UNIVERSITY OF SOUTHAMTON
FACULTY OF ENGINEERING, SCIENCE AND MATHEMATICS
School of Electronics and Computer Science

Methods of Frequency Tuning Vibration Based Micro-Generator

by
Dibin Zhu

Thesis for the degree of Doctor of Philosophy

October 2009

UNIVERSITY OF SOUTHAMPTON

ABSTRACT

FACULTY OF ENGINEERING, SCIENCE AND MATHEMATICS
SCHOOL OF ELECTRONICS AND COMPUTER SCIENCE

Doctor of Philosophy

METHODS OF FREQUENCY TUNING VIBRATION BASED MICRO-GENERATOR

by Dibin Zhu

A vibration based micro-generator is an energy harvesting device that couples a certain transduction mechanism to the ambient vibration and converts mechanical energy to electrical energy. In order to maximize available power, micro-generators are typically inertial devices that operate at a single resonant frequency. The maximum output power is generated when the resonant frequency of the generator matches the ambient vibration frequency. The output power drops significantly if these two frequencies do not match due to the high Q-factor of the generator. This thesis addresses possible methods to overcome this limit of vibration based micro-generators, in particular, method of tuning the resonant frequency of the generator to match the ambient vibration frequency.

This thesis highlights mechanical and electrical methods of resonant frequency tuning of a vibration based micro-generator. The mechanical frequency tuning is realized by applying an axial tensile force to strain the cantilever structure of the generator. A tunable micro-generator with a tuning range from 67.6 Hz to 98Hz and a maximum output power of 156.6μW at a constant low vibration acceleration level of $0.59 m \cdot s^{-2}$ was designed and tested. The tuning mechanism was found not to affect the damping of the generator. A closed loop frequency tuning system as well as the frequency searching algorithms has been developed to realize automatic frequency tuning using the proposed mechanical tuning method. The model of duty cycle of the system was established and it was proved theoretically that a reasonable duty cycle can be achieved if the generator and tuning system is designed properly.

The electrical tuning method is realized by changing the load capacitance of the generator. Models of piezoelectric and electromagnetic generators using electrical tuning methods were derived. The model of the electromagnetic generator has also been experimentally verified. The electrically tunable generator tested has a maximum 3dB bandwidth of 4.2Hz.

In conclusion, resonant frequency tuning using mechanical methods presented in the thesis have larger tuning range than that using electrical methods. However, frequency tuning using electrical tuning methods consumes less power than that using mechanical methods for the same amount of tuning range.

Contents

List of Figures

List of Tables

Declaration of Authorship

I, Dibin Zhu declare that the thesis entitled ‘Methods of Frequency Tuning Vibration Based Micro-Generator’ and the work presented in the thesis are my own. I confirm that:

- This work was done wholly or mainly while in candidature for a research degree at this University;
- Where any part of this thesis has previously been submitted for a degree or any other qualification at this University or any other institution, this has been clearly stated;
- Where I have consulted the published work of others, this is always clearly attributed;
- Where I have quoted from the work of others, the source is always given. With the exception of such quotations, this thesis is entirely my own work;
- I have acknowledged all main sources of help;
- Where the thesis is based on work done by myself jointly with others, I have made clear exactly what was done by others and what I have contributed myself;
- Parts of this work have been published as listed in section 1.3 of this thesis.

Signed:

Date:

Acknowledgements

I sincerely thank my supervisor Dr Steve Beeby for his guidance and helpful academic suggestion for my PhD study over the past three and half years. I also want to take this opportunity to gratefully acknowledge the help from Professor Neil White, Dr John Tudor and Dr Russel Torah. I also appreciate very much that staff from Perpetuum Ltd. including Dr Stephen Roberts, Mr Thomas Mouille and Dr Adam Wasenczuk for sharing their ideas with me and their technical help. Also, I would like to thank Mr David Brennan for his effort to turn those drawings into practical devices.

I also wish to thank the people who locate or used to locate in Bay 5 in the ESD lab, including Andrew, Stephen, Somphop, Siti, Ivo, Noreha, Kiwi and Ghaithaa, who made Bay 5 such an interesting place to work at.

Last but not lease, I can never forget the support from my parents and grandparents who are far away in China. Without their love and support, I could never have gone this far. I would like to especially thank my beloved wife, Xiaoqian, who accompanies with me in this foreign country and makes my life more meaningful. I appreciate it from the bottom of my heart. This thesis is dedicated to all my family and friends.

Nomenclature

a	Vibration acceleration
B	Magnetic flux density
b	Damping coefficient
b_e	Electrically induced damping coefficient
b_m	Mechanically induced damping (parasitic damping) coefficient
D	Electrical displacement (charge density)
d	Piezoelectric strain coefficient
E	Electric field density
e.m.f.	Electro-motive force
F_b	Buckling force
F_e	Damping force
f_r	Resonant frequency
$\boldsymbol{g}$	Standard gravity ($1\boldsymbol{g} = 9.8\ \mathrm{m{\cdot}s^{-2}}$)
J	Current density
k	Spring constant
L_c	Coil inductance
m	Proof mass
m_c	Mass of the cantilever
m.m.f	Magnetomotive force
N	Number of turns of the coil
P	Power
P_e	Maximum electrical energy extracted by the transduction mechanism
P_L	Power delivered to the resistive load
P_m	Mechanical loss
Q	Quality (Q)-factor
Q_e	Q-factor at optimum load
Q_{OC}	Open circuit Q-factor
R_c	Coil resistance
R_L	Load resistance

$\mathscr{R}$	Reluctance
Y	Young's modulus of the material
y	Movement of vibration
z	Displacement of the proof mass
Z	Maximum displacement of the proof mass
δ	Mechanical strain
ε	Dielectric constant of the piezoelectric material
ϕ	Transformation factor
η_a	Efficiency of the actuator
η_g	Efficiency of the generator
K	Electromagnetic coupling factor
μ	Permeability
σ	Mechanical stress Conductivity
ω_r	Resonant angular frequency
Ψ	Magnetic flux
ζ_e	Electrically induced damping factor
ζ_m	Mechanically induced damping factor
ζ_T	Total damping factor of the system

Chapter 1

Introduction

1.1 Research Objectives

Vibration-based micro-generators, as a new source of energy conversion, have been studied for many years. Academic Institutions around the world have developed a number of vibration-based micro-generators that produce useful power levels of hundreds of microwatts to several milliwatts [1]. Furthermore, some companies, e.g. Perpetuum Ltd [2], Mide Technology Corporation [3] and EnOcean GmbH [4] have commercialized this technology. However, the disadvantages of the vibration-based micro-generator are as obvious as its advantages. The working environment of the existing vibration-based micro-generator is quite limited. Almost all of the existing vibration-based micro-generators are designed to work in one particular environment. Their performance largely depends on the frequency of the ambient vibration. To make generators produce more energy, all resonant generators are designed to have very high Q-factor. Therefore, if the resonant frequency of the generator does not match the ambient vibration frequency, the output power level will decrease

dramatically. This drawback severely restricts the development of the vibration-based micro-generator.

To date, there are generally two possible solutions to this problem. The first is to tune the resonant frequency of a single generator periodically so that it matches the frequency of ambient vibration at all times. The second solution is to widen the bandwidth of the generator. This research is focused on finding suitable methods to tune the resonant frequency of the vibration-based micro-generator to match the ambient vibration frequency. Resonant frequency tuning will be studied by means of two methods. The first is to tune the resonant frequency of the vibration-based micro-generator using an intermittent and mechanical tuning method, in particular, changing mechanical strain of the structure. The second is to tune the resonant frequency by adjusting the electrical load of the vibration-based micro-generator.

1.2 Novelty in the Thesis

Novelties in this thesis include:

- Theoretically and experimentally proving the feasibility of resonant frequency tuning by applying an axial tensile force to the cantilever of the vibration based micro-generator;
- Design and fabrication of a tunable vibration based micro-generator;
- Development of a closed loop resonant frequency tuning system and two frequency searching algorithms;
- Establishment of models of frequency tuning piezoelectric and electromagnetic generators using electrical tuning methods;
- Experimental verification of the model of the electrically tunable electromagnetic generator.

1.3 Declaration

Most research work presented in this thesis was done by the author except:

- Part of the derivation of model of electrical tuning for electromagnetic generators (Equations (7.21) to (7.26) in Chapter 7), which was derived by Dr Stephen Roberts from Perpetuum Ltd.;

- Design and fabrication of the electrically tunable electromagnetic generator presented in Section 7.5.1. The generator was designed by Mr Thomas Mouille from Perpetuum Ltd and fabricated by Perpetuum Ltd.

1.4 Document Structure

In Chapter 2, the background of this research including transduction methods of vibration-based micro-generators are introduced followed by analysis of electromagnetic vibration-based micro-generators. Chapter 3 summarizes the existing strategies for increasing the operating bandwidth of vibration energy harvesters. In Chapter 4, the principle of the frequency tuning using mechanical methods is introduced. A preliminary test testifying the theory is then described. In Chapter 5, simulation and optimization of a tunable vibration-based electromagnetic micro-generator are presented followed by experimental characterization of this generator. A closed-loop automatic frequency tuning system has been developed. Details of the system together with analysis of the duty cycle of the system are given in Chapter 6. In Chapter 7, resonant frequency tuning using electrical methods is detailed. The principle as well as modeling of the method is presented. Two prototypes of electrically tunable electromagnetic generators have been tested, compared and discussed. The mathematical model has also been verified. Chapter 8 concludes details of this project and outlines future development in this area.

1.5 Publications

Publications during my PhD study have been restricted by Perpetuum Ltd for commercial reasons. An agreement has been signed by the author with Perpetuum Ltd to confirm that every publication regarding resonant frequency tuning using mechanical and electrical methods has to be approved by Perpetuum Ltd for five years from 2006. Any publication is not allowed before some key techniques are patented by Perpetuum Ltd. The first application of patent was submitted in January 2008. Therefore, there is no paper published before then. That is why only one paper has been published so far. However, there are some more papers having been submitted or being revised. Here is a list of papers related to my PhD study.

1) D. Zhu, S. Roberts, M. J. Tudor and S. Beeby 2008 Closed loop frequency tuning of a vibration-based micro-generator, *The 8th International Workshop on Micro and Nanotechnology for Power Generation and Energy Conversion Applications, November 9-12, 2008, Sendai, Japan*.
2) D. Zhu, M. J. Tudor and S. Beeby, Strategies for increasing the operating bandwidth of vibration energy harvesters: a review (submitted to *Measurement Science and Technology*).
3) D. Zhu, S. Roberts, M. J. Tudor and S. Beeby, Design and experimental characterization of a tunable vibration-based electromagnetic micro-generator (submitted to *Sensors and Actuators*).
4) D. Zhu, S. Roberts, M. J. Tudor and S. Beeby, Closed loop frequency tuning of an electromagnetic micro-generator (being revised).

Chapter 2

Fundamentals

2.1 Power supply strategies for Wireless Sensor Network

In the last decade, wireless communication has become more and more important and its application more widespread. Many standards and protocols have emerged to meet requirements for all kinds of wireless communication, e.g. infra-red for short range point-to-point (P2P) communication, IEEE 802.11 for Wireless Local Area Network (WLAN), IEEE 802.15 and Bluetooth for wireless Personal Area Network (PAN). Wireless systems offer a number of advantages over wired systems: they are flexible, easy to deploy and they can be placed in locations inaccessible to wired systems. Furthermore, the layout of nodes in the wireless system can be easily changed without considering or re-routing cabling. One of the most promising applications of wireless system is Wireless Sensor Networks (WSN).

WSN have been deployed in a wide variety of applications in recent years for the monitoring of the environment, machines, structural health and by the military for surveillance and security [5, 6]. Since each node in WSN has no physical connection to the outside world, it must have its own power supply. At present, the default power source for WSN is a battery. However, a battery has some disadvantages: it is quite bulky, has a finite amount of energy so may need periodic replacement and contains potentially hazardous chemicals. In some applications, WSN are deployed in harsh environments which may be difficult to access to replace the batteries. Therefore, it is preferred to make WSN 'self-powered' essentially scavenging their power from the surrounding environment. Recent advances in low-power sensor technology and wireless links have reduced their power requirements to only a few milliwatts [7, 8], which makes self-powered WSN feasible.

Some possible energy sources [9, 10] for WSN include photonic energy [11], thermal energy [12] and mechanical energy [1]. These sources can be used to replace or recharge the battery and increase the lifetime and capacity of WSN. Among these sources, photonic energy has already been widely used and solar cells provide excellent power density. However, solar cells are obviously not suitable in low light or dirty conditions, or in embedded applications. Thermal energy can be converted to electrical energy by the Seebeck effect but the working environment for thermo-powered sensors is restricted. Mechanical energy can be found almost anywhere that WSN may potentially be deployed which makes converting mechanical energy from ambient vibration into electrical energy an attractive approach for powering wireless sensors. The source of mechanical energy can be a moving human body or a vibrating structure. The frequency of the mechanical excitation depends on the source: less than 10Hz for human movements and over 30Hz for machinery vibrations [13]. Such devices are termed as vibration-based micro-generators. The research covered in this thesis is based on a vibration-based micro-generator.

In Section 2.2, classification of vibration-based micro-generators and principle of each transducer are described. A wide range of reported vibration-based micro-generators are summarized in Tables 2.1, 2.2 and 2.3 according to their transduction priciples. These tables are produced based on lists in [1] with some updated generators since its publication. Advantages and disadvantages of each transducer

have been listed and compared. In Section 2.3, issues regarding vibration-based micro-generators, especially electromagnetic generators, are analyzed. In addition, the effect of mechanical damping on the optimum resistive load and the maximum output power has been studied in Section 2.3.2. In Section 2.4, limitations of existing vibration-based micro-generators have been discussed, which introduces the objective of this project.

2.2 Vibration-based Micro-generator

In vibration energy harvesting, a particular transduction mechanism such as electromagnetic [14], electrostatic [15] and piezoelectric [16] is used to extract electrical energy from motion. The generator also requires a mechanical system to couple environmental displacements to the transduction mechanism. This mechanical system has to be designed to maximize the coupling between the mechanical energy source and the transduction mechanism. Most vibration-based micro-generators are single degree of freedom second order spring-mass system consisting of an inertial frame that transmits the vibration to a suspended inertial mass to produce a relative displacement or cause mechanical strain. The transduction mechanism can then generate electrical energy by exploiting the relative displacement or strain.

2.2.1 Electromagnetic (EM) Generators

Electromagnetic induction was discovered by Michael Faraday in 1831. Faraday's law of electromagnetic induction states that an electrical current will be induced in any closed circuit when the magnetic flux through a surface bounded by the conductor changes. This applies whether the field itself changes in strength or the conductor is moved through it. In an electromagnetic generator, permanent magnets are used to produce strong magnetic field and coil is used as the conductor. Either the permanent magnet or the coil is fixed to the frame while the other is attached to the inertial mass. The relative displacement caused by the vibration makes the transduction mechanism work and generate electrical energy. The induced voltage, also known as electromotive force (*e.m.f*), across the coil is proportional to the strength of the magnetic field, the velocity of the relative motion and the number of turns of the coil. An electromagnetic generator has high output current level at the expense of low voltages.

Figure 2.1 shows two commonly seen examples of electromagnetic generators.

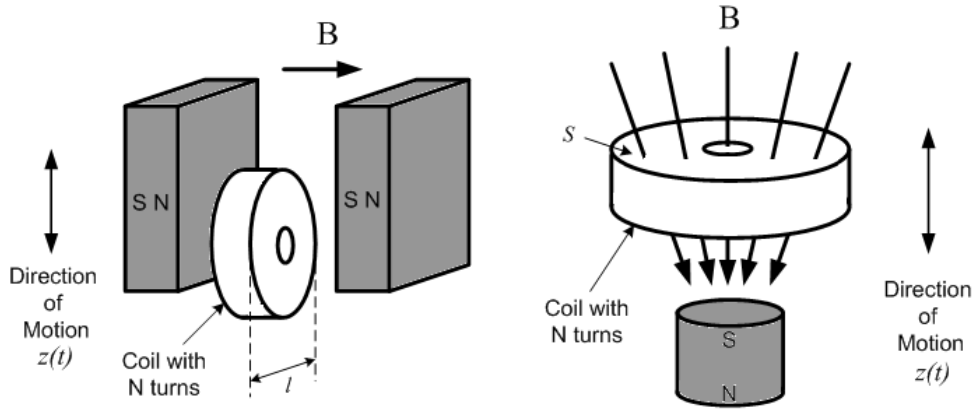

(a) (b)

Figure 2.1. Electromagnetic generators.

For the case in Figure 2.1a, the magnetic field is uniform. The magnetic field cut by the coil varies with the relative displacement between magnets and the coil. In this case, the induced electromotive force is given by:

$$e.m.f. = -N \cdot l \cdot B \cdot \frac{dz}{dt} \tag{2.1}$$

where N is the number of turns of the coil, l is the effective length of the coil, B is the flux density going through the coil and $\frac{dz}{dt}$ is the relative velocity between the magnets and the coil.

For the case in Figure 2.1b, the magnetic field varies with the distance apart from the magnet. The induced electromotive force is given by:

$$e.m.f. = -N \cdot S \cdot \frac{dB}{dz} \cdot \frac{dz}{dt} \tag{2.2}$$

where S is the effective area of the coil and $\frac{dB}{dz}$ is the gradient of the magnetic flux density along the direction of relative motion between magnets and the coil.

In both cases, the induced *e.m.f.* is a function of velocity of relative movement *z(t)*. Therefore, both expressions can be expressed by:

$$e.m.f. = \mathrm{K} \cdot \frac{dz}{dt} \tag{2.3}$$

where K is the electromagnetic coupling factor. K equals $-N \cdot l \cdot B$ and $-N \cdot S \cdot \frac{dB}{dz}$ in both cases, respectively. It represents the change in coupled flux per unit displacement.

Figure 2.2 shows a circuit representation of an electromagnetic generator with a resistive load, R_L. The relation between the current through the load and the induced *e.m.f* is given by:

$$e.m.f. + i \cdot (R_L + R_c) + L_c \frac{di}{dt} = 0 \tag{2.4}$$

where R_c and L_c are the resistance and inductance of the coil, respectively.

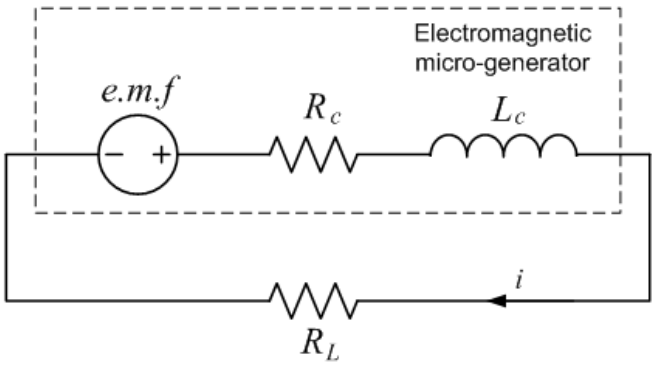

Figure 2.2. Circuit representation of an electromagnetic generator.

Electromagnetic generators perform better in macro scale than in micro scale [17]. Particularly, generators integrated with MEMS with electroplated coils and magnets may not be able to produce useful power levels. Table 2.1 lists some reported electromagnetic generators with their main characteristics.

Table 2.1. Summary of electromagnetic generators.

Reference	*f* (Hz)	Excitation level ($m \cdot s^{-2}$)	Mass (g)	Volume (mm^3)	P (μW)	Power Density ($\mu W \cdot mm^{-3}$)	Structure Material
Williams [18] (2001)	4400	382	0.0023	5.4	0.3	0.0556	GaAs Polyimide
Ching [19] (2002)	110	95.5	N/A	1000	830	0.83	Copper
Glynne-Jones [20] (2004)	322	2.7	N/A	840	180	0.214	Steel
Koukharenko [21] (2006)	1615	3.92	N/A	100	0.104	0.00104	Silicon
Saha [22] (2006)	84	7.8	25	800[a]	3500	4.375	Copper
Beeby [23] (2007)	52	0.589	0.66	150	46	0.307	BeCu
Wang [24] (2007)	121.25	14.7	0.0312	10[a]	$60mV_{pp}$ OC	N/A	Copper
Külahand [25] (2008)	25	N/A	15.6[a]	2000[a]	3.97	0.00199	Styrene

[a] Estimated or Extrapolated from data in reference OC: Open Circuit

2.2.2 Electrostatic (ES) Generators

The basis of electrostatic generator is the variable capacitor. The variable capacitance structure is driven by mechanical vibrations. The capacitance varies between maximum and minimum value. If the charge on the capacitor is constrained, charge will move from the capacitor to a storage device or to the load as the capacitance decreases. Thus, mechanical energy is converted to electrical energy. Electrostatic generators can be classified into three types, i.e. In-Plane Overlap (Figure 2.3a) which varies the overlap area between electrode fingers, In-Plane Gap Closing (Figure 2.3b) which varies the gap between electrode fingers and Out-of-Plane Gap Closing (Figure 2.3c) which varies the gap between two large electrode plates [15].

A simplified circuit for an electrostatic generator using charge constrained conversion is shown in Figure 2.4. V_{in} is a pre-charged reservoir, which could be a capacitor or a rechargeable battery. C_v is a variable capacitor, which is one of the three types mentioned above. C_{par} is the parasitic capacitance associated with the variable capacitor structure and any interconnections, which limits the maximum voltage. C_L is the storage capacitor or any kind of load.

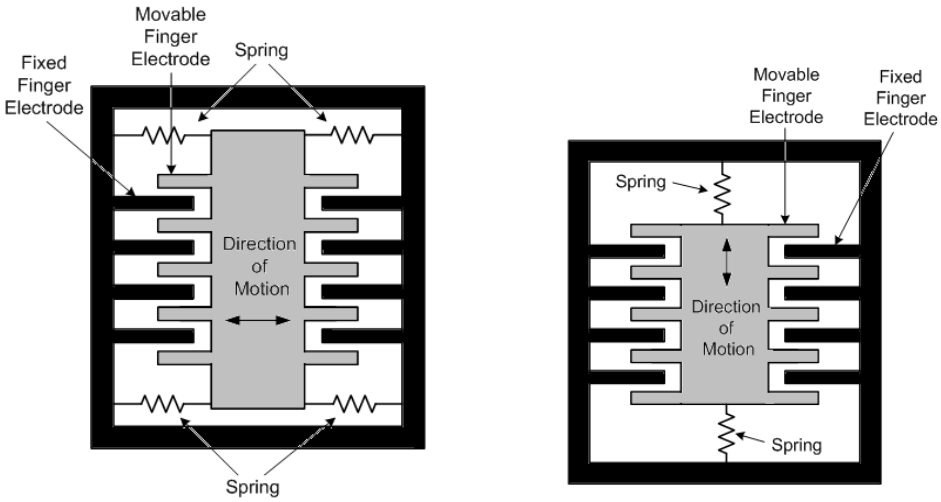

(a) In-Plane Overlap (b)In-Plane Gap Closing

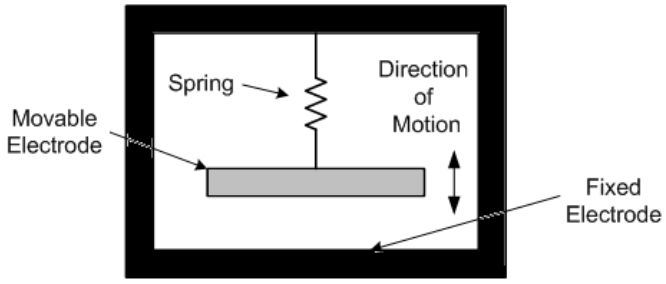

(c) Out-of-Plane Gap Closing

Figure 2.3. Electrostatic generators.

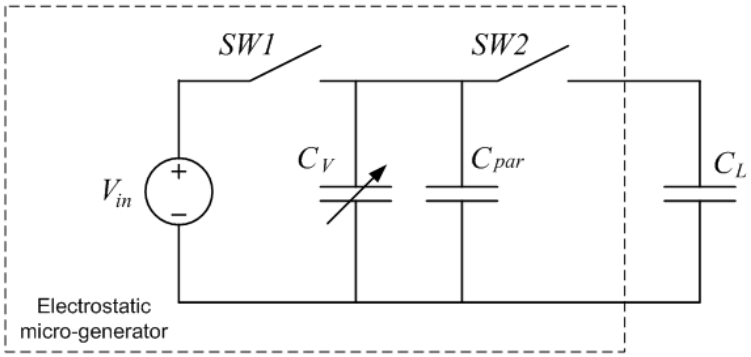

Figure 2.4. Circuit representation for an electrostatic generator.

The maximum voltage across the load is given by:

$$V_{\max} = \frac{C_{\max} + C_{par}}{C_{\min} + C_{par}} \cdot V_{in} \tag{2.5}$$

And the maximum energy converted from mechanical domain to electrical domain is:

$$E_{\max} = \frac{1}{2}\left(C_{\max} - C_{\min}\right) \cdot V_{\max} \cdot V_{in} \tag{2.6}$$

An electrostatic generator can be easily realized in MEMS version. Since the fabrication process of electrostatic generators is similar to that of VLSI, electrostatic generators can be assembled with VLSI without difficulties. Unfortunately, electrostatic generators require an initial polarizing voltage or pre-charged electrets. Therefore, they can hardly become a separate power source. However, they can be used to charge a battery. Table 2.2 lists some reported electrostatic generators with their main characteristics.

Table 2.2. Summary of electrostatic generators.

Reference	*f* (Hz)	Excitation level ($m \cdot s^{-2}$)	Mass (g)	Volume (mm^3)	P (μW)	Power Density ($\mu W \cdot mm^{-3}$)	Type
Meninger [26] (2001)	2520	N/A	N/A	75	8	0.11	IPO
Tashiro [27] (2002)	6	1	780	N/A	36	N/A	OP
Mitcheson [28] (2003)	30	50	0.1	750	3.7	0.0049	N/A
Arakawa [29] (2004)	10	3.9	N/A	800	6	0.0075	IPO
Despesse [30] (2005)	50	8.8	104	1800	1052	0.584	IPGC
Kuehne [31] (2006)	1000	1.96	N/A	N/A	4.28	0.079	IPO
Yen [32] (2006)	1560	82.32	N/A	N/A	1.8	N/A	OP
Sterken [33] (2007)	500	9.8	N/A	N/A	5	N/A	OP
Lo [34] (2008)	50	576.6	54	50000	17.98	0.00036	OP

IPO: In-Plane Overlap IPGC: In-Plane Gap Closing OP: Out-of-plane

2.2.3 Piezoelectric (PZ) generators

The piezoelectric effect was discovered by Pierre and Jacques Curie in 1880. It is the ability of some materials (notably crystals and certain ceramics) to generate an electric potential in response to applied mechanical stress. The electrical polarization

is proportional to the applied strain. This is the piezoelectric effect used for mechanical to electrical energy conversion. Commonly used materials for piezoelectric power generation are PZT, PVDF [35] and Macro-Fiber Composite (MFC) [36].

Piezoelectric micro-generators typically work in either d33 mode (Figure 2.5a) or d31 mode (Figure 2.5b). In the d33 mode, a force is applied in the same direction as the poling direction, such as the compression of a piezoelectric block that is poled on its top and bottom surfaces. In the d31 mode, a force is applied in the direction perpendicular to the poling direction, an example of which is a bending beam that is poled on its top and bottom surfaces. Generally, the d31 mode has been the most commonly used coupling mode although the d31 mode yields a lower coupling coefficient than the d33 mode [35]. This is because that the typically used structures working in the d31 mode are a cantilever or a double-clamped beam. When such structures bend, it produces much more stress than compressing a structure working in the d33 mode.

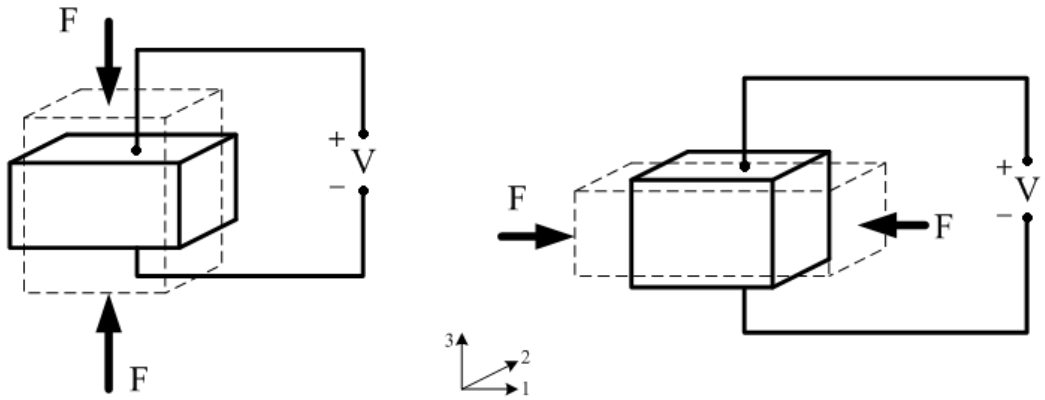

(a) (b)

Figure 2.5. Piezoelectric generators (a) d33 mode (b) d31 mode.

The constitutive equations for a piezoelectric material are given by:

$$\delta = \frac{\sigma}{Y} + d \cdot E \tag{2.7}$$

$$D = \varepsilon \cdot E + d \cdot \sigma \tag{2.8}$$

where δ is mechanical strain, σ is mechanical stress, Y is the Young's modulus of the material, d is the piezoelectric strain coefficient, E is the electric field, D is the electrical displacement (charge density) and ε is the dielectric constant of the piezoelectric material.

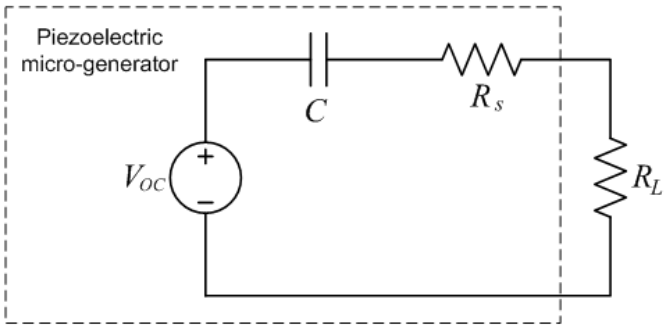

Figure 2.6. Circuit representation of a piezoelectric generator.

Figure 2.6 shows a circuit representation of a piezoelectric generator with a resistive load, R_L. C is the capacitance between two electrodes and R_s is the resistance of the piezoelectric material. The voltage source, V_{OC}, is the open circuit voltage resulting from Equation (2.8) when the electrical displacement is zero. It is given by:

$$V_{OC} = -\frac{d \cdot t}{\varepsilon} \cdot \sigma \tag{2.9}$$

where t is the thickness of the piezoelectric material.

Piezoelectric generators have the simplest structure among the three transducers and they can produce appropriate voltages for electronic devices. However, the mechanical properties of the piezoelectric material may limit overall performance and lifespan of the generator. Although piezoelectric thin films can be integrated into a MEMS fabrication process, the piezoelectric coupling is greatly reduced. Therefore, the potential for integration with microelectronics is less than that for electrostatic micro-generators. Table 2.3 lists some reported piezoelectric generators with their main characteristics.

Table 2.3. Summary of piezoelectric generators.

Reference	*f* (Hz)	Excitation level ($m \cdot s^{-2}$)	Mass (g)	Volume (mm^3)	P (μW)	Power Density ($\mu W \cdot mm^{-3}$)	Material
White [37] (2001)	80	2.3	0.8	125	2.1	0.0168	Screen printed PZT
Roundy [13] (2003)	120	2.5	9.2	1000	375	0.375	PZT
Lu [38] (2004)	7000	N/A	N/A	N/A	1600	N/A	PZT-PIC255
Jeon [39] (2005)	13.9	106	N/A	0.027[a]	1	37.04	PZT
Fang [40] (2006)	608	9.8	0.0016[a]	0.6[a]	2.16	3.6	PZT
Marzencki [41] (2007)	1500	3.92	0.0009[a]	5	0.03	0.006	AlN
Jeong [42] (2008)	120	0.98	N/A	N/A	500	22	PMNZT
Kok [43] (2008)	230	9.8	N/A	N/A	0.27	N/A	PZT

[a] Extrapolated from data in reference

2.2.4 Other Transduction Mechanisms

Magnetostrictive materials are also used to extract electrical energy from ambient vibration. These materials deform when placed in a magnetic field and it can induce changes in magnetic field when it is strained. Magnetostrictive materials are generally used in piezoelectric-magnetostrictive composites. Such composites were originally used in magnetic field sensors and have recently been adopted in energy harvesting

Huang et al [44] reported two energy harvesting devices based on a Terfenol-D/PZT/ Terfenol-D composite. Their device produced 1.2mW of power when excited at $5 m \cdot s^{-2}$ at 30Hz. Recently, Wang et al [45] reported a new vibration energy harvester based on magnetostrictive material, Metglas 2605SC with electromagnetic pickup. Experimentally, the maximum output power and power density on the load resistor can reach 200μW and $900 \mu W \cdot cm^{-3}$, respectively, at a low frequency of 58Hz. For a working prototype under a vibration with resonance frequency of 1.1kHz and peak acceleration of $8.06 m \cdot s^{-2}$, the average power and power density during charging the ultracapacitor can achieve 576μW and $606 \mu W \cdot cm^{-3}$, respectively,

2.2.5 Comparisons of Transduction Mechanisms

The main advantages and disadvantages of each type of transduction mechanism are summarized in Table 2.4.

Table 2.4. Comparisons of different transduction mechanisms of vibration-based micro-generators.

Type	Advantages	Disadvantages
Electromagnetic	♦ No external voltage source ♦ No mechanical constraints needed ♦ High output current	♦ Difficult to integrate with MEMS fabrication process ♦ Poor performance in micro scale ♦ Low output voltage
Electrostatic	♦ Easy to integrate with MEMS fabrication process ♦ High output voltage	♦ Mechanical constraints needed ♦ External voltage source or pre-charged electret needed ♦ Low output current
Piezoelectric	♦ Simple structure ♦ No external voltage source ♦ Compatible with MEMS ♦ High output voltage ♦ No mechanical constraints Needed	♦ Thin films have poor coupling ♦ Poor mechanical properties ♦ High output impedance ♦ Charge leakage ♦ Low output current
Magnetostrictive	♦ Ultra-high coupling coefficient ♦ High flexibility	♦ Nonlinear effect ♦ May need bias magnets ♦ Difficult to integrate with MEMS fabrication process

Since electrostatic and piezoelectric transducers are compatible with MEMS, they are more suitable to be deployed in micro or nano-scale systems while electromagnetic and magnetostrictive transducers are suitable for macro-scale systems. Roundy et al [46] calculated the theoretical maximum energy density of the first three transducers. It was concluded that piezoelectric and electromagnetic transducers have similar energy density which is about ten times of that of electrostatic transducers.

Table 2.5 lists some commercially available vibration-based micro-generators. To the date, only generators with electromagnetic and piezoelectric transducers can be found on the market, which indicates that these two transducers are more feasible in practice. This consideration agrees with Roundy's calculation.

Table 2.5. Summary of vibration-based micro-generators available on the market.

Model	*f* (Hz)	Excitation level ($m \cdot s^{-2}$)	Total Mass (g)	Volume (mm^3)	P (mW)	Transducer
Mide Technology Corporation						
Volture PEH20w [47]	80-175[a]	13.7	85.14	39963 (Total device) 388.55 (Piezo wafer)	2-24	PZ
Volture PEH25w [48]	50-140[a]	13.7	85.14	40543 (Total device) 194.27 (Piezo wafer)	2.5-24	PZ
Perpetuum Ltd						
PMG-17 [49]	100/120	9.8	655	522682 (Total device)	45	EM
PMG-27 [50]	17.2	0.49	400	467711 (Total device)	4	EM

[a] Tunable by changing the length of the cantilever manually

PZ: Piezoeletric EM: Electromagnetic.

2.3 Analysis of Vibration-based Micro-generators

Vibration-based micro-generators, as a new source of energy, have received increasing levels of attention in the last decade. Since vibration can be found almost anywhere that WSN may potentially be deployed, electrical energy converted from mechanical energy in ambient vibrations is often an attractive approach for powering wireless sensors. Extracting energy from vibration requires a transduction mechanism to generate electrical energy from motion as mentioned earlier in this chapter. Vibration energy is best suitable for inertial generators with the mechanical component attached to an inertial frame which acts as the fixed reference. The inertial frame transmits the vibrations to a suspended inertial mass producing a relative displacement between them or change in mechanical strain. Therefore, the majority of generators are based upon a spring-mass system with a characteristic resonant

frequency.

The generic model of vibration-based micro-generators was first developed by Williams and Yates [51]. This model has been experimentally found to represent the vibration-based micro-generators accurately, especially electromagnetic generators. Details of this model will be given in Appendix A. Some key characterizations of this model regarding to this research and some more derivations are presented in this section.

2.3.1 Output Power of Electromagnetic Micro-generators

The average power dissipated within the damper, i.e. the sum of the power generated by the electromagnetic transducer and the power wasted in the parasitic damping, is as follows [51]:

$$P(\omega) = \frac{m\zeta_T Y^2 \left(\frac{\omega}{\omega_r}\right)^3 \omega^3}{\left[1-\left(\frac{\omega}{\omega_r}\right)^2\right]^2 + \left[2\zeta_T \frac{\omega}{\omega_r}\right]^2} \tag{2.10}$$

where m is the mass, ζ_T is the total damping, Y is the tip displacement of the mass and ω_r is the resonant frequency.

When the generator is at resonance, i.e. $\omega = \omega_r$, the power dissipation reaches maximum. The maximum dissipated power is:

$$P = \frac{mY^2\omega_r^3}{4\zeta_T} \tag{2.11}$$

or

$$P = \frac{mY^2\omega_r^3}{4(\zeta_e + \zeta_m)} \tag{2.12}$$

where ζ_e and ζ_m are electrical damping and mechanical damping, respectively.

The power dissipation is the sum of maximum electrical energy extracted by the transduction mechanism, P_e, and mechanical loss, P_m. P_e and P_m are as follows:

$$P_e = \frac{\zeta_e m Y^2 \omega_r^3}{4(\zeta_e + \zeta_m)^2} \tag{2.13}$$

$$P_m = \frac{\zeta_m m Y^2 \omega_r^3}{4(\zeta_e + \zeta_m)^2} \tag{2.14}$$

Maximum power conversion from mechanical domain to electrical domain occurs when $\zeta_e = \zeta_m$, i.e. damping arising from the electrical domain equals to mechanical losses. Therefore, the maximum electrical power that can be extracted by the micro-generator, P_e, is given by:

$$P_e = \frac{P}{2} = \frac{m Y^2 \omega_r^3}{16\zeta_m} \tag{2.15}$$

Since the peak acceleration of the base, a, is given by $a = Y\omega^2$, Equation (2.15) can be rewritten as:

$$P_e = \frac{m \cdot a^2}{16\omega_r \cdot \zeta_m} \tag{2.16}$$

As the open circuit Q-factor, $Q_{OC} = \frac{1}{2\zeta_m}$, Equation (2.16) can be written as:

$$P_e = \frac{m \cdot a^2}{8\omega_r} \cdot Q_{OC} \tag{2.17}$$

The power delivered to the resistive load, P_L, is a function of the coil and load resistance, which is given by:

$$P_L = P_e \cdot \frac{R_L}{R_L + R_c} = \frac{m \cdot a^2}{16\omega_r \cdot \zeta_m} \cdot \frac{R_L}{R_L + R_c} \tag{2.18}$$

$$P_L = P_e \cdot \frac{R_L}{R_L + R_c} = \frac{m \cdot a^2}{8\omega_r} \cdot Q_{OC} \cdot \frac{R_L}{R_L + R_c} \tag{2.19}$$

It is found via Equation (2.18) and (2.19) that the maximum power delivered to the electrical domain is inversely proportional to damping factor, i.e. proportional to the Q-factor. Hence, when designing a vibration-based micro-generator to achieve maximum power output, it is important to design the generator to have a high Q-factor (i.e. low damping factor) and that the generator is excited at its resonant frequency. Figure 2.7 shows an example of the power spectrum of a vibration-based micro-generator of resonant frequency 50Hz with various Q-factors and damping factors. It can be seen that, for generators with a high Q-factor (i.e. low damping factor), the output power drops significantly if the frequency of operation is away from the generator's resonance. When the Q-factor is lower (i.e. damping factor is higher), the peak output power decreases while the bandwidth of the generator increases and the devices becomes less sensitive to frequency shifts at the expense of lower maximum generated power.

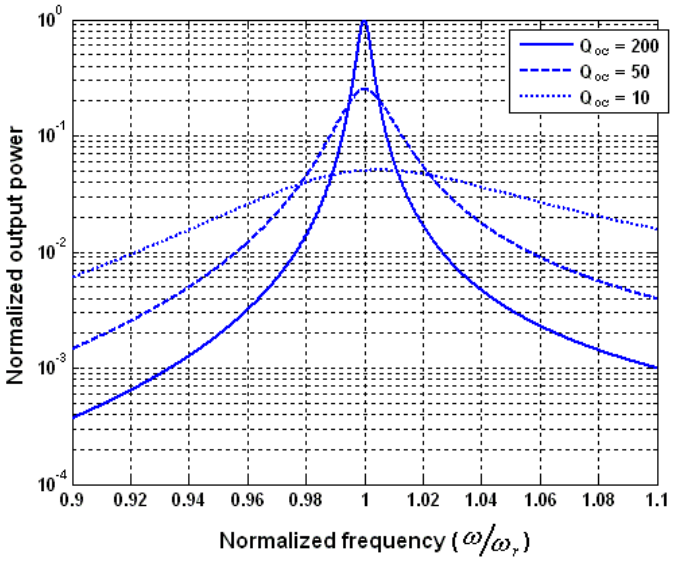

Figure 2.7. Power spectrum of a generator with various Q-factors.

2.3.2 Optimum Resistive Load

When load resistance is much larger than coil resistance, almost 100% of the extracted electrical power is delivered to the load. Increasing the load resistance results in a decrease in electrically induced damping, which also increases the output voltage. However, the output power does not always increase with the increase of the load resistance. If the resistive load is selected properly, maximum generated power as well as the most efficient power transfer to the load can be achieved at the same time.

For electromagnetic generator, the electrically induced damping factor, ζ_e, is:

$$\zeta_e = \frac{\mathrm{K}^2}{2m\omega(R_L + R_c)} \tag{2.20}$$

where K is the electromagnetic coupling factor as defined in Section 2.2.1.

Substituting Equation (2.20) into Equation (2.13) and considering $a = Y\omega^2$ give another expression of maximum electrical energy extracted by the transduction mechanism as follows:

$$P_e = \frac{\mathrm{K}^2 m^2 a^2 (R_L + R_c)}{2\left[\phi^2 + 2m\omega_r (R_L + R_c)\zeta_m\right]^2} \tag{2.21}$$

Therefore, the power delivered to the resistive load is given by:

$$P_L = P_e \cdot \frac{R_L}{R_L + R_c} = \frac{\mathrm{K}^2 m^2 a^2 R_L}{2\left[\phi^2 + 2m\omega_r (R_L + R_c)\zeta_m\right]^2} \tag{2.22}$$

Figure 2.8 shows an example of electrical power delivered to the load resistor versus load resistance. The maximum power delivered to the resistive load occurs at an optimum load resistance.

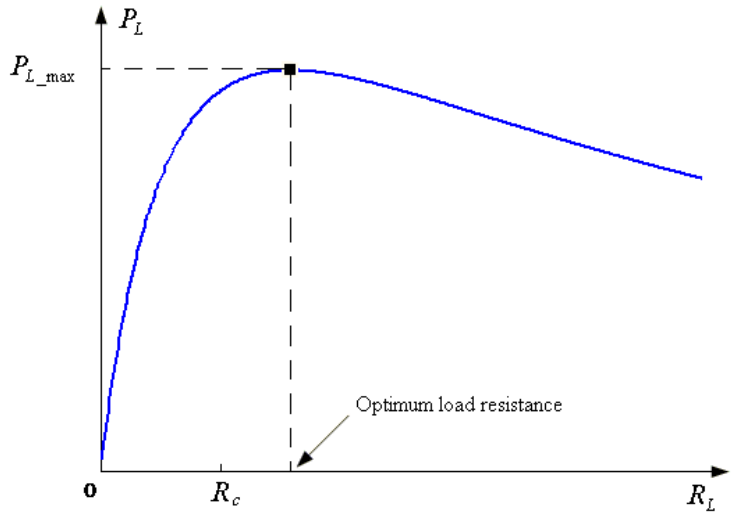

Figure 2.8. Electrical power delivered to the load resistor vs. load resistance.

The maximum power delivered to the resistive load, the optimum load resistance and the transfer efficiency depends on the mechanical damping factor. When the mechanical damping factor is zero, the output power is totally dependent on the electrical loads.

2.4 Limitation of Vibration-based Generators

The mathematical analysis described in Section 2.3 shows that maximum power is generated when the resonant frequency of the generator matches the frequency of the ambient vibration. As generators are usually designed to have a high Q-factor for better performance, the generated power drops dramatically if these two frequencies don't match. Most reported generators are designed to work only at one particular frequency [1]. For applications such as moving vehicles, human movement and wind induced vibration where the frequency of ambient vibration changes periodically, the efficiency of generators with one fixed resonant frequency is significantly reduced since the generator will not always be at resonance. This limitation must be overcome if vibration-based micro-generators are to be widely applicable in powering wireless systems. Solutions to this problem include tuning the resonant frequency of the micro-generator as well as widening the bandwidth of the generators. Details of both solutions will be presented in the next chapter.

2.5 Conclusions

Several power supply strategies for wireless sensor networks have been introduced in this chapter. Attention has been paid especially to vibration-based micro-generators. A particular transduction mechanism is used to extract electrical energy from motion. The main transduction mechanisms are electromagnetic, electrostatic, piezoelectric and magnetostrictive.

Equation (2.10) gives a good guideline in designing vibration-based micro-generators. It is found that the maximum power converted from the mechanical domain to the electrical domain is proportional to the mass and vibration acceleration and inversely proportional to resonant frequency as well as mechanical (electrical) damping factor. This means that more power can be extracted if the inertial mass is increased or the generator can work in the environment where the vibration level is high. For a fixed resonant frequency, the generator has to be designed to make the mechanical damping as small as possible. For a generator with constant mechanical damping, the generated electrical power drops with an increase of the resonant frequency.

Furthermore, if the micro-generator is connected to the optimum resistive load, both maximum power extracted by the transduction mechanism and the most efficient power delivery from generator to resistive load can be realized. The maximum power delivered to the resistive load, the optimum load resistance as well as the transfer efficiency depends on the mechanical damping factor. If the mechanical damping factor is zero, i.e. no mechanical damping, the output power is totally dependent on the electrical loads. Therefore, it is highly important to minimize the mechanical damping in designing the micro-generator.

A limitation of the vibration-based micro-generators is their narrow operating frequency range. Solutions to this problem include tuning the resonant frequency of the micro-generator and widening the bandwidth of the generator. Details will be given in Chapter 3.

Chapter 3

Strategies for Increasing the Operating Frequency Range of Vibration-based Micro-generators

3.1 Introduction

Mathematical analysis presented in Chapter 2 showed that maximum power is generated when the resonant frequency of the generator matches the frequency of the ambient vibration. As generators are usually designed to have a high Q-factor for better performance, the generated power drops dramatically if these two frequencies don't match. Most reported generators are designed to work only at one particular frequency [1]. For applications such as moving vehicles, human movement and wind induced vibration where the frequency of ambient vibration changes periodically the efficiency of generators with one fixed resonant frequency is significantly reduced

since the generator will not always be at resonance. This limitation must be overcome if vibration-based micro-generators are to be widely applicable in powering wireless systems. To date, there are, in general, two approaches to solving this problem.

The first is to adjust, or tune, the resonant frequency of a single generator so that it matches the frequency of the ambient vibration at all times. This can be achieved by changing the mechanical characteristics of the structure or electrical load of the generator. Changing the mechanical characteristics of a generator has previously been called passive or active tuning depending on the approach [52]. Passive tuning is defined as a tuning mechanism that operates periodically. This approach only consumes power during the tuning operation and uses negligible energy once the generator is matched to the frequency of the ambient vibrations. Active tuning is defined as a tuning mechanism that is continuously applied even if the resonant frequency equals the ambient vibration frequency. Since both of these approaches involve some form of active process, a more precise classification scheme defining tuning mechanisms as either intermittent (previously called passive) or continuous (previously called active) is used throughout this thesis.

The second approach is to widen the bandwidth of the generator. This can be achieved by, for example, employing:

- An array of structures each with a different resonant frequency;
- An amplitude limiter;
- Non-linear (e.g. magnetic) springs;
- Bi-stable structures;
- A large inertial mass (large device size) with a high degree of damping.

This chapter reviews vibration powered generators that demonstrate these approaches as well as those reported frequency tuning strategies for other resonant devices that are potentially applicable for tuning vibration-based micro-generators. The following Section describes the theory behind tuning strategies, compares the power consumption for continuous and intermittent tuning mechanisms and suggests criteria for evaluating tuning mechanisms. Section 3.3 introduces the potential mechanical parameters that can be adjusted to achieve frequency tuning and reviews the

approaches presented in the literature to date. Section 3.4 discusses the theory of electrical tuning for piezoelectric generators and presents example devices. Section 3.5 contains examples of wide bandwidth generators that demonstrate the principles introduced above. Section 3.6 gives a tabulated summary of devices presented to date categorised into three approaches: continuous tuning, intermittent tuning and generator arrays. Section 3.7 compares tuning strategies and presents theoretical power output versus frequency graphs for a large size wide bandwidth device, a generator array and a single tunable generator. This analysis considers four scenarios enabling a broad comparison between approaches.

3.2 Strategies to Tune Resonant Frequency

3.2.1 Intermittent versus Continuous Tuning

As described in the introduction of this chapter, continuous tuning is applied constantly to the generator and therefore consumes more energy than intermittent tuning. It was concluded by Roundy [52] that generators using a continuous tuning mechanism can never produce a net increase in power output as the power required to tune the resonant frequency will always exceed the increase in output power resulting from the frequency tuning. However, the derivation presented was not correct as is shown below in Equations (3.11) to (3.15). For clarity, the derivation in [52] is reproduced here in Equations (3.1) to (3.10).

The analysis covers resonant frequency tuning achieved by providing an additional force proportional to the generator's displacement (i.e. altering stiffness) or acceleration (i.e. altering mass) using a tuning actuator [52].

The power required by the tuning actuator, $P_a(t)$, is:

$$P_a(t) = k_a z(t)\frac{dz(t)}{dt} = m_a \frac{dz(t)}{dt}\cdot\frac{d^2 z(t)}{dt^2} \tag{3.1}$$

where k_a is the actuator stiffness, $z(t)$ is the displacement of the proof mass and m_a is the mass of the actuator. The untuned resonant frequency, ω_1, and the new resonant frequency, ω_2, are given by:

$$\omega_1 = \sqrt{\frac{k}{m}} \tag{3.2}$$

$$\omega_2 = \sqrt{\frac{k + k_a}{m}} \tag{3.3}$$

The actuator stiffness, k_a, can be represented as:

$$k_a = m\omega_2^2 - k = m\left(\omega_2^2 - \omega_1^2\right) \tag{3.4}$$

Hence, Equation (3.1) can be written as:

$$P_a(t) = \frac{1}{2} m\omega_2\left(\omega_2^2 - \omega_1^2\right)Z^2 \sin(2\omega_2 t) \tag{3.5}$$

As the maximum displacement of the proof mass, Z, can be expressed as:

$$Z = \frac{a}{2\zeta_T \omega_2^2} \tag{3.6}$$

where a is the excitation acceleration and ζ_T is the total damping factor, the magnitude of the power needed for actuation becomes:

$$\left|P_a\right| = \frac{m\left(\omega_2^2 - \omega_1^2\right)a^2}{8\zeta_T^2 \omega_2^3} \tag{3.7}$$

There will be a net increase in power output only if the power generated at the new frequency, ω_2, after deducting the actuation power ($P_{out2}(\omega_2)$) is larger than the power output without tuning at ω_2 ($P_{out1}(\omega_2)$), (shown in Figure 3.1) i.e. the following inequality is true.

$$\left|P_{out2}(\omega_2)\right| - \left|P_a\right| \geq \left|P_{out1}(\omega_2)\right| \tag{3.8}$$

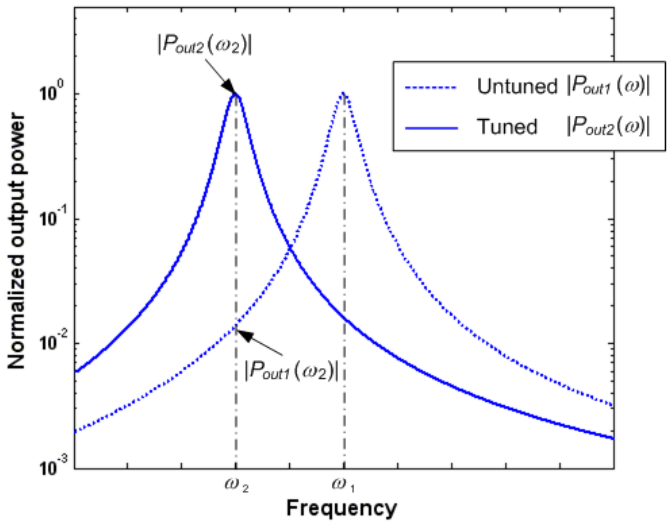

Figure 3.1. Power spectrum of untuned and tuned generator.

$P_{out2}(\omega_2)$ is the maximum power the generator outputs at the new resonance given by:

$$\left|P_{out2}(\omega_2)\right| = \frac{m\zeta_e a^2}{8\omega_2\zeta_T^2} \tag{3.9}$$

$P_{out1}(\omega_2)$ is the output power at ω_2 when the generator has the original resonant frequency, ω_1, given by:

$$\left|P_{out1}(\omega_2)\right| = \frac{m\zeta_e r^2 a^2}{4\zeta_T^2 r^2\omega_1 + \omega_1\left(1-r^2\right)^2} \tag{3.10}$$

where $r = \omega_2/\omega_1$.

Hence, it was found in [52] that, based on Equations (3.7), (3.9) and (3.10), inequality (3.8) will never be true, which drew the conclusion that a net increase in power output can never be produced using an active tuning mechanism. This is the end of the derivation in [52].

However, the average power of a time-varying signal within a period, T, cannot simply be represented by its maximum value as was stated in Equation (3.7). It is given by:

$$P = \frac{1}{T}\int_0^T P(t)dt \tag{3.11}$$

The displacement of the proof mass in single degree of freedom second order spring-mass systems, $z(t)$, is given by [53]:

$$z(t) = \frac{\omega^2 Y}{\sqrt{\left(\omega_r - \omega\right)^2 + \left(\frac{b\omega}{m}\right)^2}}\sin\left(\omega t + \varphi\right) \tag{3.12}$$

where $\varphi = \tan^{-1}\left(\frac{b\omega}{k - \omega^2 m}\right)$, b is the damping coefficient and k is the spring constant.

The power available within the generator is:

$$P = b\left(\frac{dz(t)}{dt}\right)^2 \tag{3.13}$$

Substituting Equation (3.12) into Equation (3.13) leads to the time-varying expression of power available within the generator as:

$$P(t) = \frac{m\zeta_T Y^2\left(\frac{\omega}{\omega_r}\right)^3\omega^3}{\left[1-\left(\frac{\omega}{\omega_r}\right)^2\right]^2 + \left[2\zeta_T\frac{\omega}{\omega_r}\right]^2} + \frac{m\zeta_T Y^2\left(\frac{\omega}{\omega_r}\right)^3\omega^3}{\left[1-\left(\frac{\omega}{\omega_r}\right)^2\right]^2 + \left[2\zeta_T\frac{\omega}{\omega_r}\right]^2}\cos\left(2\omega t + 2\varphi\right) \tag{3.14}$$

Using Equation (3.11), the expression of power available within the generator can be derived in the same way as Equation (2.10).

Based on Roundy's equations, substitution of Equation (3.5) into Equation (3.11) leads to the average power of the actuation as:

$$|P_a| = \frac{1}{T}\int_0^T P_a(t)dt = \frac{1}{T}\int_0^T \left[\frac{1}{2}m\omega_2\left(\omega_2^2 - \omega_1^2\right)Z^2\sin(2\omega_2 t)\right]dt = 0 \qquad (3.15)$$

In practice, actuation power can never be zero if the tuning mechanism is activated. Roundy et al used the maximum power rather than the average power of actuation in their derivation and drew the conclusion that the active tuning can never produce a net increase of output power. In addition, only the situation where the tuning force is proportional to the generator's displacement or acceleration was studied in [52]. For most cases, tuning force is not linked to the generator's movement and methods of calculating actuation power may vary according to the way in which tuning force is applied. Therefore, the analysis in [52] does not apply to all situations.

However, it is apparent that intermittent tuning has an advantage over a continuous tuning mechanism because it is switched off once the device is at resonance and therefore consumes less energy than continuous mechanisms.

3.2.2 Evaluating Tuning Approaches

The suitability of different tuning approaches will depend upon the application but in general terms the key factors for evaluating a tuning mechanism for adjusting the resonant frequency of vibration-based micro-generators are:

- The energy consumed by the tuning mechanism should be as small as possible and must not exceed the energy produced by the generator;
- The mechanism should achieve a sufficient operational frequency range;
- The tuning mechanism should achieve a suitable degree of frequency resolution;
- The generator should have as high as possible Q-factor to achieve maximum power output and the strategy applied should not increase the damping, i.e. decrease Q-factor, over the entire operational frequency range.

A generator's resonant frequency can be tuned by both mechanical and electrical methods. Mechanical tuning alters the resonant frequency by changing the mechanical properties of the structure. Electrical tuning alters the resonant frequency by adjusting the electrical load. The principles of both methods as well as existing approaches to

realize them are described in the following Sections.

3.3 Mechanical Tuning Methods

As most reported vibration energy harvesting devices are based on a cantilever [1], this structure will be used in the following theoretical analyses of mechanical tuning. The principles demonstrated are, however, generally applicable to all mechanical resonator structures. This Section covers mechanisms that achieve tuning by:

- Changing dimensions;
- Moving the centre of gravity of proof mass;
- Variable spring stiffness;
- Straining the structure.

A comprehensive review of each mechanical tuning mechanism reported in the literature to date is presented after a brief analysis of the theory.

The resonant frequency of a spring-mass structure is given by:

$$f_r = \frac{1}{2\pi}\sqrt{\frac{k}{m}} \tag{3.16}$$

where k is the spring constant and m is the inertial mass. When tuning the resonant frequency of the generator, one can change either the spring constant or the mass.

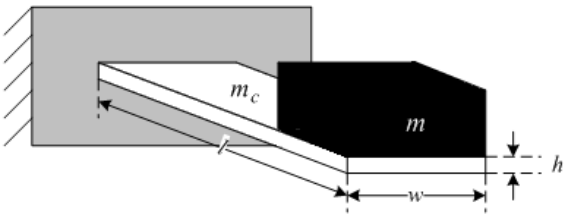

Figure 3.2. Cantilever with mass.

The spring constant of a resonator depends on its materials and dimensions. For a cantilever with a mass at the free end (Figure 3.2), the resonant frequency is given by [54]:

$$f_r = \frac{1}{2\pi}\sqrt{\frac{Ywh^3}{4l^3\left(m + 0.24m_c\right)}} \tag{3.17}$$

where Y is Young's modulus of the cantilever material, w, h and l are the width, thickness and length of the cantilever, respectively and m_c is the mass of the cantilever. The resonant frequency can be tuned by adjusting all these parameters. Each parameter in Equation (3.17) is discussed in the following Sections.

In addition, it is important to mention that if actuators are involved in changing the mechanical properties of the resonant structure, the tuning mechanisms can be operated by a control system to automatically tune the generator.

3.3.1 Changing Dimensions

In practice, it is difficult to change the width, w, and thickness, h, of a cantilever while changing the length, l, is feasible. Furthermore, modifying l is suitable for intermittent tuning. The approach requires that the cantilever base clamp be released and re-clamped in a new location along the length of the beam thereby changing the effective length (and hence frequency). There is no power required to maintain the new resonant frequency. Furthermore, as the resonant frequency is inversely proportional to $l^{3/2}$ thus modifying l can significantly change f_r.

Suppose l is the original length of the cantilever and l' is the modified length of the cantilever, $l' = l + \Delta$, where Δ is the difference between them. The mass of cantilever is then changed to $m_c' = whl'\rho$, where ρ is the density of the cantilever material while the original mass of cantilever is $m_c = whl\rho$. Then, the new resonant frequency becomes:

$$f_r' = \frac{1}{2\pi}\sqrt{\frac{Ywh^3}{4l'^3\left(m + 0.24m_c'\right)}} = \frac{1}{2\pi}\sqrt{\frac{Ywh^3}{4(l+\Delta)^3\{m + 0.24[wh(l+\Delta)]\rho\}}} \tag{3.18}$$

And the ratio of the tuned frequency to the original frequency called the normalised resonant frequency is:

$$\frac{f_r'}{f_r} = \sqrt{\frac{l^3(m+0.24m_c)}{l'^3(m+0.24m_c')}} = \sqrt{\frac{l^3(m+0.24whl\rho)}{(l+\Delta)^3\{m+0.24[wh(l+\Delta)]\rho\}}} \tag{3.19}$$

Figure 3.3 shows the normalized resonant frequency with the variation of cantilever length where a negative Δ/l means the new cantilever beam is shorter than its original length and thus has a higher resonant frequency. A positive Δ/l means the cantilever beam has been lengthened giving a lower resonant frequency. Figure 3.3 shows it is more effective to tune the resonant frequency by shortening the cantilever beam.

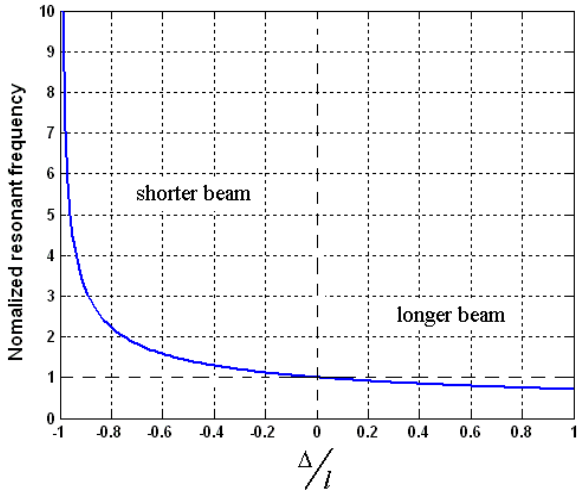

Figure 3.3. Normalized resonant frequency with variation of cantilever lengths.

An example of this approach is described in a patent by Gieras et al [55]. Figure 3.4 shows the side view of the proposed device. The electromagnetic generator consists of a cantilever with a set of magnets fixed to its free end. The cantilever is clamped to a base using screws. A coil is placed between the magnets to pick up output power. A slider is connected to a linear actuator which moves the slider back and forth to adjust the effective length of the cantilever, L and hence the resonant frequency of the generator.

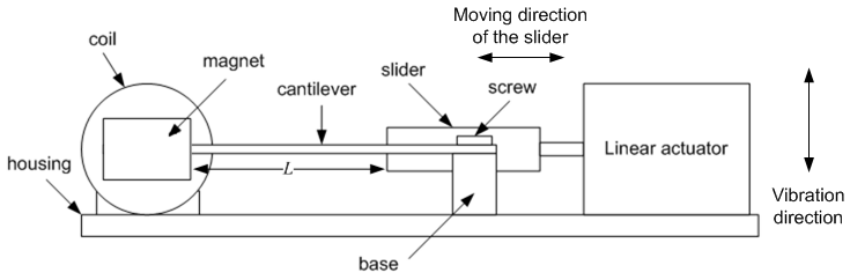

Figure 3.4. Side view of a proposed self-adjustable energy harvesting system.

3.3.2 Moving Centre of Gravity of Proof Mass

It is difficult to add or remove mass after a generator has been fabricated. However, the resonant frequency of a cantilever structure can be adjusted by moving the centre of gravity of the inertial mass. Figure 3.5 shows the side view of a cantilever with a mass on the free end.

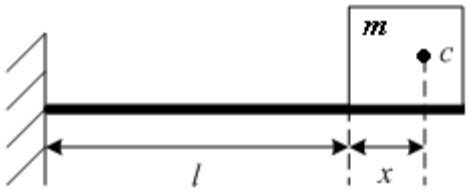

Figure 3.5. Side view of a cantilever structure.

The length of the cantilever without the mass is l and the proof mass on its free end is m. The centre of gravity of the proof mass is located at c and the distance between c and the end of the cantilever is x. The tuned resonant frequency of this structure can be approximated as [56]:

$$f_r' = \frac{1}{2\pi}\sqrt{\frac{Ywh^3}{12ml^3}\cdot\frac{r^2+6r+2}{8r^4+14r^3+\frac{21}{2}r^2+4r+\frac{2}{3}}} \tag{3.20}$$

where w and h are the width and thickness of the cantilever, respectively and $r = \frac{x}{l}$.

The resonant frequency of such a generator, considering that the mass of the cantilever beam is negligible compared to the proof mass, Equation (3.17) can be

rewritten as:

$$f_r = \frac{1}{2\pi}\sqrt{\frac{Ywh^3}{4l^3 m}} \tag{3.21}$$

Hence, the ratio of the tuned frequency to the original frequency is

$$\frac{f_r'}{f_r} = \sqrt{\frac{1}{3}\cdot\frac{r^2+6r+2}{8r^4+14r^3+\frac{21}{2}r^2+4r+\frac{2}{3}}} \tag{3.22}$$

Figure 3.6 shows the normalized resonant frequency with variation of the position of the centre of gravity of the proof mass. The further the centre of gravity of the proof mass is from the end of the cantilever, the lower the resonant frequency.

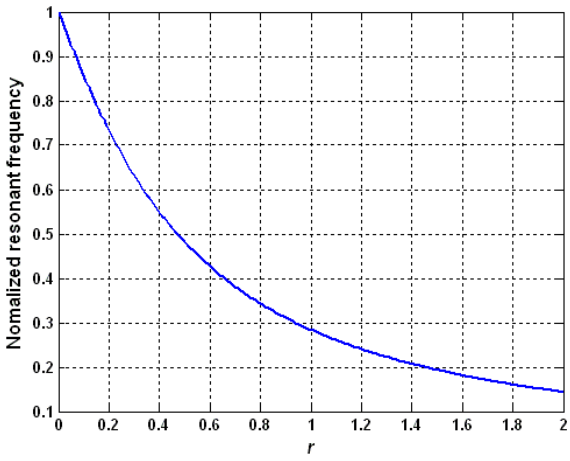

Figure 3.6. Normalized resonant frequency with variation of centre of gravity positions.

Wu et al [57] reported a piezoelectric generator using this principle as shown in Figure 3.7. The proof mass of this device consisted of two parts: a fixed mass was attached to the cantilever and the other part was a movable screw. The position of the centre of gravity of the proof mass could be adjusted by changing the position of the movable screw. A fastening stud was used to fix the screw when tuning was finished. The size of the fixed mass is 10mm × 12mm × 38mm and the movable mass is an M6

screw of length of 30mm. The resonant frequency of the device was tuned from 180Hz to 130Hz by moving the screw from one end to the other end (Figure 3.8). The output voltage dropped with increasing resonant frequency.

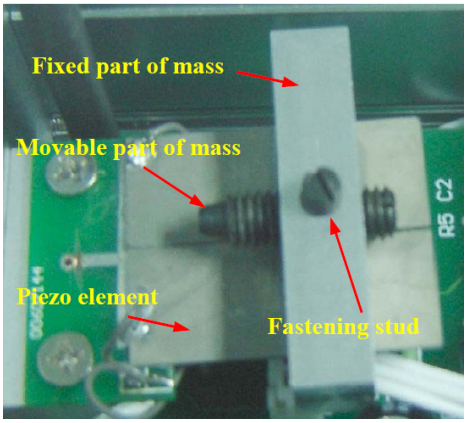

Figure 3.7. Picture of the piezoelectric cantilever prototype with movable mass [56].

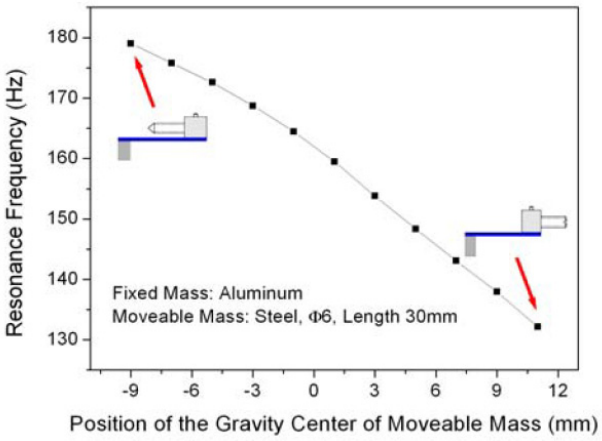

Figure 3.8. Experimental result of frequency adjustment [57].

This approach is suitable for fine frequency tuning of the generator before installation if the vibration frequency in the working environment is not time-varying.

3.3.3 Variable Spring Stiffness

One commonly used method is to soften the spring stiffness. The principle is to apply a 'negative' spring in parallel to the mechanical spring. Therefore, the effective spring constant of such device, k_{eff}, becomes:

$$k_{eff} = k_m + k_a \tag{3.23}$$

where k_m is the mechanical spring constant and k_a is an additional 'negative' spring stiffness (Figure 3.9). The modified frequency becomes:

$$f_r = \frac{1}{2\pi}\sqrt{\frac{k_{eff}}{m}} = \frac{1}{2\pi}\sqrt{\frac{k_m + k_a}{m}} \tag{3.24}$$

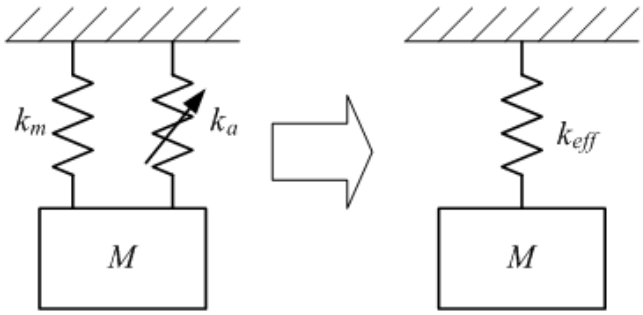

Figure 3.9. Model of devices with softened spring stiffness.

The negative spring k_a can be applied electrostatically, piezoelectrically, magnetically or thermally. Examples of these approaches are described below. Most of these examples are tunable resonators and not energy harvesters but the principles are identical. It is important to note, however, that the additional inertial mass present in an energy harvester (as opposed to the purely resonant structures) will reduce the tuning effectiveness and increase the power required to tune compared to the values quoted. It should also be noted that the following variable spring stiffness devices are all continuously operated except the one on which the negative spring is applied magnetically.

3.3.3.1 Electrostatic

Scheibner [58,59] reported a vibration detector consisting of an array of eight comb resonators each with a different base resonant frequency. A single resonator is shown in Figure 3.10. Each resonator comb is tuned by electrostatically softening the structure by applying a tuning voltage to the electrodes marked 'V_{Tun}'. The device was designed so that the resonator array had overlapping tuning ranges which allowed continuous measurements in the frequency range of the device from 1kHz to 10kHz. Figure 3.11 shows the tuning range of each resonator. The tuning voltage varied from 0V to 35V. The total size of the sensor chip is 7mm × 10mm.

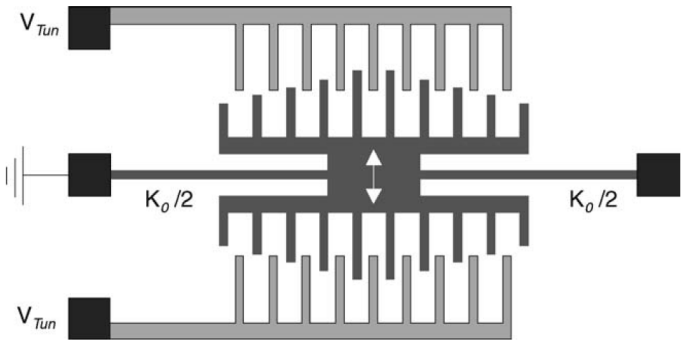

Figure 3.10. Resonance tuning by electrostatic-softening [59].

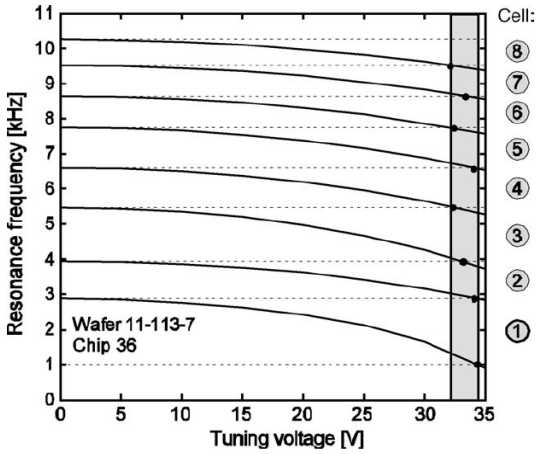

Figure 3.11. Resonance tuning of the array [59].

Adam [60] realized a tuning range from 7.7% to 146% of the central frequency of 25kHz of a resonator with a single comb structure (Figure 3.12). The driving voltage ranged from 0V to 50V (Figure 3.13). The total size was not mentioned in the paper but is estimated from the SEM scale to be no larger than 500μm × 500μm.

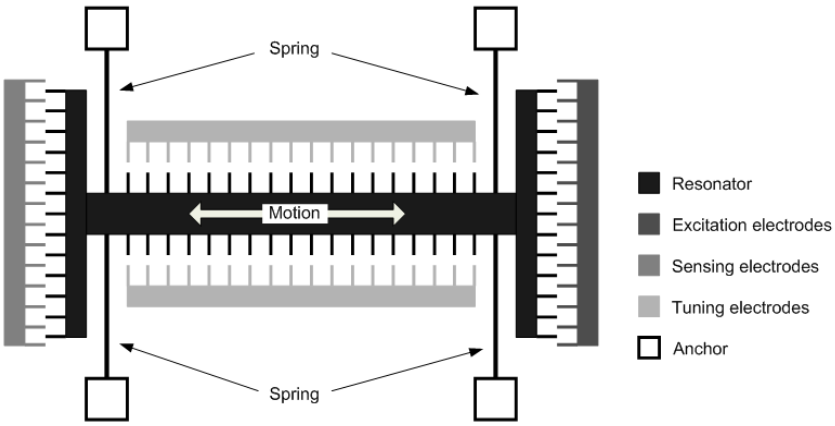

Figure 3.12. Schematic diagram of a single comb structure (after [60]).

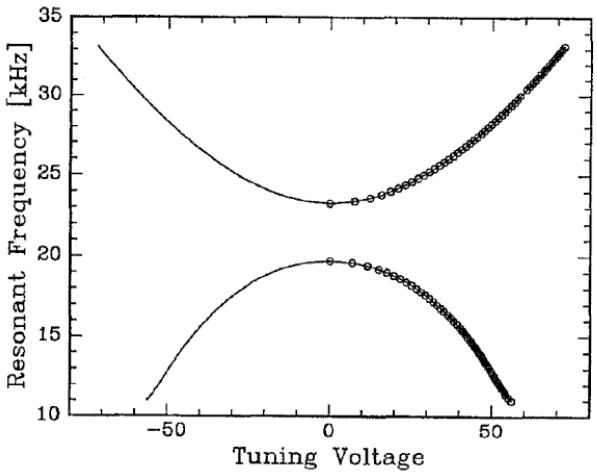

Figure 3.13. Resonance tuning of a single comb structure [60].

Lee et al [61] presented a frequency tunable comb resonator with curved comb fingers (Figure 3.14). Fingers of the tuning comb were designed to be curved shape to generate a constant electrostatic stiffness or linear electrostatic force that is independent of the displacement of the resonator under a control voltage. Experimentally, the resonant frequency of a laterally driven comb resonator with 186 pairs of curved contour fingers was reduced by 55% from the initial frequency of 19 kHz under a bias voltage of 150V (Figure 3.15). The corresponding effective stiffness was decreased by 80% from the initial value of 2.64N/m. The total size of the resonator is 460μm × 840μm. It was concluded that the closed-form approach of the comb-finger profile can be applied to other comb shaped actuators for frequency control whilst achieving linear electrostatic stiffness with respect to displacement.

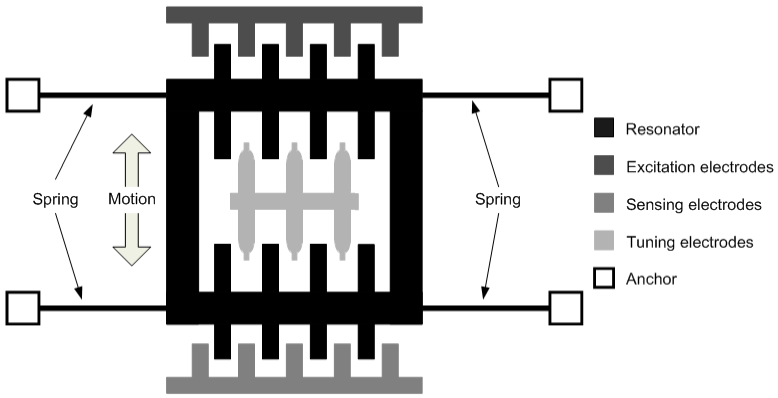

Figure 3.14. Schematic diagram of a comb resonator with curved tuning fingers (after [61]).

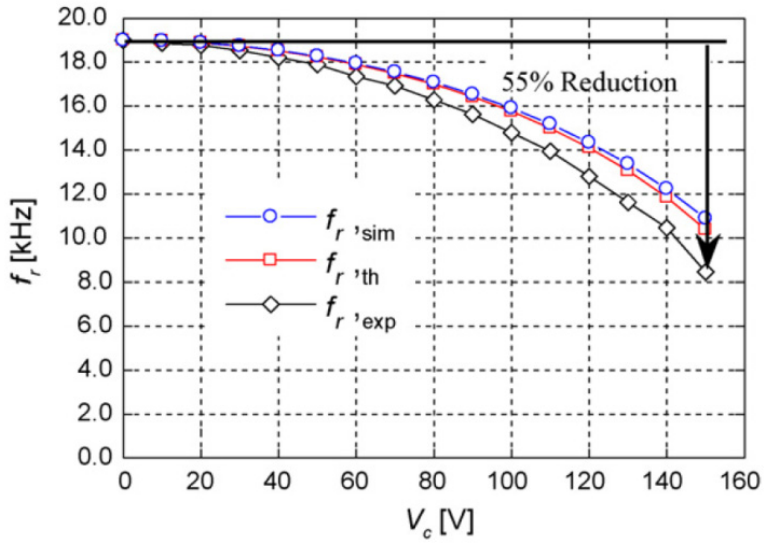

Figure 3.15. Resonance tuning of a comb resonator with curved tuning fingers [61].

Piazza et al [62] developed a micromachined, piezoelectrically actuated and sensed, high-Q single-crystal silicon (SCS) resonator with voltage-tunable centre frequency (Figure 3.16). Piezoelectric transduction was integrated with capacitive fine-tuning of the resonator centre frequency to compensate for any process variations. The resonant frequency could be tuned by 6kHz based on an untuned resonant frequency of 719kHz by applying an electrostatic force beneath the cantilever (Figure 3.17). The driving voltage varied from 0 to 20V. The dimensions of this resonator are 200μm × 20μm × 4.2μm.

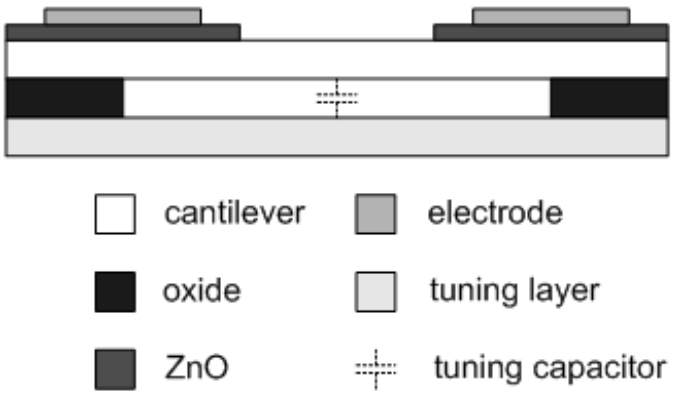

Figure 3.16. Voltage-tunable, piezoelectrically-transduced SCS resonators: Q-enhanced configuration (after [62]).

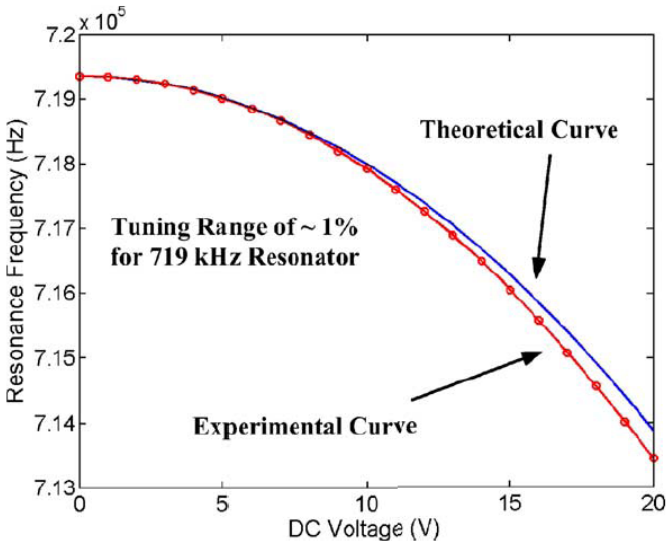

Figure 3.17. Electrostatic fine-tuning characteristic for a 719kHz piezo-resonator [62].

Yao et al [63] compared frequency tuning by applying either axial force (discussed further in Section 3.4) or transverse force on the resonator electrostatically as shown in Figure 3.18. Frequency tuning by applying transverse force was tested experimentally. It was found that the resonant frequency may increase or decrease with the applied tuning voltage depending on where the tuning electrode is placed with respect to the excitation electrode and the resonating rod. When the tuning electrode was placed on the same side of the excitation electrode as indicated in Figure 3.18(b), the resonant frequency decreased with the increase of applied voltage. When the tuning electrode was placed on the opposite side of the excitation electrode as indicated in Figure 3.18(c), the resonant frequency increased with the increase of applied voltage.

A micromachined resonator having an out-of-plane natural resonant frequency of 0.96MHz and a Q-factor of 4370 had a linear tuning range (with respect to the transverse tuning force) of 60kHz with a maximum required DC tuning voltage of 35V (Figure 3.19). Another resonator with untuned resonant frequency of 149.5kHz was tuned to 139.5kHz by applying a DC tuning voltage of 30V (Figure 3.20). The actual dimensions of these devices were not mentioned. The idea was later patented by Thiesen and O'Brian in 2006 [64].

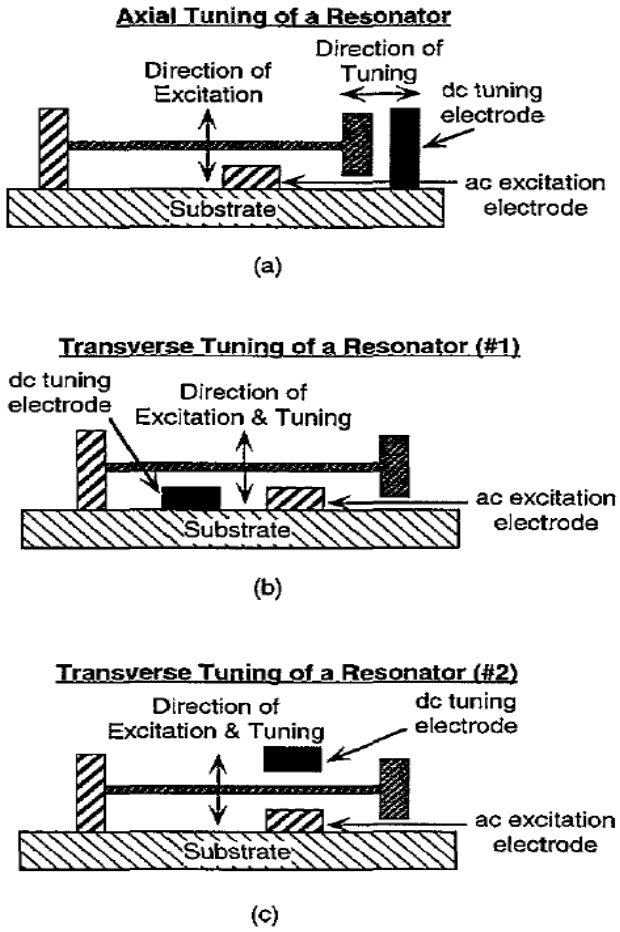

Figure 3.18. Schematic drawing of a simple resonator showing axial loading (a), and transverse loading with the excitation and the tuning electrode on the same side (b) and on the opposite side (c) of the resonating rod. [63]

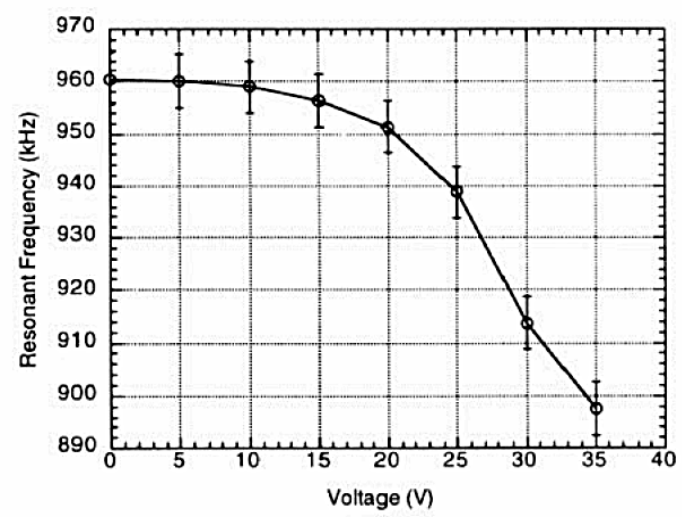

Figure 3.19. Measured resonant frequency vs. the tuning dc voltage with an untuned resonant frequency of 0.96MHz (tuning mechanism as in Figure 3.18b) [63].

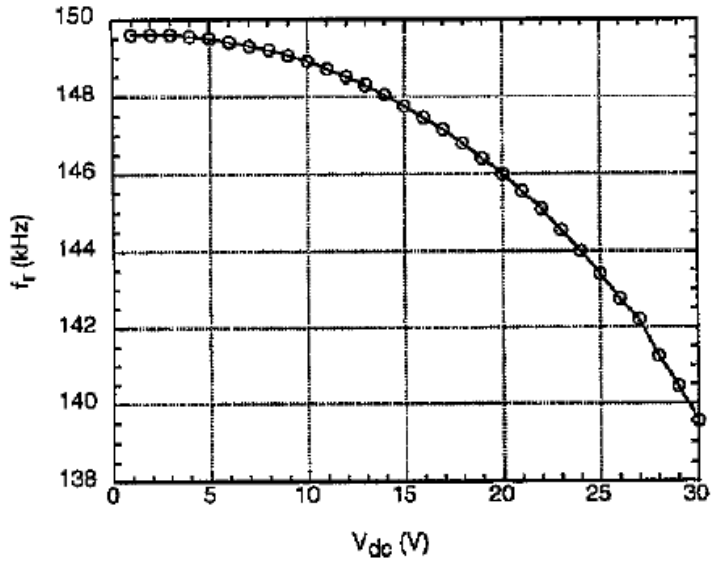

Figure 3.20. Measured resonant frequency vs. the tuning dc voltage with an untuned resonant frequency of 1495.5kHz (tuning mechanism as in Figure 3.18b) [63].

3.3.3.2 Piezoelectric

Peters et al [65] reported a tunable resonator, shown in Figure 3.21a, potentially suitable as a resonator structure for vibration energy harvesting. The adjustment of the resonant frequency was provided by mechanical stiffening of the structure using piezoelectric actuators. A piezoelectric actuator was used because piezoelectric materials can generate large forces with low power consumption. Two actuators, one clamped and one free, are connected together. The free actuator can oscillate around the axis of rotation if a suitable excitation is applied to the clamp. The stiffness of the structure was increased by applying an electrical potential to both actuators which changes the shape of the structure as shown in Figure 3.21c. Thus, the natural frequency of the rotational mass-spring system increased. The tuning voltage was chosen to be ±5V leading to a measured resonance shift of ±15% around the initial resonant frequency of 78Hz, i.e. the tuning range was from 66Hz to 89Hz (Figure 3.22).

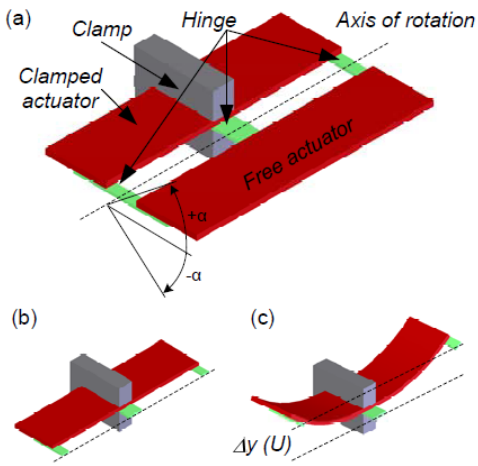

Figure 3.21. (a) Schematic of the resonator (b) cross-Section without applied voltage and (c) with applied voltage [65].

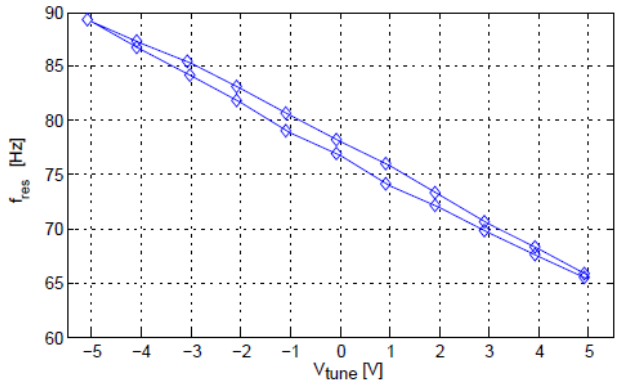

Figure 3.22. Measured resonant frequency vs. applied tuning voltage [65].

3.3.3.3 Magnetic

Challa et al [66] reported an intermittently tuned piezoelectric micro-generator, 50cm^3 in volume, with a frequency range of 22 to 32Hz based on an original resonant frequency of 26Hz. The tuning was realized by manually applying a magnetic force perpendicularly to the cantilever generator as shown in Figure 3.23. By varying the distance between the two sets of tuning magnets on the beam and the stationary magnets, the resonant frequency of the generator can be altered. The maximum tuning distance was 3cm. The proposed generator produced 240 to 280μW power at 0.8m·s^{-2} acceleration but the tuning mechanism had the unwanted side effect of varying damping over the frequency range as shown in Figure 3.24. The device was made of discrete components. The dimension of the piezoelectric cantilever is 34mm × 20mm × 0.92mm and the effective mass is 45.8g.

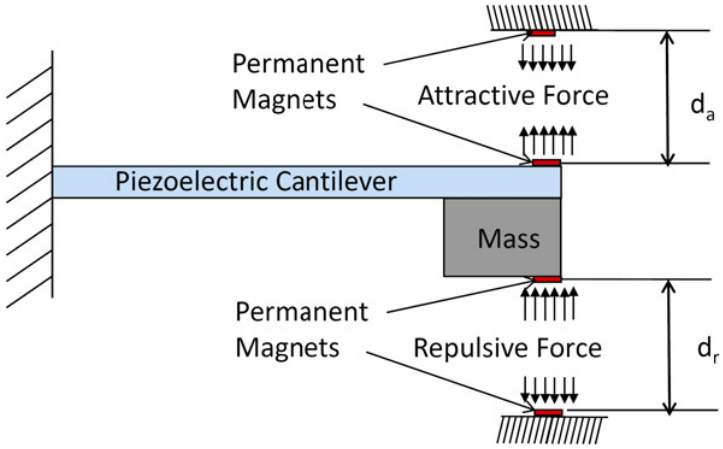

Figure 3.23. Schematic of a tunable piezoelectric generator [66].

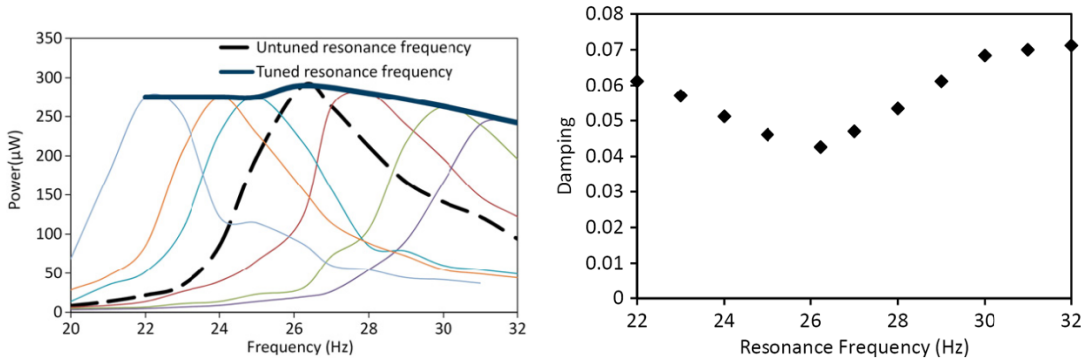

(a) (b)

Figure 3.24. Output power (a) and damping (b) vs. resonant frequency [66].

3.3.3.4 Thermal

Remtema and Lin [67] used a resistive heater to generate a thermal stress on a straight-beam spring (Figure 3.25), which caused up to 6.5% frequency change based on a resonant frequency of 31kHz with a maximum temperature at 255°C. The power consumption during the process was 25mW. Figure 3.26 shows the percentage change of resonant frequency with variation of power consumed in tuning. The size of the device is estimated to be less than 500μm × 700μm from the author's description. The thermal approach is unlikely to be practical for energy harvesting since it is inherently high power and is a continuous tuning mechanism.

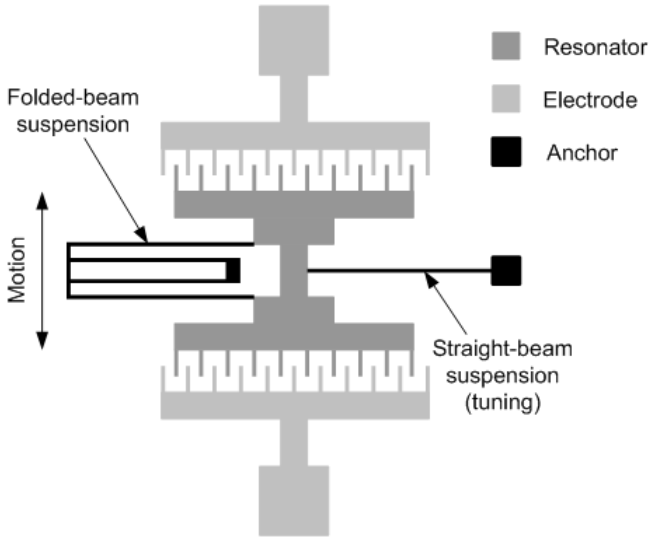

Figure 3.25. Schematic diagram of a comb-shape micro resonator with a straight-beam for active frequency tuning via localized stressing effects (after [67]).

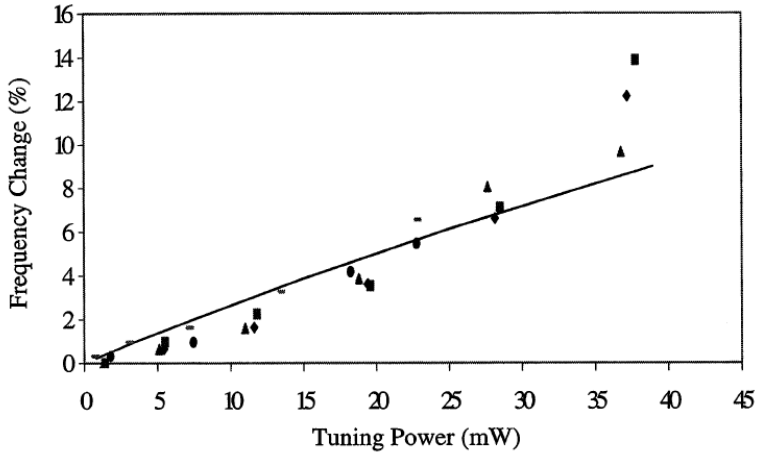

Figure 3.26. Measured frequency change vs. tuning power [67].

Syms et al [68] reported frequency tuning by applying constrained thermal expansion on a simple unfolded resonator (Figure 3.27). The tuning range was from -25% to +50% with power consumption from 1.5 to 10mW (Figure 3.28). The tuning sensitivity obtained with this tuning method was 33% per mW. It is estimated from the annotation in Figure 3.27 that the device is no larger than 3000μm × 3000μm.

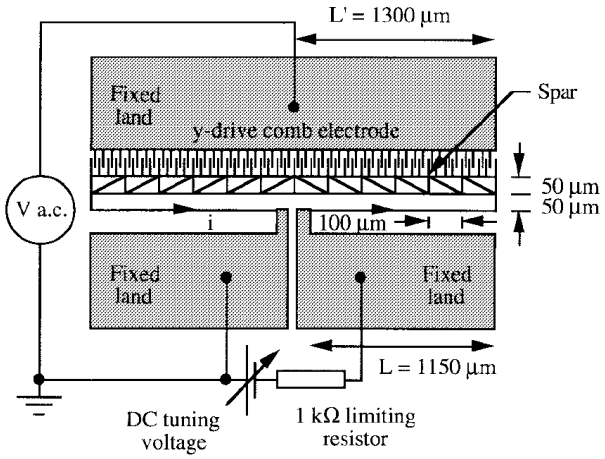

Figure 3.27. Layout and connection of laterally resonant comb-drive actuator used for tuning experiments [68].

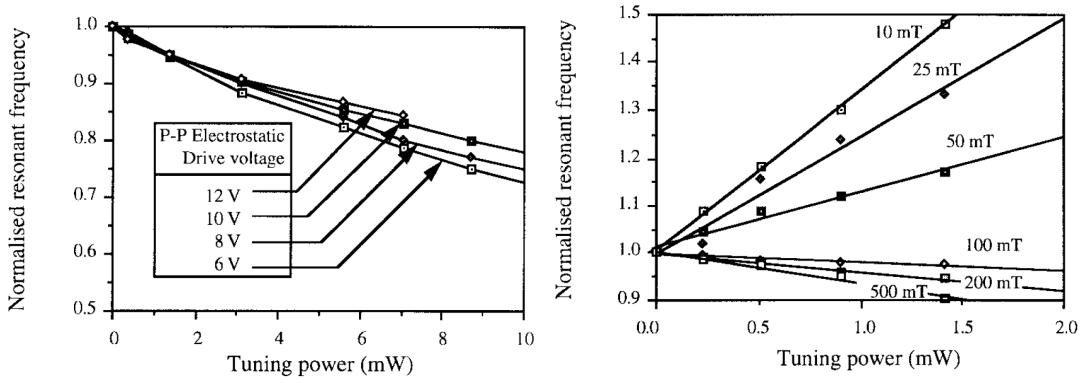

(a) (b)

Figure 3.28. Variation of resonant frequencies with tuning power (a) at different electrostatic drive voltage (b) gas pressure [68].

3.3.4 Straining the Structure

The effective stiffness of the structure can be varied by applying a stress and therefore placing it under strain. The following theoretical analyses focus on straining a cantilever and a clamped-clamped beam. The resonant frequency of a cantilever structure can be tuned by applying an axial load. In vibration energy harvesting, most devices are based on cantilever structures especially the clamped-free (Figure 3.29) and clamped-clamped (Figure 3.30) cantilever. An axial tensile load applied to a cantilever (Figure 3.29a, 3.30a) increases the resonant frequency of the cantilever while an axial compressive load applied to a cantilever (Figure 3.29b, 3.30b) decreases the resonant frequency of the cantilever.

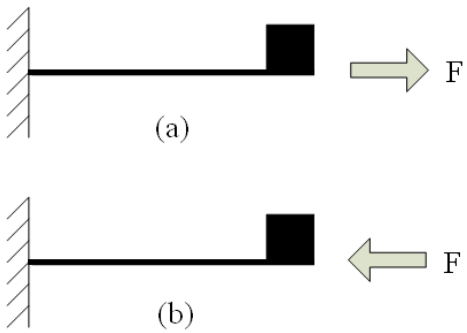

Figure 3.29. Axial tensile (a) and compressive (b) load on a clamped-free cantilever.

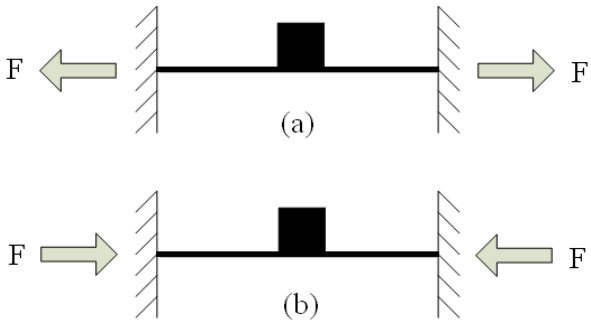

Figure 3.30. Axial tensile (a) and compressive (b) load on a clamped-clamped beam.

An approximate formula for the resonant frequency of a uniform cantilever in mode i with an axial load, f_{ri}', is given by [69]:

$$f_{ri}' = f_{ri} \cdot \sqrt{1 + \frac{F}{F_b} \cdot \frac{\lambda_1^2}{\lambda_i^2}} \tag{3.25}$$

where f_{ri} is the resonant frequency in mode i without load, F is the axial load and F_b is the axial load required to buckle the beam, i.e. to make the fundamental resonant frequency zero. F is positive for a tensile load and negative in the compressive case. Variable λ_i is a dimensionless load parameter which is a function of the beam boundary conditions applied to the cantilever for the i^{th} mode of the beam. It is given by the i^{th} positive solution of Equation (3.26) for a cantilever and of Equation (3.27) for a clamped-clamped beam [70].

$$\cos\lambda \cdot \cosh\lambda + 1 = 0 \tag{3.26}$$

$$\cos\lambda \cdot \cosh\lambda - 1 = 0 \tag{3.27}$$

The majority of cantilever based micro-generators operate in the fundamental flexural mode (mode 1); the resonant frequency of a uniform cantilever in mode 1 with an axial load, f_{r1}', is given by:

$$f_{r1}' = f_{r1} \cdot \sqrt{1 + \frac{F}{F_b}} \tag{3.28}$$

The ratio of the tuned frequency to the original frequency is:

$$\frac{f_r'}{f_r} = \sqrt{1 + \frac{F}{F_b}} \tag{3.29}$$

The buckling load F_b of a cantilever and a clamped-clamped beam are given by Equations (3.30) and (3.31), respectively [71]:

$$F_b = \frac{\pi^2 \cdot E \cdot w \cdot h^3}{48 \cdot l^2} \tag{3.30}$$

$$F_b = \frac{\pi^2 \cdot E \cdot w \cdot h^3}{3 \cdot l^2} \tag{3.31}$$

where E is the Young's modulus of the material of the cantilever and w, h and l are the width, thickness and length of the cantilever, respectively.

Figure 3.31 shows the change in resonant frequency of a cantilever with axial load. It shows that a compressive load is more efficient in frequency tuning than a tensile load. If the compressive force is larger than the buckling load, the cantilever beam will buckle and no longer oscillate in mode 1. If a very large tensile force is axially applied to the cantilever, i.e. much greater than the buckling load, the resonant frequency will approach that of a straight tensioned cable as the force associated with the tension in the cantilever becomes much greater than the beam stiffness.

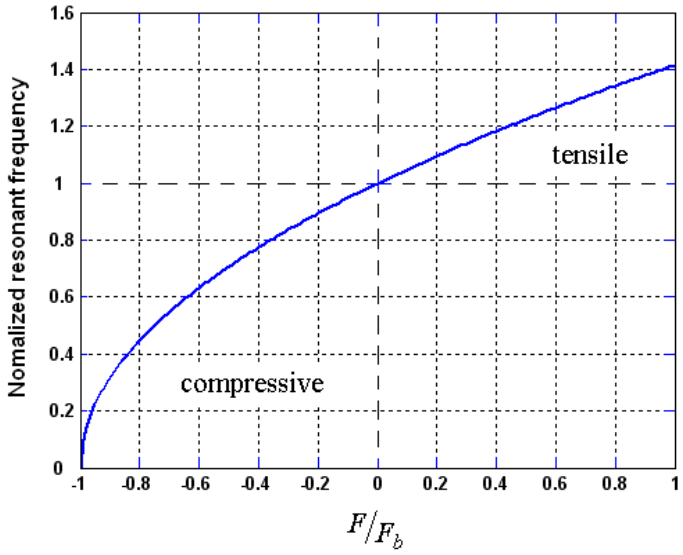

Figure 3.31. Normalized resonant frequency with variation of axial loads.

The following Sections give examples of clamped-clamped beam and cantilever beam structures.

3.3.4.1 Clamped-clamped Beam Structures

Cabuz *et al* [72] realized resonant frequency tuning by an applying an axial force on a micromachined resonant beam electrostatically as shown in Figure 3.32. One end of the resonator was clamped on a fixed support while the other end was connected to a movable support. The moveable support could rotate around a torsion bar as a voltage was applied across two tuning electrodes. The torsion bar converted the vertical tuning motion into an axial force along the resonator. Upward rotation induces a compressive stress in the resonator while downward rotation induces a tensile stress. The tuning range was 16Hz based on a centre frequency of 518Hz (Figure 3.33) with driving voltage from 0 to 16V. The dimensions of the resonator are 1000μm × 200μm × 3μm and the dimensions of the movable support are 12.5mm^2 × 0.3mm. This is an example of continuous tuning.

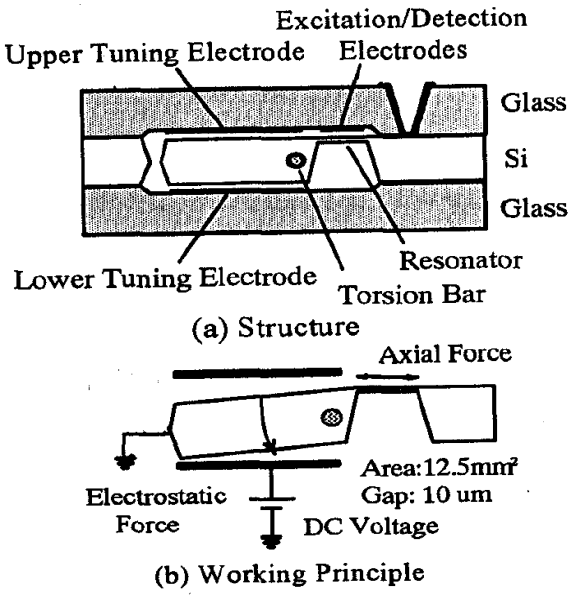

Figure 3.32. Structure for fine resonance frequency tuning at device level by an electrostatically induced axial force [72]

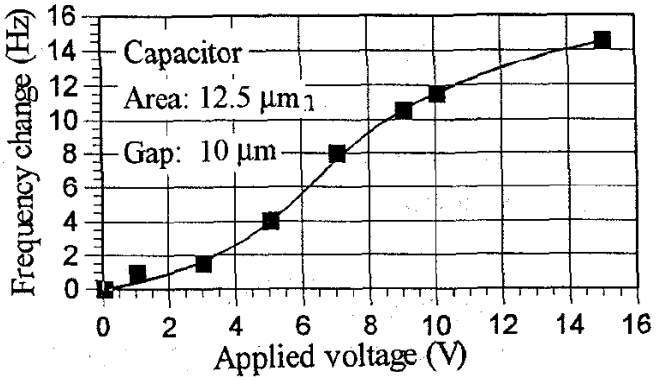

Figure 3.33. Resonant frequency change vs. applied voltage [72].

Leland and Wright [73] successfully tuned the resonant frequency of a vibration-based piezoelectric generator by manually applying an axial compressive preload directly on the cantilever using a micrometer (Figures 3.34 and 3.35). The tuning range was from 200 to 250Hz. This device generated 300 to 400μW of power at an acceleration of $9.8 m \cdot s^{-2}$. It was determined that a compressive axial preload could reduce the resonance frequency of a vibration energy scavenger by up to 24% but it also increased the total damping (Figure 3.36). The piezoelectric bimorph has dimensions of 31.7mm × 12.7mm × 0.509mm and the weight of the proof mass is 7.1g. This is an example of intermittent tuning, but it is not automated and has to be done manually.

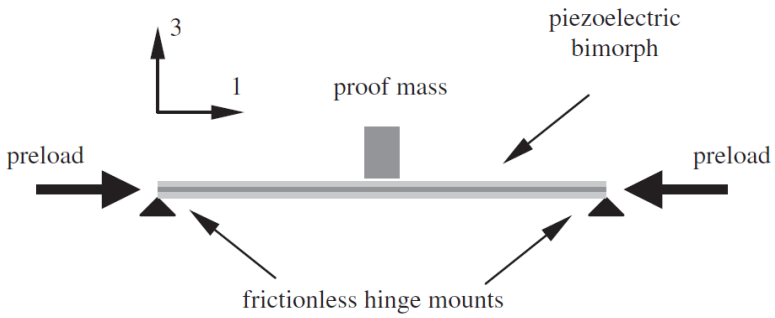

Figure 3.34. Schematic of a simply supported piezoelectric bimorph vibration energy scavenger [73].

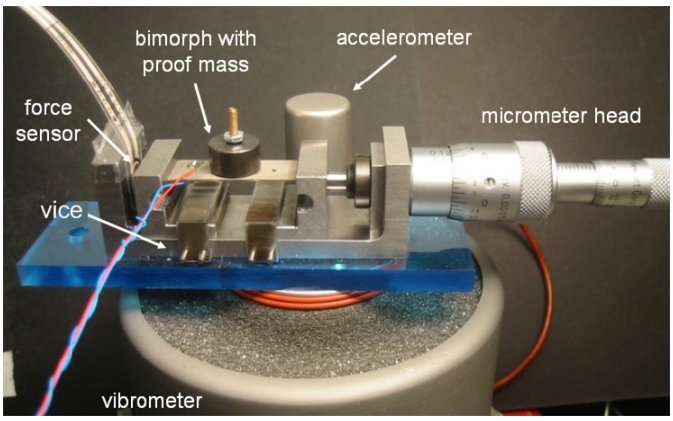

Figure 3.35. Experimental apparatus [73].

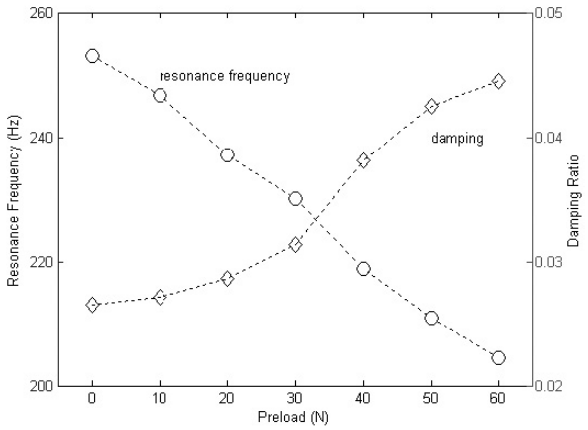

Figure 3.36. Resonance frequency and damping vs. preload [73].

3.3.4.2 Cantilever Structures

Mukherjee [74] patented the idea of applying axial force to a vibrating cantilever beam sensing element using electrostatic force. The resonator consisted of two sets of comb-like structures (Figure 3.37). The set closer to the anchor was used for sensing

while the other set was used for frequency tuning. The two tuning electrodes provided a voltage across the structure at the free end and the two electrodes which applied an axial tensile or compressive end load to the cantilever. The resonant frequency of the beam was approximately 15.5kHz. This is an example of continuous tuning which achieved a tuning range of -0.6% to 3.3% of its untuned resonant frequency, i.e. about 600Hz. The cantilever buckled when $50V_{DC}$ was applied to provide a compressive force. This is an example of continuous tuning.

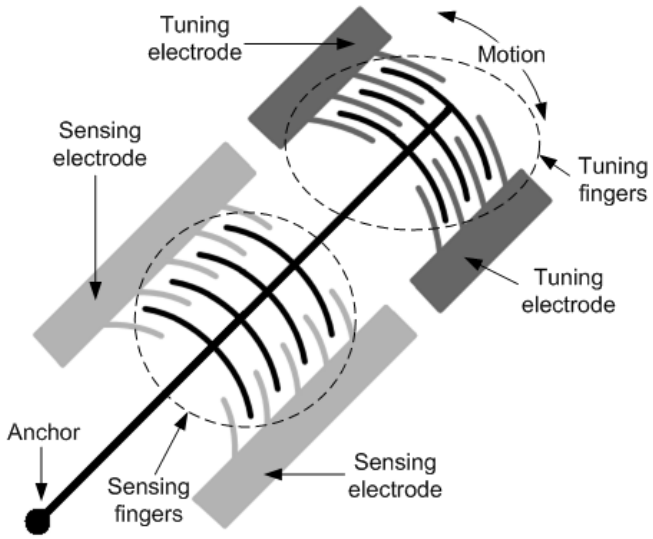

Figure 3.37. Resonator with actuator at the free end (after [74]).

Hu et al [75] theoretically investigated an axial preloading technique to adjust the behaviour of a piezoelectric bimorph. Computational results show that resonance occurred when the natural frequency of the bimorph was adjusted to be adjacent to the external driving frequency by preloading. The mechanism for an axial preload to improve the bimorph performance at varying-frequency vibrations was examined in detail. A method for applying an axial preload to a piezoelectric bimorph was suggested and is shown in Figure 3.38. It comprises a mechanical bolt running through the central metal layer and fixed at the left-hand side edge wall. A capped stiff metal plate was attached to the bolt at the free end of the cantilever. A clockwise torsion of the bolt can produce a compressive preload to the bimorph, and conversely, an anticlockwise torsion of the bolt produces a force to pull the capping plate to move towards the right-hand side, which can generate a tensile preload to the bimorph. This is an example of manual intermittent tuning.

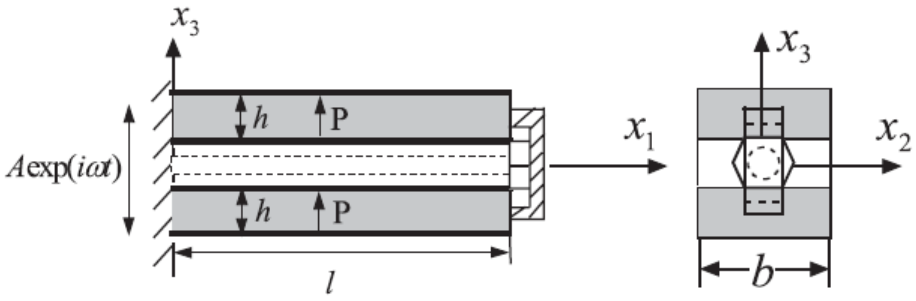

Figure 3.38. A method to apply axial preload to a piezoelectric bimorph [75].

This principle was demonstrated by Eichhorn et al [76]. Figure 3.39 shows a schematic diagram of the test device. The piezoelectric generator consisted of a piezo-polymer-composite cantilever beam with arms on both sides to enable the application of an axial force to the free end of the beam. The arms were connected to the base with two wings. These wings were used to transmit the force to the arms, which in turn apply the load to the free end of the beam. The tuning force was applied by a screw and a steel spring. The axial load depends linearly on the deflection of the spring, which in turn was proportional to the number of revolutions of the screw. The spring pushes the whole generator base against two blocks of which the counter pressure generates the pre-stress in the arms and the stabilizing wings. The screw, spring and generator were all mounted on the same aluminium frame. This is another example of manual intermittent tuning.

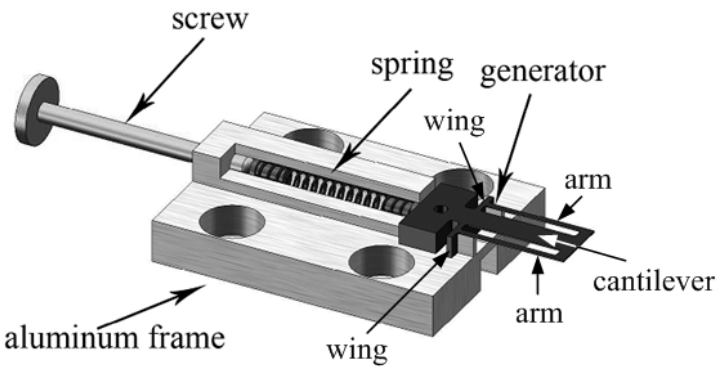

Figure 3.39. Schematic diagram of the test device [76].

In tests only a compressive load was applied. Figure 3.40 shows the test results of this generator under vibration level of 63.7m·s^{-2}. It was found that with the increase of compressive load, the resonant frequency, output voltage and the Q-factor reduced.

By cutting notches on the wings the tuning efficiency was increased. With notches in the wings, a resonant frequency shift of more than 20% was achieved with a total force of 22.75N (Figure 3.41). The tuning range was from 290Hz to 380Hz with compressive load up to 22.75N. The dimensions of the cantilever are 20mm × 5mm × 0.44mm and the overall width of the device including arms is 13mm.

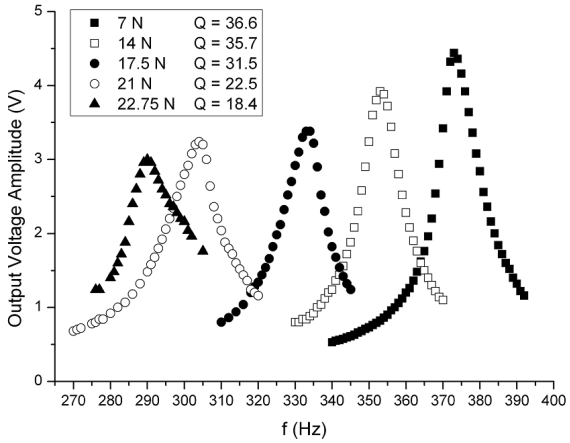

Figure 3.40. Test results under vibration of 63.7 m·s^{-2} [76].

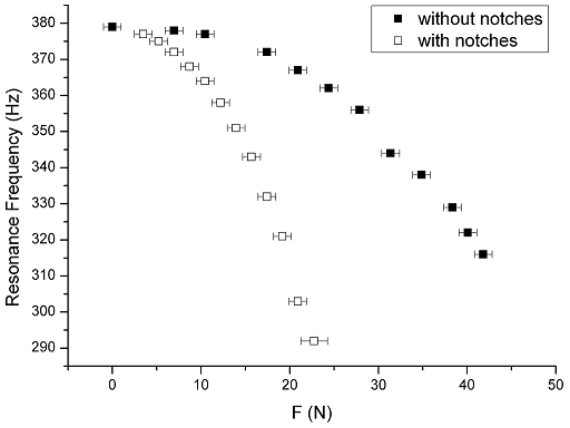

Figure 3.41. Comparison of tuning efficiency of wings with and without notches [76].

Another method of applying axial load to a cantilever based micro-generator is reported by Zhu et al [77] who presented a tunable electromagnetic vibration-based micro-generator with closed loop frequency tuning. Frequency tuning was realized by applying an axial tensile magnetic force to the micro-generator. Details of this method will be presented in this thesis.

3.4 Electrical Tuning Methods

All the frequency tuning methods mentioned above are based on mechanical methods. The following Sections describe methods to tune the resonant frequency of a vibration-based micro-generator electrically.

3.4.1 Principle

The basic principle of electrical tuning is to change the electrical damping by adjusting the load, which causes the power spectrum of the generator to shift. As resistive loads reduce the efficiency of power transfer and load inductances are difficult to be varied, it is most feasible to adjust capacitive loads to realize electrical tuning. Detailed models of electrical tuning for both piezoelectric and electromagnetic micro-generators will be given in Chapter 7.

3.4.2 Examples of Electrically Tunable Micro-generators

Charnegie [78] presented a piezoelectric micro-generator based on a bimorph structure and adjusted its load capacitance. Again, one piezoelectric layer was designed for energy harvesting while the other is used for frequency tuning (Figure 3.42).

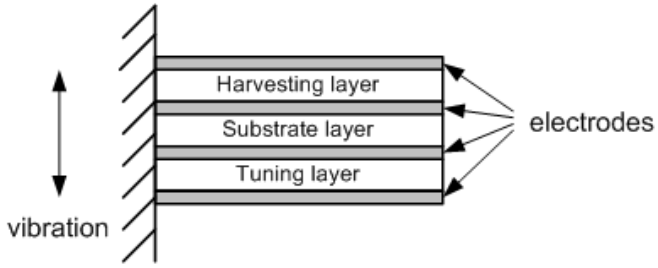

Figure 3.42. Piezoelectric bimorph used for electrical frequency tuning.

The test results showed that if only one layer was used for frequency tuning (Figure 3.43a), the resonant frequency can be tuned an average of 4Hz with respect to the untuned frequency of 350Hz, i.e. 1.14% tuning by adjusting the load capacitance from 0 to 10mF (Figure 3.44a). If both layers were used for frequency tuning (Figure 3.43b), the tuning range was an average of 6.5Hz, i.e. 1.86% of tuning by adjusting the same amount of the load capacitance (Figure 3.45a). It was found that if one layer was used for tuning and the other for energy harvesting (Figure 3.43a), the output

power did not reduce with the increase of the load capacitance (Figure 3.44b). However, if both frequency tuning and energy harvesting were achieved using the same layer (Figure 3.43b), the output power decreased when the load capacitance became larger (Figure 3.45b).

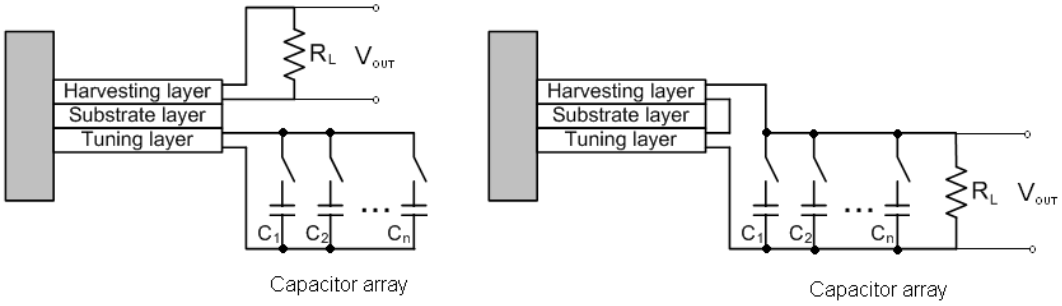

(a) (b)

Figure 3.43. Frequency tuning and energy harvesting using (a) the same layer (b) different layer.

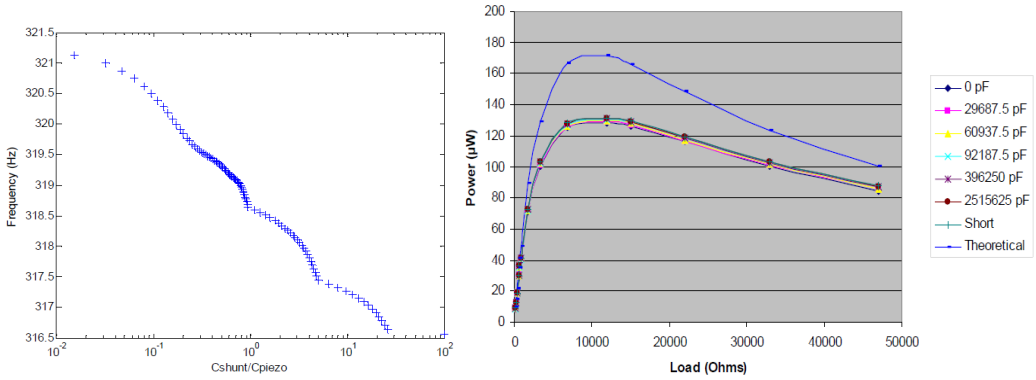

(a) (b)

Figure 3.44. Resonant frequency (a) and output power (b) vs. load capacitance while tuning and energy harvesting in different layers [78].

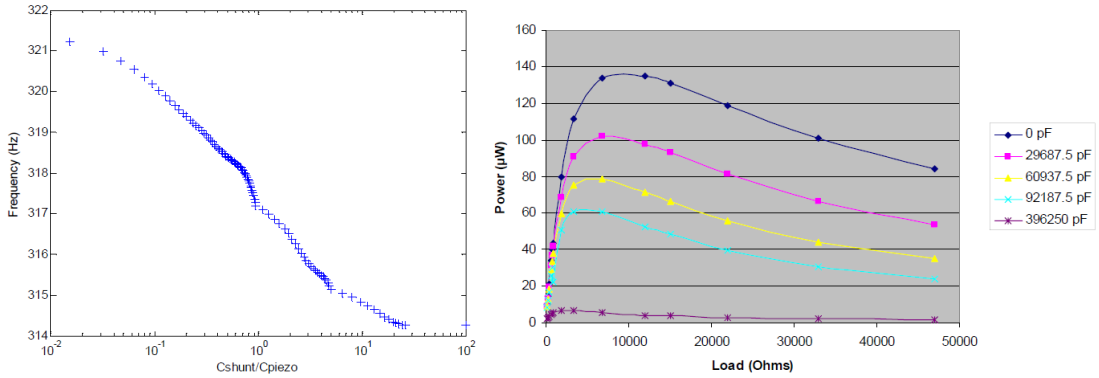

(a) (b)

Figure 3.45. Resonant frequency (a) and output power (b) vs. load capacitance while tuning and energy harvesting in same layers [78].

Wu et al [79] also used this method to tune the resonant frequency of a generator composed of a piezoelectric bimorph cantilever. The upper piezoelectric layer was used for frequency tuning while the lower layer was used for energy harvesting. The tunable bandwidth of this generator was 3Hz between 91.5Hz and 94.5Hz. The charging time of the generator was compared with and without the tuning system. Experimentally, it was found that, when the device was excited under random frequencies from 80Hz to 115Hz, the average harvesting output power of the generator with tuning was about 27.4% higher than that without tuning and the charging time was shortened by using tuning system. These results showed a significant improvement of average harvested power output by using an electrical tuning method.

3.5 Strategies to Widen Bandwidth

The other commonly used solution to increase the operational frequency range of a vibration energy harvesting generator is to widen the bandwidth. To date, strategies to widen the bandwidth include using a generator array consisting of small generators with different resonant frequencies, introducing an amplitude limiter to the device, employing non-linear and bi-stable structures and designing a large generator with a large inertial mass and high degree of damping. In this Section, details of generator array, amplitude limiter and nonlinear and bi-stable structures will be covered. The strategy of employing a single large generator will not be detailed as it can be simply described using Equation (2.10) while it will be considered in the comparison of different strategies later in this chapter.

3.5.1 Generator Array

In this method, the bandwidth is widened by designing a generator consisting of an array of small generators, each of which has different dimensions and mass and hence different resonant frequencies (Figure 3.46). Thus, the assembled generator has a wide operational frequency range whilst the Q-factor does not decrease. Figure 3.47 shows the power spectrum of a generator array which is a combination of the power spectra of each small generator. The frequency band of the generator is thus essentially increased. The drawback of this approach is the added complexity of fabricating an array of generators and the increased total volume of the device depending upon the

number of devices in the array. Furthermore, only one small generator in the array works at a certain frequency, which is not volume efficient.

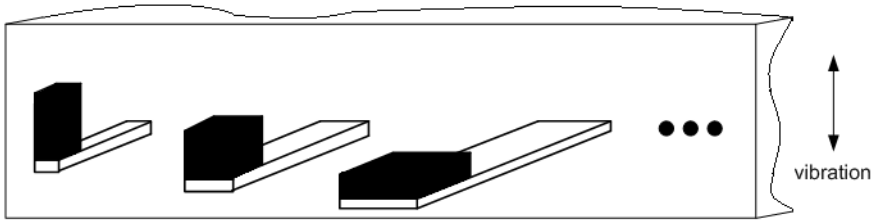

Figure 3.46. A mechanical band-pass filter with a set of cantilever beams.

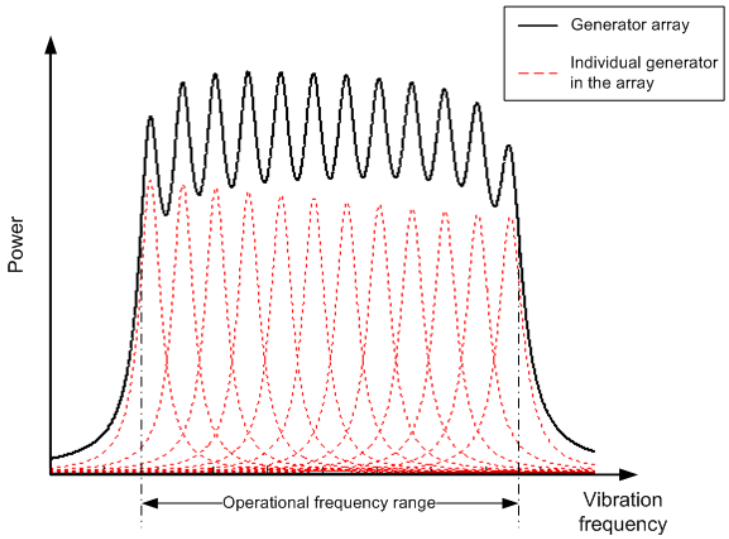

Figure 3.47. Power spectrum of a generator array.

Shahruz [80] developed a device which consisted of a set of cantilever beams with proof masses at their tips. The dimensions of each beam and mass were different and were chosen appropriately to make the whole device work as a band-pass filter. Each beam is an individual generator. Since these beams had different resonant frequencies, the filter could automatically 'select' one beam to resonate at one particular frequency based on the driving vibration frequency. A generator based on such a filter will work at various frequencies, i.e. effectively widening the operational frequency range.

Xue et al [81] presented an approach for designing broadband piezoelectric harvesters by integrating multiple piezoelectric bimorphs with different aspect ratios into a system, primarily with different thicknesses of piezoelectric layers, h. Figure 3.48 shows a schematic diagram of the array.

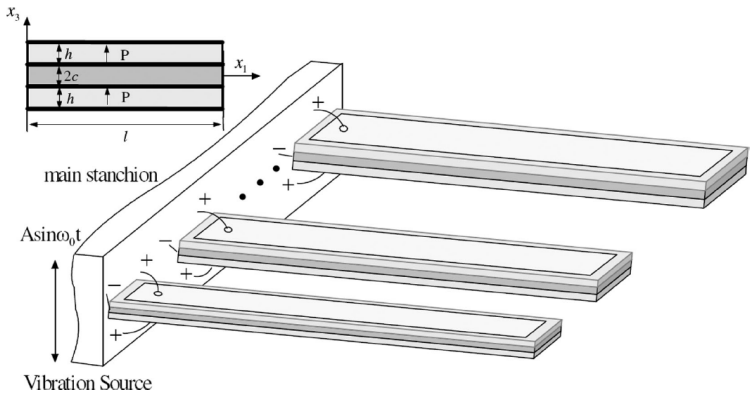

Figure 3.48. Schematic illustration of a piezoelectric bimorphs harvesting system [80].

The effect of connecting piezoelectric bimorphs in series and in parallel on improving energy harvesting performance was discussed. It was found that the bandwidth of a generator can be widened by connecting multiple piezoelectric bimorphs with different aspect ratios in series. In addition, the bandwidth of the generator can be shifted to the dominant frequency domain of the ambient vibrations by increasing or decreasing the number of piezoelectric bimorphs in parallel. Numerical results showed that the bandwidth of the piezoelectric energy harvesting devices can be tailored by the connection patterns (i.e., in series and in parallel) among piezoelectric bimorphs (Figure 3.49 and 3.50).

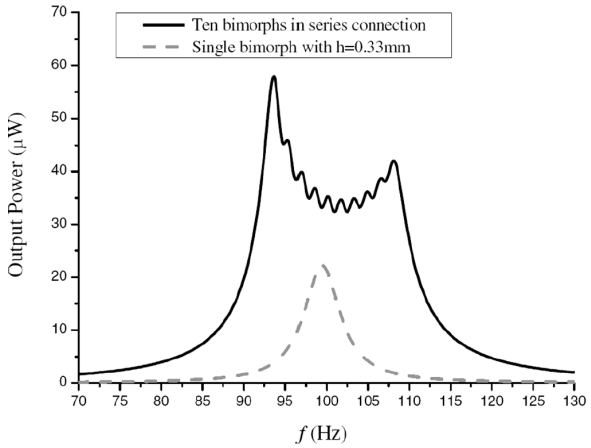

Figure 3.49. Comparison of power spectrum for a single piezoelectric bimorph and ten piezoelectric bimorphs in series with various thicknesses of piezoelectric layer, *h* [81].

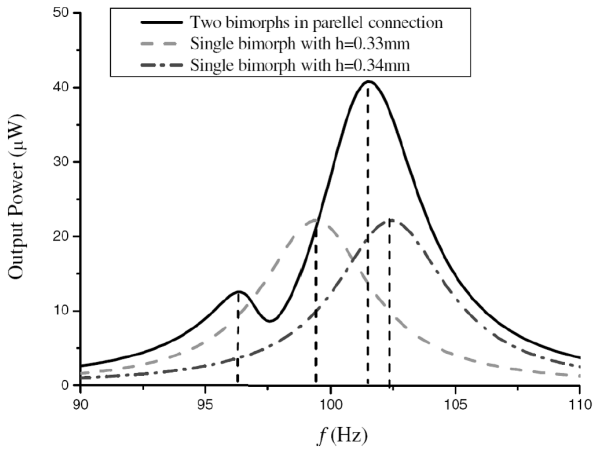

Figure 3.50. Effect of piezoelectric bimorphs in parallel on harvester performance [81].

Feng et al [82] presented a micromachined piezoelectric generator with a wide vibration bandwidth. The device was designed to achieve an optimal Figure of Merit (FOM) which is defined as $(\text{Bandwidth})^2 \times$ (the maximum displacement of cantilever structures under a given acceleration under static conditions). The dimensions of the generator are 3mm × 3mm × 5mm and it consisted of four cantilever structures connected in parallel, which were fabricated to achieve a flexible membrane with minimum residual stress capable of a large displacement. Each cantilever had different mass or centre of gravity and so a different resonant frequency (Figure 3.51). The designed generator was targeted at producing microwatts to milliwatts in a wide mechanical vibration range from 300 to 800Hz (Figure 3.52) but no test results were reported to date.

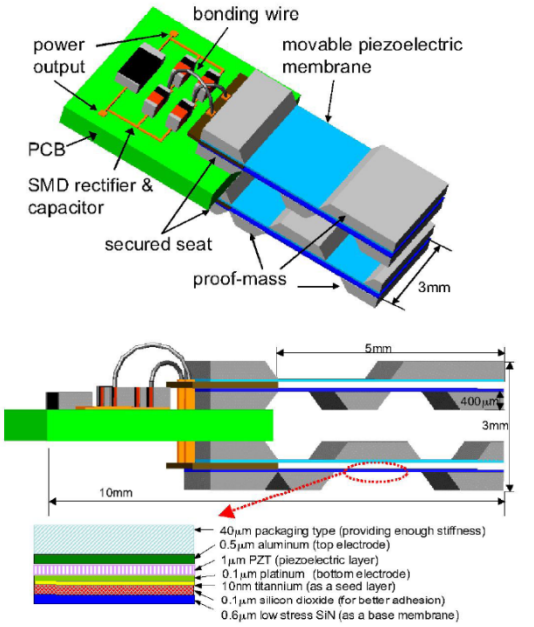

Figure 3.51. Conceptual diagram of the piezoelectric wide-bandwidth microgenerator [82].

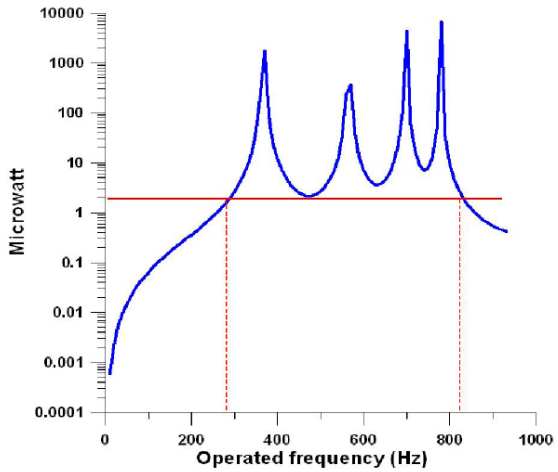

Figure 3.52. Estimated power generation with the power range of μW to mW in a wide bandwidth [82].

A multifrequency piezoelectric generator intended for powering autonomous sensors from background vibrations was presented by Ferrari et al [83]. The generator consisted of multiple bimorph cantilevers with different natural frequencies of which the rectified outputs were fed to a single storage capacitor. A generator with three commercially available piezoelectric bimorph cantilevers was examined. Each cantilever has the same dimensions of 15mm × 1.5mm × 0.6mm and different masses, 1.4g, 0.7g and 0.6g, respectively. The generator was used to power a battery-less

sensor module that intermittently read the signal from a passive sensor and sent the measurement information via RF transmission, forming an autonomous sensor system. It was found that the sensor module could be sufficiently powered, thereby triggering the transmission, even for an excitation frequency that was off resonance for all of the cantilevers. At resonance none of the cantilevers used alone was able to provide enough energy to operate the sensor module. Experimentally, it showed that a generator array operating with wideband frequency vibrations provides improved overall energy conversion over a single generator at the expense of larger volume.

Sari et al [84] reported a micromachined electromagnetic generator with a wide bandwidth. The generator consists of a series of cantilevers with various lengths and hence resonant frequencies (Figure 3.53). These cantilevers are distributed in a 12.5mm × 14mm area. The length of the cantilevers increased gradually so that the cantilevers have overlapping frequency spectra with the peak powers at similar but different frequencies. This resulted in a widened bandwidth as well as an increase in the overall output power.

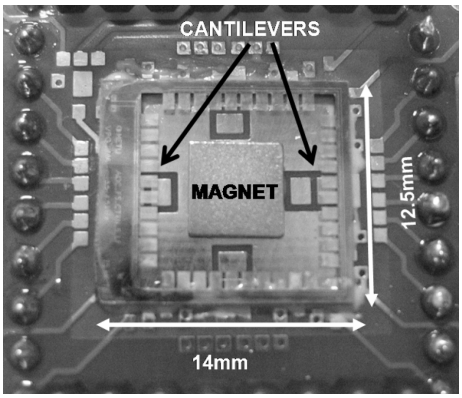

Figure 3.53. Photograph of a wide band electromagnetic generator [84].

The generator used an electromagnetic transducer to transduce power. A large magnet was fixed in the middle of the cantilever array and coils were fabricated by sputtering and patterning metal on top of the cantilevers. The coils moved with ambient vibration relative to the static magnet and the coils were connected in series. Experimentally, the device generated 0.5μW continuous power at 20mV voltage between 3.3 and 3.6kHz of ambient vibration. Figure 3.54 shows the power spectrum of this generator.

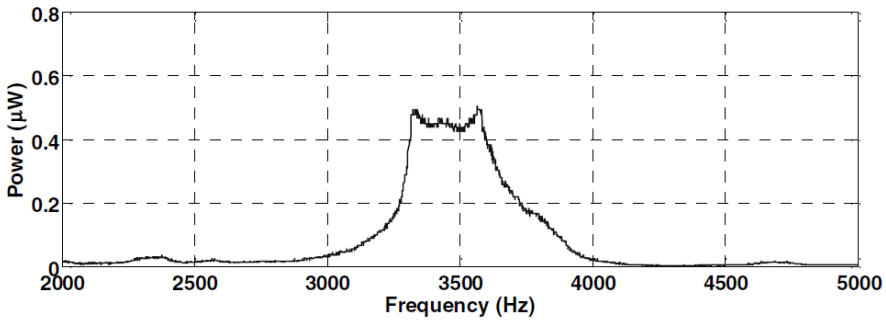

Figure 3.54. Power spectrum of Sari's generator [84].

3.5.2 Amplitude Limiter

Another method of increasing the bandwidth of a vibration-based micro-generator was reported by Soliman et al [85]. The bandwidth of the device was increased by using a mechanical stopper (amplitude limiter) to limit the amplitude of the resonator (Figure 3.55, 3.56). The theory behind this method is complex and details can be found in [85]. It was found that this method increases the bandwidth of the generator during an up-sweep, i.e. when the excitation frequency was gradually increased. The bandwidth remained the same in a down-sweep, i.e. when excitation frequency was gradually reduced. This phenomenon is caused mainly because of the non-linearity of the device, which will be discussed in Section 3.53. Experimental measurements showed that the up-sweep bandwidth was 240% wider than that of the architecture without a stopper at the half-power level but the maximum output voltage was 30% less (Figure 3.57). The dimensions of the cantilever are 45.3mm × 10mm × 1.02mm and the mass is extrapolated to be 2.92g.

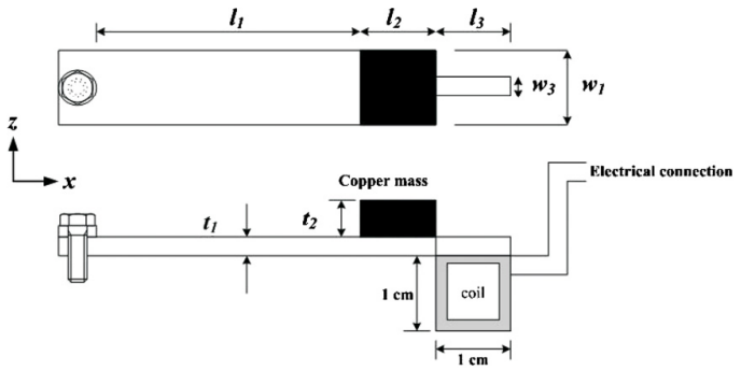

Figure 3.55. Top and side view of the device [85].

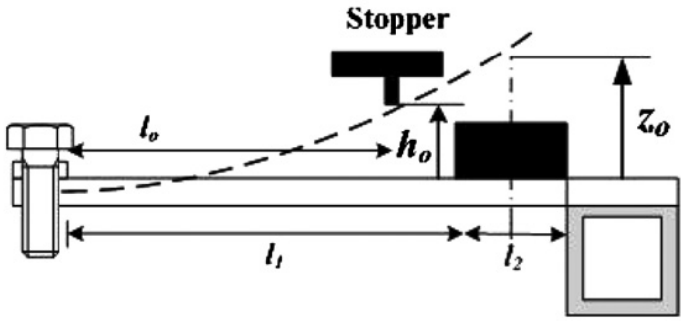

Figure 3.56. Increase the bandwidth using a stopper [85].

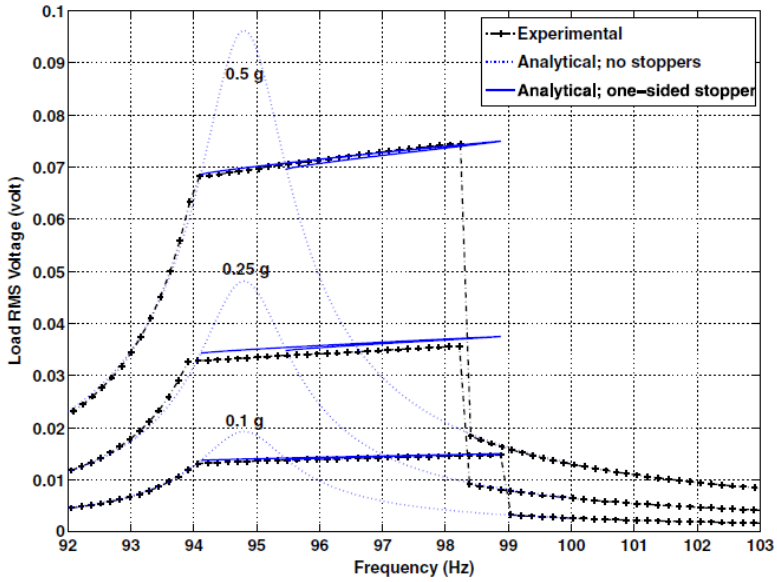

Figure 3.57. Voltage on load vs. excitation frequency [85].

3.5.3 Non-linear Generators

The theory of vibration energy harvesting using non-linear generators was investigated by Ramlan et al [86]. Instead of using conventional second order model as Equation (2.10), non-linear generators were modelled using Duffing's Equation as follows:

$$m\frac{d^2z(t)}{dt^2} + b\frac{dz(t)}{dt} + kz(t) + k_n[z(t)]^3 = -m\frac{d^2y(t)}{dt^2} \tag{3.32}$$

where the spring force is the combination of linear force, $kz(t)$ and non-linear force, $k_n[z(t)]^3$. Solving Equation (3.32) gives the frequency-amplitude relationship as:

$$\Omega_a(Z) = \left(\frac{3}{4}\alpha Z^2 + \left(1 - 2\zeta^2\right) - \frac{\left(a^2 - 3\alpha\zeta^2 Z^4 + 4\zeta^2 Z^2\left(\zeta^2 - 1\right)\right)^{\frac{1}{2}}}{Z} \right)^{\frac{1}{2}} \tag{3.33}$$

$$\Omega_b(Z) = \left(\frac{3}{4}\alpha Z^2 + \left(1 - 2\zeta^2\right) + \frac{\left(a^2 - 3\alpha\zeta^2 Z^4 + 4\zeta^2 Z^2\left(\zeta^2 - 1\right)\right)^{\frac{1}{2}}}{Z} \right)^{\frac{1}{2}} \tag{3.34}$$

where Ω_a and Ω_b are frequencies, α is proportional to the non-linear spring factor, k_n, Z is the amplitude of the proof mass, ζ is the damping factor and a is the normalized excitation acceleration.

Such devices have a hardening or softening spring which has the effect of shifting the resonant frequency upwards or downwards. Numerical and analytical studies showed that a device with a hardening spring has a larger bandwidth over which power can be harvested due to the shift in the resonance frequency. Their analysis also showed that the bandwidth of the hardening system depends on the damping ratio, the nonlinearity and the input acceleration (Figure 3.58). Ideally, the maximum amount of power harvested by a system with a hardening stiffness is the same as the maximum power harvested by a linear system, irrespective of the nonlinearity, although this possibly occurs at a different frequency depending on the nonlinearity. It should be pointed out that the output power and bandwidth of the non-linear generators depends on the direction of approach of the vibration frequency to the resonant frequency. For a hard non-linearity, this approach will only produce an improvement when approaching the device resonant frequency from a lower frequency. For a soft non-linearity, this approach will only produce an improvement when approaching the device resonant frequency from a higher frequency. It is unlikely that these conditions can be guaranteed in real application.

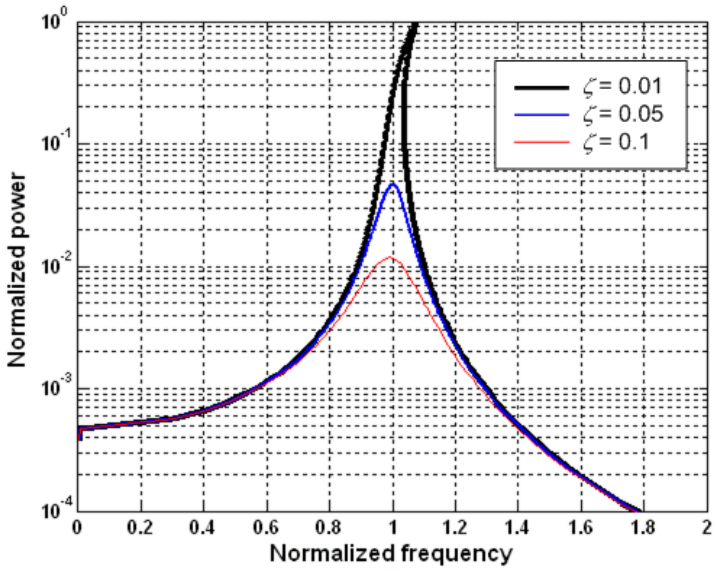

(a) Various damping ratio

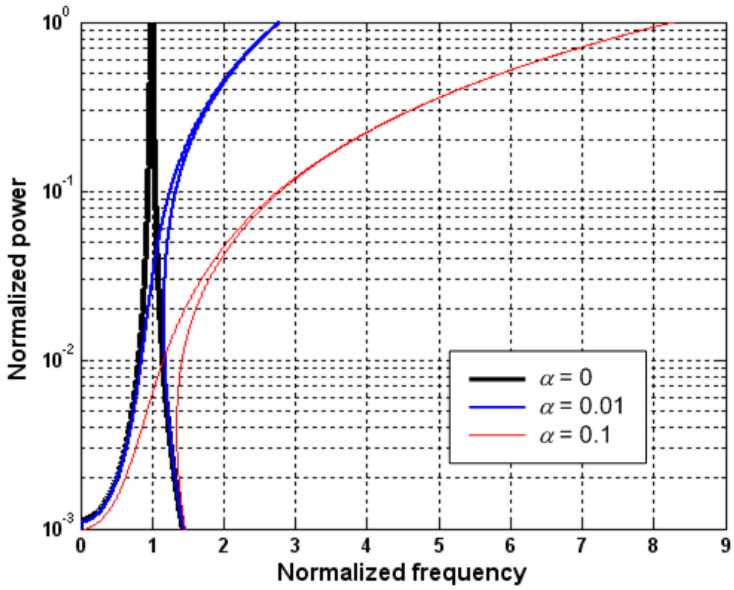

(b) Various non-linearity

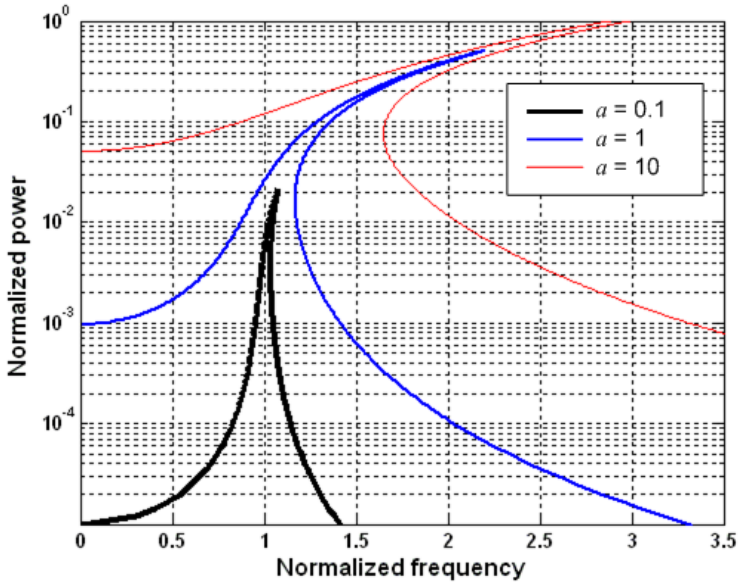

(c) Various input acceleration

Figure 3.58. Power spectrum of non-linear generators.

Non-linear generators can be conveniently realized by using a magnetic spring instead of a conventional spring. Spreemann et al [87] reported a tunable electromagnetic vibration energy harvester with a magnetic spring, which combined a tuning mechanism with the non-linear structure. Instead of using a linear suspension, this device was implemented using a rotary suspension (Figure 3.59). The use of magnetic spring magnets resulted in a nonlinear restoring force. The nonlinear restoring force provides low resonance frequencies within a small generator volume and small changes in the spring magnet's position cause a significant change in the spring characteristic. As shown experimentally in Figure 3.60, the resonant frequency shifted by about 30Hz for a displacement of 1.5mm of each spring magnet. The maximum output decreased with the increase of the magnet spacing, i.e. as the resonant frequency decreased, which accords with the conclusion drawn from Equation (2.16). Also the bandwidth of the device increased as the space between magnets became smaller, i.e. non-linearity increased. This agrees with the analysis result shown in Figure 3.57. The generator has a volume of approximately 2.5cm^3.

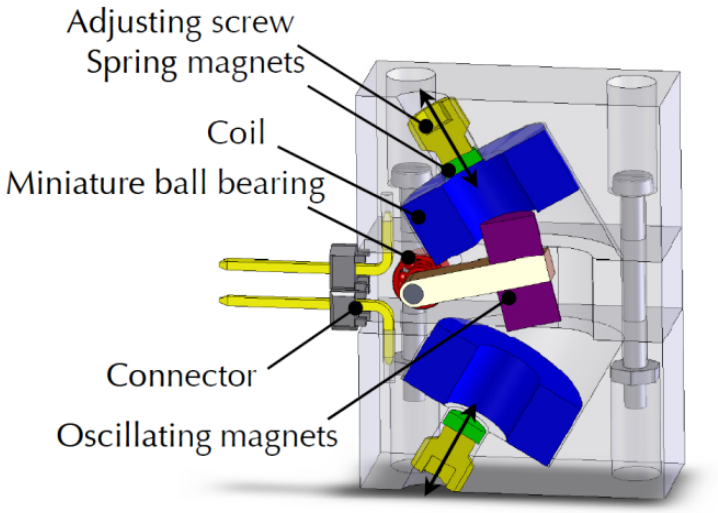

Figure 3.59. Half-Section of the device [87].

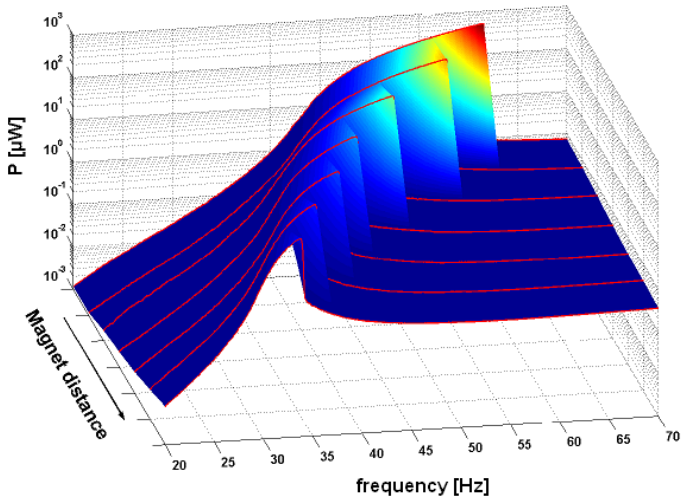

Figure 3.60. Measured output power [87].

In addition, the design and analysis of an energy harvesting device with magnetic restoring forces to levitate an oscillating centre magnet was presented by Mann et al [88]. Figure 3.61 shows the schematic diagram of the device. The device used two outer magnets that were mechanically attached to a threaded support. A centre magnet was placed between the two outer magnets and the magnetic poles were oriented to repel the centre magnet, thus suspending the centre magnet with a nonlinear restoring force. The nonlinearity allows the linear resonance to be tuned by simply changing the spacing between outer and centre magnets (Figure 3.62).

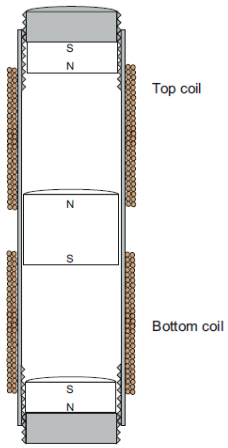

Figure 3.61. Schematic diagram of magnetically levitated generator [88].

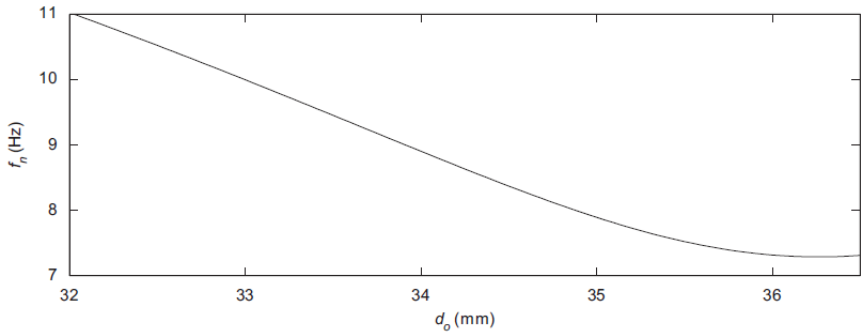

Figure 3.62. Change in the linear resonances as a function of the magnet spacing [88].

The mathematical model for the energy harvesting device was derived by Mann et al and examined for the case of harmonic base excitation. It was found theoretically and experimentally that the response for both linear and nonlinear systems scales almost linearly within some regimes of excitation amplitudes (Figure 3.63a). However, once the nonlinearities have been sufficiently engaged, as shown in Figure 3.63b, the peak response of the nonlinear system no longer scales linearly and is relocated away from linear resonance. Thus, the ability to tune the restoring forces is an essential consideration for applications with a fixed frequency harmonic excitation so that the best performance can be obtained. Additionally, in the frequency response for the nonlinear system, relatively large amplitudes persist over a much larger range of frequencies, which could prove beneficial for applications with either fixed or varying excitation inputs. Furthermore, the maximum output power of such devices is delivered to the electrical load at a frequency away from linear resonance.

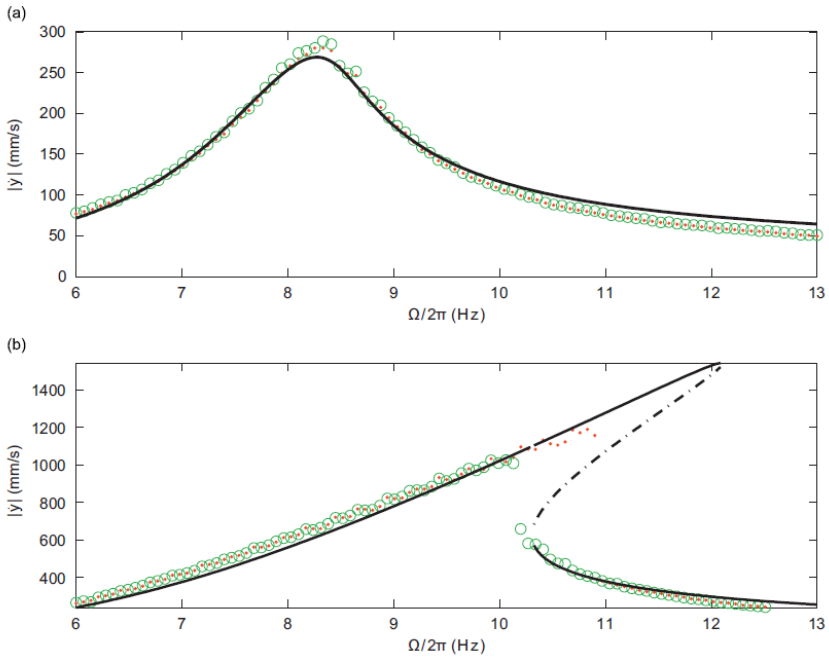

Figure 3.63. Experimental velocity response amplitudes from forward (dots) and reverse frequency sweeps (circles) are compared with theory. Theoretical predictions are separated into stable solutions (solid line) and unstable solutions (dashed line). (a) excitation level of $2.1 m \cdot s^{-2}$ (b) excitation level of $8.4 m \cdot s^{-2}$ [88].

Burrows et al [89, 90] reported another non-linear generator. It consisted of a linear spring with the non-linearity caused by the addition of magnetic reluctance forces. Figure 3.64 shows the schematic diagram of the non-linear generator. The flux concentrator guides the magnetic flux through the coil. The vibration of the magnets causes a change in direction of the magnetic flux, which induces a voltage across the coil. The reluctance force between the magnets and the flux concentrator resulted in the non-linearity. Theoretically, it was found that, for given displacement and mass, there is more energy stored in a non-linear system than a linear system as the force on the spring at a given peak displacement will be higher than in the linear case and the mass velocity will be higher when it passes zero displacement. In addition, the generator experimentally showed a wider bandwidth during an up-sweep, i.e. when the excitation frequency was gradually increased while the bandwidth was much narrower during a down-sweep, i.e. when the excitation frequency was gradually decreased.

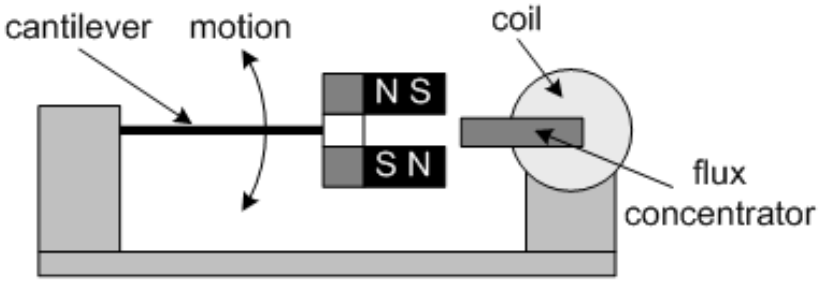

Figure 3.64. Schematic diagram of a non-linear generator (after [90]).

3.5.4 Bi-stable Structures for Vibration Energy Harvesting

Ramlan et al [86] studied a bi-stable structure for energy harvesting (also termed the snap-through mechanism). These structures employ a negative stiffness which has the effect of steepening the displacement response of the resonator as a function of time resulting in a higher velocity for a given input excitation. Their analysis revealed that the amount of power harvested by a nonlinear device is $4/\pi$ greater than that of the tuned linear device provided the device produces a square wave output for a given sinusoidal input. Numerical results also showed that more power is harvested by the mechanism if the excitation frequency is much less than the generator's resonant frequency. Although the bi-stable mechanism cannot produce a square wave like response under all operating conditions, it offers better performance than the linear mechanism at lower frequencies than the resonant frequency of the linear device. Bi-stable devices also have the potential to cope with mismatch between resonant frequency and vibration frequency.

Dogheche et al [91] have reported a piezoelectric Micro-machined Ultrasonic Transducer (pMUT) used as a mechanical to electrical energy scavenger. The resonator was a silicon membrane of which the thickness varied from 1 to 5μm and of four different diameters, 132, 200, 400 and 600μm. Different pMUT devices have been tested using a hand shaking excitation ranging from 4.9 to 19.6m·s^{-2}. The experimental results showed that the pMUT device can generate power in both linear (elastic) and non-linear (bi-stable) mechanical behaviours.

3.6 Summary

Tables 3.1 and 3.2 summarize continuous and intermittent tuning methods. The continuous tuning devices relate to resonator devices and have not yet been applied to vibration energy harvesting. The intermittent tuning summary table contains information from actual vibration energy harvesters. Table 3.3 summarizes generator arrays.

Table 3.1. Summary of continuous tuning methods.

Reference	Untuned resonant frequency (Hz)	Tuning range (Hz)	Size	Tuning voltage (V)	Sensitivity (Hz/V)
Scheibner [59]	Multiple	1 – 10k	$7 \times 10mm^2$	0 - 35	257
Adams [60]	25 k	1.9 - 36.5k	$500 \times 10\mu m^2$	0 - 50	692
Lee [61]	19 k	5.55 – 19k	$460 \times 840\mu m^2$	0 - 150	89.67
Piazza [62]	719 k	713 – 716k	$200 \times 20 \times 4.2\mu m^3$	0 - 20	300
Yao [63]	960 k	900 – 960k	N/A	0 - 35	1714
Yao [63]	149.5 k	139.5 - 149.5k	N/A	0 - 30	333
Peters [64]	78	66 - 89	N/A	-5 - +5	2.3
Remtema [67]	31 k	31 – 33k	$500 \times 700\mu m^2$	0 – 25mW	80Hz/mW
Syms [68]	N/A	-25% - 50%	$3000 \times 5000\mu m^2$	1.5 - 10mW	8.8%/mW
Cabuz [72]	518	518 - 534	$1000 \times 200 \times 3\mu m^3$	0 - 16	1
Mukherjee [74]	15.5 k	15.4 - 16	N/A	0 - 50	12

Table 3.2. Summary of intermittent tuning methods used in vibration energy harvesting.

Reference	Untuned resonant frequency (Hz)	Tuning range (Hz)	Mass (g)	Size (mm^3)	Tuning force (N)	Excitation level ($m \cdot s^{-2}$)	Output power (μW)	sensitivity	Affect on damping
Wu [57]	N/A	130 - 180	N/A	10 × 12 × 38 [a]	N/A [b]	1.96	5 – 11V_{oc}	1.67Hz/mm	N/A
Challa [66]	26	22 - 32	45.8	34 × 20 × 0.92	N/A [c]	0.8	240 – 280	0.33Hz/mm	↑ [e]
Leland [73]	250	200 - 250	7.1	31.7 × 12.7 × 0.509	0 - 60	9.8	300 – 400	0.83Hz/N	↑ [e]
Eichhorn [76]	380	290 - 380	N/A	20 × 5 × 0.44	0 - 22.75	63.7	3 - 4.5V_{oc}	3.96Hz/N	↑ [e]
Zhu [77]	45	67.6 - 98	N/A	N/A	N/A [d]	0.588	61.6 - 156.6	8Hz/mm	-- [f]

[a] Size of the mass
[b] Change in position of centre of gravity: 30mm
[c] Tuning distance: 30mm
[d] Tuning distance: 3.8mm
[e] Damping increased with tuning mechanism
[f] Damping stayed constant for most of the tuning range and increased when tuning force became large

Table 3.3. Summary of generator array.

Reference	Tuning range (Hz)	Number of cantilever	Power level (μW)
Xue [81]	92 - 110	10	> 30 [a]
Feng [82]	300 - 800	4	> 2 [a]
Sari [84]	3300 - 3600	40	> 0.5

[a] Simulation results

3.7 Comparisons of Different Strategies

It has been proven theoretically and demonstrated experimentally that both tuning resonant frequency and widening the bandwidth of vibration-based micro-generators can increase their operational frequency range.

To compare the performance of a single generator with a wide bandwidth, a generator array and a single tunable generator with constant damping, typical specifications of these three types of generators have been chosen. G1, G2 and G3, listed in Table 3.4, represent a single generator with a wide bandwidth, a generator array and a single tunable generator with constant damping, respectively. Figure 3.65 shows the comparison of power spectra of these three types of generator.

Table 3.4. List of specifications in Figure 3.65.

Figure	Operational frequency range	Q-factor of G1	Q-factor of G2	Number of individual generator in G2, n	Resonant frequencies of individual generators in G2	Q-factor of G3	Mass ratio (G1:G2:G3)
3.65a	94 % - 106 %	10	100	9	91.5 % + n * 1.8 %	200	30:15:1
3.65b	94 % - 106 %	10	200	12	92.5 % + n * 1.2 %	200	30:10:1
3.65c	55 % - 183 %	1	10	31	47 % + n * 5 %	200	200:100:1
3.65d	55 % - 183 %	1	100	45	47 % + n * 3 %	200	200:90:1

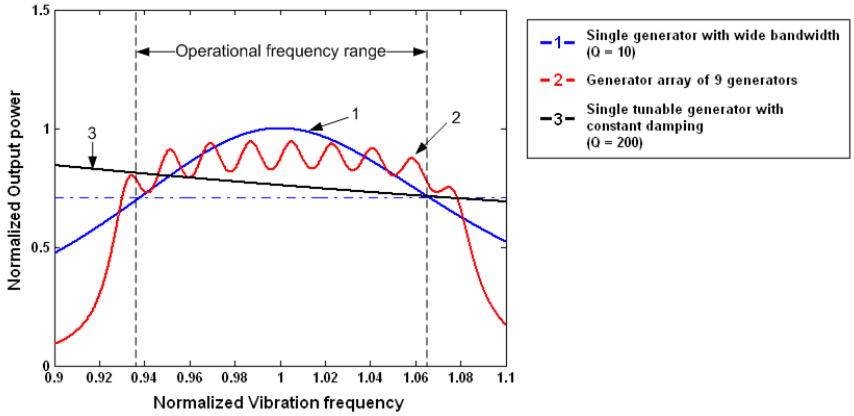

(a) Curve 1 and 3 are both single generators. Curve 2 consists of a generator array of 9 generators of Q-factor of 100.

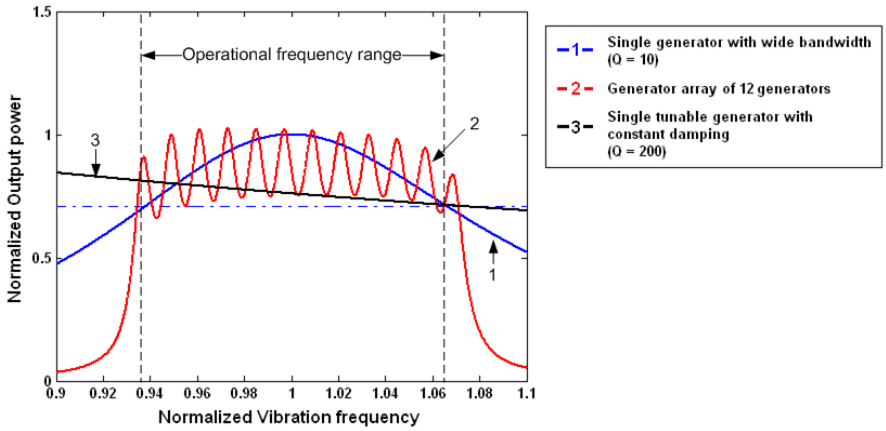

(b) Curve 1 and 3 are identical to Figure 3.65(a). Curve 2 now consists of a generator array of 12 generators of Q-factor of 200.

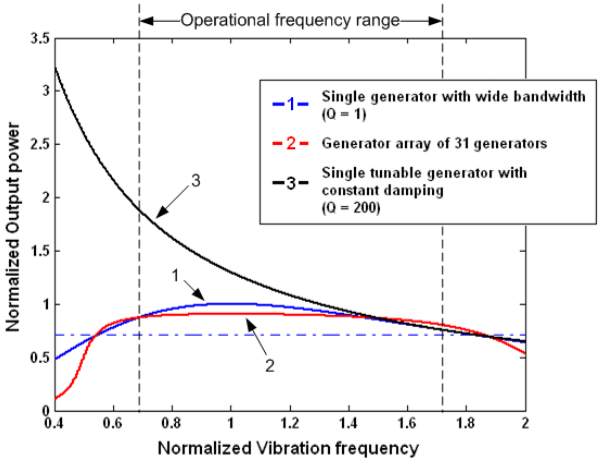

(c) For curve 1, the Q-factor has been reduced to 1. Curve 2 shows a generator array of 31 generators of Q-factor of 10. Curve 3 has the same Q-factor as in Figure 3.65(a) and (b) but with higher mass.

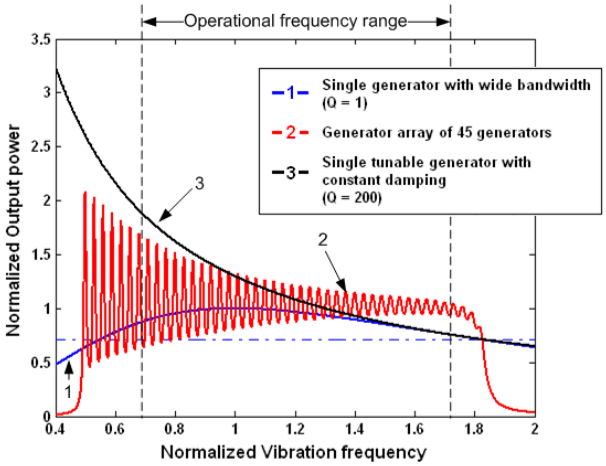

(d) Curves 1 and 3 are identical to Figure 3.65(c). Curve 2 now consists of a generator array of 45 generators of Q-factor of 100.

Figure 3.65. Comparison of a single generator with a wide bandwidth, a generator array and a single tunable generator with constant damping.

When the Q-factor of a single generator decreases, its bandwidth increases. To generate the same output power level as those within the original bandwidth, a single generator has to be larger as the bandwidth increases.

If a generator array is used to widen the operational frequency range, one can design a few larger individual generators with low Q-factor with large resonant frequency gap between generators or many smaller individual generators with high Q-factor but

small resonant frequency gap between generators. By contrast, it is much easier to design small tunable generators with constant damping to cover the same amount of operational frequency range at the cost of extra energy to power the frequency tuning mechanisms.

Table 3.5 compares the advantages and disadvantage of different strategies to increase operational frequency range of vibration-based micro-generators.

Table 3.5. Comparisons of different strategies.

Strategies	Advantages	Disadvantages
Mechanical tuning	● High efficiency	○ Extra system and energy are required ○ Responds to only one frequency at a time ○ Slow response to change in vibration frequency
♦ Change dimension	● Does not affect damping	○ Difficult to implement ○ Not suitable for tuning in situ[1]
♦ Change centre of gravity	● Does not affect damping	○ Not suitable for tuning in situ
♦ Change spring stiffness continuously	● Suitable for in situ tuning	○ Consumes energy when generators work at resonance
♦ Apply axial load (Change spring stiffness intermittently)	● Easy to implement ● Suitable for in situ tuning ● No energy is required when generators work at resonance ● Damping is not affected when tensile load is applied	○ Increased damping when compressive load is applied
Electrical tuning	● Easy to implement ● No energy is required when generators work at resonance ● Suitable for in situ tuning	○ Low efficiency

[1] Tuning while the generator is mounted on the vibration source and working

Strategies	Advantages	Disadvantages
Widen bandwidth	● No tuning mechanism required ● Respond to different frequencies at the same time ● Immediate response to change in vibration frequency	○ Complexity in design
♦ Generator array	● Damping is not affected	○ Complexity in design ○ Low volume efficiency
♦ Use mechanical stopper	● Easy to implement	○ Fatigue problem ○ Decrease in maximum output power
♦ Non-linear generators	● Better performance at excitation frequencies higher than resonant frequency	○ Complexity in design ○ Hysteresis
♦ Bi-stable structure	● Better performance at excitation frequencies much lower than resonant frequency	○ Complexity in design

3.8 Conclusions

As most practical applications for vibration-based micro-generators exhibit frequency variations over time, it is not possible to guarantee that fixed frequency generators will always work at resonance and produce maximum output power. Mechanisms have to be employed to increase the operational frequency range of vibration-based micro-generators. There are two possible solutions, i.e. tuning the resonant frequency of a single generator and widening the bandwidth of the generator. Practical realizations of each solution and their characteristics are summarized in this Section.

3.8.1 Tuning the Resonant Frequency of a Single Generator

The first solution, i.e. tuning the resonant frequency of a single generator, requires a certain mechanism to periodically adjust the resonant frequency so that it matches the frequency of ambient vibration at all times, maximum power can then be generated at various frequencies without reducing the Q-factor and with high efficiency per unit volume. Intermittent tuning has advantages over continuous tuning as it is more efficient because the tuning mechanism is turned off when the generator is at the right

frequency thereby consuming negligible energy, which makes producing a net output power more probable.

Among mechanical methods of frequency tuning, changing the dimensions of the structure and the position of the centre of gravity are potentially suitable for intermittent tuning. However, they are less suitable for continuous tuning since it is problematic to change and maintain the new dimensions of the structure or the centre of gravity of the proof mass during operation. The most suitable approach to changing the dimensions of the structure is to change its length. This requires the structure clamp is removed, the length adjusted and then the structure re-clamped. It is important that in each tuning procedure that the structure is clamped properly, otherwise the performance of the generator will be severely affected by introducing damping effects through the supports. Therefore, these two methods are not suitable for in situ tuning (tuning while the generator is mounted on the vibration source and working) or tuning with automatic control.

Alternatively the frequency can be tuned by changing the spring stiffness intermittently or continuously. They are both suitable for in situ tuning but intermittently changing the spring stiffness is always preferred for efficiency reasons. However, extra systems and energy are required to realize tuning using mechanical methods.

It is important to mention that the efficiency of mechanical tuning methods also depends on the size of the structure. The smaller the resonator, the higher the efficiency of the tuning mechanism.

Resonant frequency tuning by adjusting the electrical load has been practically shown to be feasible. This method consumes little energy as it does not involve any change in mechanical properties. The only energy consumed is in the electronic switches and control unit, which is typically far less than that consumed in mechanical tuning methods. In addition, it is much easier to implement than mechanical methods. However, the tuning efficiency to date is quite low and this method cannot achieve a large tuning range. An extra closed loop system also has to be introduced to control

the tuning process.

3.8.2 Widening the Bandwidth of the Generator

For the second solution, i.e. to widen the bandwidth, an obvious problem is that there is a trade-off between the system bandwidth and the Q-factor. Wider bandwidth means, for a single resonator, a lower Q-factor, which reduces the maximum output power. Bandwidth can also be effectively widened by designing a generator consisting of an array of small generators, each of which works at a different frequency. Thus, the assembled generator has a wide operational frequency range whilst the Q-factor does not decrease. However, this assembled generator must be carefully designed so that each individual generator does not affect the others. This makes it more complex to design and fabricate. Additionally, at a particular source frequency, only a single or a few individual generators contribute to power output so the approach is volume inefficient.

Another method used to increase the bandwidth is to use an amplitude limiter to limit the amplitude of the resonator. The drawbacks are that this method causes the maximum output power to drop by limiting vibration amplitude and the repeating mechanical contact between the cantilever and the mechanical stopper may result in earlier fatigue induced failure in the cantilever beam.

Furthermore, non-linear generators and generators with bi-stable structures are two further potential solutions to increase the operational frequency range of vibration-based micro-generators. They can improve performance of the generator at higher and lower frequency bands relative to its resonant frequency, respectively. However, the mathematical modelling of these generators is more complicated than that of linear generators, which increases the complexity in design and implementation. Besides, there is hysteresis in non-linear generators. Performance during down-sweep (or up-sweep) can be worse than that during up-sweep (or down-sweep) or worse than the linear region depending on sweep direction as explained in Section 3.5.3.

In conclusion, for vibration energy harvesting, possible strategies to increase the operation frequency range include:

- Changing spring stiffness intermittently (preferred) or continuously;
- Straining the structure intermittently (preferred) or continuously;
- Adjusting the capacitive load;
- Using a generator array;
- Employing non-linear and bi-stable structures.

To realize these strategies properly, the following issues have to be considered. For intermittent mechanical tuning, the tuning system has to be designed to consume as little energy as possible and not to affect the damping so as to make the generator harvest maximum power. In addition, currently commercially available linear actuators are still large in size compared to the mm scale micro-generator. To keep tunable generators of reasonable size, it is important to use miniature actuators. Generators using electrical tuning must be well designed in order to achieve sufficient coupling between the mechanical and electrical domains to enable larger tuning ranges. Moreover, non-linear generators and generators with bi-stable structures have not been sufficiently developed and further attention should be paid to practically implement them.

In the next four chapters, detailed analysis and practical effort to tune the resonant frequency of electromagnetic vibration-based micro-generators using mechanical and electrical tuning methods to match the ambient vibration frequency will be presented.

Chapter 4

Resonant Frequency Tuning using Mechanical Methods

4.1 Introduction

In this chapter, mechanical methods used to tune the resonant frequency of vibration-based micro-generators based on a cantilever structure, particularly applying an axial force to the cantilever, is presented. As strain in the cantilever changes, its resonant frequency is tuned. The principle of this method is presented in Section 4.2. To minimize unwanted effects on the cantilever vibrations, a contactless magnetic force provided by two tuning magnets is used to apply the axial force. A numerical method of calculating the magnetic force between two magnets is given afterwards. A preliminary test that has been done to prove this method will be demonstrated in Section 4.3. The test gives a good guidance to optimizing this method and designing a tunable electromagnetic vibration-based micro-generator.

4.2 Principle

The principle of this method has been briefly introduced in Section 3.3.4.2 and it will be detailed here.

4.2.1 Model of the Mechanical Tuning Mechanism

An axial tensile load applied to a cantilever (Figure 4.1a) increases the resonant frequency of the cantilever while an axial compressive load applied to a cantilever (Figure 4.1b) decreases the resonant frequency of the cantilever.

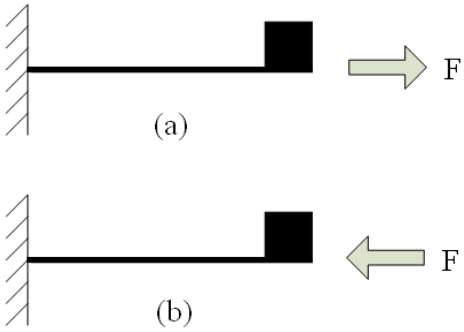

Figure 4.1. Axial tensile (a) and compressive (b) load on a clamped-free cantilever.

An approximate formula for the resonant frequency of a uniform cantilever in mode i with an axial load, f_{ri}', is given by [69]:

$$f_{ri}' = f_{ri} \cdot \sqrt{1 + \frac{F}{F_b} \cdot \frac{\lambda_1^2}{\lambda_i^2}} \tag{4.1}$$

where f_{ri} is the resonant frequency in mode i without load. F is the axial load. F is positive if the load is tensile and F is negative if the load is compressive. F_b is the axial load required to buckle the beam, i.e. to make the fundamental resonant frequency zero. λ_1 is a dimensionless load parameter which is a function of the beam boundary conditions applied to the cantilever for mode 1 of the beam and λ_i is the same parameter for mode i. λ_i is given by the ith positive solution of Equation (4.2) [70]:

$$\cos\lambda \cdot \cosh\lambda + 1 = 0 \tag{4.2}$$

Since most micro-generators with a cantilever structure work at a resonance of mode 1, the resonant frequency of a uniform cantilever in mode 1 with an axial load, f_{r1}', is given by:

$$f_{r1}' = f_{r1} \cdot \sqrt{1 + \frac{F}{F_b}} \tag{4.3}$$

The buckling load F_b is given by:

$$F_b = \frac{\pi^2 \cdot Y \cdot I}{4 \cdot l^2} \tag{4.4}$$

where Y is the Young's modulus of the material of the cantilever, l is the span of the cantilever and I is the area moment of inertia which is, for this structure, give by:

$$I = \frac{w \cdot h^3}{12} \tag{4.5}$$

Thus, the buckling load can be rewritten as:

$$F_b = \frac{\pi^2 \cdot Y \cdot w \cdot h}{48 \cdot l^2} \tag{4.6}$$

Figure 4.2 shows the change in resonant frequency of a cantilever with axial load. It shows that a compressive load is more efficient in frequency tuning than a tensile load. Effects of both tensile load and compressive load on parasitic damping in the generator have been investigated in a preliminary test which will be presented separately in Section 4.3.6 and Section 4.3.8. If a very large tensile force is axially applied to the cantilever, the resonant frequency will approach that of a straight tensioned cable as the force associated with the tension in the cantilever becomes much greater than the beam stiffness.

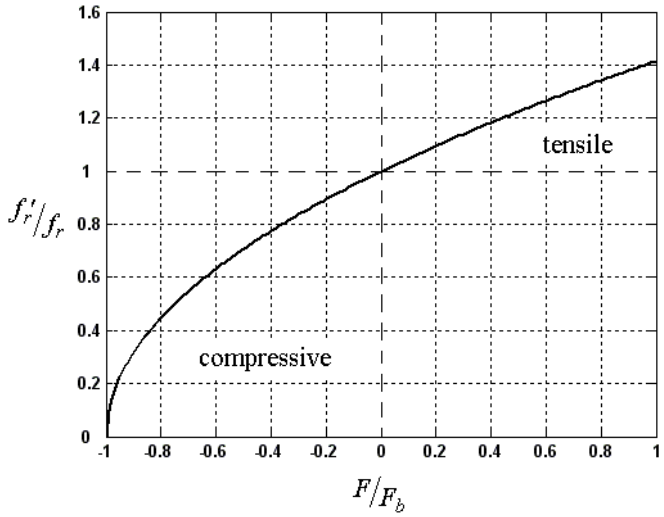

Figure 4.2. Change in resonant frequency with axial load.

4.2.2 Method of Applying Axial Force

Figure 4.3 shows the schematic diagram of the tuning mechanism. The resonant frequency tuning is realized by applying axial force to the cantilever. The tuning force is provided by the repelling (Figure 4.3a) or attractive (Figure 4.3b) force between two tuning magnets with similar or opposite poles facing each other. One magnet is fixed at the free end of a cantilever while the other is placed axially in line with the cantilever and is moveable along the span of the cantilever. As the distance between the two tuning magnets is adjusted, the axial load on the cantilever changes, and hence the resonant frequency of the cantilever is tuned. The areas where the two magnets face each other are curved to maintain a constant gap between them over the amplitude range of the generator.

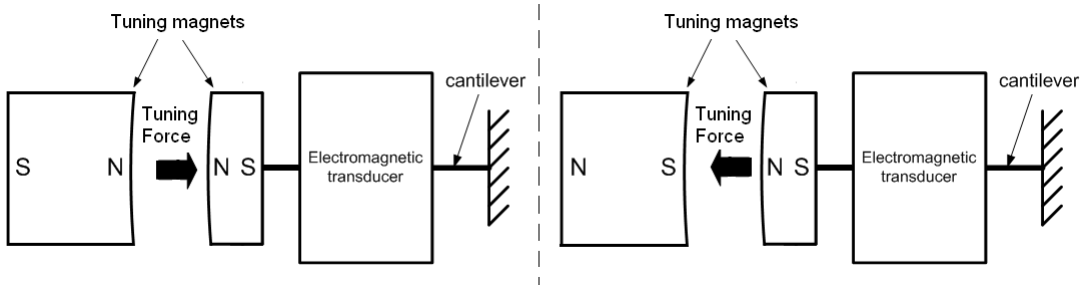

(a) (b)

Figure 4.3. Schematic diagram of tuning mechanism (a) compressive force (b) tensile force.

4.2.3 Calculation of Magnetic Force

The calculation of magnetic force between simple shape magnets can be performed numerically. Only final equation is given here. A detailed description of this calculation can be found in [92].

Figure 4.4 shows two cubic magnets whose centres are o and o', respectively.

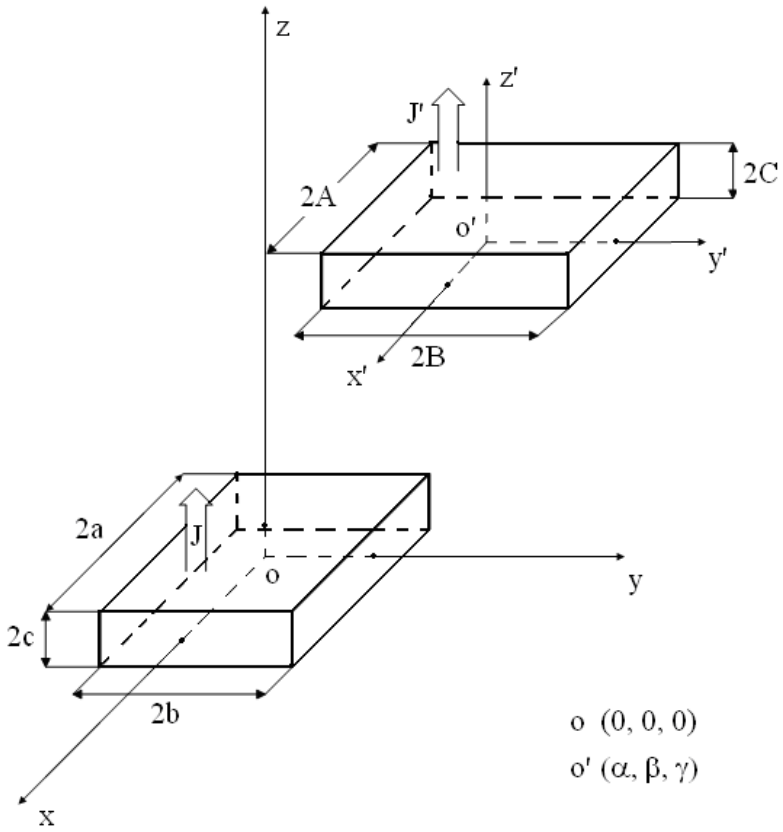

Figure 4.4. Magnet configuration 1.

Their sides are respectively parallel and they are separated by α, β and γ in x, y and z direction (centre to centre), respectively. The dimensions of the lower magnet are 2a × 2b × 2c and that of the upper one is 2A × 2B × 2C. The magnetisations of the two magnets, J and J' are uniform. Their poles are in the z-axis. The magnetic force between these two permanent magnets can be calculated using the following equations:

$$F = \frac{J \cdot J'}{4\pi\mu_0} \sum_{i=0}^{1} \sum_{j=0}^{1} \sum_{k=0}^{1} \sum_{l=0}^{1} \sum_{p=0}^{1} \sum_{q=0}^{1} (-1)^{i+j+k+l+p+q} \phi\left(u_{ij}, v_{kl}, w_{pq}, r\right) \qquad (4.7)$$

For F_x,

$$\phi_x = \frac{1}{2}\left(v_{ij}^2 - w_{pq}^2\right)\cdot \ln\left(r - u_{ij}\right) + u_{ij} v_{kl} \cdot \ln\left(r - v_{kl}\right) + v_{kl} w_{pq} \cdot \tan^{-1} \frac{u_{ij} v_{kl}}{r w_{pq}} + \frac{1}{2} r u_{ij} \tag{4.8}$$

For F_y,

$$\phi_y = \frac{1}{2}\left(u_{ij}^2 - w_{pq}^2\right)\cdot \ln\left(r - v_{kl}\right) + u_{ij} v_{kl} \cdot \ln\left(r - u_{ij}\right) + u_{ij} w_{pq} \cdot \tan^{-1} \frac{u_{ij} v_{kl}}{r w_{pq}} + \frac{1}{2} r v_{kl} \tag{4.9}$$

For F_z,

$$\phi_z = -u_{ij} \cdot w_{pq} \cdot \ln\left(r - u_{ij}\right) - v_{kl} \cdot w_{pq} \cdot \ln\left(r - v_{kl}\right) + u_{ij} \cdot v_{kl} \cdot \tan^{-1} \frac{u_{ij} \cdot v_{kl}}{r \cdot w_{pq}} - r \cdot w_{pq} \tag{4.10}$$

where

$$u_{ij} = \alpha + (-1)^j A - (-1)^i a$$

$$v_{kl} = \beta + (-1)^l B - (-1)^k b$$

$$w_{pq} = \gamma + (-1)^q C - (-1)^p c$$

$$r = \sqrt{u_{ij}^2 + v_{kl}^2 + w_{pq}^2}$$

For the situation that two cubic magnets share the same central line along the thickness and the area where these two magnets face each other overlaps perfectly (shown in Figure 4.5), i.e. $\alpha = \beta = 0$ and $\gamma = d + (c + C)/2$. Therefore, F_x and F_y are negligible and F_z is the force between two magnets. Equation (4.7) and (4.10) gives a method of calculation of magnetic force between cubic magnets.

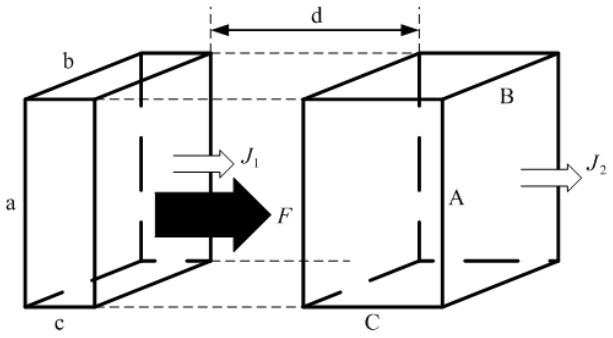

Figure 4.5. Magnetic configuration 2.

In this particular application, although the areas where the two magnets face each other are curved to maintain a constant gap between them over the amplitude range of the generator, they can be regarded as two rectangular parallelepipedic magnets since the curvatures are small. Therefore, as an approximation, Equation (4.7) and (4.10) can still be applied.

4.3 Preliminary Tests

4.3.1 Realization of Tuning Mechanism

Realization of the proposed tuning mechanism is shown in Figure 4.6. The micro-generator and the tuning mechanism are mounted on the same housing so that there is no relative displacement between them. The movable tuning magnet is attached to a linear actuator and the distance between the two tuning magnets, hence the tuning force is adjusted by the linear actuator.

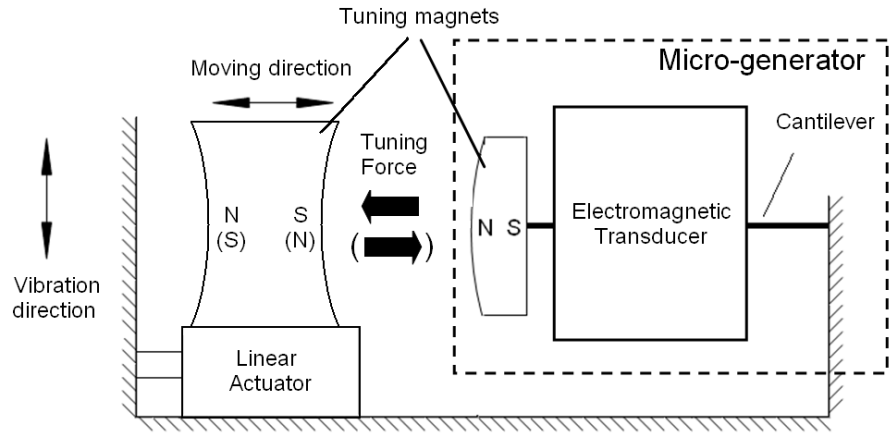

Figure 4.6. Realization of the tuning mechanism.

4.3.2 Generator tested in the Preliminary Test

The generator tested in the preliminary test is shown in Figure 4.7. It was modified from a generator previously developed in our group. The beam has been redesigned to accommodate the tuning magnet. A resonator consisting of magnets and a cantilever beam is clamped to a base where a coil is fixed.

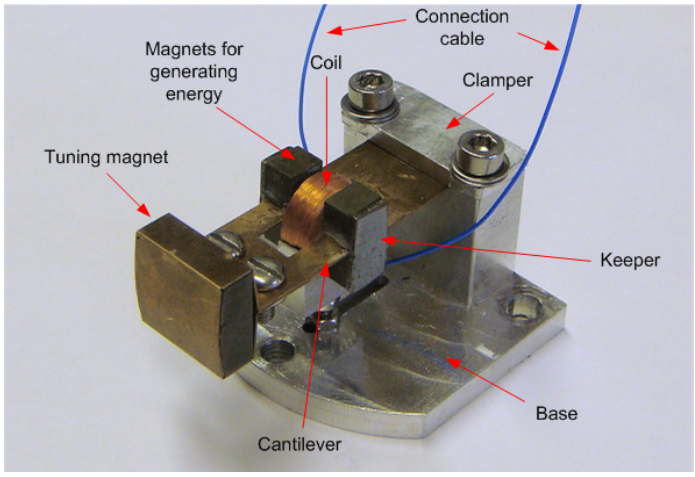

Figure 4.7. Generator tested in the preliminary test.

Figure 4.8 gives the dimensions of the cantilever. It is 0.3 mm thick and made of Beryllium Copper (BeCu) [93], a material possessing good mechanical properties, especially excellent fatigue characteristics. The Young's modulus and Poisson's ratio of BeCu are 117GPa and 0.34, respectively, which will be used throughout the future simulation.

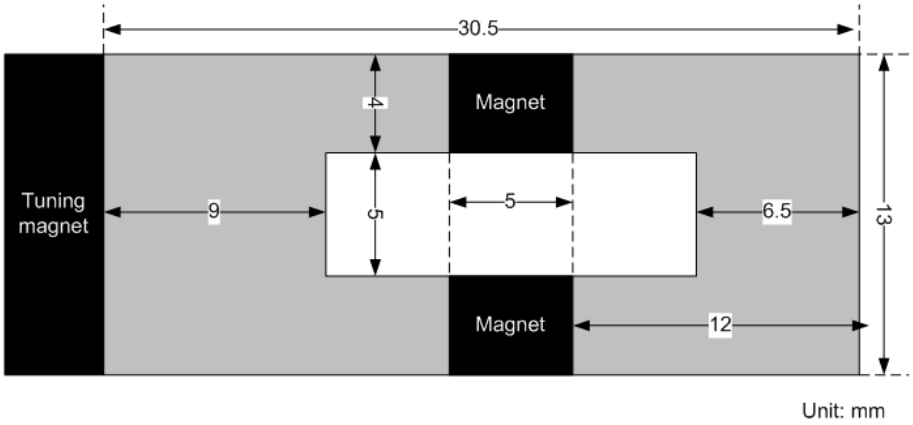

Figure 4.8. Dimension of the cantilever.

The magnetic circuit of this generator is shown in Figure 4.9. Two mild steel keepers were used to couple the magnetic flux between top and bottom magnets, which

ensures a uniform magnetic field within the air gap. The coil is attached to the base of the generator. The four-magnet structure is fixed to a cantilever beam and vibrates with the ambient vibration. The magnets move with respect to the static coil so that the induced current is generated within the coil according to the Faraday's law. Both tuning magnet and magnets for generating power are made of Neodymium Iron Boron (NdFeB) [94], a high energy density rare earth magnet.

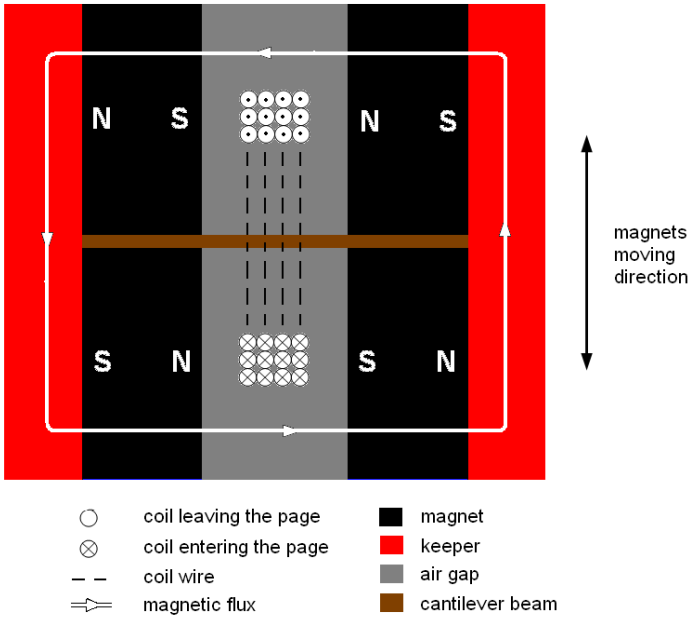

Figure 4.9. Cross section of the four-magnet arrangement.

Each magnet has the dimension of 5mm × 4mm (a) × 5mm and the dimensions of the keeper are 10mm × 5mm × 0.7mm, where (a) indicates the polarization direction. This gives this generator the total mass of 12.4g and its estimated untuned resonant frequency is 27.19Hz according to Equation (3.16).

The outer and inner diameter of the coil is 10mm and 4mm, respectively. The coil thickness is 4mm. The measured coil resistance is 337Ω. Thus, the estimated number of turns is 2540 with a fill factor of 0.6.

4.3.3 Test setup

The generator was tested on a shaker (Labworks ET-126 [95]) with a programmable resistance box and a PC with LabVIEW software [96] collecting the data (Figure 4.10).

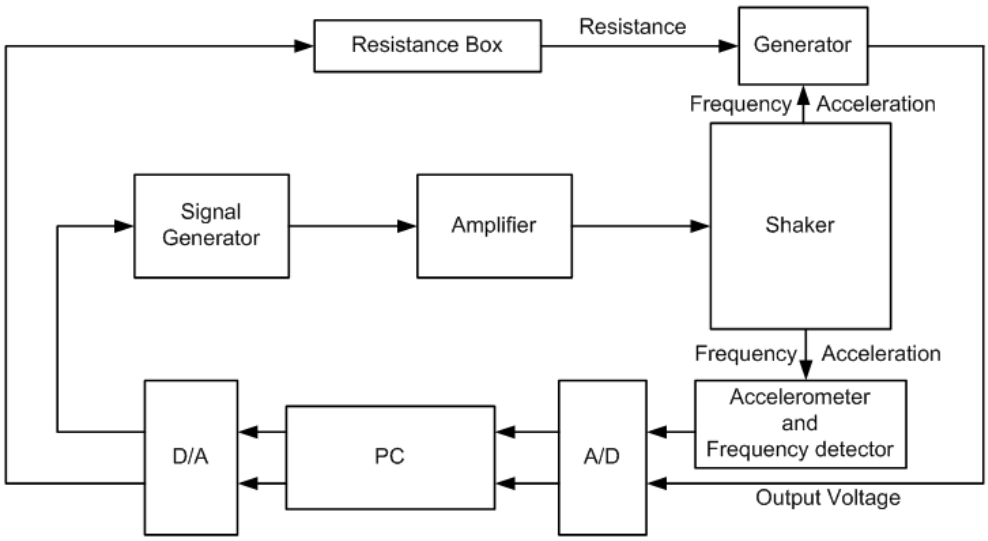

Figure 4.10. Block diagram of test platform.

The frequency and acceleration of the vibration is first set in the PC via a LabVIEW application. The signal generator outputs a sinusoid signal with the preset frequency and a certain peak voltage. This control signal is fed into a shaker to produce the target vibration. An accelerometer is used to detect the acceleration of the vibration produced by the shaker and a specially designed pulse counting circuit is used to detect the frequency of the vibration. The PC monitors the output of these sensors and adjusts the control signal to ensure the vibration is exactly what is wanted. The micro-generator to be tested is riveted securely on the shaker to minimize the loss in mechanical coupling. Additionally, the load resistance of the generator can be adjusted in the PC as well and the output voltage across the load is recorded by the PC via LabVIEW. This system is suitable for fully characterizing the generator over a wide range of acceleration levels, load resistances and frequencies. In this test, the vibration acceleration was set to be $0.49 m \cdot s^{-2}$, i.e. $50 m\boldsymbol{g}$ ($1\boldsymbol{g} = 9.8 m \cdot s^{-2}$) as a simulation of the vibration level of a commercially available pump.

The test platform of the system is shown in Figure 4.11. Tuning magnets (5) is attached to the free end of the cantilever resonator on the generator (4). The other tuning magnet (3) is fixed on a slider (2) which is able to slide along a track. The movement of the slider is controlled by the linear actuator (1). The linear actuator used here is Haydon® 21000 Series Size 8 linear actuator, E21H4(AC)-5 [97]. Its operation voltage is 5V and power consumption is 2.45W. The resolution of the

actuator is 0.01mm/step. It is controlled by the microcontroller via two H-bridge circuits (Figure 4.12). All components in the test were powered by an external power source. In this application, half stepping is used. Table 4.1 lists the stepping sequence of the stepper motor. In intermittent tuning, the new resonant frequency should be maintained with little energy being consumed. For the stepper motor, it must keep the position of the tuning magnet when the tuning is finished. In other word, the magnetic force between two tuning magnets cannot exceed the static holding force of the stepper motor.

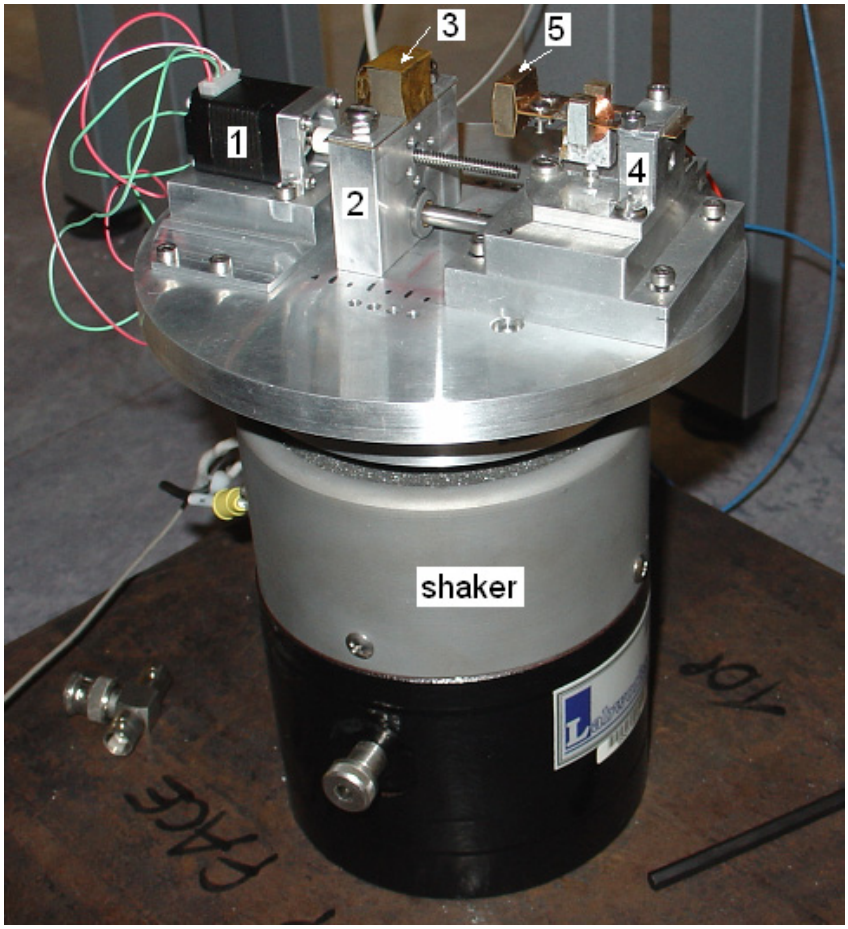

Figure 4.11. Test platform in the preliminary test

(1. Linear actuator; 2. Slider; 3. Tuning magnet 1; 4. Micro-generator; 5. Tuning magnet 2).

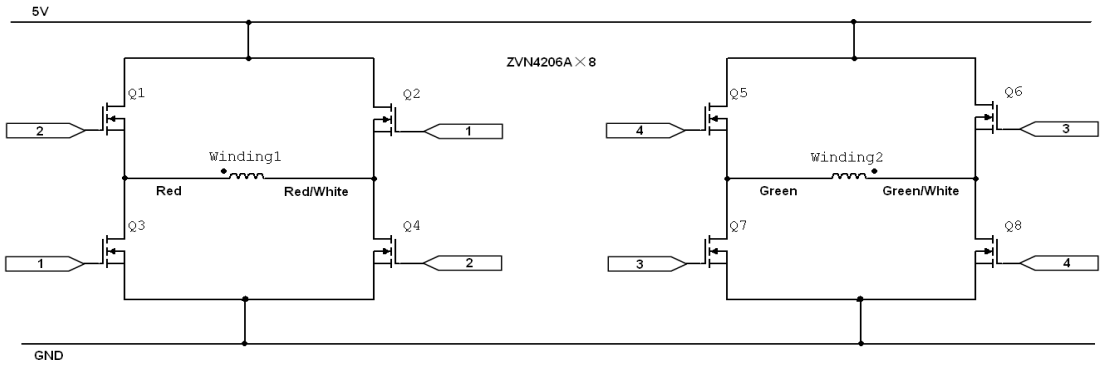

Figure 4.12. Control circuit of the stepper motor.

Table 4.1. Half-stepping sequence

Step	Q2-Q3	Q1-Q4	Q6-Q7	Q5-Q8
1	ON	OFF	ON	OFF
2	OFF	OFF	ON	OFF
3	OFF	ON	ON	OFF
4	OFF	ON	OFF	OFF
5	OFF	ON	OFF	ON
6	OFF	OFF	OFF	ON
7	ON	OFF	OFF	ON
8	ON	OFF	OFF	OFF
1	ON	OFF	ON	OFF

Figure 4.13 shows the static holding force of this stepper motor. In this application, the speed of the stepper motor was set to be 400step/sec. Therefore, the maximum static holding force is about 26N.

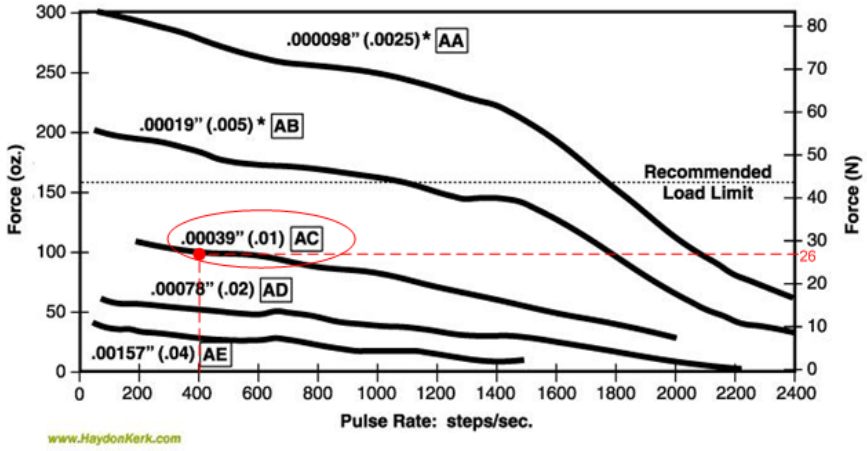

Figure 4.13. Performance curves-21000 Series Size 8 Linear actuator [95].

4.3.4 Tuning Magnet and Tuning Force

Figure 4.14 shows the dimensions of the two tuning magnets. As mentioned above, since the curvatures of the curved surfaces are small, as an approximation, they can be regarded as two parallelepipedic magnets so that Equation (4.7) to (4.10) can be applied. Table 4.2 lists the dimensions of the two magnets corresponding to the variables in Equation (4.7) and (4.10).

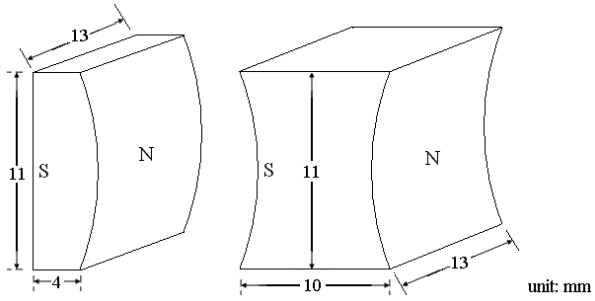

Figure 4.14. Dimension of the tuning magnets.

Table 4.2. Dimensions of the two magnets corresponding to the variables in Equation (4.10) and (4.13).

axis	x	y	z
Magnet 1	2a = 13 mm	2b = 11 mm	2c = 10 mm
Magnet 2	2A = 13 mm	2B = 11 mm	2C = 4 mm

These two magnets are made of NdFeB (N38H). A typical value of its magnetisation is 1.22T [98]. Figure 4.15 shows the numerical calculation of the tuning force versus distance between two tuning magnets. The compressive force and tensile force are the same in value for the same set of magnets but opposite in direction. The buckling force for this structure is 9.08N according to Equation (4.6). Therefore, the minimum distance between the two tuning magnets is 8.9mm when compressive force is applied.

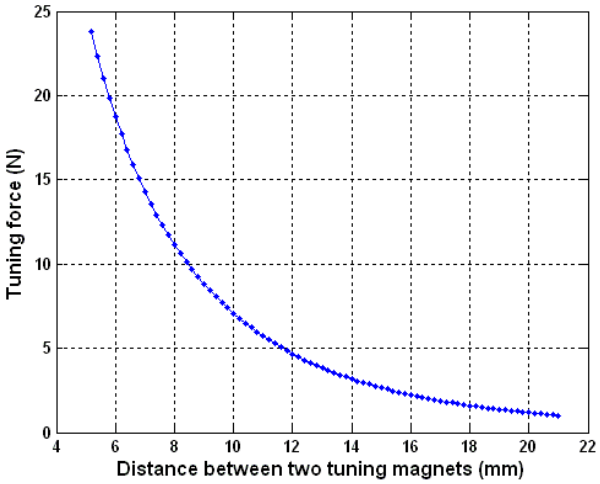

Figure 4.15. Numerical calculation of tuning force vs. distance between two tuning magnets.

It is found that when tensile force is applied and the two tuning magnets were less than 5 mm apart, the linear actuator holding the movable tuning magnet cannot keep the position of the slider because the attractive force is larger than the static holding force of the actuator. The movable tuning magnet is pulled by the attractive force towards the generator and the two magnets finally stick to each other. Since this causes the failure of the system, the distance between two tuning magnets has to be more than 5mm at all times in this application.

This result agrees with numerical calculation, which proves the accuracy of the model mentioned in Section 4.2.3. As it is difficult to measure the force between the two tuning magnets directly, the values of tuning force in this test are all obtained via numerical calculation.

4.3.5 Resonant Frequency under Tensile Loads

Figure 4.16 and 4.17 show the resonant frequency of the micro-generator with variation of tensile tuning forces and distances between the two tuning magnets, respectively. Test results have been compared with the simulation results in ANSYS Workbench [99] and found to be in reasonable agreement with the simulation. Note that only the axial load was applied in the simulation and loads on other directions were not taken into account. The resonant frequency has been tuned from 35Hz to 68Hz by varying the distance between the two tuning magnets from 4.8mm to 18mm.

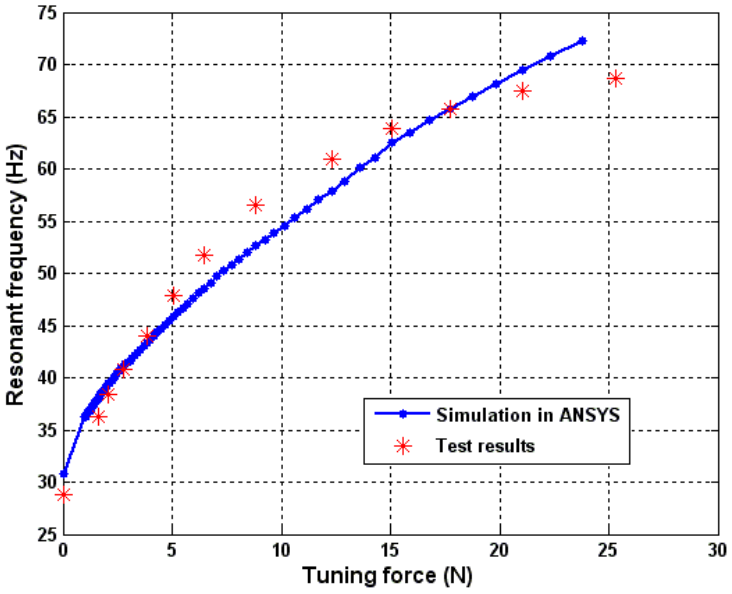

Figure 4.16. Resonant frequency with variation of tensile tuning forces.

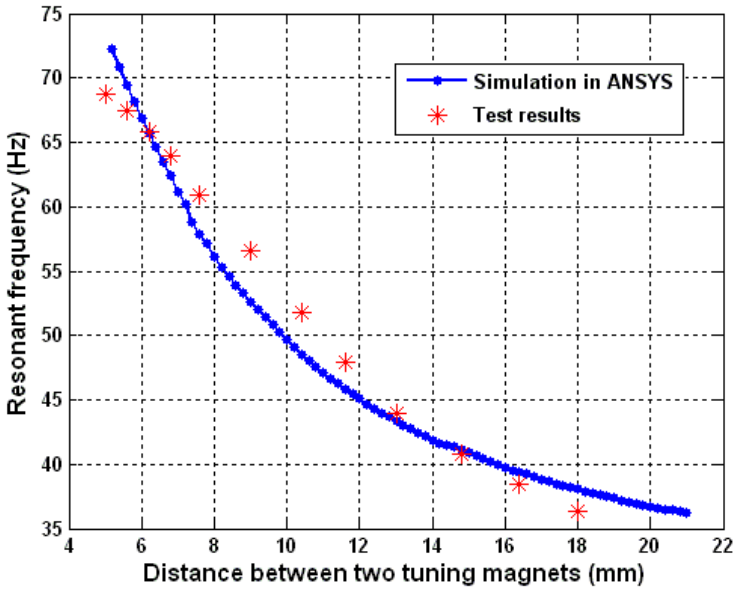

Figure 4.17. Resonant frequency vs. distances between tuning magnets when tensile force is applied.

It is found in Figure 4.16 that when the tuning force became large, the resonant frequency was lower than expected. The reason for this is that when a tensile load much greater than the buckling force is applied to a beam, the resonant frequency approaches that of a straight tensioned cable and does not increase any more because the force associated with the tension in the beam becomes much greater than the beam stiffness.

4.3.6 Power Output under Tensile Loads

Figure 4.18 shows test results of the power spectra of the generator with various resonant frequencies under tensile loads. It is found that the Q-factor of the generator with tensile loads became higher than that of the generator without any tuning. As predicted in Equation (2.17), the output power reduces with the increase of the resonant frequency. Additionally, when the resonant frequency approached the upper boundary of the tuning range, i.e. when the tuning force was large, the output power of the generator dropped lower than constant damping situation, which means that the total damping increased as the tuning force becomes large.

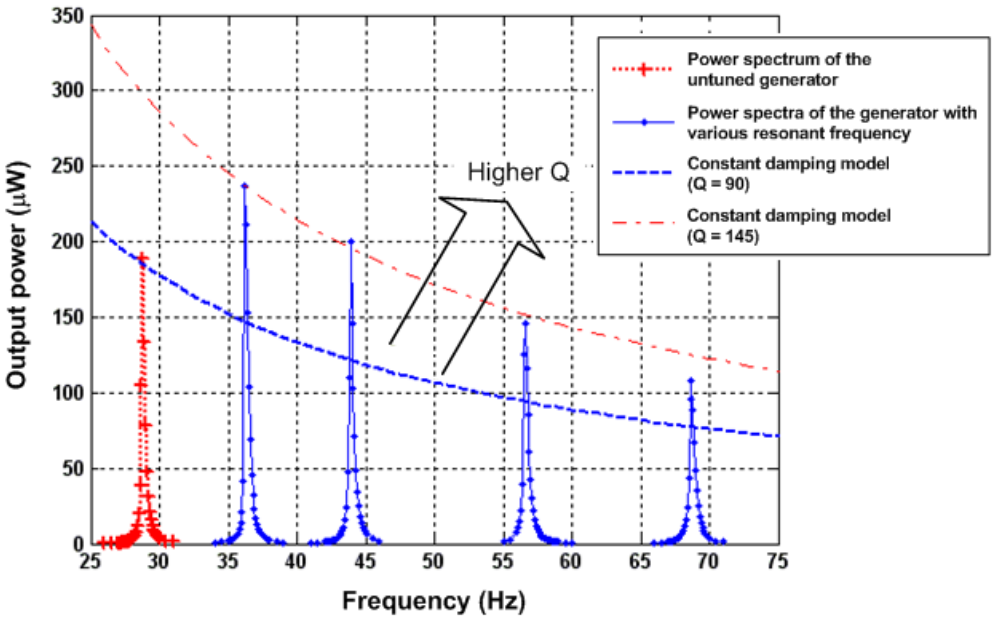

Figure 4.18. Power spectra of the generator with various resonant frequencies under tensile loads.

4.3.7 Resonant Frequency under Compressive Loads

Figure 4.19 shows the resonant frequency of the micro-generator with variation of compressive tuning forces and distance between two tuning magnets, respectively. Similarly, test results have been compared with the simulation results in ANSYS Workbench. The resonant frequency has been tuned from 18Hz to 1.2Hz by varying the distance between the two tuning magnets from 18mm to 15mm.

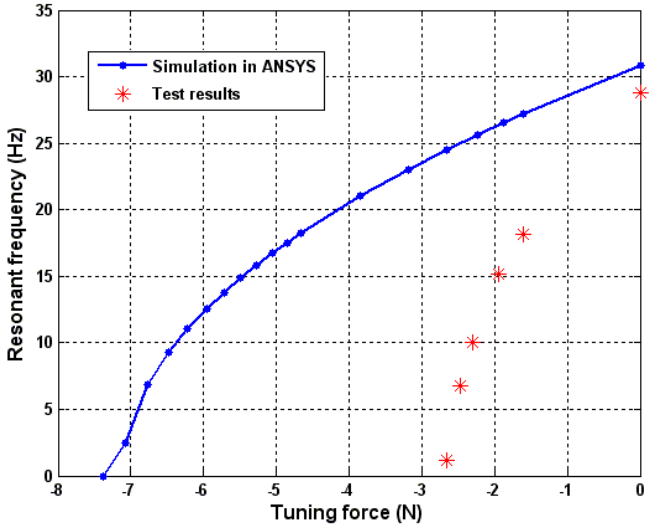

Figure 4.19. Resonant frequency vs. distance between tuning magnets when compressive force is applied.

The test results did not match the simulation results. Experimentally, the resonant frequency of the generator decreased more than expected under compressive loads. The reason for this is that in the practical situation, the cantilever was bent due to the compressive loads and the mass had an initial displacement when it was static. As the generator started vibrating, the mass had a larger displacement in one direction than that in the other one. When the compressive load became large, the inertial displacement of the mass was so large that it hardly vibrated. However, in the simulation, only the axial load was applied while the initial displacement of the proof mass and loads on other directions were not taken into account.

4.3.8 Power Output under Compressive Loads

Figure 4.20 shows test results of the power spectra of the generator with various resonant frequencies under compressive loads. It is found that the Q-factor of the generator decreased significantly when compressive loads were applied. As discussed in Chapter 2, the generator must have a high Q-factor to produce more output power. Although tuning by applying compressive force is more sensitive than tuning by tensile loads, this characteristic makes frequency tuning by applying compressive loads less useful than tuning by applying tensile loads.

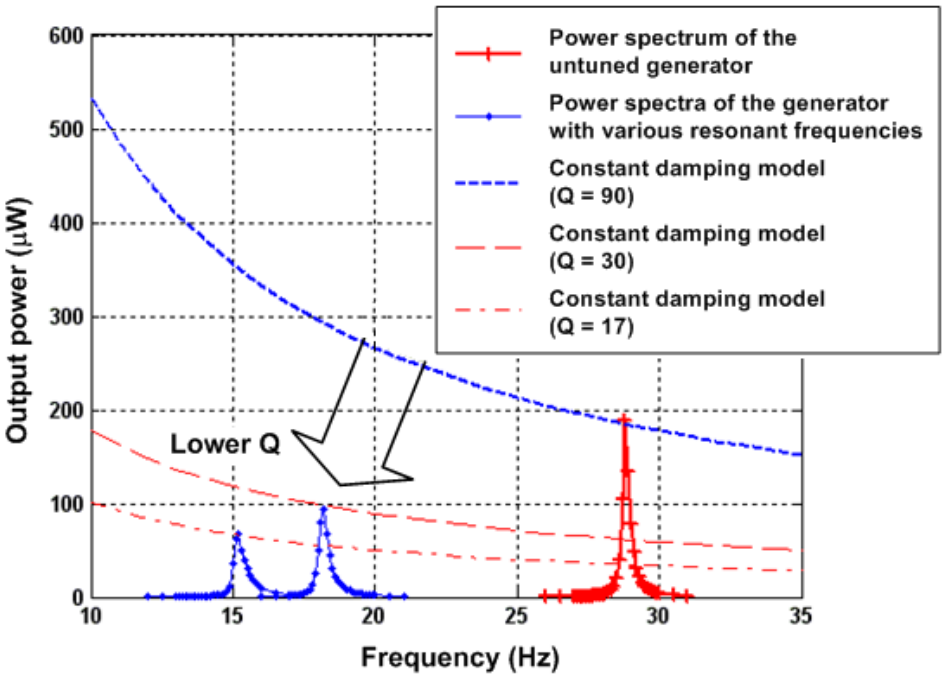

Figure 4.20. Power spectra of the generator with various resonant frequencies under compressive loads.

4.4 Conclusions

This chapter detailed the realization of resonant frequency tuning of a vibration-based generator by applying axial loads to the cantilever structure. The axial loads are provided by the interacting force between two tuning magnets. Theoretically, it has been proved that both axial tensile and compressive loads can change the resonant frequency of a cantilever structure. An axial tensile load can increase the resonant frequency while an axial compressive load can decrease the resonant frequency. The theoretical analysis also showed that the resonant frequency of a cantilever structure is more sensitive to compressive load than tensile load, i.e. resonant frequency changes more by applying the compressive load than by applying the same amount of tensile load.

A prototype of a generator has been tested. The generator consisted of a cantilever, an electromagnetic transducer and a tuning magnet attached to the free end of the cantilever. The untuned resonant frequency of the generator is 27Hz. The other tuning magnet is fixed on a slider which can move axially alone the cantilever span. The distance between two magnets can be manually adjusted and thus the tuning force.

Experimentally, it was proved that the resonant frequency of the generator could be tuned by applying axial load. Under tensile loads, the resonant frequency has been tuned from 35Hz to 68Hz by varying the distance between the two tuning magnets from 4.8mm to 18mm. It is found that, when the tuning force became large, the resonant frequency was lower than expected because, when a tensile load much greater than the buckling force is applied to a beam, the resonant frequency approaches that of a straight tensioned cable and does not increase any more because the force associated with the tension in the beam becomes much greater than the beam stiffness. Furthermore, the Q-factor of the generator with tensile loads became higher than that of the generator without any tuning and the output power reduces with the increase of the resonant frequency as predicted. As long as the tensile load is applied, the Q-factor stayed constant for most of the tuning range. However, the Q-factor decreased when the tensile load became large.

Under compressive loads, the resonant frequency has been tuned from 18Hz to 1.2Hz by varying the distance between the two tuning magnets from 18mm to 15mm. The resonant frequency decreased significantly for a small tuning force. It showed a larger decrease than the simulation results suggested. Furthermore, the Q-factor of the generator dropped a lot as the resonant frequency decreased, i.e. the compressive load increased, which is a fatal drawback for this method as a useful tuning mechanism.

It is concluded that applying axial tensile loads to a cantilever is the better method to tune the resonant frequency of the vibration-based micro-generator with a cantilever structure compared to applying axial compressive loads because an axial tensile load increases the Q-factor of the generator while an axial compressive load decreases the Q-factor. In the next two chapters, more details will be given on designing a miniature tunable micro-generator using this tuning method and making the frequency tuning completely automatic, i.e. to make the tunable micro-generator work at its resonant frequency matching ambient vibration frequency at all times.

Chapter 5

Simulation, Optimization and Performance of a Tunable Electromagnetic Generator

5.1 Introduction

In Chapter 4, a preliminary test of resonant frequency tuning on an electromagnetic generator using a mechanical method has been presented. These test results verify the feasibility of tuning the resonant frequency of a vibration-based micro-generator with a cantilever structure by applying an axial force. As frequency tuning by applying tensile force has more advantages over frequency tuning by applying compressive force, in the following research, only frequency tuning by applying tensile loads are investigated. In this chapter, design of a miniature tunable electromagnetic generator tuned by applying a tensile force is detailed. The overview of the generator is first

addressed in Section 5.2. After that, methods of optimizing the magnetic field, including magnetic circuit theory, magnetic field theory and computer assisted simulation, are introduced in Section 5.3 to 5.6. All dimensions have been optimized so that the generator outputs the maximum power and has the maximum tuning efficiency using these methods. The target of this design is to build a tunable micro-generator smaller than 2 cm^3 in volume with the generator capable of producing $5V_{pp}$ output voltage when the generator is shaken at $0.59m{\cdot}s^{-2}$ ($60m\boldsymbol{g}$, $1\boldsymbol{g} = 9.8m{\cdot}s^{-2}$) with a tuning range of 70 to 100Hz. Performance of the optimized generator including tuning range, output power, Q-factor and the efficiency of the generator is given in Section 5.7.

5.2 Overview of Design

The electromagnetic micro-generator presented in this paper was designed by the author and has the similar electromagnetic layout as a generator previously developed as part of an EU funded research project 'VIBES' [23]. Compared to VIBES generator, this generator is slightly bigger and a tuning magnet is fixed to the free end of the cantilever so that mechanical tuning method can be applied. Figure 5.1 shows the overall design of the tunable vibration-based electromagnetic micro-generator. In Figure 5.1(c), a DIP-16 socket is placed next to the generator as a reference of its dimensions.

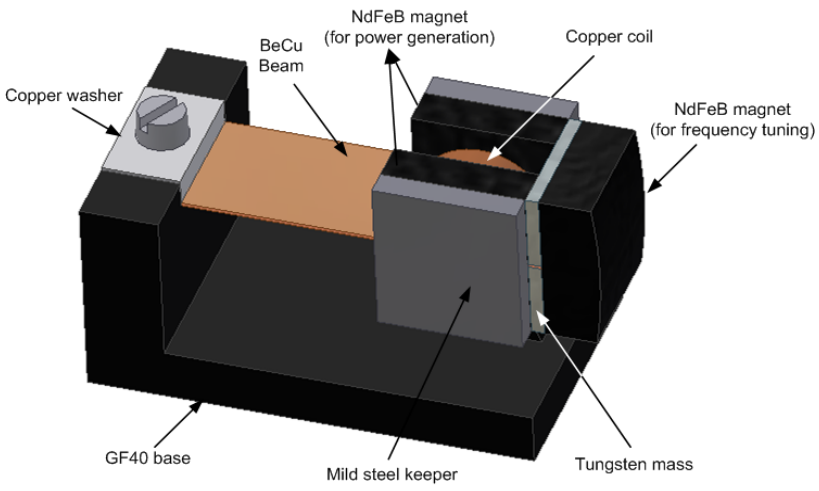

(a) Model

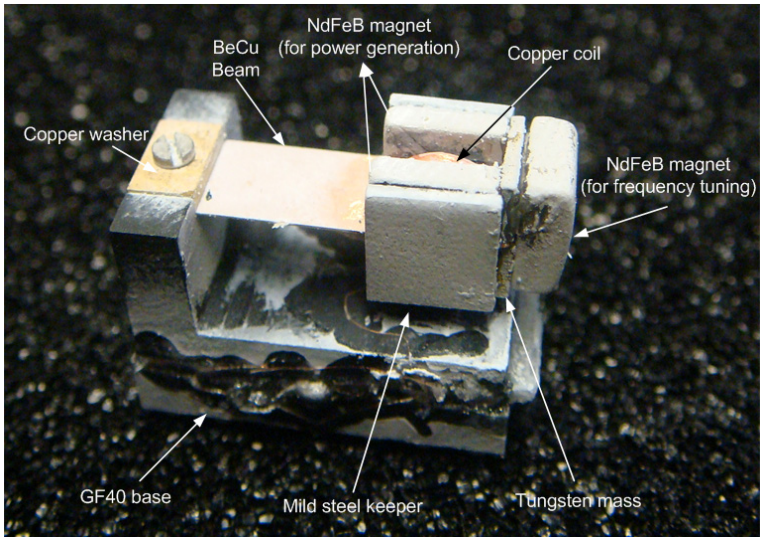

(b) Photo

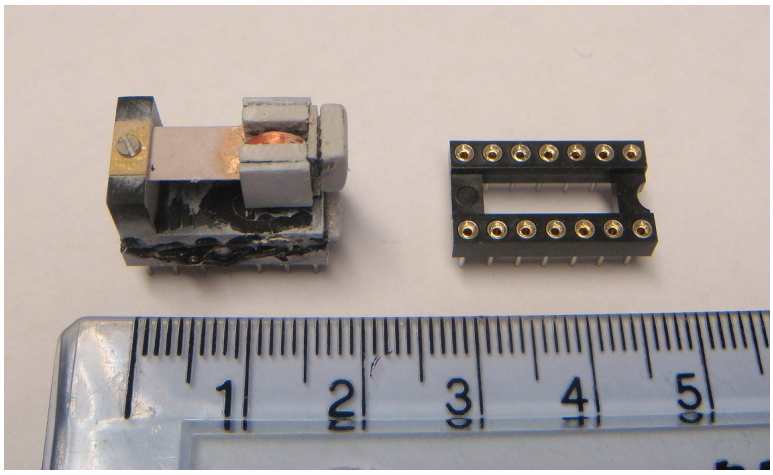

(c) Generator with indication of its dimensions

Figure 5.1. Tunable electromagnetic micro-generator.

5.2.1 Electromagnetic transducer

The magnetic circuit of this generator is shown in Figure 5.2. Two mild steel keepers were used to couple the magnetic flux between the top and bottom magnets, which ensured a uniform magnetic field within the air gap. Detailed analysis of the magnetic field will be given in Section 5.5. The coil was attached to the housing of the generator. The four-magnet structure was fixed to a cantilever beam and vibrated with the ambient vibration. The magnets moved with respect to the static coil so that the induced current was generated within the coil according to the Faraday's law.

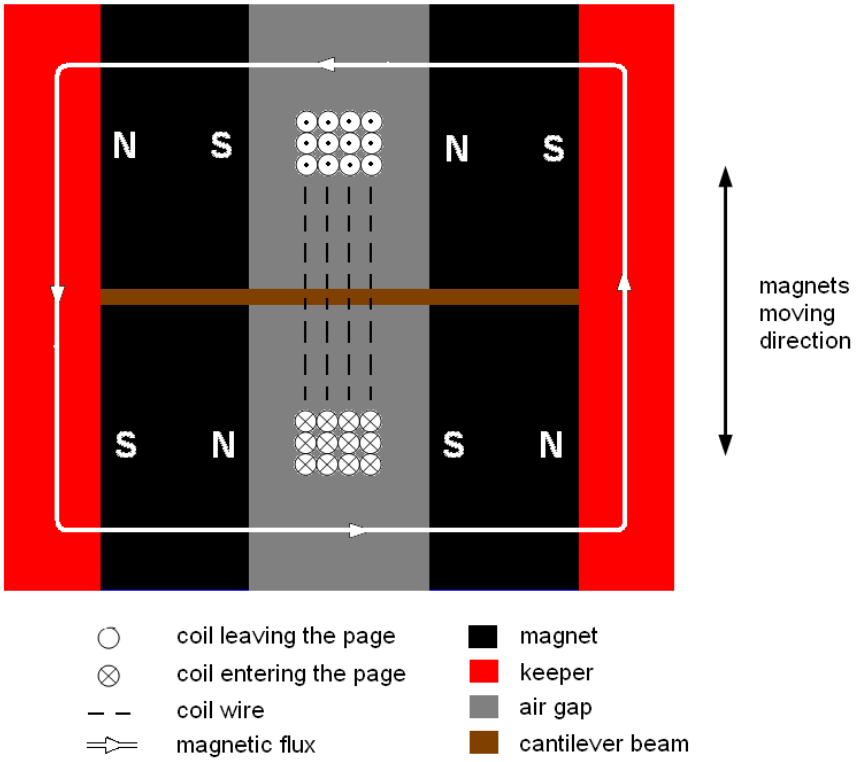

Figure 5.2. Cross section of the four-magnet arrangement.

5.2.2 Tuning mechanism

The schematic diagram of the tuning mechanism has been shown in Figure 4.6[1]. The generator and the tuning mechanism were mounted on the same housing so that there was no relative displacement between them. The tuning force was provided by the attractive force between two tuning magnets with opposite poles facing each other. One magnet was fixed at the free end of a cantilever while the other was attached to an actuator and placed axially in line with the cantilever. The tuning magnet attached to the actuator was larger than the one on the generator along the vibration direction so that they always overlap perfectly during operation. The distance between the two tuning magnets was adjusted by the linear actuator. Thus, the axial load on the cantilever was changed.

5.2.3 Micro-generator design

Each component of the generator was fabricated separately using conventional manufacturing processes. All magnets, mild steel keepers and additional tungsten mass were glued to the cantilever beam with cyanoacrylate with the aid of an

[1] Only the tensile force is applied in this case.

alignment jig. This assembly was then clamped onto the base using an M1 sized nut and a copper washer. The coil was bonded to the coil support pre-machined on the base. Table 5.1 summarizes materials for each component and the reasons for selection.

Table 5.1. Material of each component.

Component	Material	Reason for selection
Magnet	NdFeB	High energy density
Keeper	Mild steel	Ferromagnetic material
Additional mass	Tungsten alloy	High density
Beam	BeCu	Excellent fatigue characteristics
Base	Tecatron GF40	High rigidity, non ferromagnetic

5.3 Q-factor under tuning force

As mentioned in Section 3.2.2, a tuning mechanism should not reduce the Q-factor of the generator. In this section, the effect of the tuning force on the Q-factor of the generator is studied.

Figure 5.3 shows the forces on the resonator along the *z* axis. To make this figure easy to understand, the transducer is omitted as the tuning force is only applied on the tuning magnet 1 and it is assumed that the tuning magnet 1 has the overall mass of the generator. In addition, the resonator is assumed to travel only along the *z* axis to make the analysis simpler. Therefore, only forces along the *z* axis have to be studied. Additionally, it is assumed that the tuning forces on other directions than *z* direction do not affect the total damping.

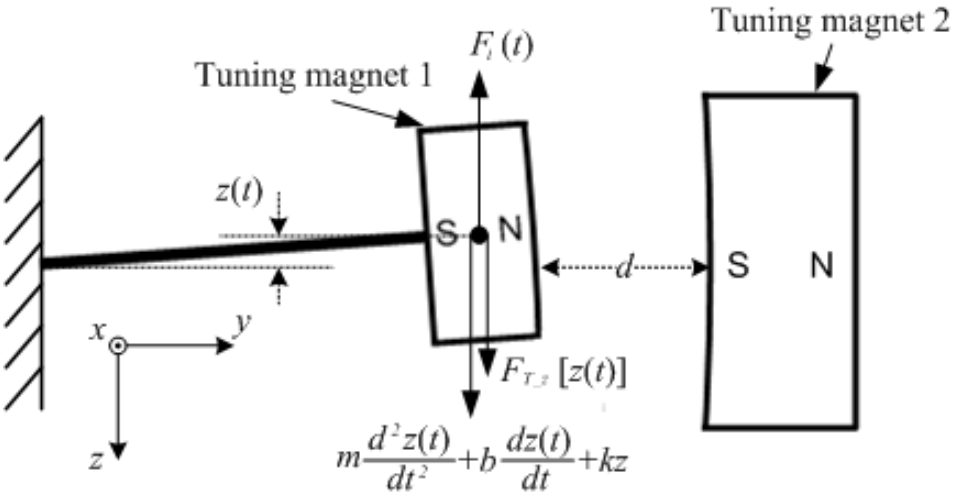

Figure 5.3. Forces on the resonator.

The dynamic model in this situation is given by:

$$m\frac{d^2z(t)}{dt^2}+b\frac{dz(t)}{dt}+kz(t)+F_{T\_z}[z(t)]=F_i(t) \tag{5.1}$$

where m, b, k, $z(t)$ are mass, damping coefficient spring constant and relative motion of the mass with respect to the housing, respectively. $F_{T\_z}[z(t)]$ is the z component of the magnetic force introduced by two tuning magnets, which can be calculated using Equation (4.7) with:

$$\phi=\frac{1}{2}\left(u_{ij}^2-w_{pq}^2\right)\cdot\ln\left(r-v_{kl}\right)+u_{ij}\cdot v_{kl}\cdot\ln\left(r-u_{ij}\right)+u_{ij}\cdot w_{pq}\cdot\tan^{-1}\frac{u_{ij}\cdot v_{kl}}{r\cdot w_{pq}}+\frac{1}{2}r\cdot v_{kl}$$

$$u_{ij}=(-1)^j\cdot A-(-1)^i\cdot a$$

$$v_{kl}=z(t)+(-1)^l\cdot B-(-1)^k\cdot b$$

$$w_{pq}=d+\frac{C+c}{2}+(-1)^q\cdot C-(-1)^p\cdot c$$

$$r=\sqrt{u_{ij}^2+v_{kl}^2+w_{pq}^2}\ .$$

and $F_i(t)$ is the inertial force on the mass, which is give by:

$$F_i(t) = -m\frac{d^2 z_h(t)}{dt^2} \tag{5.2}$$

where $z_h(t)$ is the displacement of the vibration source.

The Q-factor of the generator is given by:

$$Q = \frac{Z}{Z_h} \tag{5.3}$$

where Z and Z_h are the maximum values of $z(t)$ and $z_h(t)$, respectively.

As it is difficult to analytically solve the differential Equation (5.1), numerical methods can be used to obtain a numerical solution. In this case, the fourth-order Runge–Kutta method was adopted [100]. Figure 5.4 shows an example of the numerical solution to Equation (5.1). The waveform after the solution being converged was treated as an approximation to the actual solution.

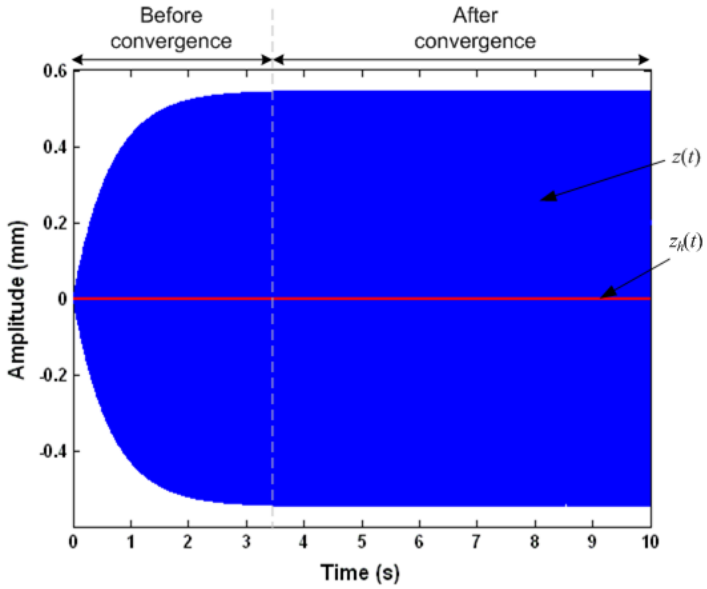

(a)

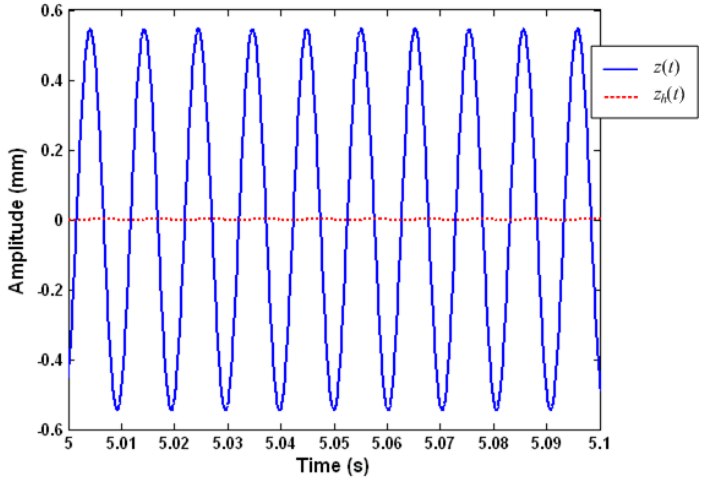

(b)

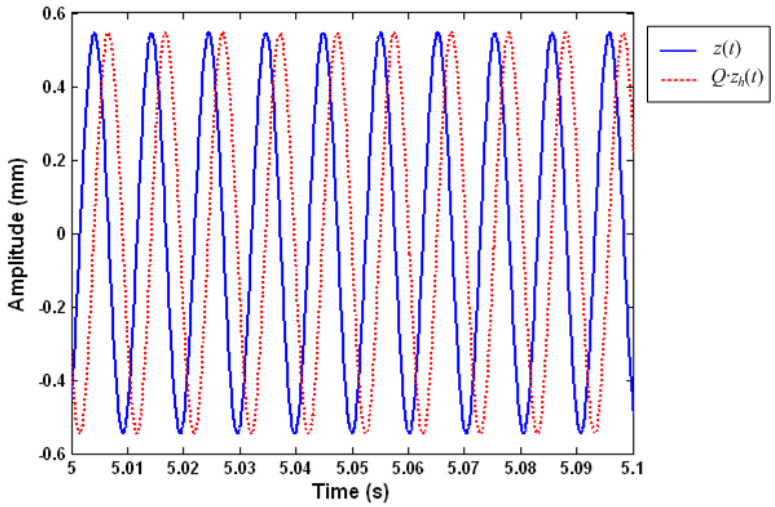

(c)

Figure 5.4. Numerical solution of differential Equation (5.1) (a) overall waveform (b) detailed waveform (comparison of amplitude) (c) detailed waveform (comparison of phase).

Figure 5.5 shows the numerical results of the Q-factor with various distances between the two tuning magnets and acceleration levels. It was found that as the excitation level became higher, the distance between two tuning magnets at which Q-factor of the generator started reducing significantly became smaller. In other words, when the excitation level becomes small, the tuning force capable of increasing total damping also becomes small. For a fixed distance between the two tuning magnets (tuning force), the higher the excitation level, the higher the Q-factor. For a fixed Q-factor, the higher the excitation level, the closer the two tuning magnets.

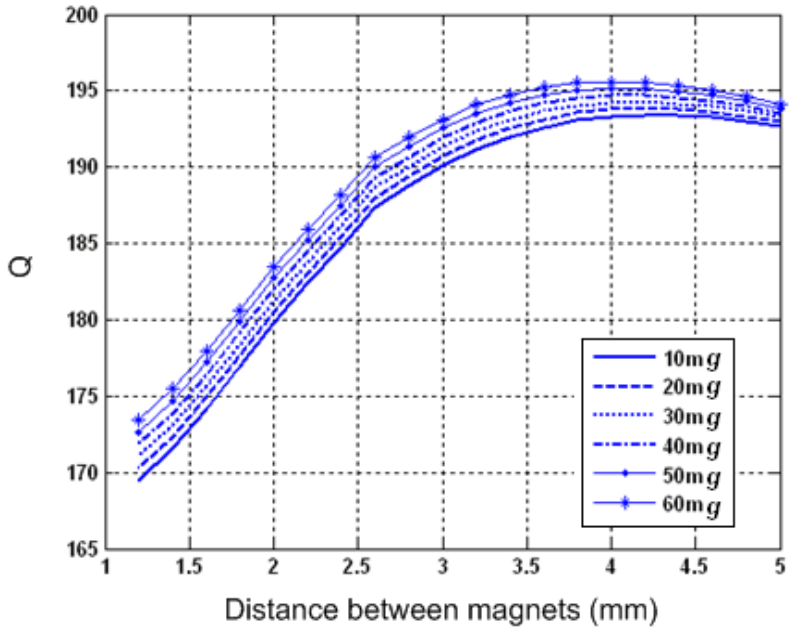

Figure 5.5. Q-factor with various distances between two tuning magnets and acceleration levels.

5.4 Cantilever Beam

5.4.1 Material Selection

Common materials used as beam materials include Single-Crystal Silicon (SCS) [101,102], Stainless Steel 320 Full Hard (SS320FH) [102,103] and Beryllium Copper (BeCu) [23] because of the cyclical stressing of the beam during operation.

Single crystal silicon is elastic to fracture and therefore will not change its material properties or dimensions as a result of being cyclically stressed. Silicon also does not suffer from fatigue failure. Silicon beams can be fabricated by DRIE etching through the thickness of a wafer. However, the Single-Crystal Silicon beams have been found to be too brittle to handle during assembly [23].

Both Stainless Steel 320 FH and BeCu have excellent elastic properties and fatigue characteristics without the brittleness of silicon. The metal beams are fabricated by a combination of photolithography and spray etching, which involves coating both sides of the metal sheet with a UV sensitive photoresist and using contact lithography to define the beam shape. The resist is developed after exposure, which leaves regions of

the metal sheet exposed to a Ferric Chloride etchant which is sprayed simultaneously to both sides. This etches through the exposed metal leaving the desired beam geometry. This is a straightforward batch fabrication process that enables numerous structures to be fabricated simultaneously on each metal sheet.

In this application, BeCu was selected as beam material for its excellent mechanical properties, in particular excellent fatigue characteristics.

5.4.2 Thickness

The resonant frequency of the generator depends on the dimensions of the beam and the inertial mass. For given inertial mass of 2.4g and a beam length of 13mm and width of 5mm, the untuned resonant frequency and tuning range when the tuning force changes from 1N to 6.67N as a function of beam thicknesses are shown in Figure 5.6. These results were obtained from a prestressed ANSYS modal analysis. It was found that the thinner the beam, i.e. the lower the spring constant of the cantilever, the lower the untuned resonant frequency and the larger tuning range. For this generator, a 120μm thick beam was chosen to give a predicted untuned resonant frequency of 45.2Hz and a tuning range from 66.4Hz to 108.8Hz.

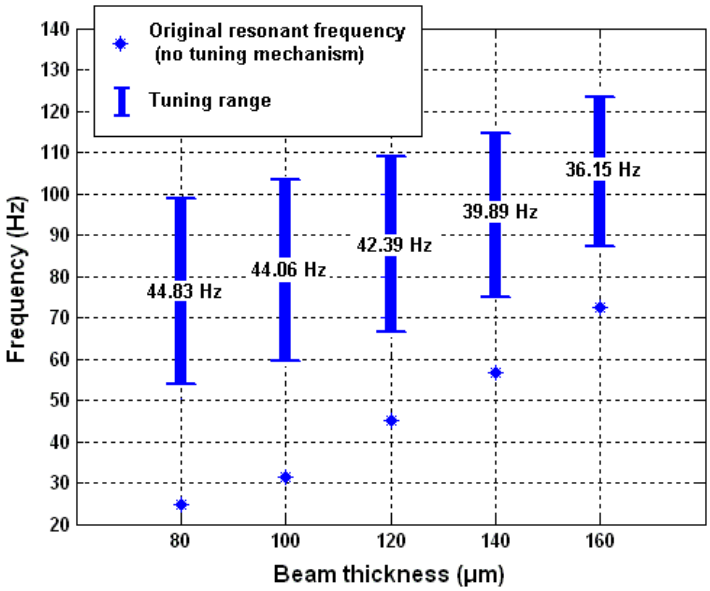

Figure 5.6. Base resonant frequency and tuning range with variation of beam thicknesses.

5.5 Analysis of the Magnetic Field in the Air Gap

The purpose of this analysis is to optimize the dimensions of the magnets and length of the air gap to maximize the magnetic flux density within the air gap. Three approaches have been used to conduct the magnetic field analysis: (1) magnetic circuit approach (2) analysis based on magnetic field theory and (3) computer assisted simulation. The first two approaches have been used to optimize the design and the last was used to verify the optimization.

5.5.1 Magnet Material Selection

Due to the limitation of the volume of the micro-generators, a magnetic material having a strong energy density is inevitable to achieve a high output power density. Most commonly used permanent magnet materials include Alnico magnet, Ceramic (ferrite) magnet and rare earth magnets such as samarium-cobalt (SmCo) and neodymium-iron-boron (NdFeB).

Alnico permanent magnets are made primarily from aluminum, nickel, cobalt, copper, iron and sometimes titanium. As it is mechanically strong, they can be either cast or sintered. It can be used in very high temperature, up to 524 to 549℃. Ceramic permanent magnets are composed of strontium carbonate and iron oxide. They are the least expensive material of the four but tooling is quite expensive. Due to its brittleness and manufacturing process, the shapes of magnets made of ceramic magnets have to be simple. Ceramic magnets have lower service temperature than alnico but higher than rare earth magnets. Permanent Samarium Cobalt magnets (SmCo) are composed of samarium, cobalt and iron. They are extremely strong for their small size, metallic in appearance and found in simple shapes such as rings, blocks and discs. They have good temperature stability and can be used in high temperature up to 250℃. However, SmCo is very expensive. As another rare earth magnet, Neodymium-iron-boron (NdFeB) materials have the similar mechanical properties as SmCo. They are the most powerful magnets in the world. Their working temperature is up to 120℃ and they are much cheaper than SmCo. The drawback is that NdFeB corrodes and they must be coated for long term maximum energy output [104].

NdFeB is therefore most suitable for this application. The remanence flux density (Br) and the relative permeability (μ_r) of NdFeB magnets are 1.23T and 1.1, respectively and its density is 7,500kg·m^{-3}.

5.5.2 Magnetic Circuit Theory

Most magnetic devices such as motors and generators consist of ferromagnetic materials that have a high relative permeability. Magnetic flux lines are continuous and form closed paths, which is similar to electric current and electric circuits. Therefore, concepts in electric circuits can be applied to solve their analogous magnetic circuit. Table 5.2 lists the analogy between electric and magnetic circuits. Table 5.3 and Table 5.4 list equations and laws for them, respectively [105, 106].

Table 5.2. Analogy between electric and magnetic circuits.

Electric	Magnetic
Conductivity, $\boldsymbol{\sigma}$ (Ω^{-1}·m^{-1})	Permeability, $\boldsymbol{\mu}$ (H·m^{-1})
Electric field density, $\boldsymbol{E}$ (V·m^{-1})	Magnetic field intensity, $\boldsymbol{H}$ (A·m^{-1})
Current density, $\boldsymbol{J}$ (A·m^{-2})	Flux density, $\boldsymbol{B}$ (T, Wb·m^{-2})
Current, $\boldsymbol{I}$ (A)	Magnetic flux, $\boldsymbol{\Psi}$ (Wb)
Electromotive force (*emf*) (voltage), $\boldsymbol{V}$ (V)	Magnetomotive force (*mmf*), $\boldsymbol{\mathcal{F}}$ (A)
Resistance, $\boldsymbol{R}$ (Ω)	Reluctance, $\boldsymbol{\mathcal{R}}$ (A·Wb^{-1})

Table 5.3. Equations for electric and magnetic circuits.

Electric	Magnetic
$emf = IR = \int E \cdot dL$	$mmf = \Psi R = \int H \cdot dL$
$I = \int_s J \cdot dS$	$\Psi = \int_s B \cdot dS$
Potential $\phi = \int E \cdot dL$	Potential $\Omega = \int H \cdot dL$
$E = -\nabla\phi$	$H = -\nabla\Omega$
$J = \sigma E$	$B = \mu H$

L: Length of the medium.

S: Cross-sectional area of the medium.

Table 5.4. Laws for electric and magnetic circuits.

	Electric	Magnetic
Ohm's Law	$R = \frac{V}{I} = \frac{L}{\sigma S}$	$\mathscr{R} = \frac{mmf}{\Psi} = \frac{L}{\mu S}$
	$V = EL = IR$	$mmf = HL = \Psi\mathscr{R} = NI$
Kirchhoff's Law	$\Sigma I = 0$	$\Sigma\Psi = 0$
	$\Sigma V - \Sigma RI = 0$	$\Sigma mmf - \Sigma\Psi\mathscr{R} = 0$

N: Number of turns of the coil.

I: Electric current in the coil.

As Kirchhoff's current and voltage laws can be applied in magnetic circuit, the rules for adding voltages and for combining series and parallel resistances also hold for *mmf*s and reluctance.

Thus, for *n* magnetic circuit elements in series

$$\Psi_1 = \Psi_2 = \Psi_3 = \cdots = \Psi_n \tag{5.4}$$

and

$$\mathscr{F} = \mathscr{F}_1 + \mathscr{F}_2 + \mathscr{F}_3 + \cdots + \mathscr{F}_n \tag{5.5}$$

Thus, for *n* magnetic circuit elements in parallel

$$\Psi = \Psi_1 + \Psi_2 + \Psi_3 + \cdots + \Psi_n \tag{5.6}$$

and

$$\mathscr{F}_1 = \mathscr{F}_2 = \mathscr{F}_3 = \cdots = \mathscr{F}_n \tag{5.7}$$

However, there are still some differences between electric and magnetic circuits. Firstly, magnetic flux does not flow as current does. Also, permeability, μ, varies with

flux density, B, in a magnetic circuit because there are normally ferromagnetic (nonlinear) materials used in magnetic devices while conductivity, σ, is independent of current density, J, in an electric circuit. Due to these differences, the magnetic circuit approach can only be an approximation in magnetic field analysis.

Recalling the magnetic circuit of this generator shown in Figure 5.2, its perspective view is shown in Figure 5.7 which can be represented as shown in Figure 5.8. $\mathcal{F}_1$, $\mathcal{F}_2$, $\mathcal{F}_3$ and $\mathcal{F}_4$ represent four identical magnets. $\mathcal{R}_{m1}$, $\mathcal{R}_{m2}$, $\mathcal{R}_{m3}$ and $\mathcal{R}_{m4}$ are their respective reluctance. $\mathcal{R}_{k1}$ and $\mathcal{R}_{k2}$ are reluctance of two keepers while $\mathcal{R}_{g1}$ and $\mathcal{R}_{g2}$ are reluctance of two air gaps.

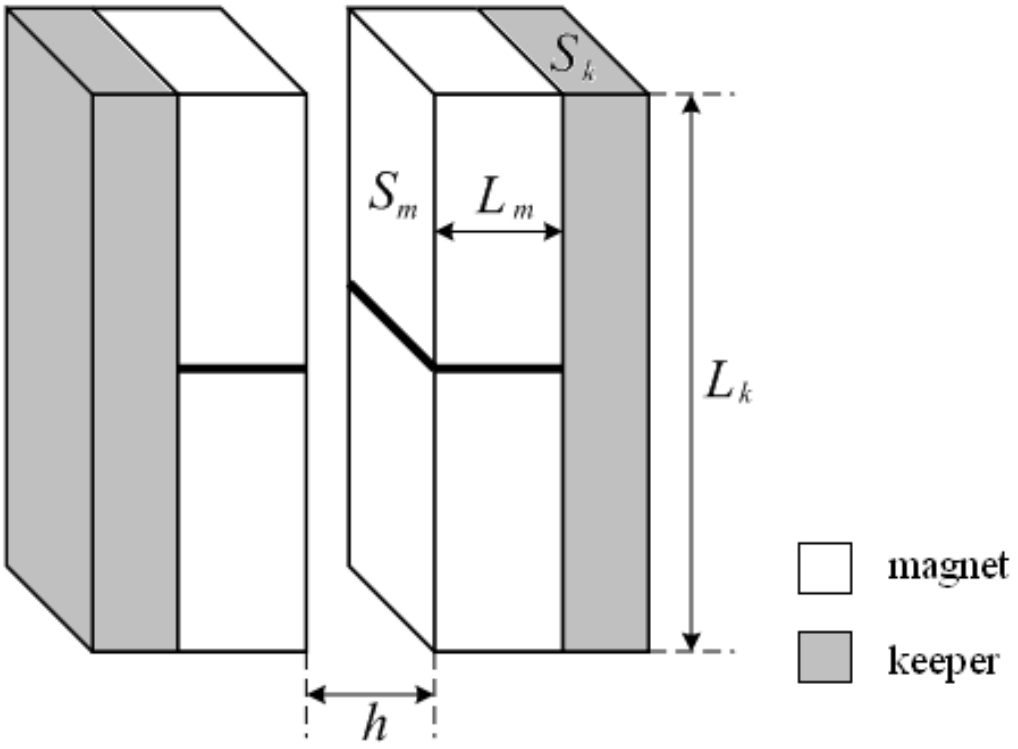

Figure 5.7. Perspective view of the magnetic circuit of the generator.

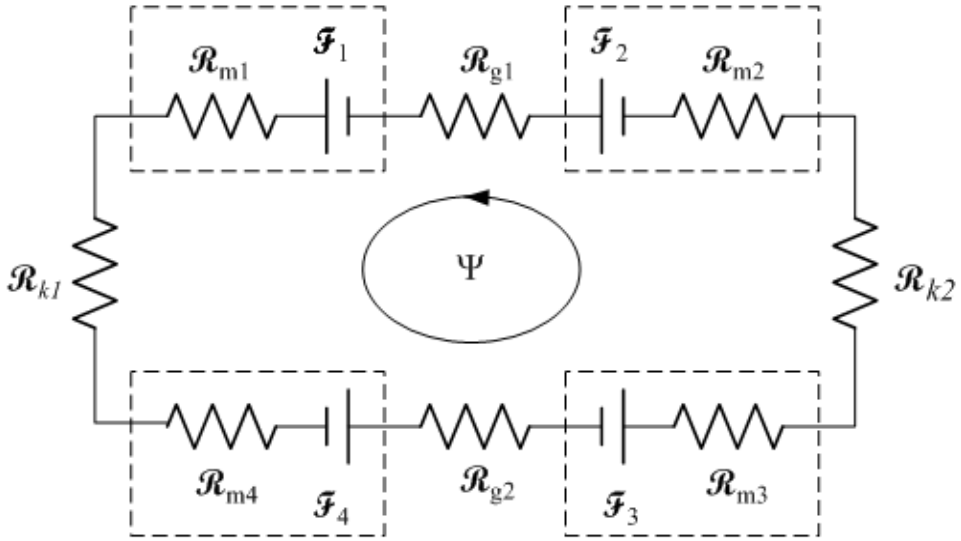

Figure 5.8. Magnetic circuit of the generator.

Magnetomotive forces of these magnets are given by:

$$\mathcal{F}_1 = \mathcal{F}_2 = \mathcal{F}_3 = \mathcal{F}_4 = H_c \cdot L_m = \frac{B_r \cdot L_m}{\mu_m \cdot \mu_0} \tag{5.8}$$

where H_c and B_r are magnetic coercivity and magnetic retentivity. L_m is the length of the magnet along the polarization direction. μ_m and μ_0 are relative permeability of the magnet material and the permeability of vacuum, respectively. Reluctances of these magnets are as follows:

$$\mathcal{R}_{m1} = \mathcal{R}_{m2} = \mathcal{R}_{m3} = \mathcal{R}_{m4} = \frac{L_m}{\mu_m \cdot \mu_0 \cdot S_m} \tag{5.9}$$

where S_m is the cross section area of the pole area.

Reluctances of the two keepers are given by:

$$\mathcal{R}_{k1} = \mathcal{R}_{k2} = \frac{L_k}{\mu_k \cdot \mu_0 \cdot S_k} \tag{5.10}$$

where L_k is the length of the keeper. μ_k are relative permeability of the keeper material and S_k is the cross sectional area of the keeper.

Reluctances of air gaps are given by:

$$\mathcal{R}_{g1} = \mathcal{R}_{g2} = \frac{h}{\mu_0 \cdot S_g} \tag{5.11}$$

where h is the length of the air gap. S_g is the effective cross sectional area of the air gap. Due to the flux fringing in the air gap, the effective cross sectional area of the air gap is a function of the length of the air gap (Figure 5.9).

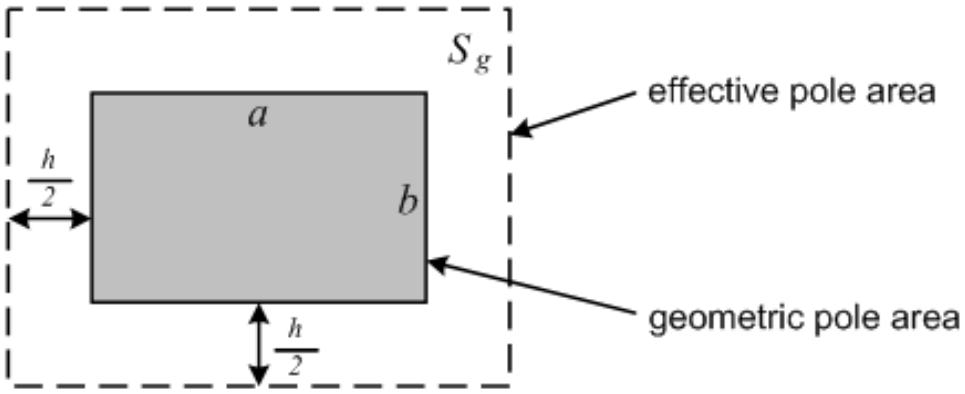

Figure 5.9. Effect of flux fringing on reluctance of the air gap.

Therefore, the magnetic flux, Ψ, in this magnetic circuit is given by:

$$\Psi = \frac{\mathcal{F}_1 + \mathcal{F}_2 + \mathcal{F}_3 + \mathcal{F}_4}{\mathcal{R}_{m1} + \mathcal{R}_{m2} + \mathcal{R}_{m3} + \mathcal{R}_{m4} + \mathcal{R}_{k1} + \mathcal{R}_{k2} + \mathcal{R}_{g1} + \mathcal{R}_{g2}} \tag{5.12}$$

The magnetic field flux density in the air gap is:

$$B = \frac{\Psi}{S_g} \tag{5.13}$$

5.5.3 Magnetic Field Theory

A bar magnet or a small current loop is usually referred to as a magnetic dipole. The magnetic field $\vec{B}$ at an observation point $P(r, \theta, \phi)$ due to a circular loop carrying current $\vec{I}$ as in Figure 5.10 is determined using the following method.

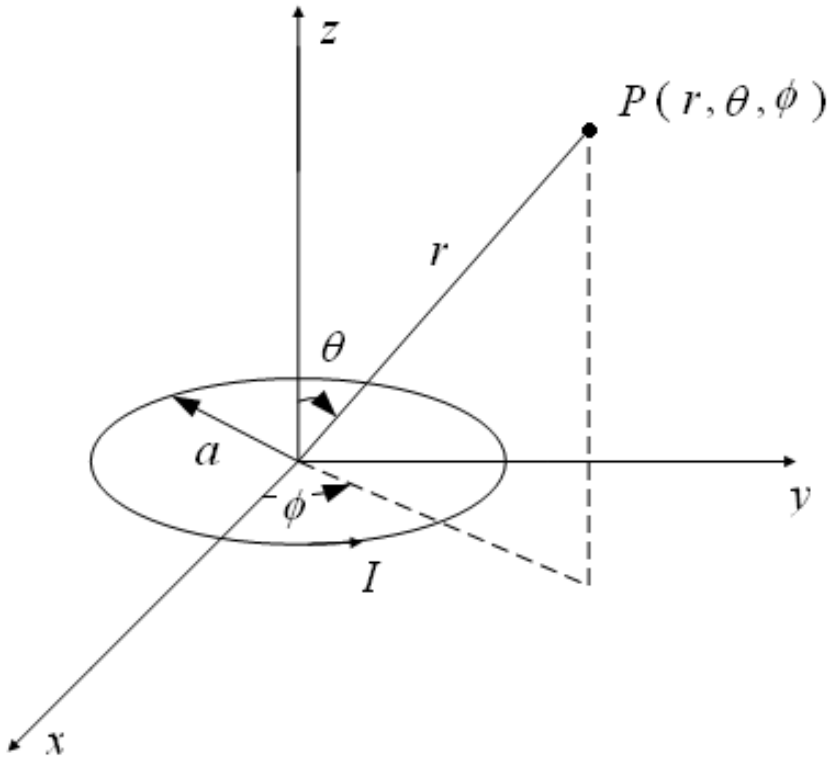

Figure 5.10. Magnetic field at *P* due to a current loop.

The magnetic vector potential at *P* is:

$$\vec{\Omega} = \frac{\mu_0 \vec{I}}{4\pi} \oint \frac{d\vec{I}}{r} \tag{5.14}$$

At far-field where $r >> a$, the loop appears small at the observation point. $\vec{\Omega}$ has only a ϕ-component given by:

$$\vec{\Omega} = \frac{\mu_0 I \pi \cdot a^2 \sin\theta}{4\pi \cdot r^2} \cdot \vec{e}_\phi \tag{5.15}$$

or

$$\vec{\Omega} = \frac{\mu_0 \vec{m} \times \vec{e}_r}{4\pi \cdot r^2} \tag{5.16}$$

where $\vec{m} = I\pi a^2 \vec{e}_z$ is the magnetic moment of the loop and $\vec{e}_z \times \vec{e}_r = \sin\theta \cdot \vec{e}_\phi$. The magnetic flux density $\vec{B}$ can be determined by:

$$\begin{aligned} \vec{B} &= \nabla \times \vec{A} \\ &= \frac{\mu_0}{4\pi \cdot r^2 \sin\theta}\left[\left(\frac{\partial}{\partial\theta} r\sin\theta A_\phi\right)\vec{e}_r + \left(-\frac{\partial}{\partial r} r\sin\theta A_\phi\right) r\vec{e}_\theta\right] \\ &= \frac{\mu_0}{4\pi \cdot r^2 \sin\theta}\left[\left(\frac{\partial}{\partial\theta}\frac{m\sin^2\theta}{r}\right)\vec{e}_r - \left(\frac{\partial}{\partial r}\frac{m\sin^2\theta}{r}\right) r\vec{e}_\theta\right] \\ &= \frac{2\mu_0 m\cos\theta}{4\pi \cdot r^3}\vec{e}_r + \frac{\mu_0 m\sin\theta}{4\pi \cdot r^3}\vec{e}_\theta \end{aligned} \tag{5.17}$$

There are alternative corresponding forms of $\vec{B}$, which are given by:

$$\vec{B}(\vec{r}) = \frac{\mu_0}{4\pi}\left[\frac{3(\vec{m}\cdot\vec{r})\vec{r}}{r^5} - \frac{\vec{m}}{r^3}\right] \tag{5.18}$$

and

$$\vec{B}(x,y,z) = \frac{\mu_0}{4\pi} m\frac{xz}{r^5}\vec{e}_x + \frac{\mu_0}{4\pi} m\frac{yz}{r^5}\vec{e}_y + \frac{\mu_0}{4\pi} m\frac{3z^2 - r^2}{r^5}\vec{e}_z \tag{5.19}$$

The magnetic field strength can be expressed as:

$$\vec{H}(x,y,z) = \frac{m}{4\pi}\cdot\frac{xz}{r^5}\vec{e}_x + \frac{m}{4\pi}\cdot\frac{yz}{r^5}\vec{e}_y + \frac{m}{4\pi}\cdot\frac{3z^2 - r^2}{r^5}\vec{e}_z \tag{5.20}$$

For a short permanent magnetic bar, the $\vec{B}$ lines are similar to those due to a small current loop (Figure 5.11). It can also be regarded as a magnetic dipole.

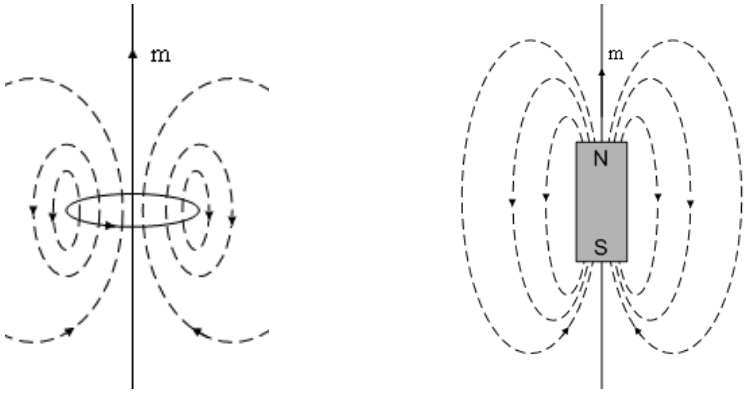

(a) (b)

Figure 5.11. The B lines due to magnetic dipoles: (a) a small current loop and (b) a bar magnet.

The dipole moment of a bar magnet is given by:

$$\vec{m} = Q_m \vec{l} \tag{5.21}$$

where $Q_m = M_p S_m$ is an isolated magnetic charge (pole strength) and $\vec{l}$ is the length of the bar. M_p is the magnetization.

In this situation, four magnets can be treated as four sets of magnetic dipole as shown in Figure 5.12. *P* is a random point within the air gap.

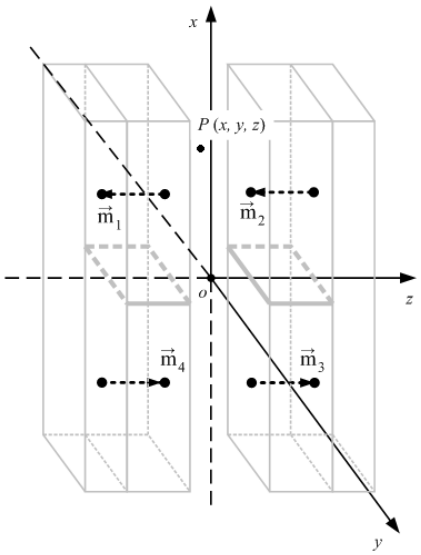

Figure 5.12. Four sets of magnetic dipole.

The total magnetic flux density at P, $\vec{B}_P$, is the sum of the magnetic flux density caused by four dipoles, i.e.:

$$\vec{B}_P = \vec{B}_{m1} + \vec{B}_{m2} + \vec{B}_{m3} + \vec{B}_{m4} \tag{5.22}$$

where $\vec{B}_{m1}$, $\vec{B}_{m2}$, $\vec{B}_{m3}$ and $\vec{B}_{m4}$ are the magnetic flux density caused by magnet m_1, m_2, m_3 and m_4, respectively.

In this particular case, only the magnetic flux density along the z axis is of interest. Therefore, the magnetic flux at P along the z axis, B_{Pz} is given by:

$$B_{Pz} = B_{m1z} + B_{m2z} + B_{m3z} + B_{m4z} \tag{5.23}$$

where B_{m1z}, B_{m2z}, B_{m3z} and B_{m4z} are the z components of $\vec{B}_{m1}$, $\vec{B}_{m2}$, $\vec{B}_{m3}$ and $\vec{B}_{m4}$, respectively. According to Equation (5.19), Equation (5.23) can be rewritten as:

$$B_{Pz} = \frac{\mu_0}{4\pi} m \sum_i^4 \frac{3z_i^2 - r_i^2}{r_i^5} \tag{5.24}$$

where r_i is the distance between P to the centre of the ith dipole and z_i is the projection of r_i on the z axis. The coordinate of the four dipoles are:

$$m1\left(h_m/2,\ 0,\ -(L_m + h)/2\right),$$

$$m2\left(h_m/2,\ 0,\ (L_m + h)/2\right),$$

$$m3\left(-h_m/2,\ 0,\ (L_m + h)/2\right),$$

and

$$m4\left(-h_m/2,\ 0,\ -(L_m + h)/2\right)$$

where h_m is the height of the magnet (dimension along x axis).

Hence z_i and r_i are as follows:

$$\begin{aligned} z_1 &= \left| z + {(L_m + h)}/{2} \right| \\ r_1 &= \sqrt{\left(x - {h_m}/{2} \right)^2 + y^2 + \left(z + {(L_m + h)}/{2} \right)^2} \end{aligned} \tag{5.25}$$

$$\begin{aligned} z_2 &= \left| z - {(L_m + h)}/{2} \right| \\ r_2 &= \sqrt{\left(x - {h_m}/{2} \right)^2 + y^2 + \left(z - {(L_m + h)}/{2} \right)^2} \end{aligned} \tag{5.26}$$

$$\begin{aligned} z_3 &= \left| z - {(L_m + h)}/{2} \right| \\ r_3 &= \sqrt{\left(x + {h_m}/{2} \right)^2 + y^2 + \left(z - {(L_m + h)}/{2} \right)^2} \end{aligned} \tag{5.27}$$

$$\begin{aligned} z_4 &= \left| z + {(L_m + h)}/{2} \right| \\ r_4 &= \sqrt{\left(x + {h_m}/{2} \right)^2 + y^2 + \left(z + {(L_m + h)}/{2} \right)^2} \end{aligned} \tag{5.28}$$

The average magnetic flux within the upper air gap (when x ≥ 0), B_{gap_u}, is given by:

$$B_{gap\_u} = \frac{\int_0^{h_m} \int_{-{w_m}/{2}}^{{w_m}/{2}} \int_{-{(L_m+h)}/{2}}^{{(L_m+h)}/{2}} B_{Pz} dz dy dz}{V_{gap}} \tag{5.29}$$

where w_m is the width of the magnet (dimension along y axis). As the device is symmetric with respect to plane yz, the average magnetic flux within the lower air gap (when x ≤ 0), B_{gap_l}, is identical to B_{gap_u}.

5.5.4 Computer Assisted Simulation

Compared to the two approaches discussed above, computer assisted simulation is the easiest and most straightforward method to analyze the magnetic field. There are

various software packages capable of such simulations, for example Ansoft Maxwell 3D [107], NISA EMAG [108], ANSYS Emag [109], INTEGRATED's CAE software [110], etc. For this application, Ansoft Maxwell 3D has been used to conduct the magnetic field simulation because of its availability, functionality and simpleness.

5.5.5 Optimization of Magnetic Field

Table 5.5 gives the magnetic constants used in the analysis. The magnet and keeper material used in the simulation is NdFeB 35 and steel, respectively.

Table 5.5. Magnetism constants.

Constant	Value	Constant	Value
H_c	$8.9 \times 10^5 A \cdot m^{-1}$	B_r	1.23T
μ_r	1.1	μ_0	$4\pi \times 10^{-7} N \cdot A^{-2}$
μ_k	4000		

The analytical results using both magnetic circuit and magnetic field theory agree with each other and have been verified in the Ansoft Maxwell 3D, which leads to the optimized dimensions of the magnets as shown in Table 5.6. After the optimization, the magnetic field within the air gap reached maximum under the restrictions of the total size and the resonant frequency of the generator. The simulation results in the Ansoft Maxwell 3D are shown in Figure 5.13.

Table 5.6. Optimized dimensions.

Variable	Value	Variable	Value
L_m	1.55mm	S_m	$16.5mm^2$
L_k	6.14mm	S_k	$5.5mm^2$
h	1.9mm	S_g	$25.5mm^2$

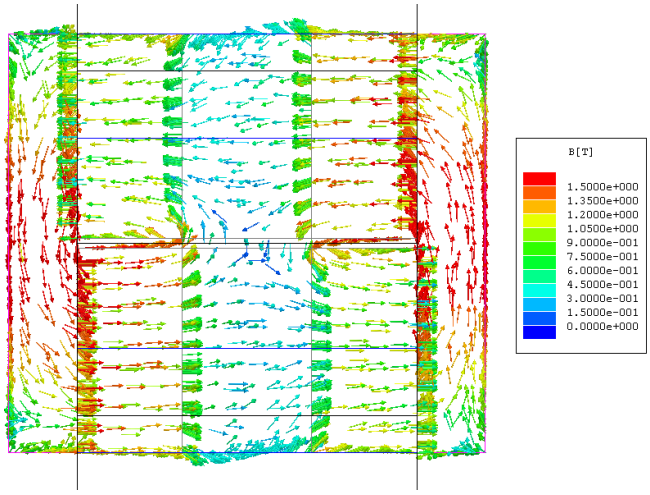

Figure 5.13. Simulation of magnetic field with optimal magnets dimension.

5.5.6 Effect of Tuning Magnets on the Magnetic Flux within the Air Gap

Compared to a previously designed generator, the main difference of this generator is the existence of the two tuning magnets. The effect these tuning magnets on the magnetic circuit of the four-magnet arrangement was simulated using Ansoft Maxwell 3D magnetic finite element (FE) software. Figure 5.14 compares the magnetic field of the generator with and without tuning magnets. It shows that magnetic flux within the air gap is barely affected by the tuning magnets. The simulation results indicate that the maximum flux density within the air gap is 0.45T.

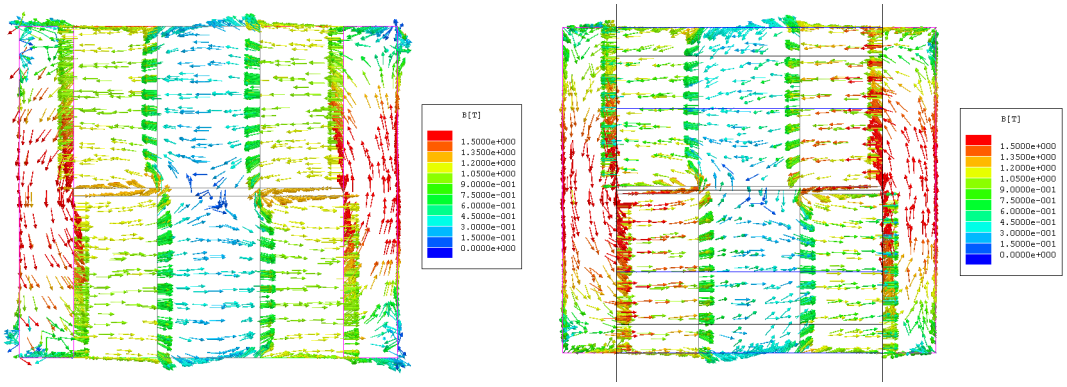

(a) (b)

Figure 5.14. Modelling of magnetic field (a) no tuning magnets (b) with tuning magnets.

5.6 Coil and Air Gap

5.6.1 Equations of coils

The number of the turns of a cylinder coil as shown in Figure 5.15 can be calculated by:

$$N = \frac{4F_c \cdot (R_o - R_i) \cdot t}{\pi \cdot d^2} \tag{5.30}$$

where F_c is the coil fill factor that is the ratio of the volume of conductor to the volume of the coil. R_o and R_i are the outer and inner radius of the coil, respectively. t is the total length of the coil and d is the diameter of the coil wire.

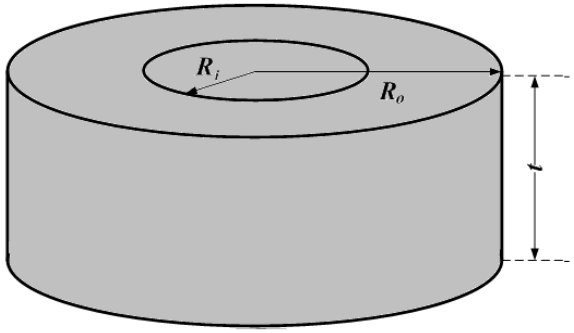

Figure 5.15. A Cylinder coil.

The coil resistance, R_c, is given by:

$$R_c = \rho \frac{L_c}{A} \tag{5.31}$$

where ρ is the electrical resistivity of the wire material, L_c is the total length of the coil wire and A is the cross area of the wire. The total wire length is:

$$L_c = \frac{4F_c \cdot (R_o^2 - R_i^2) \cdot t}{d^2} \tag{5.32}$$

The cross section area of the wire is:

$$A = \frac{\pi \cdot d^2}{4} \tag{5.33}$$

Substitution of Equation (5.32) and (5.33) into Equation (5.31) yields the formula of coil resistance can be rewritten as:

$$R_c = \rho \cdot \frac{16F_c \cdot \left(R_o^2 - R_i^2\right) \cdot t}{\pi \cdot d^4} \tag{5.34}$$

5.6.2 Optimization of Coil and Air Gap

According to Faraday's law, the induced voltage within the coil is given by:

$$V = -N\frac{d\Phi}{dt} \tag{5.35}$$

where N is the number of turns of the coil given by Equation (5.8) and $\frac{d\Phi}{dt}$ is the magnetic flux time gradient through the coil.

In order to maximize the induced voltage, the coil must have more turns while the magnetic flux gradient should be maximized. Given the limitation of generator space and winding tooling, the outer and inner radii of the coil are fixed. The wire diameter of 16 μm was chosen to give the coil more turns whilst still allowing winding. The fill factor is a function of the winding process and is typically 0.5 to 0.6. Therefore, the only parameter that can be changed to increase the number of turns is the coil thickness. Increasing the air gap can linearly increase the number of turns as shown in Figure 5.16. As the gap between the coil and the magnets is constant, the number of turns of the coil is also linear to the coil thickness. However, making the coil thicker means that the air gap between magnets has to be increased to avoid collision between the magnets and coil. Based on magnetic circuit theory, a larger air gap reduces the magnetic flux within the magnetic circuit as shown in Figure 5.18. Hence, there is a thus a tradeoff between coil thickness and magnetic flux through the coil. For a

constant gap between coil and magnets of 0.3mm, the simulation result shows that the optimum air gap and coil thickness are 1.9mm and 1.3mm, respectively. The maximum flux density within the air gap is 0.45T, which agrees with the simulation results in Ansoft Maxwell 3D discussed in Section 5.5.6. The estimated number of turns is 6950 when the fill factor is 0.5 and a voltage output of 8.1V as shown in Figure 5.18.

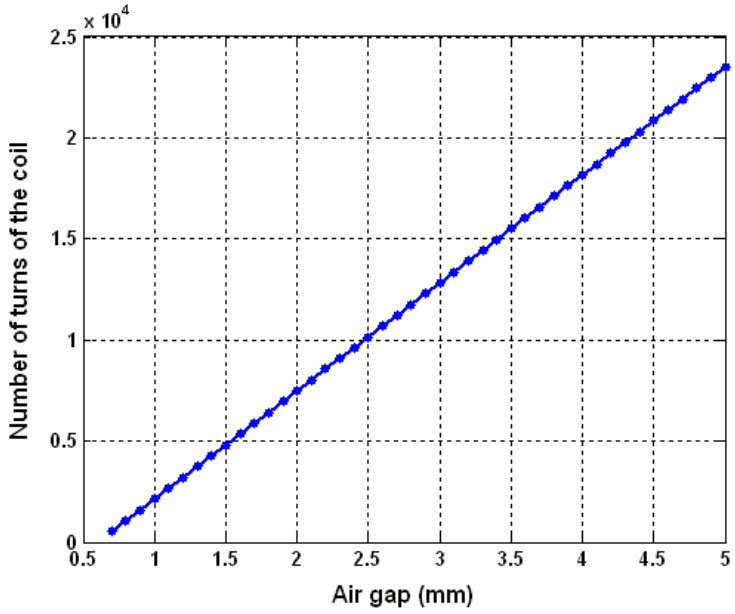

Figure 5.16. Coil turns with variation of air gap.

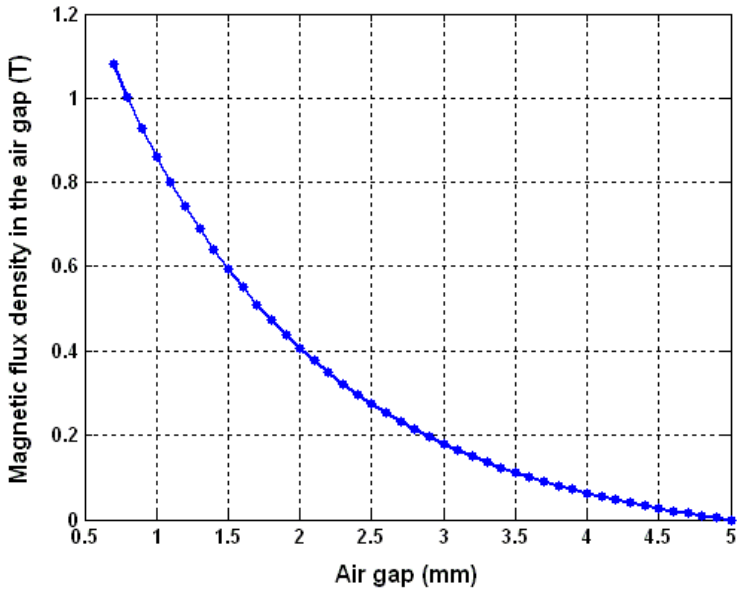

Figure 5.17. Magnetic flux density with variation of air gap.

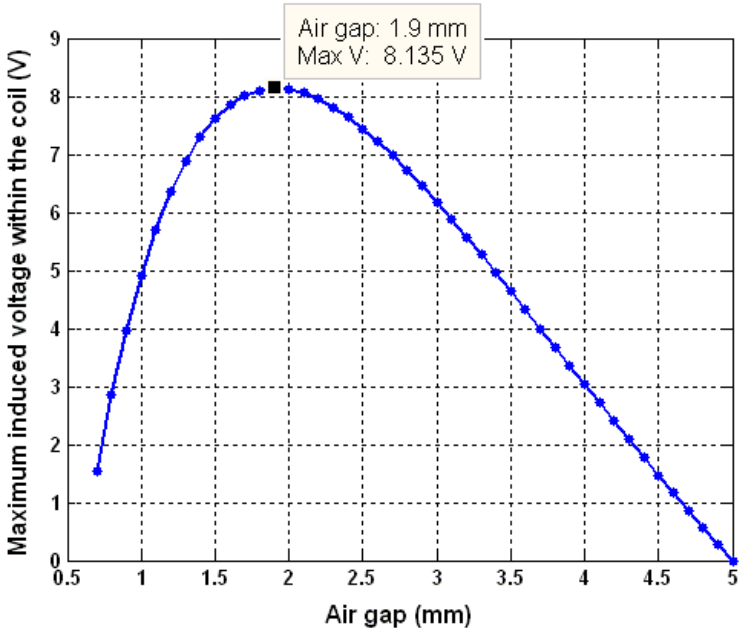

Figure 5.18. Maximum induced coil voltage with variation of air gap.

5.7 Performance of the Tunable Electromagnetic Generator

5.7.1 Test Setup

The test setup here is similar to the one in the preliminary test which has been detailed in Section 4.3.3. Briefly speaking, the generator was tested on a shaker with a programmable resistance box and a PC with LabVIEW collecting the data. The test platform of the system is shown in Figure 5.19. Tuning magnets (5) is attached to the free end of the cantilever resonator on the generator (4). The other tuning magnet (3) is fixed on a slider (2) which is able to slide along a track. The movement of the slider is controlled by the linear actuator (1). The linear actuator used here is a Haydon® 21000 Series Size 8 linear actuator, E21H4(AC)-5, which is the same one used earlier in the preliminary test discussed in Chapter 4.

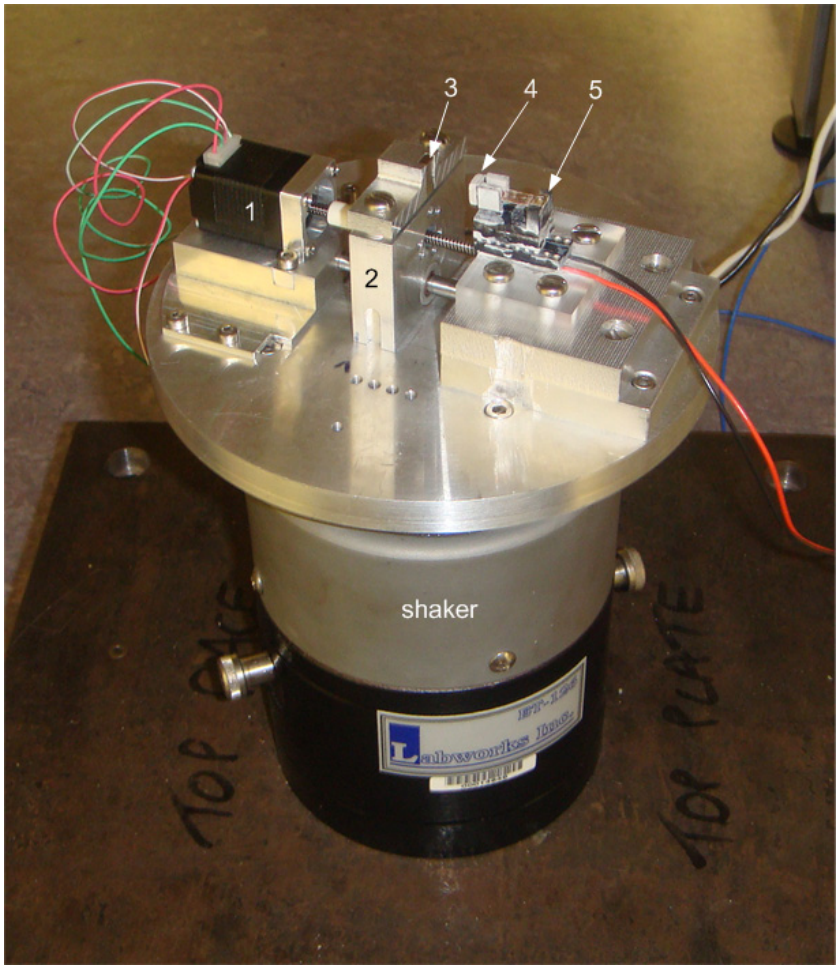

Figure 5.19. Test setup of the mechanically tunable electromagnetic generator.
(1. Linear actuator; 2. Slider; 3. Tuning magnet 1; 4. Tuning magnet 2; 5 Micro-generator.)

5.7.2 Resonant Frequency

The variation of the resonant frequency of the generator with the distance between the two tuning magnets is shown in Figure 5.20. The resonant frequency increases as the distance between the two tuning magnets is decreased, i.e. when the tuning force is increased as in Figure 5.21. The tuning range of the generator was from 67.6 to 98Hz when the distance between two tuning magnets was changed from 5 to 1.2mm. The test results followed the simulation results until the distance between two tuning magnets is less than 3mm. When this distance was less than 3mm, i.e. tuning force was larger than 2.87N, the resonant frequency increases less than indicated from simulation and approaches a limit. The reason for this is that when a tensile load much greater than the buckling force is applied to a beam, the resonant frequency approaches that of a straight tensioned cable and does not increase any more because

the force associated with the tension in the beam becomes much greater than the beam stiffness. The practical result agrees with this theoretical analysis.

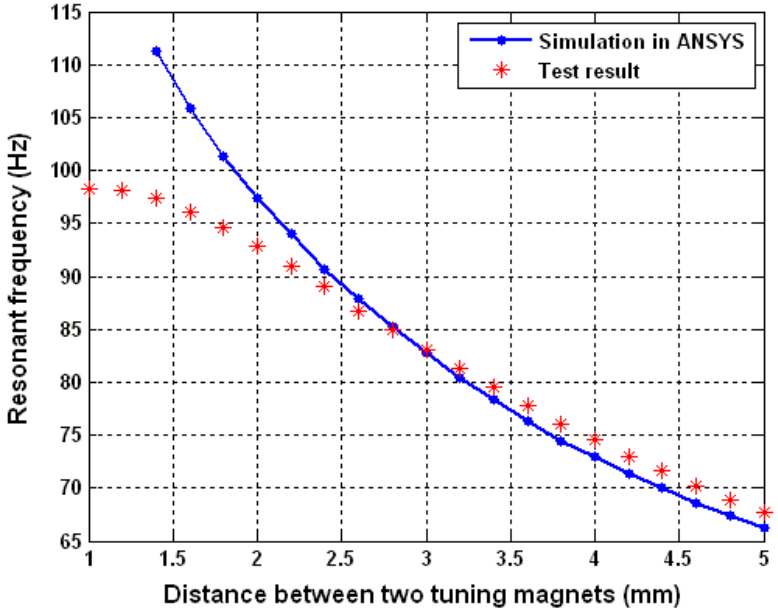

Figure 5.20. Resonant frequency with variation of distances between tuning magnets.

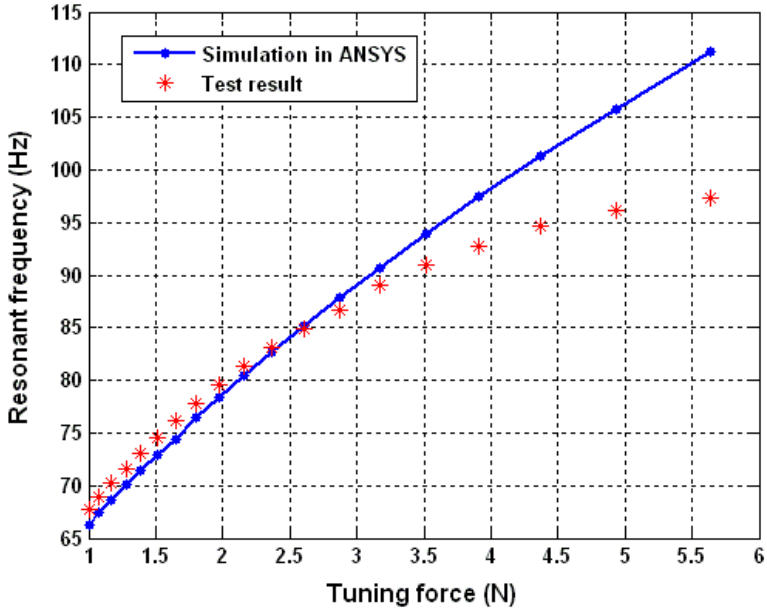

Figure 5.21. Resonant frequency with variation of tuning force.

5.7.3 Power Output

The maximum power at optimum resistive load at different resonant frequencies when

the micro-generator was excited at a vibration of 0.59m·s^{-2} is shown in Figure 5.22. It was found that the maximum output power dropped with the increase of the resonant frequency as predicted from Equation (2.16). However, when the two tuning magnets were less than 3 mm apart, i.e. when the resonant frequency was higher than 85Hz, the output power decreased more than expected. This result agreed with the test results of resonant frequency discussed in Section 4.1, which further proved that when the tuning force becomes too large, the total damping will increase and output power will reduce as predicted in Section 2.4.

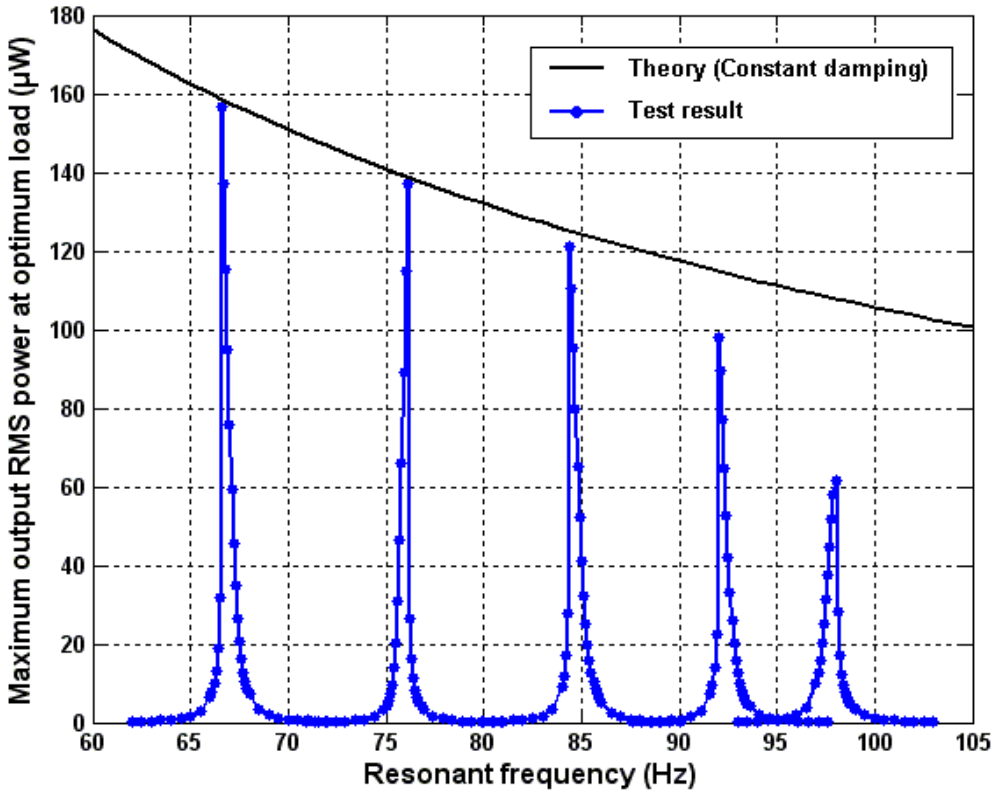

Figure 5.22. Output RMS power at optimum loads with variation of tuned resonant frequencies of the generator (excited at 0.59m·s^{-2})

Figure 5.23 shows the power spectra of the generator at optimum loads with variation of excitation level and resonant frequencies. It is found that the non-linearity of the generator became more and more apparent when the excitation level increased gradually. It is indicated from Figure 5.23 that the direction of the non-linearity[2] depends on the resonant frequency.

[2] Softening spring makes the spectrum lean to the left and hardening spring makes the spectrum lean to the right.

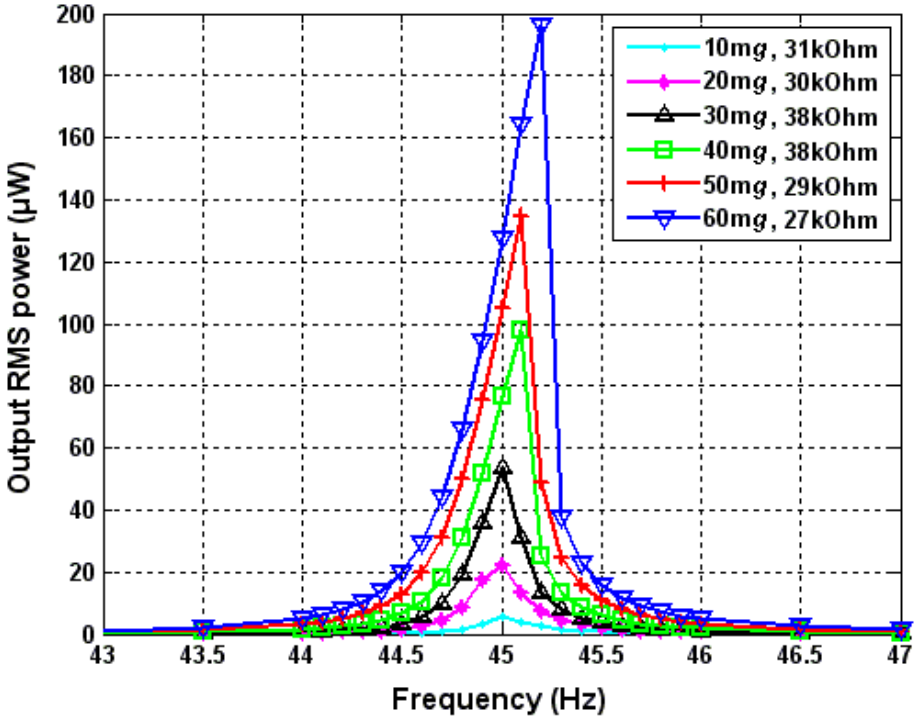
Output RMS power (μW)
Frequency (Hz)
10mg, 31kOhm
20mg, 30kOhm
30mg, 38kOhm
40mg, 38kOhm
50mg, 29kOhm
60mg, 27kOhm
0
20
40
60
80
100
120
140
160
180
200
43
43.5
44
44.5
45
45.5
46
46.5
47

(a) 45Hz

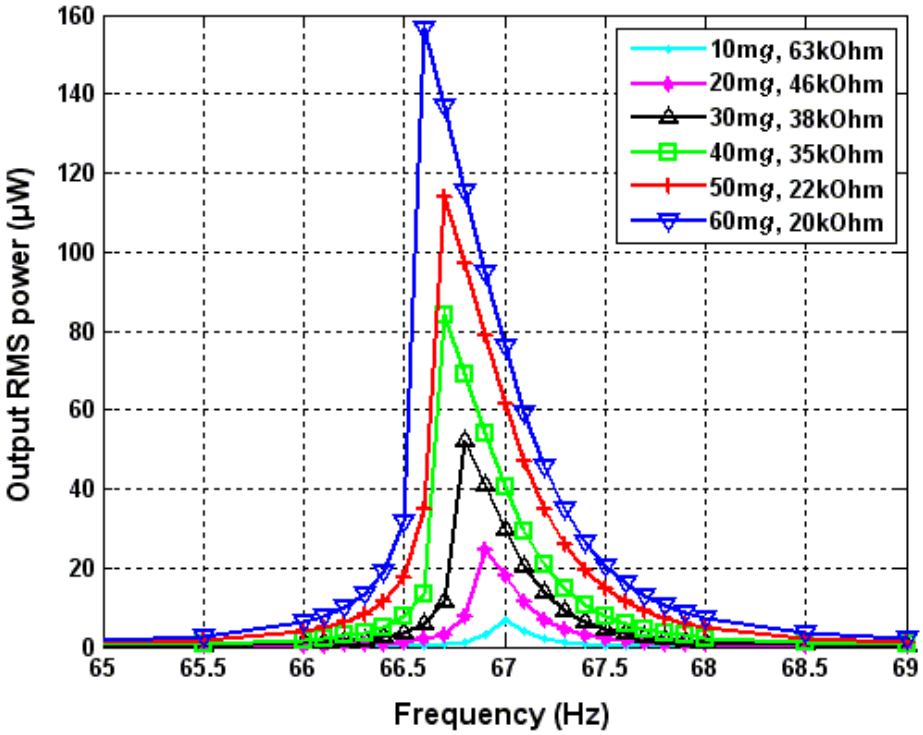
Output RMS power (μW)
Frequency (Hz)
10mg, 63kOhm
20mg, 46kOhm
30mg, 38kOhm
40mg, 35kOhm
50mg, 22kOhm
60mg, 20kOhm
0
20
40
60
80
100
120
140
160
65
65.5
66
66.5
67
67.5
68
68.5
69

(b) 67Hz

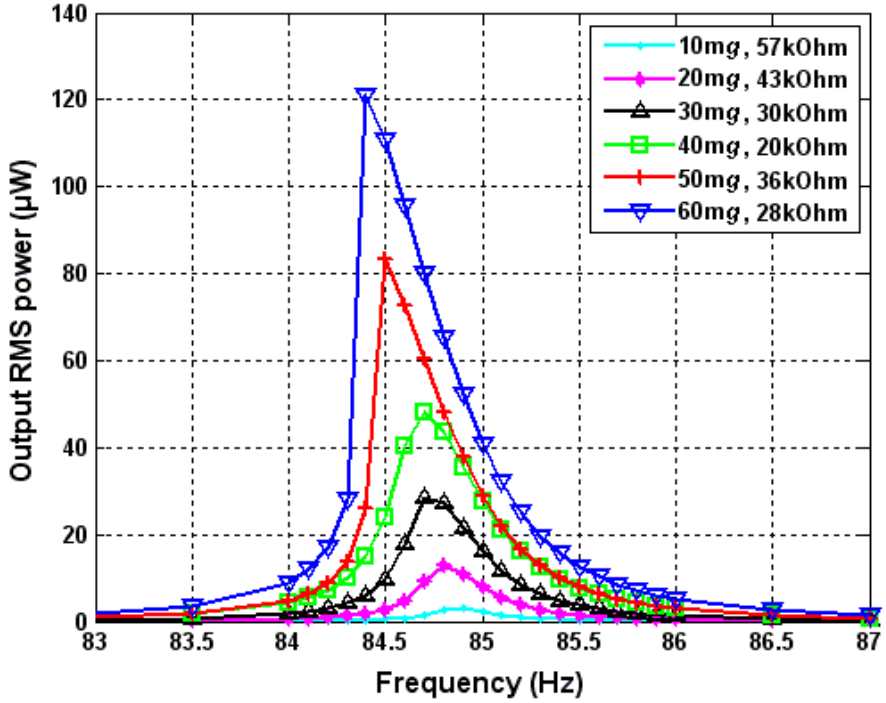

(c) 85Hz

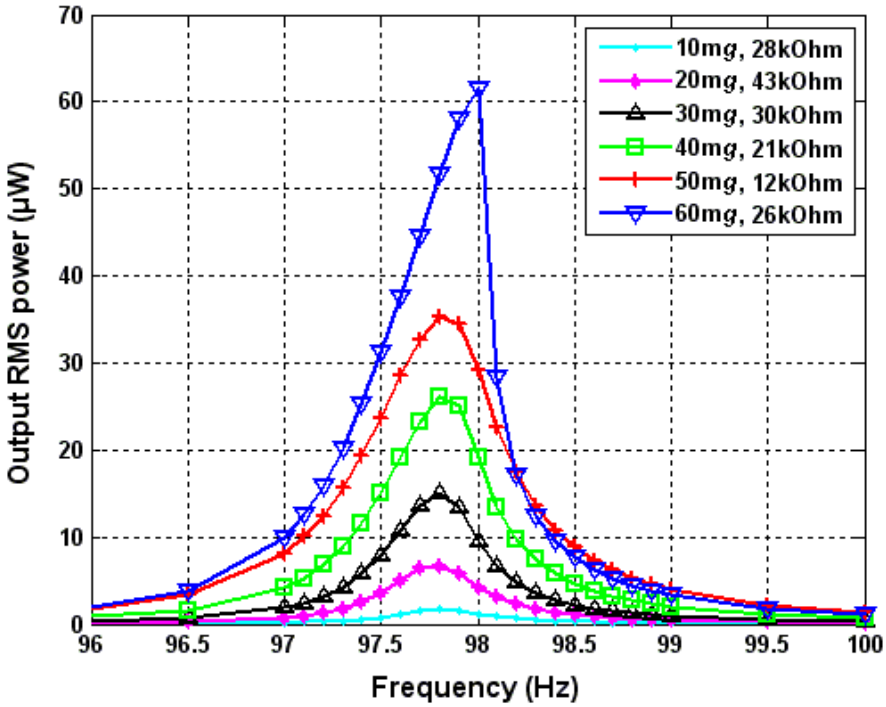

(d) 98Hz

Figure 5.23. Output RMS power at optimum loads with variation of excitation levels.

Figure 5.24 shows the maximum output RMS power at different excitation levels over the tuning range. It was found that the output power dropped by more than predicted

by the constant damping model at lower frequency if the excitation level was lower. In other words, the Q-factor drops at higher frequency if the excitation level is high, which agrees with the theoretical analysis in Section 5.3.

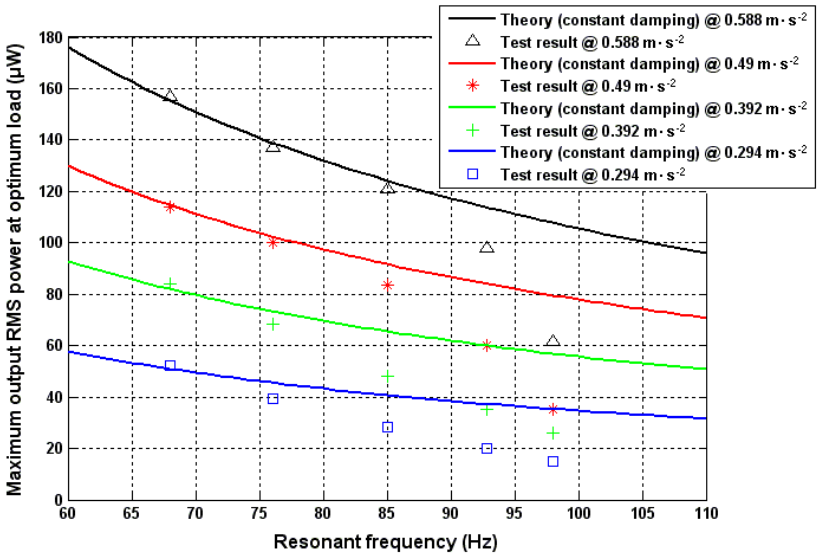

Figure 5.24. Maximum output RMS power at different excitation levels.

5.7.4 Output Voltage

Figure 5.25 shows the RMS voltage across the optimum load with the variation of vibration levels and resonant frequencies. The output voltage increased with the increase of excitation level and the decrease of resonant frequency.

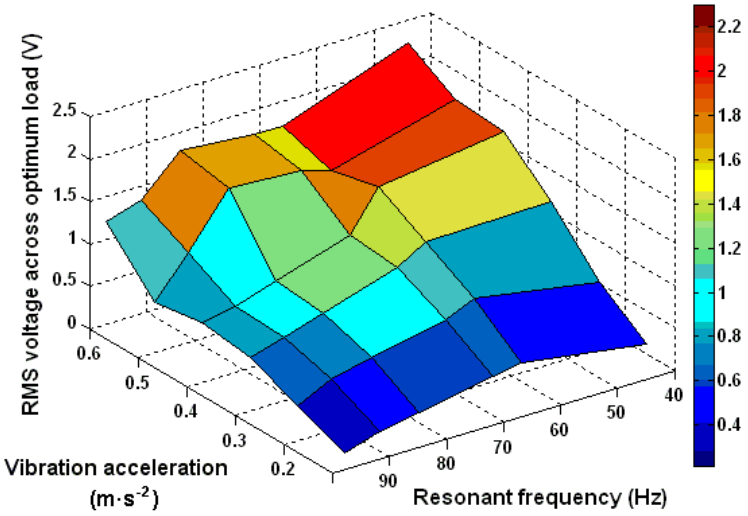

Figure 5.25. RMS voltage across optimum load with variation of vibration levels and resonant frequencies.

Figure 5.26 to 5.29 show the RMS open circuit output voltage of the generator and RMS voltage across the optimum resistive load at various resonant frequencies and excitation levels. It is found that the generator is able to output more than $2.5V_{RMS}$ at all resonant frequencies when open circuit. The voltage spectra become flat over a frequency band close to the resonant frequency under large excitations. The reason is that the displacement of the proof mass is so large that it hits the housing of the generator and thus the output voltage stops increasing.

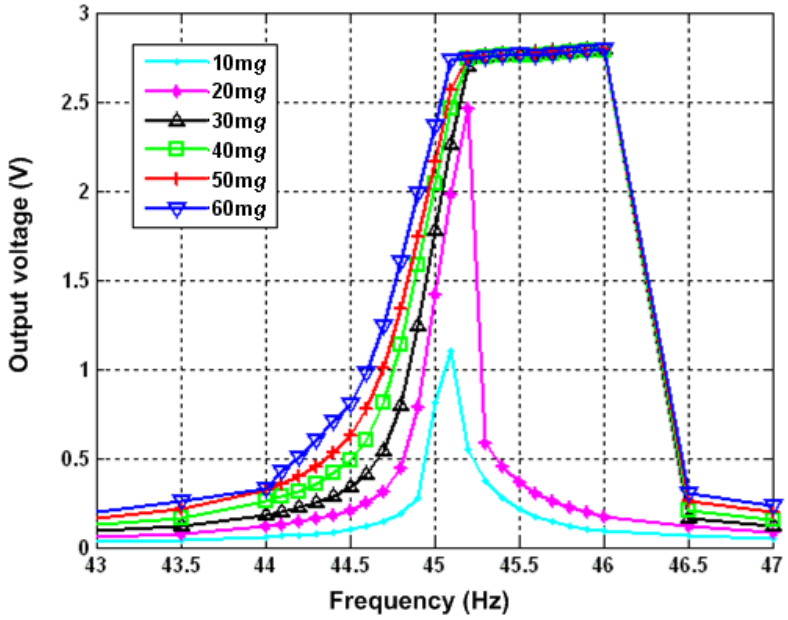

(a) Open circuit

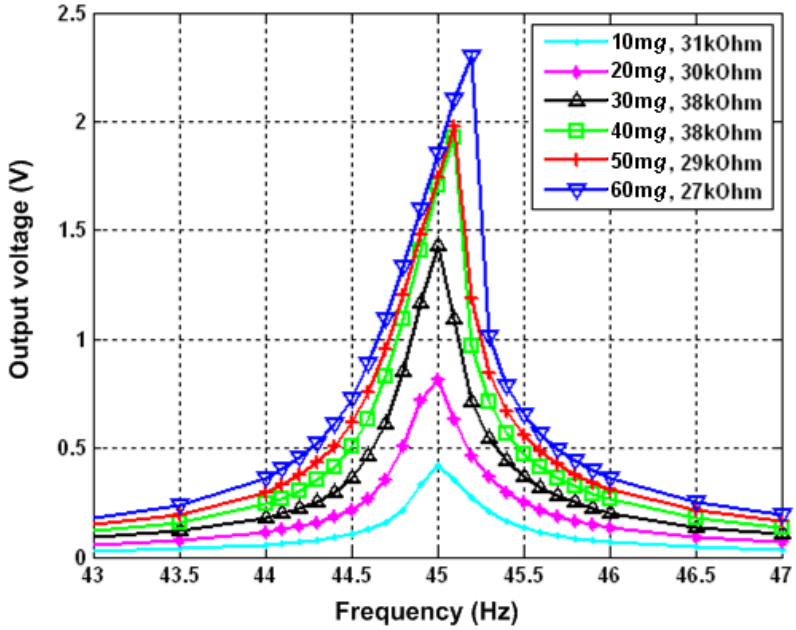

(b) Optimum load

Figure 5.26. RMS output voltage (45Hz).

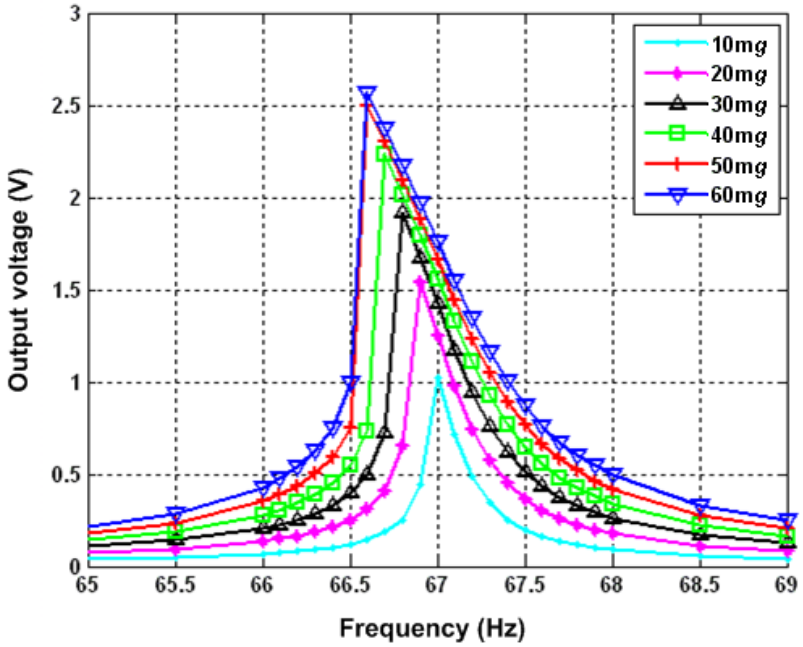

(a) Open circuit

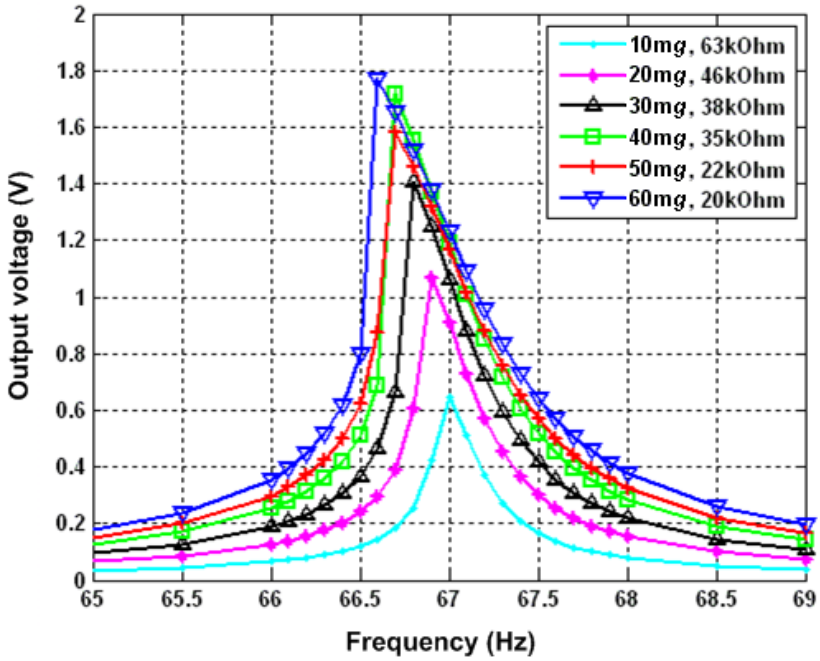

(b) Optimum load

Figure 5.27. RMS output voltage (67Hz).

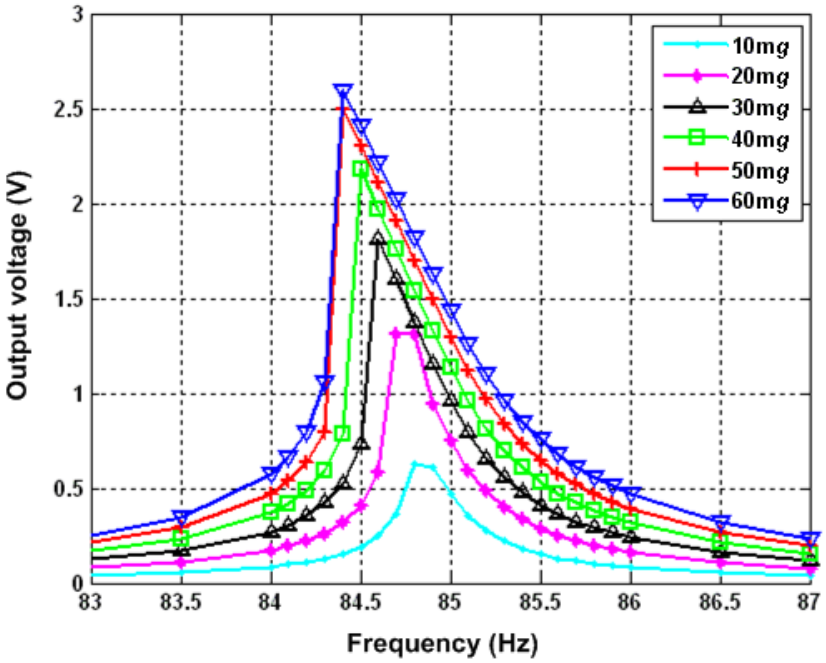

(a) Open circuit

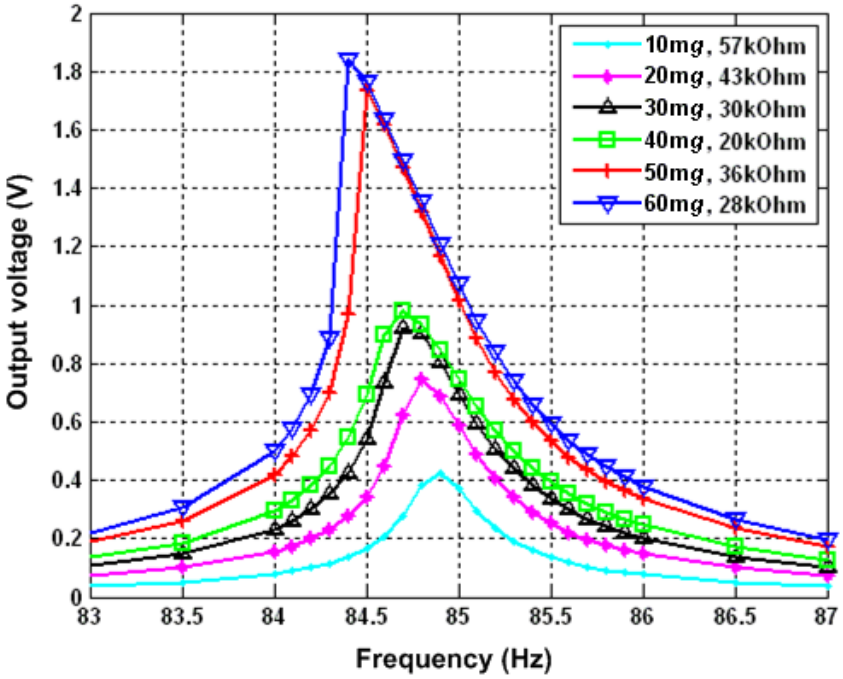

(b) Optimum load

Figure 5.28. RMS output voltage (85Hz).

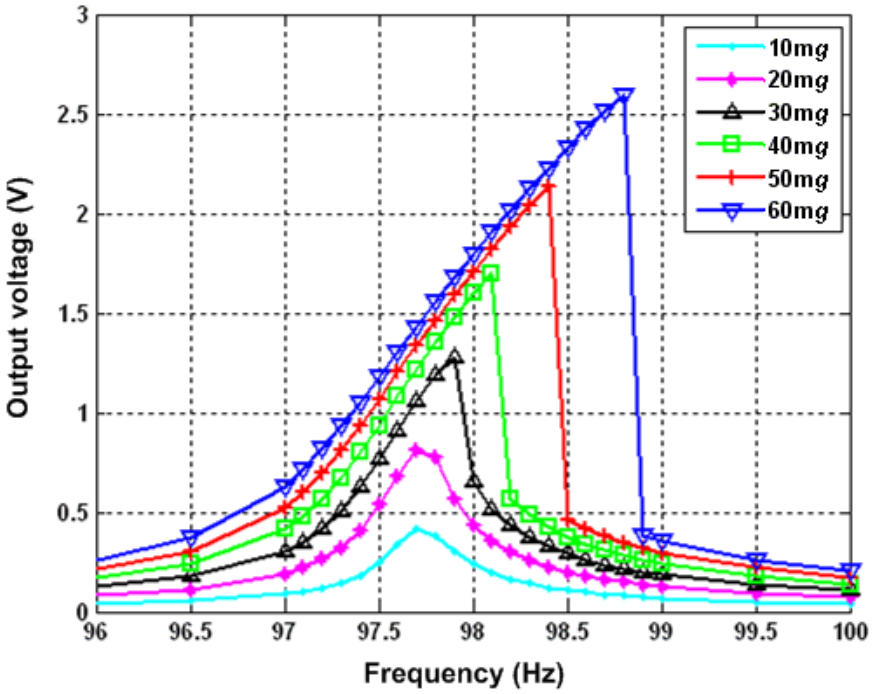

(a) Open circuit

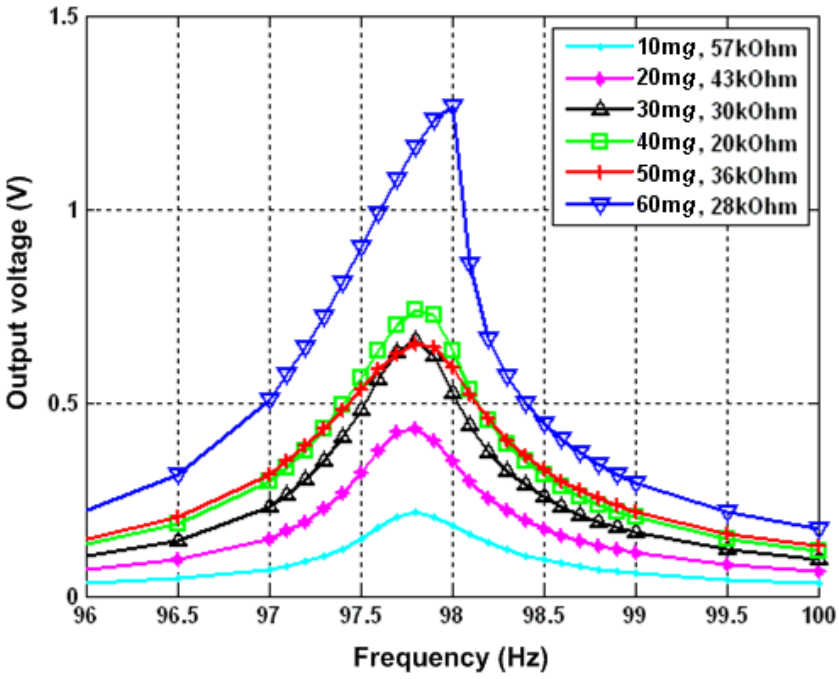

(b) Optimum load

Figure 5.29. RMS output voltage (98Hz).

5.7.5 Q-factor

The Q-factor of the generator is measured by observing the decay in the output voltage. Details of this method are given in Appendix B. Q-factor can be calculated from Equation (5.36) where f_0 is the frequency, V_1 and V_2 are the voltage amplitudes at a time interval Δt apart:

$$Q = \frac{\pi \cdot f_0 \cdot \Delta t}{\ln\left(\frac{V_1}{V_2}\right)} \tag{5.36}$$

The total Q-factor, Q_T, is the Q-factor measured when the generator is connected to the optimum load. The relationship between Q_T and the electrical and parasitic (mechanical) damping factors is given by (as Equation A.16):

$$\frac{1}{Q_T} = \frac{1}{Q_{OC}} + \frac{1}{Q_E} \tag{5.37}$$

where Q_{OC} is the open circuit Q-factor.

Figure 5.30 shows the Q-factors of the generator with various resonant frequencies under an excitation 0.59m·s^{-2}. It is found that the Q-factor reduces with the increase of the resonant frequency, i.e. the increase of the axial tensile force. This result agrees with the analysis in Section 5.3. However, the simulation results of the Q-factor in Section 5.3 are smaller than the Q-factors shown in the test. The reason is as follows. In the analysis in Section 5.3, the resonator is assumed to travel only along the vertical axis to make the analysis simple. This assumption means that the tuning magnet fixed to the free end of the cantilever is always in parallel with the movable tuning magnet. However, in practice, there is a small varying angle between these two magnets based on the position of the resonator during vibration. The magnetic force between two magnets is maximum when these two magnets are in parallel. Therefore, the actual magnetic force is smaller than predicted using the assumption above and the measured Q-factors are higher than predicted in the model described in Section 5.3.

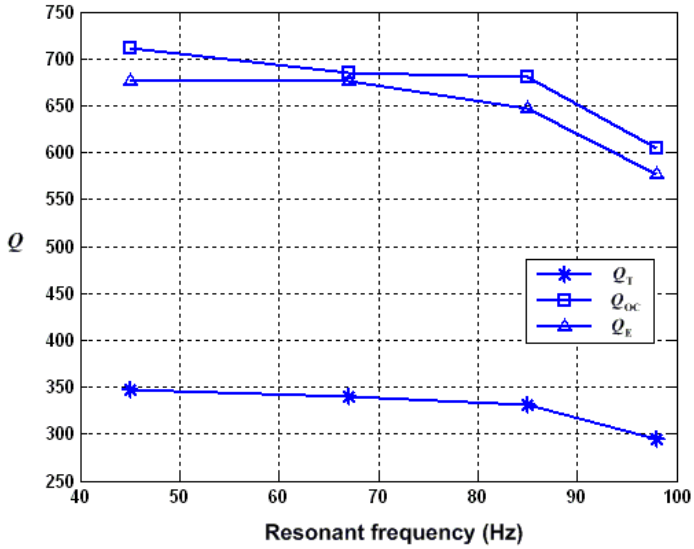

Figure 5.30. Q-factors of the generator with various resonant frequencies (0.59 m·s^{-2}).

5.7.6 Efficiency of the Generator

The efficiency of the generator, η_g, is the ratio of the power output in the optimum load, $P_{L,}$ to the maximum dissipated power within the damper, P, i.e.

$$\eta_g = \frac{P_L}{P} \tag{5.38}$$

Based on Equation (A.20), the maximum dissipated power within the damper can be written as:

$$P = \frac{ma^2}{2\omega_r} Q_T \tag{5.39}$$

Recalling the equation of the maximum power delivered to the resistive load, Equation (2.17) as:

$$P_L = P_e \cdot \frac{R_L}{R_L + R_c} = \frac{m \cdot a^2}{8\omega_r} \cdot Q_{OC} \cdot \frac{R_L}{R_L + R_c} \tag{5.40}$$

Substitution of Equation (5.39) and (5.40) into Equation (5.38) gives the expression of

the efficiency of the generator:

$$\eta_g = \frac{Q_{OC}}{4Q_T} \cdot \frac{R_L}{R_L + R_c} \tag{5.41}$$

Figure 5.31 plots the input power, predicted and measured output power with variation of resonant frequency when the generator is excited at 0.59m·s^{-2}. It shows that the generator is converting about 44% of the total power dissipated in the generator to electrical power delivered to the load.

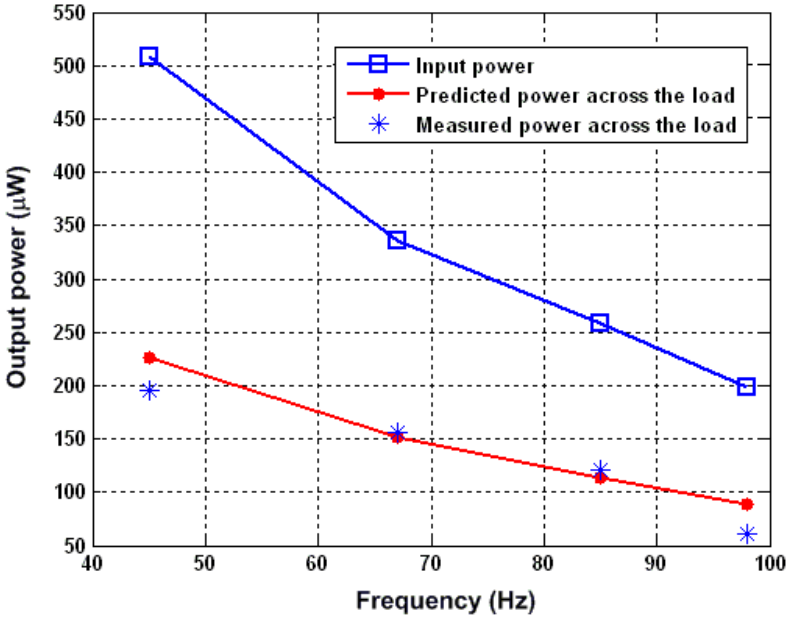

Figure 5.31. Comparison of theoretical and measured output power.

5.8 Conclusions

In this chapter, a tunable vibration-based electromagnetic micro-generator has been presented. Its resonant frequency can be tuned by applying an axial tensile load using a pair of tuning magnets. The design of the generator was optimized using magnetic circuit theory analysis, magnetic field analysis theory and computer assisted simulation in Ansoft Maxwell 3D.

The resonant frequency of the micro-generator can be tuned from 67.6 to 98Hz by changing the distance between two tuning magnets from 5 to 1.2mm, respectively.

The generator has an efficiency of 44% and delivered a power of 61.6 to 156.6μW to the electrical load over the tuning range when it was excited at a constant low vibration acceleration level of $0.59 m \cdot s^{-2}$. The generator is able to output more than $2.5 V_{RMS}$ at all resonant frequencies when open circuit.

It is found that when the tensile force became much greater than the buckling force, the resonant frequency increased less than predicted from simulation and approached a finite value. This is because that the force associated with the tension in the beam becomes much greater than the beam stiffness and the resonant frequency approaches that of a straight tensioned cable.

Importantly, it was found that the tuning mechanism does not affect the damping of the micro-generator over most of the tuning range. The maximum output power dropped with the increase of the resonant frequency as predicted. However, when the tuning force became larger than the inertial force caused by vibration, total damping was increased and the output power is less than that in the constant damping situation. In addition, it was found that an output power drops more than a constant damping model indicated occurred at a lower tuning force and hence, a lower frequency if the excitation level is lower. The reason is that when the excitation level becomes small, the tuning force capable of increasing total damping also becomes small. For a fixed tuning force, the higher the excitation level, the higher the Q-factor.

A closed loop control system developed to automatically tune the resonant frequency of this micro-generator according to ambient vibration will be presented in the next chapter.

Chapter 6

Closed-loop Resonant Frequency Tuning System

6.1 Introduction

In Chapter 5, a tunable electromagnetic micro-generator has been developed and tested. The generator was tuned by applying an axial tensile force. All the previous tests were based on manual tuning. In practical application where the frequency of ambient vibration changes occasionally, the tuning mechanism has to be automatic so that the resonant frequency of the micro-generator matches the ambient vibration frequency at all times. In Section 6.2, a closed loop frequency tuning system will be presented. It is able to detect the change in vibration frequency and take appropriate action to tune the resonant frequency of the micro-generator to match the new resonant frequency. Two tuning algorithms have been studied and compared. The duty cycle of the tuning system has also been analyzed. Finally, some guidelines to reduce

the duty cycle of the closed loop tuning system are discussed in Section 6.3.

6.2 Closed-loop Resonant Frequency Tuning System

6.2.1 System Description

The purpose of this system is to realize automatic frequency tuning. It can automatically detect the ambient vibration frequency and adjust the resonant frequency of the generator so that these two frequencies can match to make the generator produce maximum power. The tuning system can be switched between manual and automatic mode.

The tuning process is controlled by a microcontroller, schematically shown in Figure 6.1. The microcontroller detects the output voltage of the generator periodically and gives instructions to drive a linear actuator to adjust the distance between two tuning magnets and hence the tuning force. Thus, the resonant frequency of the micro-generator is changed. The microcontroller and linear actuator will ultimately be powered by the micro-generator itself. In this research, they were powered by a separate power supply to initially evaluate tuning principles and algorithms.

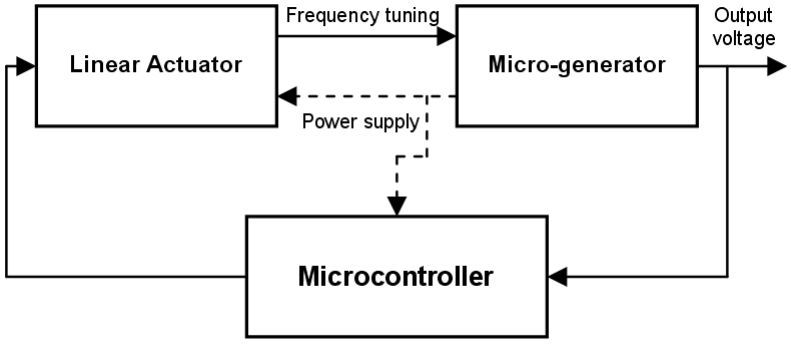

Figure 6.1. Block diagram of the closed loop tuning system.

6.2.2 Components in the System

As discussed earlier, the tuning system must consume as little power as possible. Although all components in this test were powered by an external power source, consuming less power is vital for future application. The system was aimed to be

designed as similar to the real situation as possible. Therefore, all components in the system have to be carefully selected to meet this requirement. The two main components in this tuning system are a microcontroller and a linear actuator.

Microcontroller PIC16F684 [111] of Microchip® is selected as the MCU. PIC16F684 is an 8-bit CMOS microcontroller with nanoWatt technology. It has an internal oscillator that has a wide range of software selectable frequency from 125kHz to 8MHz. A low frequency of 125kHz is selected in this application as lower internal oscillator frequency consumes less power. Its operating voltage is from 2V to 5.5V. As nanoWatt technology is involved in this microcontroller, it consumes very little power when it is in standby mode [112], which is important in this power limited application. Additionally, it integrates 8 channels of 10-bit ADC. The analogue output voltage from the generator can be injected to the microcontroller directly as feedback.

The linear actuator used in this system is the same one as used in the preliminary test, Haydon® 21000 Series Size 8 linear actuator, E21H4(AC)-5. The main specifications of this linear actuator are listed in Table 6.1.

Table 6.1. Main specifications of linear actuator E21H4(AC)-5.

Operating voltage	5V
Power	2.45W
Resolution	0.01mm/step
Speed	400step/second, i.e. 4 mm/second
Maximum static holding force	26N

6.2.3 Frequency Tuning Algorithm

As the designed generator has a high Q-factor and its spectrum is symmetrical with respect to the resonant frequency, when the ambient vibration frequency changes, it is important to know if the new frequency is higher or lower than the resonant frequency of the generator. Therefore, two algorithms have been developed and studied, i.e. voltage-only feedback and voltage-frequency feedback. The common idea behind the two algorithms is that they both consider the generator as working at resonance when the output voltage is maximum. The difference is that the second algorithm can also

detect change in vibration frequency to know if the vibration frequency is increased or decreased to save power consumed in tuning. Details and comparisons of these two algorithms are given below.

6.2.3.1 Voltage-only feedback

Figure 6.2 shows the flow chart of the voltage-only feedback algorithm. When the output voltage reaches maximum, the microcontroller assumes the micro-generator is working at resonance and stops the tuning mechanism. It switches to sleep mode to save power. The microcontroller then wakes up every duty cycle to monitor the output voltage and make a decision of whether it is necessary to trigger the tuning mechanism. If it is not necessary, the microcontroller reverts to sleep mode again.

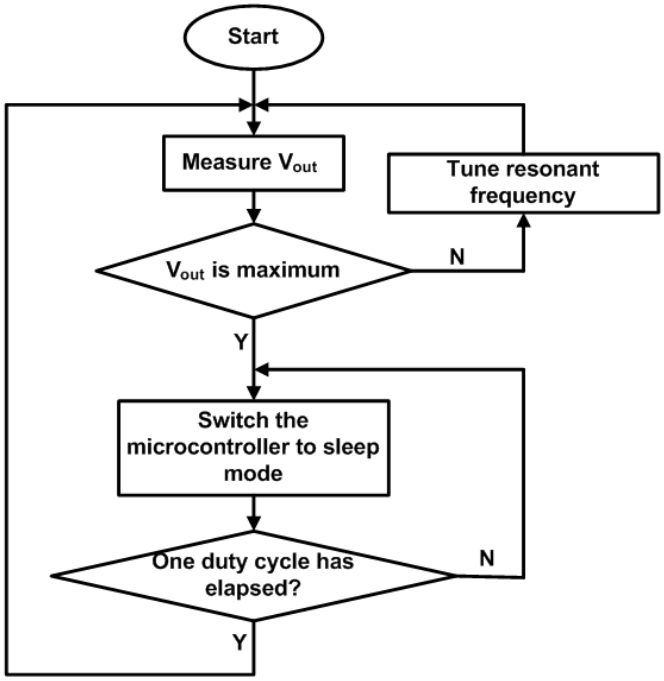

Figure 6.2. Flow chart of the voltage-only feedback algorithm.

As the desired generator has a high Q-factor and its spectrum is symmetrical with respect to the resonant frequency, when the ambient vibration frequency changes, it cannot know if the new frequency is higher or lower than the resonant frequency of the generator. Therefore, in this algorithm, the entire tuning range is traversed to find the one that matches the vibration frequency. A more detailed flow chart of this algorithm is shown in Figure 6.3.

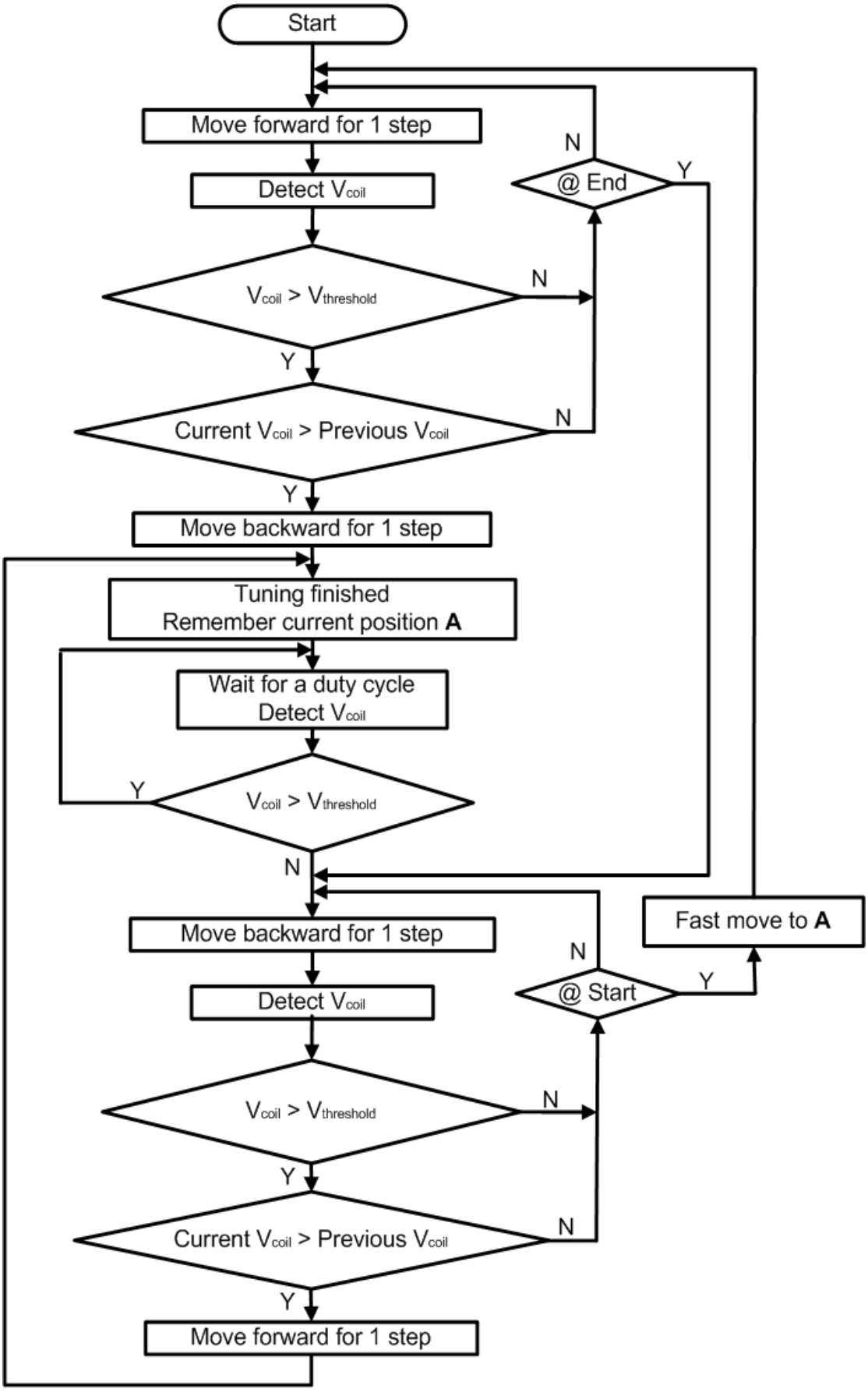

Figure 6.3. Detailed flow chart of the voltage-only feedback algorithm.

A start point and an end point are set first. The linear actuator is able to move the tuning magnet between the start and end points to cover the entire tuning range. The start point can be either the lower boundary or the higher boundary of the tuning range. Correspondingly, the end point is either the high boundary or the lower boundary of the tuning range. In this application, the start and end point means the lower and higher boundary of the tuning range, respectively.

Every time the system is reset, the program starts searching for the current vibration frequency from the start point. When the system starts running, the linear actuator gradually reduces the distance between the two tuning magnets, i.e. increasing the magnetic force and thus the resonant frequency of the generator. In the meantime, the microcontroller detects the output voltage at each resonant frequency and compares it to a preset threshold voltage, $V_{threshold}$. When the output voltage of the generator is higher than $V_{threshold}$, the microcontroller starts comparing the current output voltage to the previous output voltage. When the output voltage reaches maximum, i.e. the current output voltage is lower than the previous one and the previous one is higher than the second previous one, the generator is considered to work at its resonance, i.e. the resonant frequency matches the ambient vibration frequency. Then, the microcontroller stops the linear actuator and remembers the current position **A**. Meanwhile, it detects the output voltage every duty cycle. When the output voltage drops below $V_{threshold}$, it assumes the vibration frequency has changed and the microcontroller starts moving the tuning magnet towards the start point. If the stepper motor reaches the start point without finding the new resonant frequency, the new vibration frequency must be higher than the previous one. The linear actuator then quickly moves the tuning magnet to position **A** and searches for the new vibration frequency towards the end point. If the microcontroller cannot find the vibration frequency, it is most likely that the new vibration frequency is not within the designated tuning range. The linear actuator will wait for a duty cycle and search again towards the start point.

Briefly, the principle of this algorithm is that once the system is activated, it starts searching for the matched resonant frequency condition upwards. Any further attempts of frequency tuning start searching downwards. If there is no resonant frequency matching the vibration frequency, searches are conducted upwards again. In

principle, this algorithm sweeps the entire tuning range to find the matching resonant frequency in almost every tuning attempt. Therefore, it can also be called the frequency traversal algorithm. The drawback of this algorithm is that it is not able to distinguish changes in vibration frequency from changes in vibration acceleration when the output voltage drops, which may cause the mis-activation of the tuning system when only vibration acceleration is changed.

6.2.3.2 Voltage-frequency feedback

Figure 6.4 shows the flow chart of the voltage-frequency feedback algorithm. Its difference with the voltage-only feedback is that when the generator works at its resonance, it detects changes in frequency of the output voltage. If any increase or decrease in output frequency is detected, the system will increase or decrease the resonant frequency of the generator accordingly. If a change in vibration frequency has been detected but the system cannot tell if it is increased or decreased, the system will decrease the resonant frequency of the generator as default. A more detailed flow chart of this algorithm is shown in Figure 6.5.

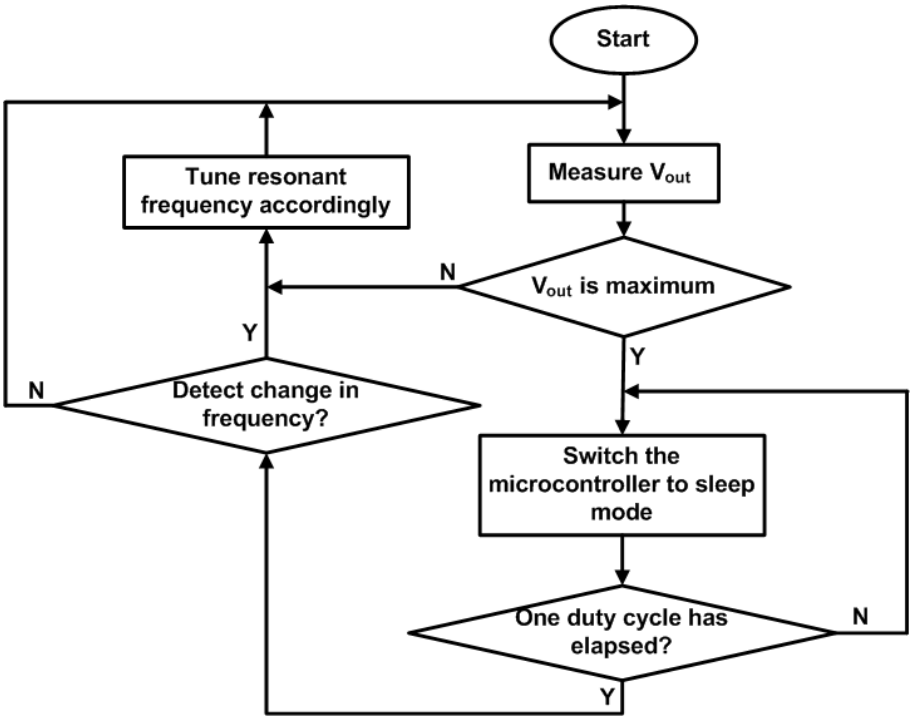

Figure 6.4. Flow chart of the voltage-frequency feedback algorithm.

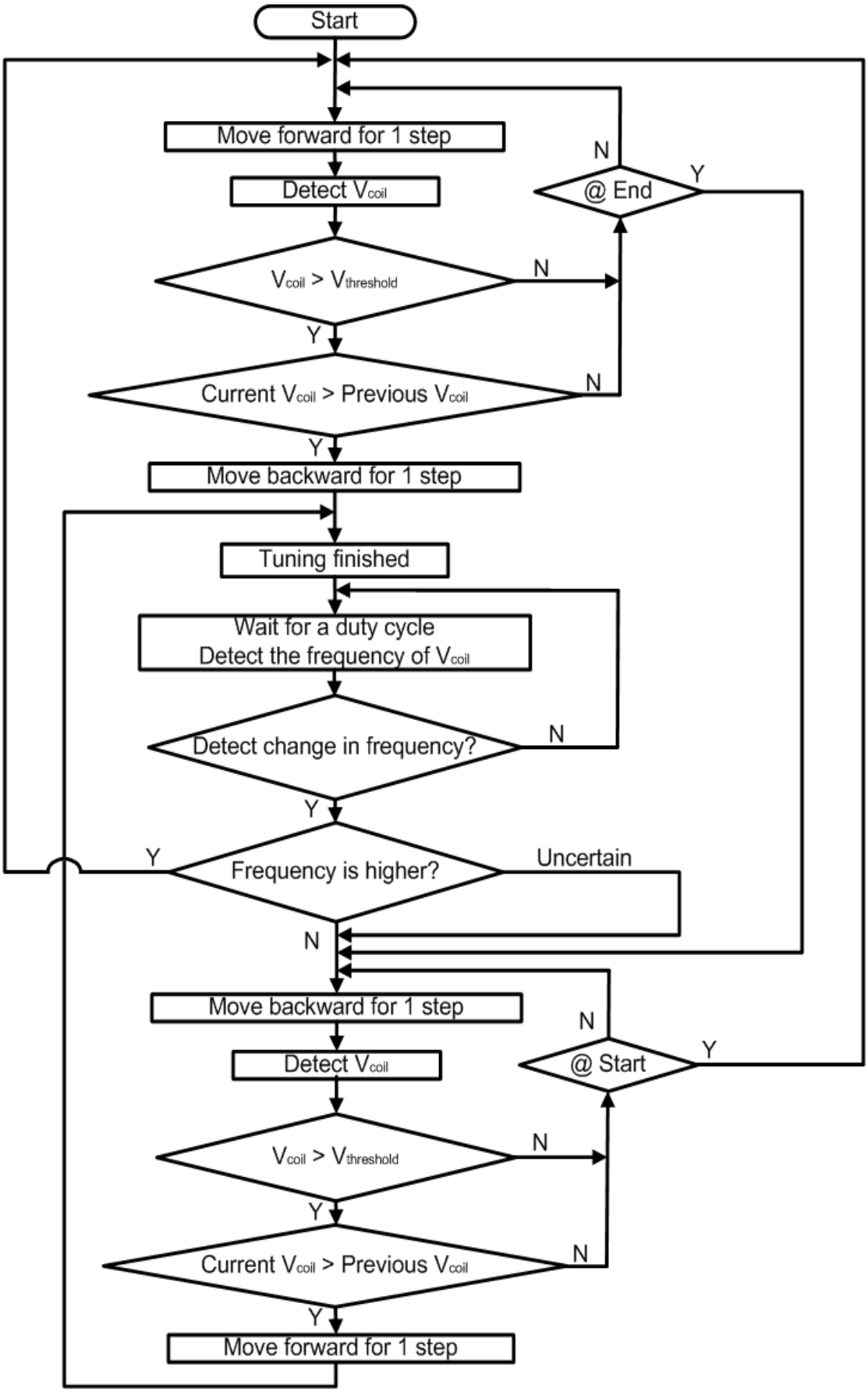

Figure 6.5. Detailed flow chart of the voltage-frequency feedback algorithm.

Detection of changes in frequency is based on the attenuation of the output voltage when the vibration frequency is moved away from the resonant frequency of the generator (as shown in Figure 6.6). As the frequency of the output voltage does not change as long as vibration frequency stays unchanged (Figure 6.7), this algorithm can avoid mis-activation of the tuning system due to change in vibration acceleration. However, when the vibration frequency changes away from the resonant frequency of the generator, the output voltage attenuates very quickly. The system may sometimes misjudge the change in vibration frequency and tune the resonant frequency on the opposite direction thus increasing the energy consumption.

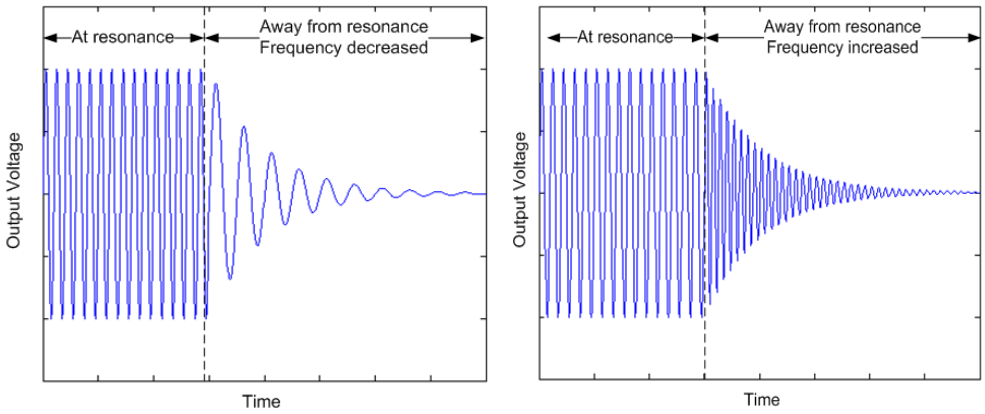

(a) (b)

Figure 6.6. Attenuation of output voltage due to change in vibration frequency (a) frequency increased (b) frequency decreased.

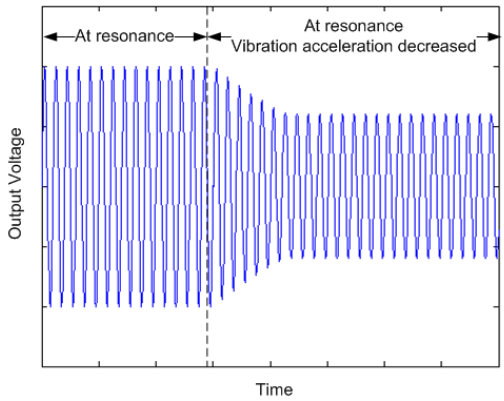

Figure 6.7. Waveform of output voltage due to change in vibration amplitude only.

6.2.4 Characterization of the System

The varying resonant frequency of the generator with distance between the two tuning magnets is shown in Figure 6.8. The resonant frequency increases as the distance

between the two tuning magnets is decreased, i.e. when the tuning force is increased. This figure is reproduced from Figure 5.21 to make description in this chapter clearer.

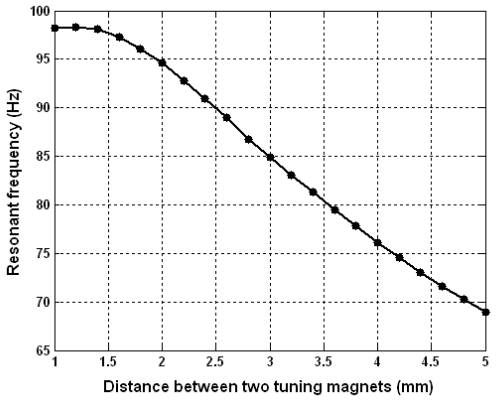

Figure 6.8. Resonant frequency with variation of distances between two tuning magnets.

Table 6.2 compares experimentally the resonant frequency of the generator when the tuning was finished with the vibration frequency as it varied using both algorithms, which shows that the closed loop frequency tuning system is successful in tracing the ambient vibration frequency. It is found that both algorithms have the same accuracy to tune the resonant frequency of the generator to match the ambient vibration frequency. The system was tested under vibration with various frequencies and constant acceleration.

Table 6.2. Resonant frequency after tuning.

Ambient vibration frequency (Hz)	**Resonant frequency of the micro-generator after tuning (Hz)**	
	Voltage-only feedback	Voltage-frequency feedback
70	70.2	70.2
75	75.1	75.0
80	79.9	80.1
85	84.8	84.9
90	90.0	90.1
95	95.1	95.0
98	98.0	98.1

6.3 Duty Cycle of the Tuning System

6.3.1 Definition of Duty Cycle

The period in which the system accumulates enough energy to perform tuning is called the duty cycle. It is important to shorten the duty cycle in practical application. The duty cycle of the closed loop frequency tuning system is given by:

$$DutyCycle = \frac{Energy\ \ consumed\ \ in\ \ tuning}{Effective\ \ power\ \ of\ \ the\ \ generator} = \frac{W/\eta_a}{P_g \cdot \eta_g} \tag{6.1}$$

where W is the effective work done by the actuator within one duty cycle. η_a and η_g are the efficiency of the actuator and the generator, respectively. P_g is the power produced by the generator. W/η_a is the actual energy consumed by the actuator including loss within the actuator and $P_g \cdot \eta_g$ is the effective power delivered to the electrical load. The duty cycle of the closed loop frequency tuning system is proportional to the effective work done by the actuator and is inversely proportional to the power generated by the generator and the efficiencies of the actuator and the generator.

Suppose that a varying magnetic force, F, is a function of distance between two tuning magnets, x, i.e. $F = f(x)$ (see Figure 6.9). If one of the magnets is fixed, the work required to move the other magnet from A to B is given by

$$W = \int_A^B F dx \tag{6.2}$$

The work is shown as the shaded area in Figure 6.9.

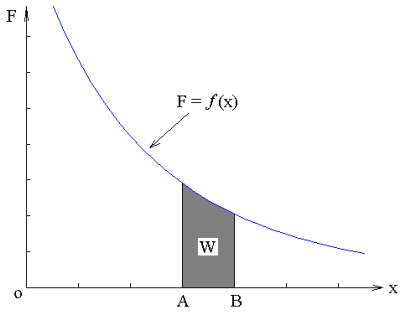

Figure 6.9. Work required to move one magnet from A to B.

6.3.2 Energy Consumed in Tuning Mechanism

Figure 6.10 shows the theoretical average energy consumed in one tuning attempt with different tuning and frequency ranges using different algorithms. One tuning attempt is defined as the entire process from a change of vibration frequency being detected until the generator is at the new resonant frequency. Marks in this figure indicate the lowest and highest frequencies in each case. It is found that the larger the tuning range, the more work the actuator must do to finish one tuning attempt. Additionally, for the same tuning range, more work has to be done if the frequency range covered is higher because tuning forces within that range become larger. As the voltage-frequency feedback algorithm is able to detect changes in vibration frequency, system using this algorithm consumes less energy in one tuning attempt than voltage-only feedback algorithm.

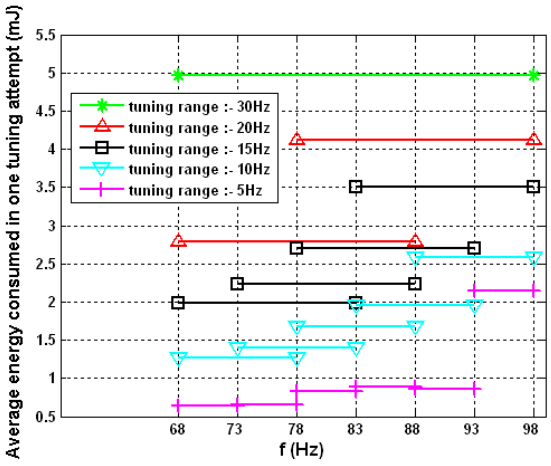

(a)

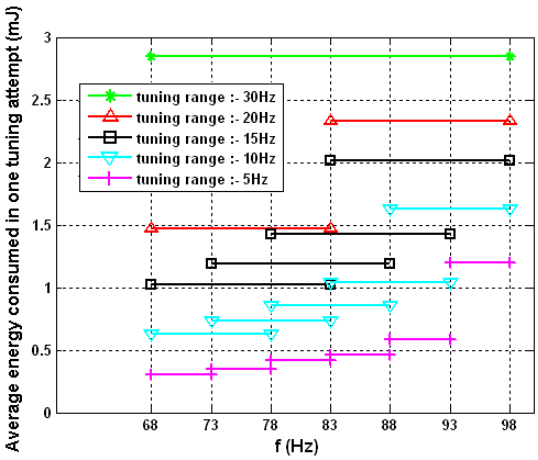

(b)

Figure 6.10. Average energy consumed in one tuning attempt with various tuning range and start frequencies (a) voltage-only feedback (b) voltage-frequency feedback.

6.3.3 Comparison of Duty Cycle using Different Algorithms

The proposed vibration-based generator, with a closed-loop frequency tuning system, generates an average of 120μW of power over the entire tuning range. Assuming typical efficiency of 60% for the actuator and the designed generator having an efficiency of 44%, the tuning duty cycles with different tuning ranges are shown in Figure 6.11. Marks in this figure indicate the lowest and highest frequencies in each case. It is found that the larger the tuning range, the longer the duty cycle. Furthermore, the duty cycle is shorter if the frequency covered is lower for the same tuning range. Since energy consumed in the system using voltage-frequency feedback algorithm is less than that consumed in the system using voltage-only feedback algorithm, the duty cycle of the voltage-frequency feedback system is shorter.

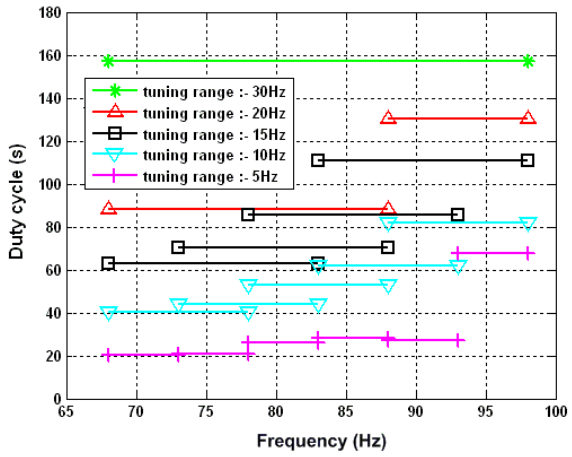

(a)

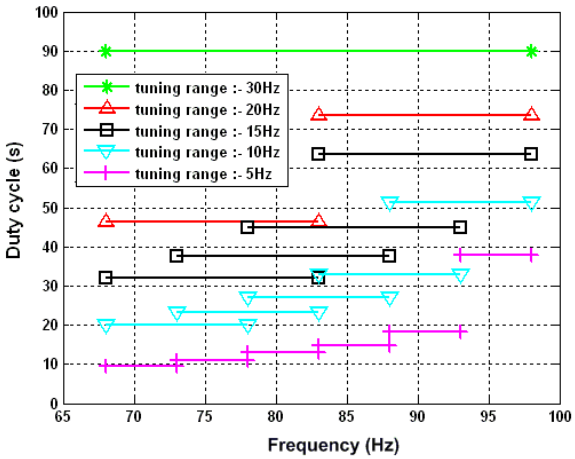

(b)

Figure 6.11. Duty cycle of the system with various tuning range and start frequencies (a) voltage-only feedback (b) voltage-frequency feedback.

Figure 6.12 shows the theoretical average duty cycle with variation of tuning range (assuming the typical average power generated by the generator is 120μW). It is found that the duty cycle increases linearly with the increase of the tuning range. The duty cycle of the system using voltage-frequency feedback algorithm is about 55% of the duty cycle of the one using voltage-only feedback algorithm with the same tuning range.

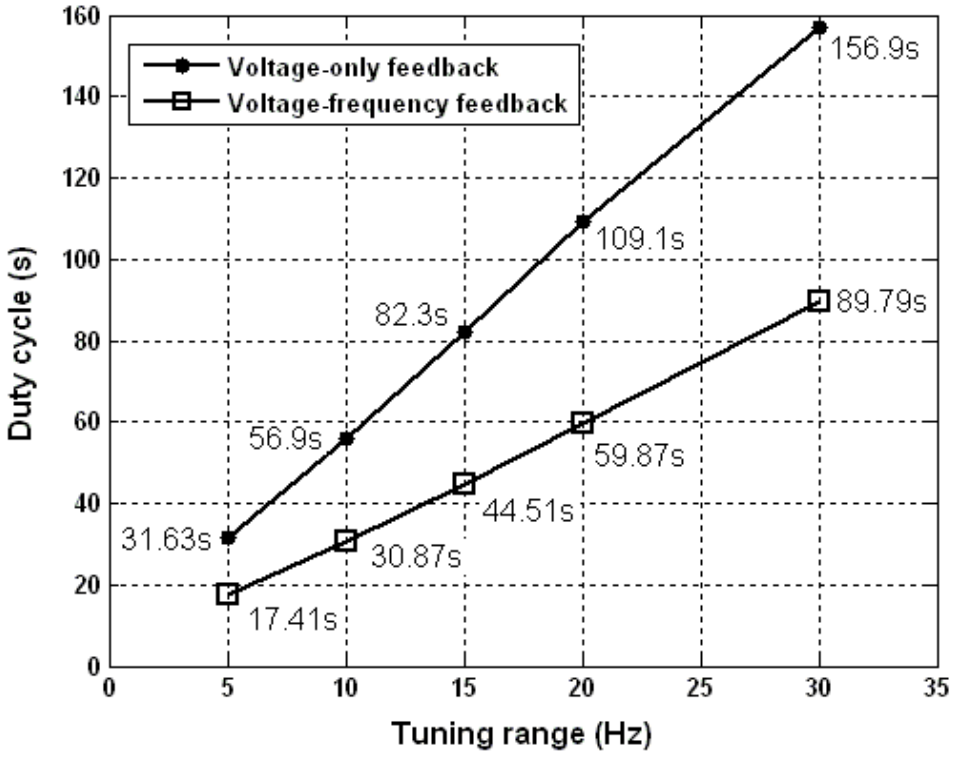

Figure 6.12. Comparisons of average duty cycle with variation of tuning range using two different algorithms.

Figure 6.13 to 6.17 show the duty cycles of the system using voltage-only feedback algorithm with different tuning ranges with variation of the efficiencies of actuator and generator assuming the average power generated by the generator is 120μW. The duty cycle drops significantly when either or both of the actuator and generator have high efficiency.

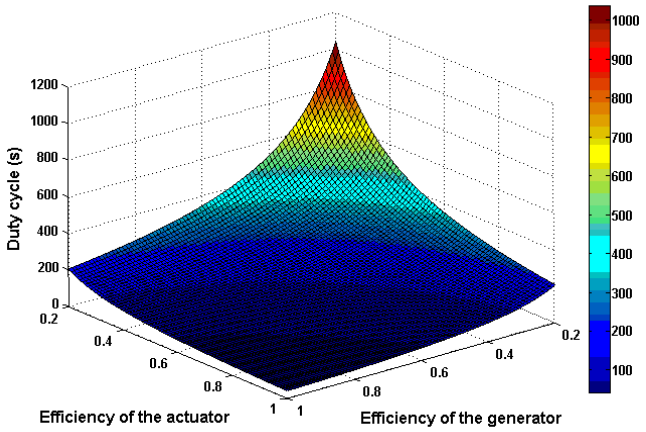

Figure 6.13. Duty cycle with variation of efficiencies of generator and actuator (Voltage-only feedback, Tuning range: 30Hz).

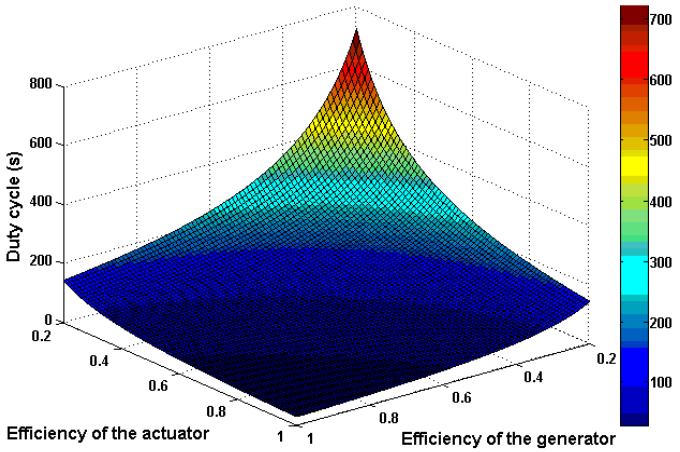

Figure 6.14. Duty cycle with variation of efficiencies of generator and actuator (Voltage-only feedback, Tuning range: 20Hz).

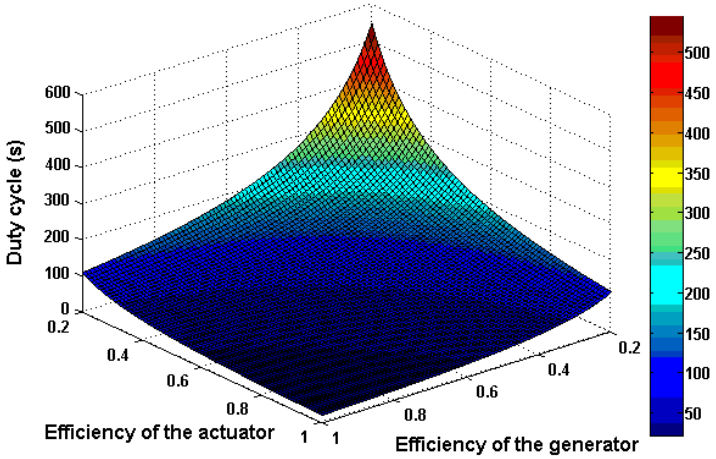

Figure 6.15. Duty cycle with variation of efficiencies of generator and actuator (Voltage-only feedback, Tuning range: 15Hz).

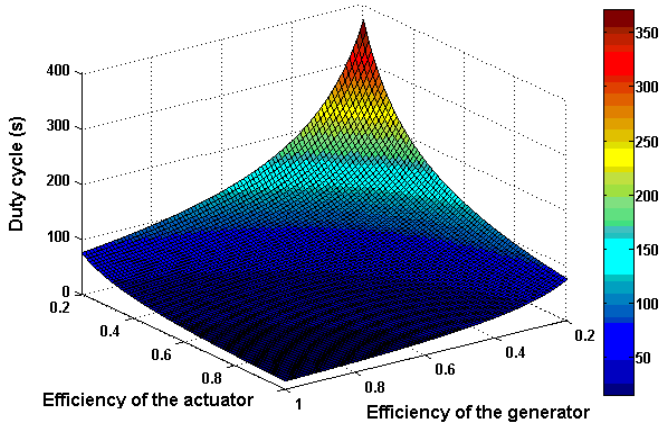

Figure 6.16. Duty cycle with variation of efficiencies of generator and actuator (Voltage-only feedback, Tuning range: 10Hz).

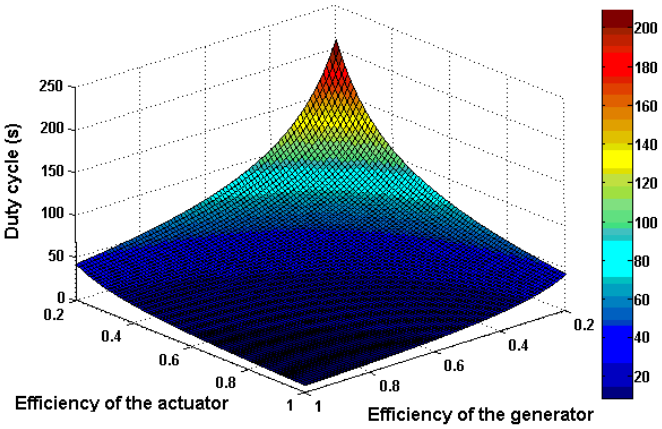

Figure 6.17. Duty cycle with variation of efficiency of the generator and actuator (Voltage-only feedback, Tuning range: 5Hz).

Figure 6.18 to 6.22 show the duty cycles of the system using voltage-frequency feedback algorithm with different tuning ranges with variation of the efficiencies of actuator and generator assuming the average power generated by the generator is 120μW. The duty cycle using this algorithm is much shorter than using the previous algorithm. Similarly, the duty cycle drops significantly when either or both of the actuator and generator have high efficiency.

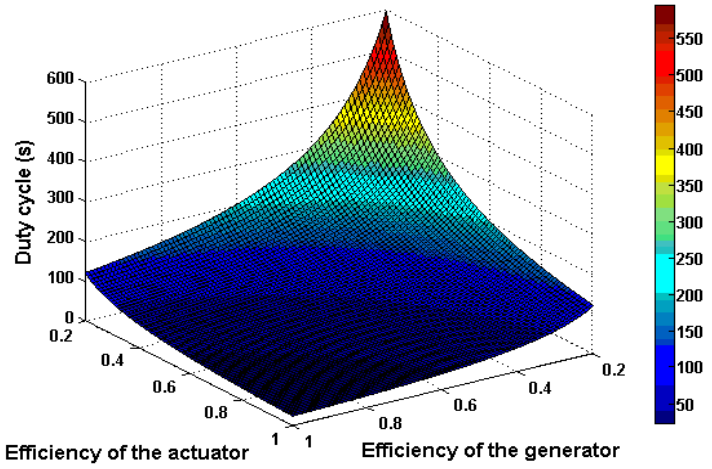

Figure 6.18. Duty cycle with variation of efficiencies of generator and actuator (Voltage-frequency feedback, Tuning range: 30Hz).

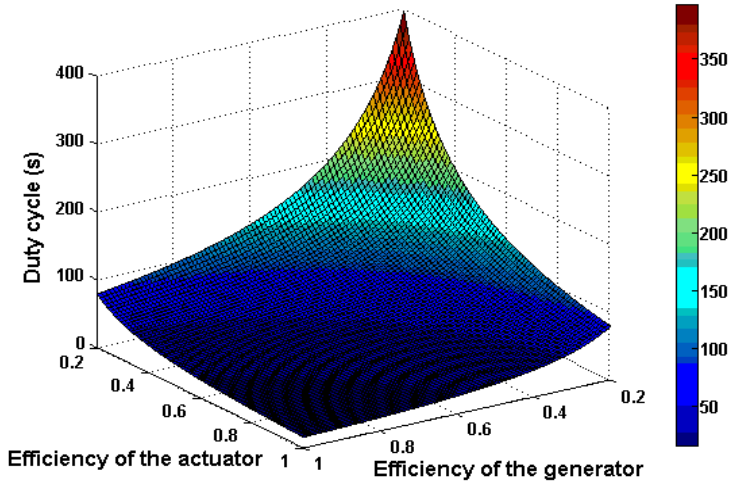

Figure 6.19. Duty cycle with variation of efficiencies of generator and actuator (Voltage-frequency feedback, Tuning range: 20Hz).

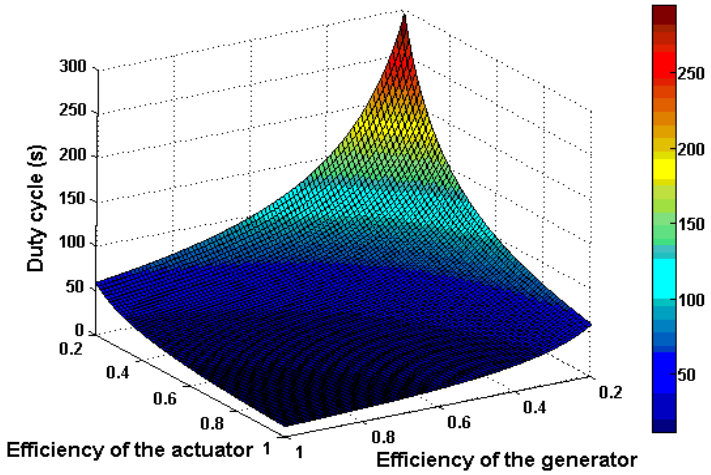

Figure 6.20. Duty cycle with variation of efficiencies of generator and actuator (Voltage-frequency feedback, Tuning range: 15Hz).

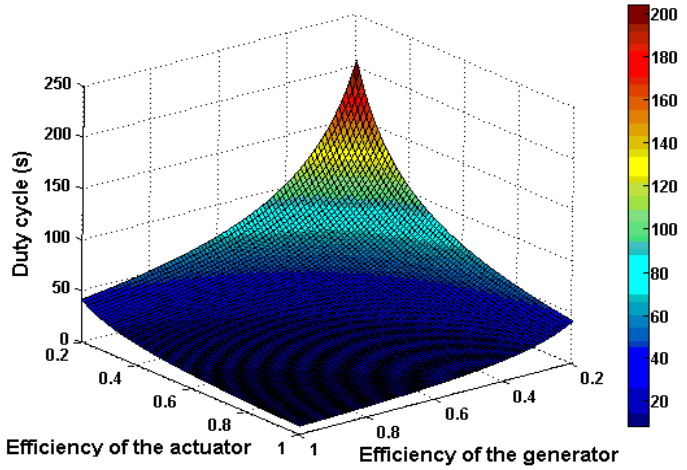

Figure 6.21. Duty cycle with variation of efficiencies of generator and actuator (Voltage-frequency feedback, Tuning range: 10Hz).

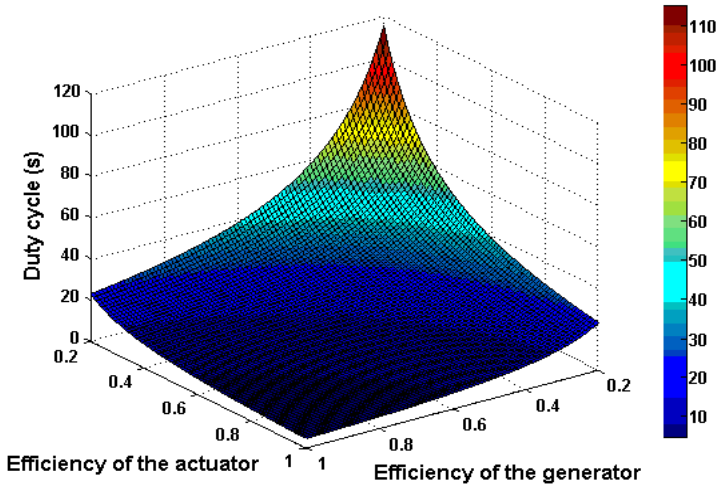

Figure 6.22. Duty cycle with variation of efficiencies of generator and actuator (Voltage-frequency feedback, Tuning range: 5Hz).

The duty cycles of the closed loop frequency tuning system using voltage-only feedback and voltage-frequency feedback algorithm when the tuning range is 30Hz (from 67.6 Hz to 98Hz) are shown in Figure 6.23 and Figure 6.24, respectively. For the voltage-only feedback algorithm, the average duty cycle of the tuning system is 2.6 minutes, i.e. about 156 seconds. Table 6.3 gives the relation between duty cycle and power level using this algorithm. If the generator generates a higher power level, the duty cycle can be reduced considerably. For the voltage-frequency feedback algorithm, the average duty cycle of the tuning system is 1.5 minutes, i.e. about 90 seconds. Table 6.4 lists the relation between duty cycle and power level using this algorithm.

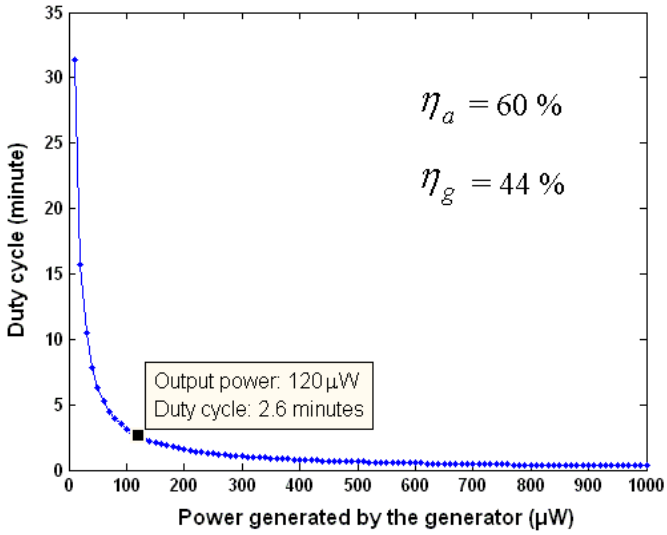

Figure 6.23. Duty cycle with variation of generated power by the micro-generator (Voltage-only feedback).

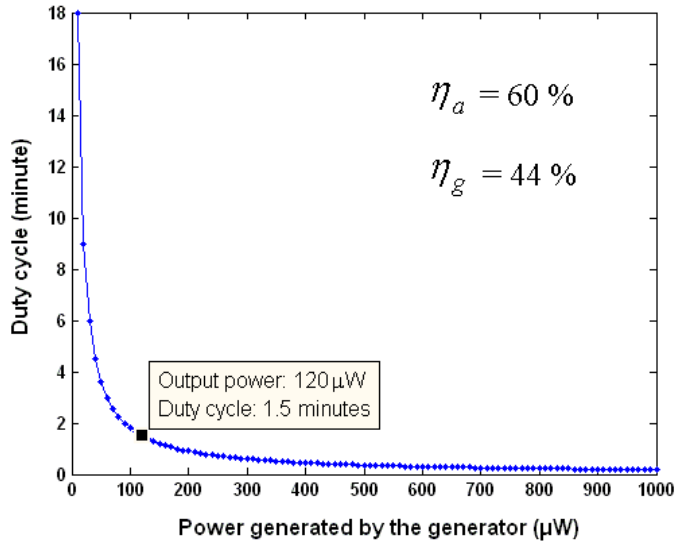

Figure 6.24. Duty cycle with variation of generated power by the micro-generator (Voltage-frequency feedback).

Table 6.3. Duty cycle Vs different power levels (Voltage-only feedback).

Power generated	Duty cycle
< 10μW	> 30 minutes
> 60μW	< 5 minutes
> 320μW	< 1 minute
> 630μW	< 30 seconds

Table 6.4. Duty cycle Vs different power levels (Voltage-frequency feedback).

Power generated	Duty cycle
< 6μW	> 30 minutes
> 35μW	< 5 minutes
> 180μW	< 1 minute
> 360μW	< 30 seconds

6.4 Conclusions

In this chapter, a closed loop tuning system developed to tune the resonant frequency to match the ambient vibration frequency has been detailed. A microcontroller was used to detect the output voltage of the micro-generator and control a linear actuator to adjust the distance between the two tuning magnets and hence the tuning force to realize the frequency tuning. In the test, all parts in the closed loop tuning system, including the microcontroller and linear actuator, were powered by a separate power supply to initially evaluate tuning principles and algorithms. The system was tested under vibration with various frequencies and constant acceleration.

Two tuning algorithms, i.e. voltage-only feedback and voltage-frequency feedback, have been tested and compared. The experimental results showed that the closed loop frequency tuning system using both algorithms successfully traced the ambient vibration frequency and tuned the resonant frequency of the micro-generator from 67.6 to 98 Hz by changing the distance between two tuning magnets from 5 to 1.2 mm, respectively.

For the voltage-only feedback algorithm, the microcontroller assumes the micro-generator is working at resonance when the output voltage reaches a maximum. It switches to sleep mode to save power when tuning is not necessary. The microcontroller then wakes up every duty cycle to monitor the output voltage and make a decision of whether it is necessary to trigger the tuning mechanism. If it is not necessary, the microcontroller reverts to sleep mode again. If a significant decrease in output voltage is detected, the microcontroller by default tunes and reduces the resonant frequency. If no resonant frequency is found matching the vibration

frequency, it then increases the resonant frequency to search for the vibration frequency again.

For the voltage-frequency feedback algorithm, the microcontroller also assumes the micro-generator is working at resonance when the output voltage reaches maximum and switches to sleep mode if tuning is not necessary. The difference of this algorithm from the voltage-only feedback is that the voltage-frequency feedback algorithm is able to detect change in frequency via attenuation of output voltage. By investigating the waveform of the output voltage, the microcontroller can tell if the vibration frequency is increased or decreased. Hence, it controls the linear actuator to tune the resonant frequency of the generator accordingly. On average, this algorithm consumes less energy in tuning than the previous one. The analysis of duty cycle proved this conclusion.

The duty cycle is defined as the period of time in which the system accumulates enough energy to perform tuning. It is proportional to the effective work done by the actuator and is inversely proportional to the power generated by the generator and the efficiencies of the actuator and the generator. It is found that the average duty cycle increases linearly with the increase of the tuning range for both algorithms. Furthermore, the duty cycle is shorter if the start frequency is lower than the target frequency for the same tuning range. The generator produces an average power of 120μW when excited at $0.59 m \cdot s^{-2}$ with a tuning range of 30Hz (from 67.6Hz to 98Hz), assuming that the actuator has the efficiency of 60% and the generator designed in this research has the efficiency 44%, respectively. The duty cycle of the proposed closed loop frequency tuning system is 2.6 minutes, i.e. about 156 seconds for system using voltage-only feedback algorithm and is 1.5 minutes, i.e. about 90 seconds for voltage-frequency feedback algorithm. It is concluded that the duty cycle can be shortened by (a) increasing the output power from the micro-generator (b) increasing the efficiency of the generator, i.e. using more efficient power conditioning circuitry (c) selecting actuators that are more efficient in transferring energy from electrical domain to mechanical domain (d) reducing the work done by the actuator, i.e. to decrease the tuning range as well the starting frequency. Furthermore, the duty cycle of a closed loop tuning system using voltage-frequency feedback algorithm is

approximately half (55%) of that of the same tuning system using voltage-only feedback algorithm. However, due to the small signal of the attenuation of output voltage during the transition between the old and the new vibration frequencies, the system using voltage-frequency feedback algorithm can sometimes misjudge the change in vibration frequency and cause unnecessary consumption of energy in frequency tuning.

In addition, the tuning system using voltage-only feedback algorithm is only able to detect the change in frequency of ambient vibration. If the amplitude and phase of the vibration change, the system may potentially be triggered by mistake. The tuning system using voltage-frequency feedback algorithm can overcome this drawback. If only amplitude of the vibration changes, the frequency feedback mechanism will avoid mis-trigger of the tuning system which could happen in system using voltage-only feedback algorithm.

Chapter 7

Resonant Frequency Tuning using Electrical Methods

7.1 Introduction

In Chapter 4, 5 and 6, resonant frequency tuning of an electromagnetic generator using mechanical methods has been detailed. A closed loop tuning system has been successfully developed to realize automatic tuning. However, one major drawback of frequency tuning using mechanical methods is that the tuning system consumes lots of energy as it changes the mechanical properties of the generator. Even when intermittent tuning is adopted, a significant amount of energy compared to the amount of energy produced by the generator is consumed in frequency tuning. Hence, an alternative more efficient power saving tuning method will be studied in this chapter. This is electrical tuning, which realizes frequency tuning by varying the electrical load of the generator. The principles of this method in both piezoelectric and

electromagnetic generators will be given in Section 7.2. The focus of this research is on the frequency tuning of electromagnetic generators using an electrical method. Some guidelines in designing an electrically tunable electromagnetic generator will be given in Section 7.3. One micro scale and one macro scale electromagnetic generator have been tested and the results are compared with the simulation results to verify the theory in Section 7.4 to 7.6.

7.2 Principle

The basic principle of electrical tuning is to change the electrical damping by adjusting the load, which causes the power spectrum of the generator to shift. Change of resistive load away from the optimum value could reduce the efficiency of power transferred to the electrical domain and load inductances are difficult to vary. It is therefore most feasible to adjust capacitive loads to realize electrical tuning. The principle of frequency tuning using electrical method in both piezoelectric and electromagnetic generators is now presented.

7.2.1 Electrical Tuning in Piezoelectric Generators

Figure 7.1 shows a schematic diagram of a bimorph piezoelectric generator with a mass, m on the tip. l_b and l_m are the effective length of the cantilever and mass, respectively. w is the width of the cantilever. t_p and t_s are the thickness of the piezoelectric layer and substrate layer, respectively and t_g is the distance from the centre of the substrate layer to the centre of the piezoelectric layer. The electrodes of the generator have been omitted in Figure 7.1.

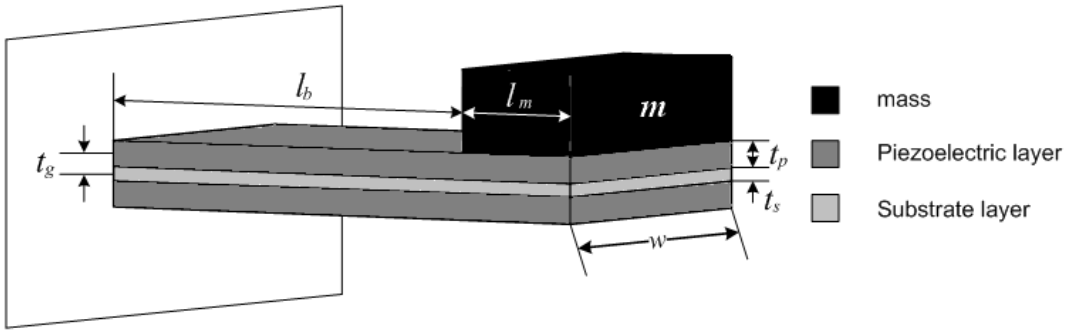

Figure 7.1. Piezoelectric bimorph generator.

Such generators can be represented using an equivalent circuit as shown in Figure 7.2. L_m, R_m and C_m represent the mass, damping, and spring in the mechanical part, respectively. C_p is the capacitance of the piezoelectric layer, C_L and R_L are the capacitive and resistive load, respectively. V is the voltage across the resistive load.

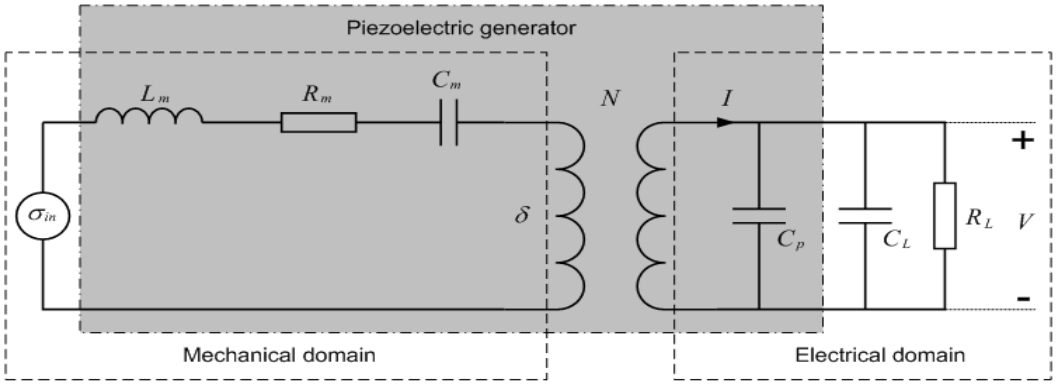

Figure 7.2. Equivalent circuit of piezoelectric generator with capacitive and resistive loads.

The transformer relates the mechanical domain to the electrical domain according to the model of the piezoelectric effect. Specifically, it relates stress (σ) to electric field (E) at zero strain, or electrical displacement (D) to strain (δ) at zero electric field. The equations for the piezoelectric effect are:

$$\delta = \frac{\sigma}{Y_p} + dE \tag{7.1}$$

$$D = \varepsilon E + d\sigma \tag{7.2}$$

where d is the piezoelectric strain coefficient, which is d_{31} for a piezoelectric bimorph as it works in 31 mode, ε is the dielectric constant of the piezoelectric material and Y_p is the Young's modulus of the piezoelectric material. Rewriting Equation (7.1) and Equation (7.2) leads to the equations for the transformer as:

$$D = -d_{31} Y_p \delta \tag{7.3}$$

Hence, the transform ratio N is given by:

$$N = -d_{31}Y \tag{7.4}$$

Equation (7.5) can be derived to present the mechanical dynamics of the system with electrical coupling. Detailed derivation of this model can be found in [113].

$$\Delta\left(s^2 + 2\zeta\omega_n s + \omega_n^2\right) = \frac{\omega_n^2 d_{31} a}{2t_c} V + b^* A_{in} \tag{7.5}$$

where Δ is Laplace transform of strain, δ, A_{in} is the vibration acceleration, ζ is the damping factor, ω_n is the untuned resonant frequency, $a = 1$ if the two piezoelectric layers are connected in series and $a = 2$ if they are connected in parallel and s is the Laplace variable. b^* is given by:

$$b^* = \frac{3t_g}{l_b^2} \cdot \frac{\left(2l_b + l_m - l_e\right)}{\left(2l_b + \frac{3}{2}l_m\right)} \tag{7.6}$$

where l_e is the length of the electrodes.

Furthermore, analysis in the electrical domain gives the following equation:

$$\Delta = \left(s + \frac{1}{R_L C_{pL}}\right) \cdot \frac{V \cdot C_{pL}}{s \cdot \Sigma} \tag{7.7}$$

where $C_{pL} = C_p + C_L$ and $\Sigma = - a \cdot d_{31} \cdot Y_c \cdot l_e \cdot w$. l_e is the length of the electrodes.

Combining Equation (7.5) and (7.7) gives the transfer function of the system as:

$$\frac{V}{A_{in}} = \frac{s \cdot \Sigma \cdot b^*}{s^3 + \left(\frac{1}{R_L C_{pL}} + 2\zeta\omega_n\right)s^2 + \left(\omega_n^2 + \frac{2\zeta\omega_n}{R_L C_{pL}} - \frac{a\Sigma\omega_n^2 d_{31}}{2t_c}\right)s + \frac{\omega_n^2}{R_L C_{pL}}} \tag{7.8}$$

which leads to the expression of the voltage across the resistive load given by:

$$V(\omega) = \frac{j\omega \cdot \Sigma \cdot b^* \cdot A_{in}}{\left[\frac{\omega_n^2}{R_L} - \left(\frac{1}{R_L} + 2\zeta\omega_n C_{pL}\right)\omega^2\right] + j\omega\left(\left(\omega_n^2 - \omega^2\right)C_{pL} + \frac{2\zeta\omega_n}{R_L} - \frac{a\Sigma \cdot \omega_n^2 d_{31}}{2t_c}\right)} \tag{7.9}$$

The power in the resistive load is given by:

$$P(\omega) = \frac{V(\omega)^2}{R_L}$$

$$= \frac{1}{R_L} \cdot \frac{\left(\omega \cdot \Sigma \cdot b^* \cdot A_{in}\right)^2}{\left[\frac{\omega_n^2}{R_L} - \left(\frac{1}{R_L} + 2\zeta\omega_n C_{pL}\right)\omega^2\right]^2 + \omega^2\left(\left(\omega_n^2 - \omega^2\right)C_{pL} + \frac{2\zeta\omega_n}{R_L} - \frac{a\Sigma \cdot \omega_n^2 d_{31}}{2t_c}\right)^2} \tag{7.10}$$

It is known that $f(x,y) = x^2 + y^2 \geq 2xy$ and that $f(x,y)$ becomes a minimum only if $x = y$ (i.e. $\frac{1}{f(x,y)}$ is maximum only if $x = y$). Therefore, Equation (7.10) reaches maximum when:

$$\frac{\omega_n^2}{R_L} - \left(\frac{1}{R_L} + 2\zeta\omega_n C_{pL}\right)\omega^2 = \omega\left(\left(\omega_n^2 - \omega^2\right)C_{pL} + \frac{2\zeta\omega_n}{R_L} - \frac{a\Sigma \cdot \omega_n^2 d_{31}}{2t_c}\right) \tag{7.11}$$

Rearranging Equation (7.11) leads to a cubic function of the form:

$$\omega^3 + X\omega^2 + Y\omega + Z = 0 \tag{7.12}$$

where:

$$X = -\left(\frac{1}{R_L C_{pL}} + 2\zeta\omega_n\right)$$

$$Y = -\left(\omega_n^2 + \frac{2\zeta\omega_n}{R_L C_{pL}} - \frac{a\Sigma \cdot \omega_n^2 d_{31}}{2t_c C_{pL}} \right)$$

$$Z = \frac{\omega_n^2}{R_L C_{pL}}$$

The real solution of (7.12) gives the function of resonant frequency with respect to the load capacitance as:

$$\omega(C_L) = \frac{\sqrt[3]{\Omega + 12\sqrt{\Psi}}}{6} - \frac{2\left(Y - \frac{X^2}{3}\right)}{\sqrt[3]{\Omega + 12\sqrt{\Psi}}} - \frac{X}{3} \tag{7.13}$$

where:

$$\Omega = 36XY - 108Z - 8X^3$$

$$\Psi = 12Y^3 - 3X^2Y^2 - 54XYZ + 81Z^2 + 12X^3Z$$

Figure 7.3 compares the resonant frequencies and power output of electrically tunable piezoelectric generators of different piezoelectric materials with the variation of load capacitance. These generators are identical except for the piezoelectric material. The coefficients used in the simulation are listed in Table 7.1.

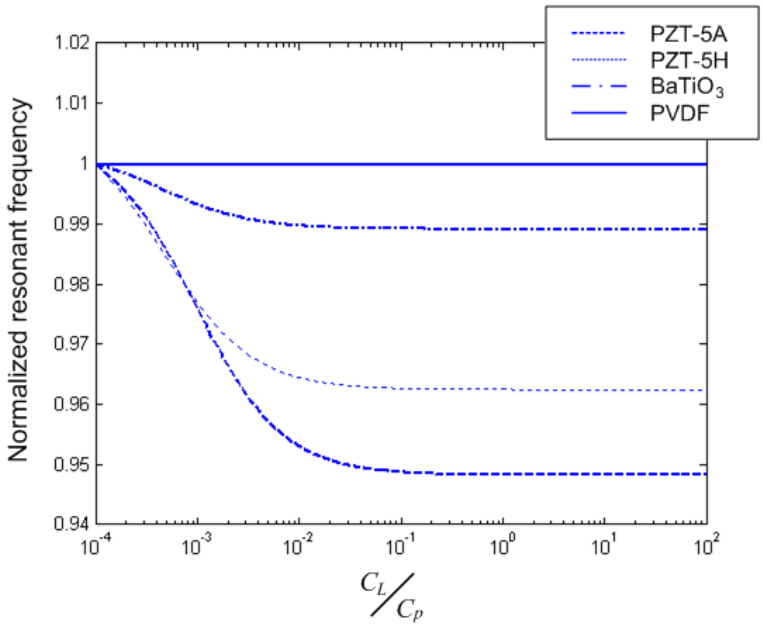

(a) Resonant frequency

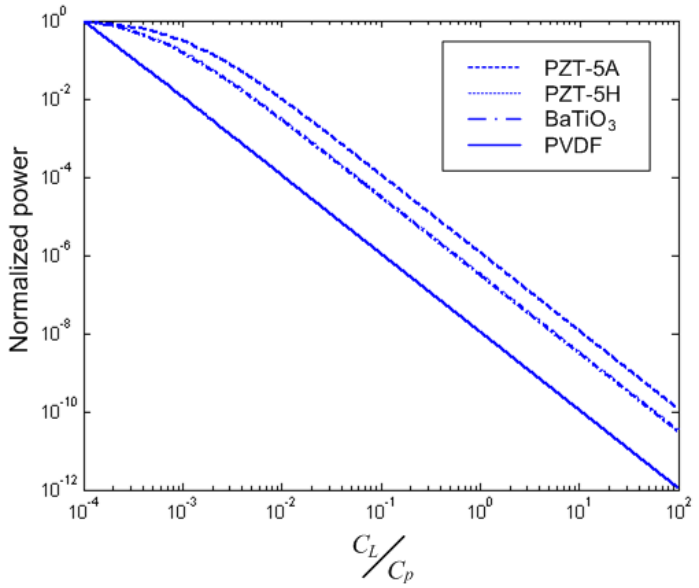

(b) Output power

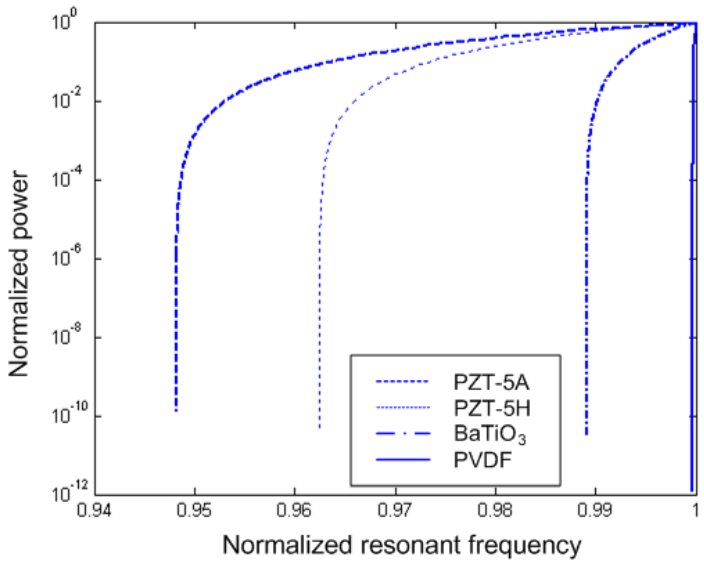

(c) Output power vs. resonant frequency

Figure 7.3. Performance of a piezoelectric generator with different piezoelectric materials.

Table 7.1. Coefficients of common piezoelectric materials [1, 114]

	PZT-5H	PZT-5A	$BaTiO_3$	PVDF
d_{31} ($\times 10^{-12}$ C·N^{-1})	-274	-171	78	23
Young's modulus (GPa)	50	50	67	2
Relative permittivity ($\varepsilon/\varepsilon_0$)	3400	1700	1700	12

The resonant frequency as well as the output power reduces with increasing load capacitance. It was demonstrated from Figure 7.3 that PZT-5H is the best of these four piezoelectric materials for an electrically tunable piezoelectric generator.

Important considerations relating to the tunability of the piezoelectric generator are:

- The material of the substrate layer and mass does not affect the tenability;
- A piezoelectric material with higher Young's modulus, strain coefficient and smaller permittivity provides a larger tuning range;
- The ratio of the thickness of the piezoelectric layer to the thickness of the substrate layer should be small to increase the tuning range;
- The capacitance of the piezoelectric layer should be minimized to increase the tuning range;

- If both piezoelectric layers are used for tuning, connection of these two layers in parallel gives a larger tuning range than connection in series;
- The total damping should be kept low to increase the tuning range.

7.2.2 Electrical Tuning in Electromagnetic Generators

The differential equation of model of vibration-based generator (as Equation A.1) is:

$$m\frac{d^2z(t)}{dt^2}+b\frac{dz(t)}{dt}+k_sz(t)=-m\frac{d^2y(t)}{dt^2} \tag{7.14}$$

where m is the mass, b is the damping coefficient k_s is the spring constant, $y(t)$ is the displacement of the generator housing and $z(t)$ is the relative motion of the mass with respect to the housing.

An equivalent electrical circuit for this system can be found by taking the Laplace transform of Equation (7.14), which, when rearranged, gives:

$$-ms^2Y(s)=sZ(s)\left(ms+b+\frac{k_s}{s}\right) \tag{7.15}$$

Equation (7.15) can be rewritten as:

$$-I(s)=E(s)\left(sC+\frac{1}{R}+\frac{1}{sL}\right) \tag{7.16}$$

where $I=\frac{m}{k_e}s^2Y(s)=\frac{m\cdot a}{k_e}$, $E(s)=k_esZ(s)$, $C=\frac{m}{k_e^2}$, $R=\frac{k_e^2}{b}$, $L=\frac{k_e^2}{k_s}$ and k_e is electrical transduction constant. Based on Equation (7.16), an equivalent electrical circuit can be found (Figure 7.4).

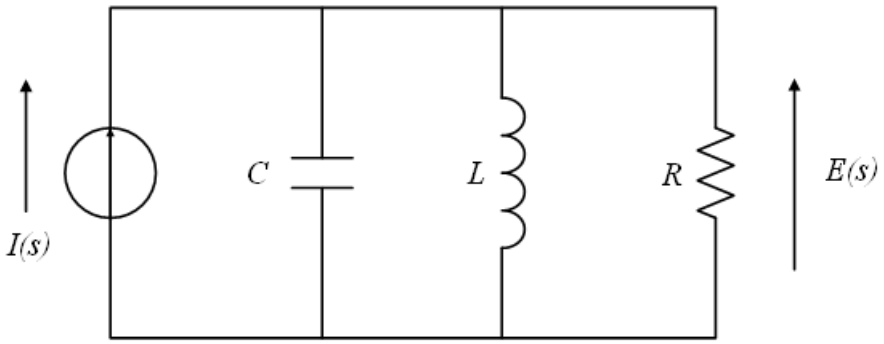

Figure 7.4. Equivalent circuit of an electromagnetic generator (mechanical domain).

Figure 7.5 shows the equivalent circuit model of an electromagnetic generator with capacitive load. R_c is the coil resistance, L_c is the coil inductance, R_L is the load resistance and C_L is the load capacitance.

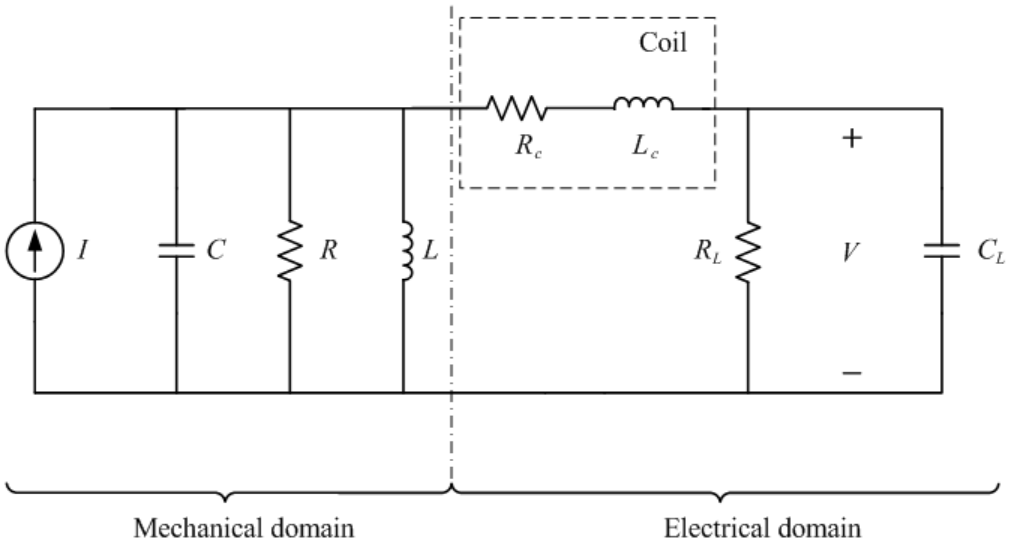

Figure 7.5. Equivalent circuit model of electromagnetic generators with capacitive load.

The existence of the coil inductance increases the complexity of the circuit and the analysis. A capacitor in series with the coil inductance, C_s, can be used to cancel the effect of the coil inductance (Figure 7.6).

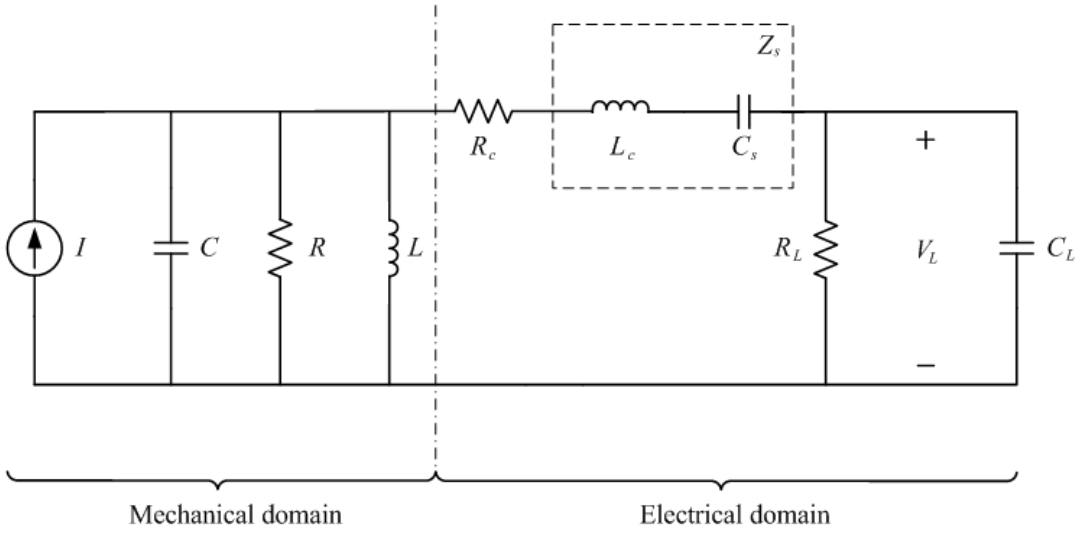

Figure 7.6. Equivalent circuit model of electromagnetic generators with capacitor connected to the coil in series.

Thus, the combined impedance of the coil inductance and the capacitor in series, Z_s, should be:

$$Z_c = 0 \tag{7.17}$$

Since

$$Z_c = \frac{1}{j\omega C} + j\omega L \tag{7.18}$$

Thus,

$$1 - \omega^2 LC = 0 \tag{7.19}$$

The value of the capacitor in series with the coil inductance is:

$$C = \frac{1}{\omega^2 L} \tag{7.20}$$

Equation (7.20) shows that the higher the resonant frequency and the value of the coil

inductance, the smaller the capacitor is needed to compensate the effect of the coil inductance. When the impedance of the coil inductance is negligible compared to the coil resistance, the effect of the coil inductance on the model can be ignored and no capacitor is needed for compensation.

Therefore, the equivalent circuit model of an electromagnetic generator with capacitive load can then be simplified as shown in Figure 7.7. The following analyses are based on the simplified mode.

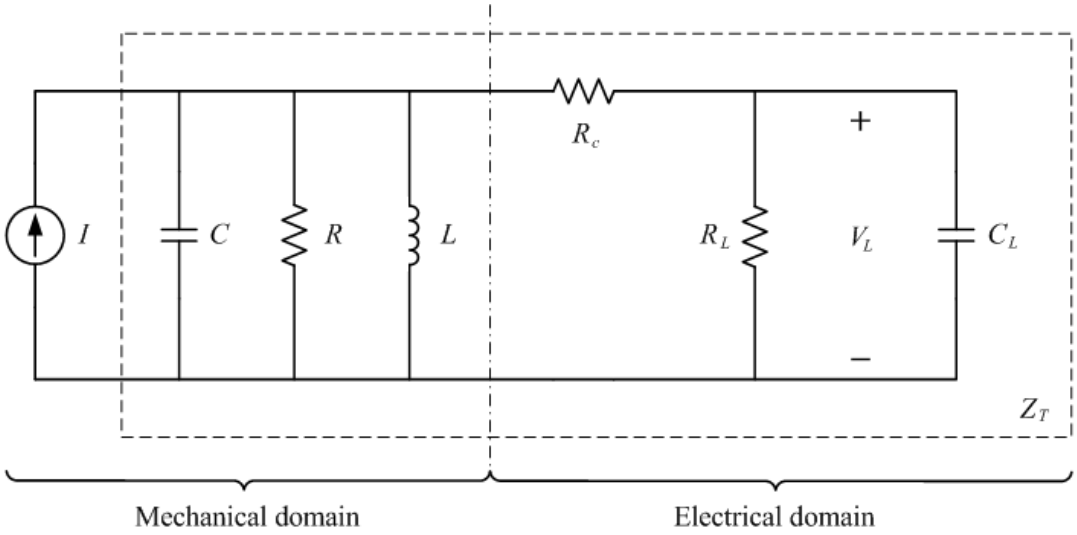

Figure 7.7. Simplified equivalent circuit model of electromagnetic generators with capacitive load.

The total impedance of this circuit, Z_T, is:

$$Z_T(\omega) = \left| \frac{1}{j \cdot \omega \cdot C + \frac{1}{j \cdot \omega \cdot L} + \frac{1}{R} + \frac{1}{R_c + \frac{1}{\frac{1}{R_L} + j \cdot \omega \cdot C_L}}} \right| \tag{7.21}$$

Therefore, the voltage across the capacitive load is:

$$V_{RR}(\omega) = I \cdot Z_T(\omega) \cdot \frac{R_L // C_L}{R_c + R_L // C_L} \tag{7.22}$$

$$V_L(\omega) = \frac{a \cdot m}{k_e} \cdot \left| \frac{1}{j \cdot \omega \cdot C + \frac{1}{j \cdot \omega \cdot L} + \frac{1}{R} + \frac{1}{R_c + \frac{1}{\frac{1}{R_L} + j \cdot \omega \cdot C_L}}} \cdot \frac{\frac{1}{\frac{1}{R_L} + j \cdot \omega \cdot C_L}}{R_c + \frac{1}{\frac{1}{R_L} + j \cdot \omega \cdot C_L}} \right| \tag{7.23}$$

The generated power is given by:

$$P(\omega) = \frac{V_L^2(\omega)^2}{R_L} \tag{7.24}$$

$$P(\omega) = \frac{a^2 \cdot m^2}{k_e^2 \cdot R_L} \left(\left| \frac{1}{j \cdot \omega \cdot C + \frac{1}{j \cdot \omega \cdot L} + \frac{1}{R} + \frac{1}{R_c + \frac{1}{\frac{1}{R_L} + j \cdot \omega \cdot C_L}}} \cdot \frac{\frac{1}{\frac{1}{R_L} + j \cdot \omega \cdot C_L}}{R_c + \frac{1}{\frac{1}{R_L} + j \cdot \omega \cdot C_L}} \right| \right)^2 \tag{7.25}$$

Finally, Equation (7.26) can be obtained by rearranging Equation (7.25) as:

$$P(\omega) = \frac{a^2 \cdot \mathrm{K}}{\omega^2} \cdot \Phi \cdot \frac{1}{\left[\frac{\omega_n^2}{\omega^2} - 1 - \Sigma \right]^2 + \left[\frac{1}{Q} + \frac{\mathrm{K}}{\omega \cdot m} \cdot \Omega \right]^2} \tag{7.26}$$

where $\mathrm{K} = \frac{k_e^2}{R_c}$

$$\Phi = \frac{r}{(1+r)^2 + \omega^2 \cdot R_L^2 \cdot C_L^2}$$

$$r = \frac{R_L}{R_c}$$

$\omega_n = \sqrt{\frac{k_s}{m}}$, is the original resonant frequency of the generator

$Q = \frac{\omega \cdot m}{b}$, is the quality factor

$$\Sigma = \frac{C_L \cdot r^2 \cdot \frac{\mathrm{K} \cdot R_c}{m}}{(1+r)^2 + \omega^2 \cdot R_L^2 \cdot C_L^2}$$

$$\Omega = \frac{(1+r) + \omega^2 \cdot R_L^2 \cdot C_L^2}{(1+r)^2 + \omega^2 \cdot R_L^2 \cdot C_L^2}$$

$P(\omega)$ reaches maximum, when

$$\frac{dP(\omega)}{d\omega} = 0 \tag{7.27}$$

i.e.

$$\frac{\omega_n^2}{\omega^2} - 1 - \Sigma = 0 \tag{7.28}$$

Thus, the frequency at which the generator produces maximum power, i.e. the new resonant frequency, ω_r, is given by:

$$\omega_r = \sqrt{\frac{\sqrt{\left(\theta + \chi - \varepsilon \cdot \omega_n^2\right)^2 + 4\varepsilon \cdot \theta \cdot \omega_n^2} - \left(\theta + \chi - \varepsilon \cdot \omega_n^2\right)}{2\varepsilon}} \tag{7.29}$$

where $\theta = (1+r)^2$

$$\chi = C_L \cdot r^2 \cdot \frac{\mathrm{K} \cdot R_c}{m}$$

$$\varepsilon = R_L^2 \cdot C_L^2$$

The new resonant frequency, ω_r, is a function of the load capacitance, C_L. Therefore, the resonant frequency can be tuned by adjusting the load capacitance.

Substitution of Equation (7.29) to Equation (7.26) yields the maximum power from the generator as follows:

$$P(\omega) = \frac{a^2 \cdot \mathrm{K}}{\omega^2} \cdot \Phi \cdot \frac{1}{\left[\frac{1}{Q} + \frac{\mathrm{K}}{\omega \cdot m} \cdot \Omega\right]^2} \tag{7.30}$$

where Φ and Ω are the same as those in Equation (7.26). As mentioned before, it is important to keep the output power constant while tuning. Two hypotheses have been made to analyse this as these hypotheses are true in most cases.

Hypothesis 1

In the equivalent circuit shown in Figure 7.7, the load resistor represents a rectification circuit. The value of load resistance is very high compared to the coil resistance as this is often the case, i.e. $R_L >> R_c$ and r is very large. Therefore, it can be assumed that

$$(1+r)^2 > 1 + r >> \omega^2 \cdot R_L^2 \cdot C_L^2 \tag{7.31}$$

Then,

$$(1+r)^2 + \omega^2 \cdot R_L^2 \cdot C_L^2 \approx (1+r)^2 \tag{7.32}$$

$$\frac{(1+r)+\omega^2 \cdot R_L^2 \cdot C_L^2}{(1+r)^2+\omega^2 \cdot R_L^2 \cdot C_L^2} \approx \frac{1}{1+r} \tag{7.33}$$

Therefore, Equation (7.26) can be simplified as:

$$P_{\max} = P(\omega_r) = \frac{a^2 \cdot \mathrm{K}}{\omega_r^2} \cdot \frac{r}{(1+r)^2} \cdot \frac{1}{\left(\frac{1}{Q} + \frac{\mathrm{K}}{\omega_r \cdot m} \cdot \frac{1}{1+r}\right)^2} \tag{7.34}$$

$$P_{\max} = \frac{a^2 \cdot \mathrm{K} \cdot r \cdot m^2}{\left[\frac{\omega_r \cdot m \cdot (1+r)}{Q} + \mathrm{K}\right]^2} \tag{7.35}$$

Equation (7.35) shows that the maximum power is a function of the resonant frequency. When the resonant frequency increases, the maximum power decreases. For a self-tuned generator, the power level must not change much while the resonant frequency is changing.

Hypothesis 2

As long as hypothesis 1 stands, there comes the second hypothesis:

$$\mathrm{K} >> \frac{\omega_r \cdot m \cdot (1+r)}{Q} \tag{7.36}$$

If Inequality (7.36) is satisfied, then:

$$\frac{\omega_r \cdot m \cdot (1+r)}{Q} + \mathrm{K} \approx \mathrm{K} \tag{7.37}$$

Therefore, the maximum power is:

$$P_{\max} = P(\omega_r) = \frac{a^2 \cdot r \cdot m^2}{\mathrm{K}} \tag{7.38}$$

which is independent of the resonant frequency.

Based on the above analysis, resonant frequency tuning for generators using electrical method is feasible. The power spectrum of the generator can be shifted by adjusting the load capacitance. The tunability[1] of an electromagnetic generator is independent of the mass, Q-factor and coil resistance of the generator and the acceleration of the vibration. However, the value of the coil resistance determines the value of load capacitance that is needed to achieve the tuning (Figure 7.8). The larger the coil resistance, the smaller the load capacitances that are needed to achieve tuning. The tunability depends mostly on K and the ratio of load resistance to coil resistance, *r*. Figure 7.9 and Figure 7.10 shows the effect of K and *r* on the tunability of the electromagnetic generator using electrical tuning method, respectively. It is found that K must be high and *r* has to be small to achieve maximum tunability. K is defined as the coupling factor and will be studied in the following section.

[1] Tunability of an electromagnetic generator using electrical tuning is defined as the tuning range across which the generator can maintain the same output power level as an untuned generator (given by Equation 7.38). The higher this tuning range, the better the tunability.

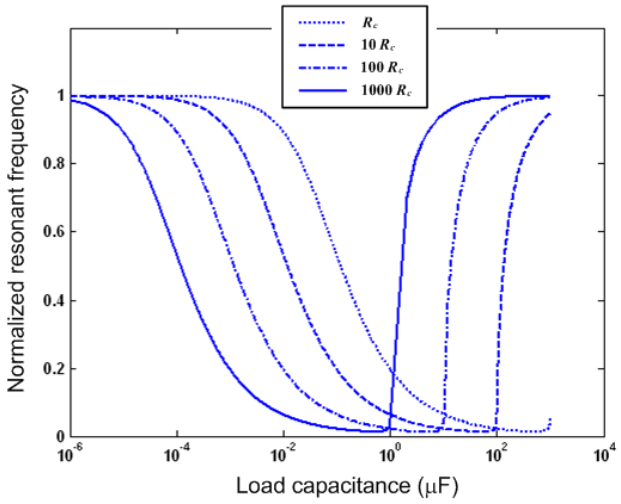

(a) Resonant frequency

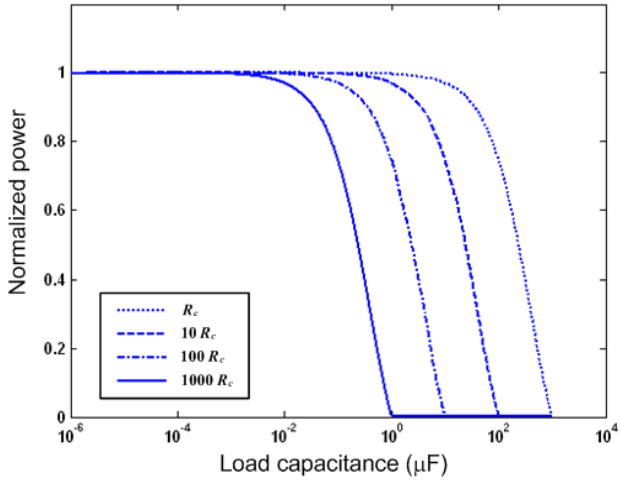

(b) Output power

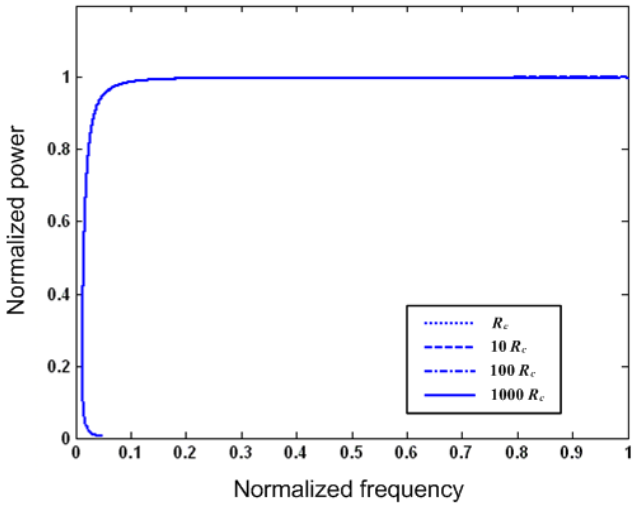

(c) Output power vs. resonant frequency

Figure 7.8. Tunability of electromagnetic generator with various coil resistances (K = 1000, r = 1).

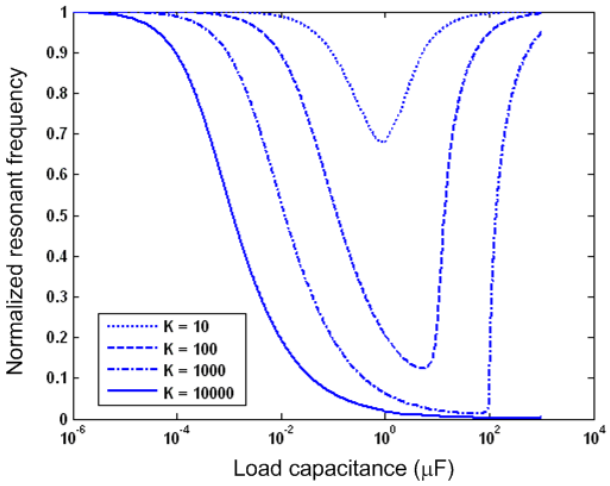

(a) Resonant frequency

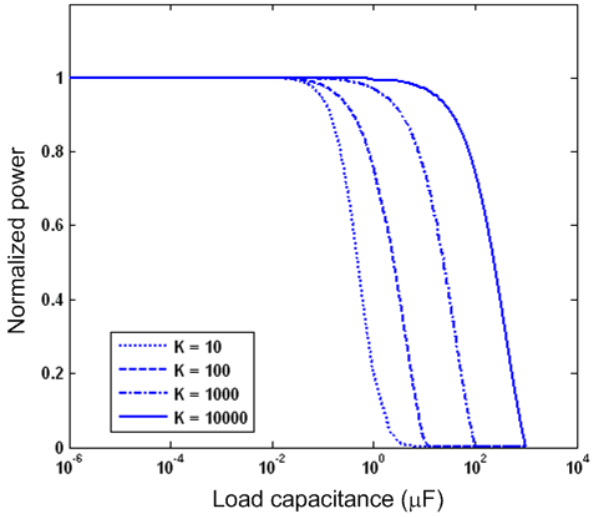

(b) Output power

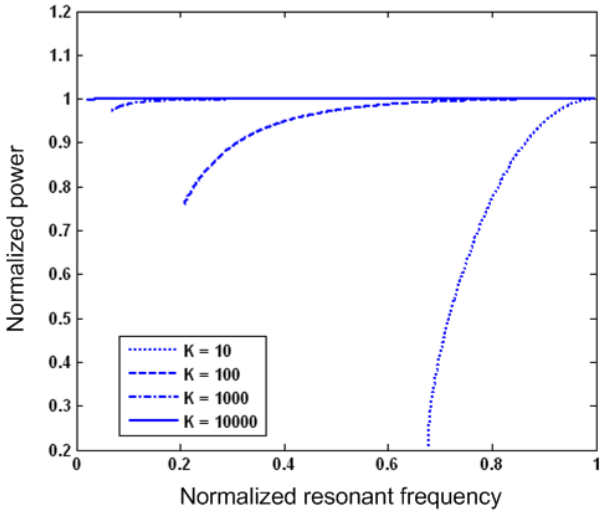

(c) Output power vs. resonant frequency

Figure 7.9. Tunability of electromagnetic generator with various K ($r = 1$).

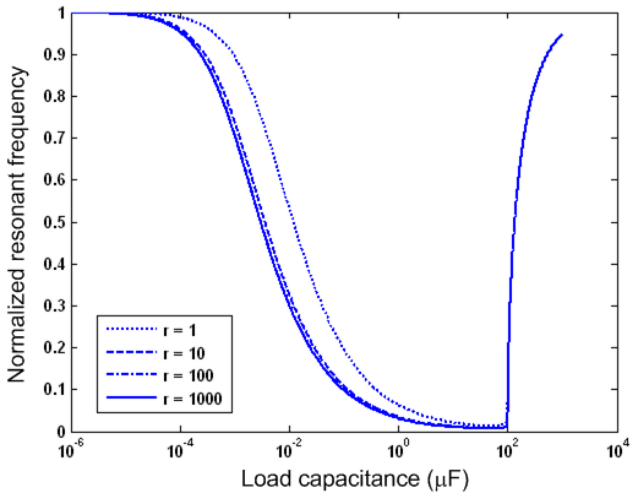

(a) Resonant frequency

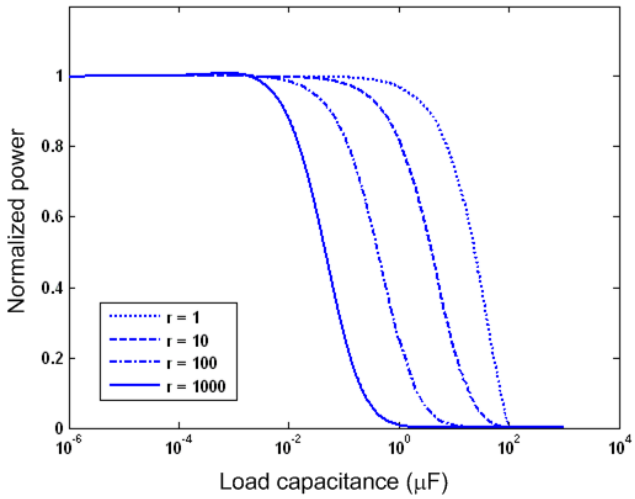

(b) Output power

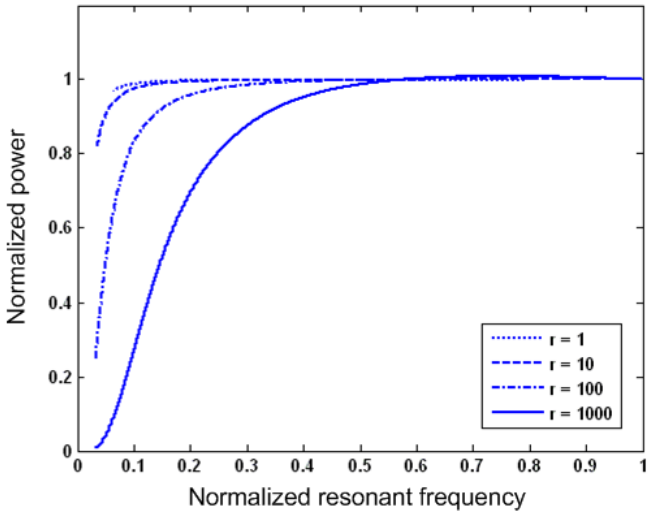

(c) Output power vs. resonant frequency

Figure 7.10. Tunability of electromagnetic generator with various *r* (K = 1000).

7.3 Analysis of Electromagnetic Coupling Factor, K

In this research, attention has been particularly paid to frequency tuning in electromagnetic generators. Therefore, in the following parts, only details relevant to electromagnetic generators are studied.

The electromagnetic coupling factor K is given by:

$$\mathrm{K} = \frac{k_e^2}{R_c} \tag{7.39}$$

where $k_e = \frac{V}{v}$ and R_c is the coil resistance, V is the induced voltage within the coil and v is the moving velocity of the mass.

According to Faraday's law of induction, the induced voltage within the inductor coil is:

$$V = -N \cdot \frac{d\phi}{dt} \tag{7.40}$$

where N is the number of turns of the coil and $\frac{d\phi}{dt}$ is the time-rate of change of magnetic flux ϕ.

Therefore, the electromagnetic coupling factor K can be rewritten as:

$$\mathrm{K} = \frac{N^2 \cdot \left(\frac{d\phi}{dt}\right)^2}{R_c \cdot v^2} \tag{7.41}$$

The parameters N and R_c are only dependent on the coil geometry and dimensions, so the coil coefficient, γ, is define as:

$$\gamma = \frac{N^2}{R_c} \tag{7.42}$$

K becomes:

$$\mathrm{K} = \gamma \cdot \frac{\left(\frac{d\phi}{dt}\right)^2}{v^2} = \gamma \cdot \frac{\left(\frac{d\phi}{dz} \cdot \frac{dz}{dt}\right)^2}{v^2} \tag{7.43}$$

Equation 7.43 can be simplified as:

$$\mathrm{K} = \gamma \cdot \left(\frac{d\phi}{dz}\right)^2 \tag{7.44}$$

To increase electromagnetic coupling factor K, the coil coefficient must be increased as well as magnetic flux within the core of the coil and also the velocity of the mass must be decreased. Also, changes in magnetic flux within unit displacement of the mass have to be increased to achieve high electromagnetic coupling factor.

7.3.1 Relationship between the Coil and K

From Equation (7.43), it is easy to find out that the larger the coil coefficient, the higher the K. In the following section, methods of increasing the coil coefficient will be discussed.

The number of the turns of the coil can be calculated by:

$$N = \frac{4F_c \cdot \left(R_o - R_i\right) \cdot t}{\pi \cdot d^2} \tag{7.45}$$

where F_c is the coil fill factor that is the ratio of the volume of conductor to the volume of the coil, R_o and R_i are the outer and inner radius of the coil, respectively. t is the total thickness of the coil and d is the diameter of the coil wire.

The coil resistance is given by:

$$R_c = \rho \frac{L_c}{A} \tag{7.46}$$

where ρ is the electrical resistivity of the wire material, L_c is the total length of the coil wire and A is the cross area of the wire. The total wire length is:

$$L_c = \frac{4F_c \cdot \left(R_o^2 - R_i^2\right) \cdot t}{d^2} \tag{7.47}$$

The cross section area of the wire is:

$$A = \frac{\pi \cdot d^2}{4} \tag{7.48}$$

Substitution of Equation (7.47) and (7.48) into Equation (7.46) yields the formula of coil resistance can be rewritten as:

$$R_c = \rho \cdot \frac{16F_c \cdot \left(R_o^2 - R_i^2\right) \cdot t}{\pi \cdot d^4} \tag{7.49}$$

Hence, the coil coefficient can be rewritten as:

$$\gamma = \frac{F_c \cdot \left(R_o - R_i\right) \cdot t}{\rho \cdot \pi \cdot \left(R_o + R_i\right)} \tag{7.50}$$

7.3.2 Relationship between the Magnetic Field and K

Assume that the resonator makes a sinusoidal movement. This movement can be

described as

$$z(t) = Z\sin(\omega t) \tag{7.51}$$

where Z is the maximum displacement of the mass and ω is the vibration frequency.

Since the magnets are part of the mass, the magnetic field within the generator changes sinusoidally. Assuming that the displacement of the mass and change in magnetic field are always in phase, the magnetic field is given by:

$$\phi(t) = \Phi\sin(\omega t) \tag{7.52}$$

where Φ is the maximum flux linkage. Therefore,

$$\frac{d\phi(t)}{dt} = \omega\Phi\cos(\omega t) \tag{7.53}$$

Hence, K can be written as:

$$\mathrm{K} = \gamma \cdot \frac{(\omega\Phi\cos(\omega t))^2}{(\omega Z\cos(\omega t))^2} \tag{7.54}$$

$$\mathrm{K} = \gamma \cdot \frac{\Phi^2}{Z^2} \tag{7.55}$$

K is proportional to the square of the maximum magnetic flux linkage and inverse-proportional to the square of the maximum displacement of the mass (magnets). Therefore, the layout of the magnets must be carefully designed so that a large magnetic field strength can be achieved within the small travel range of the magnets.

7.3.3 Key Points in Designing Electromagnetic Generators Capable of Electrical Tuning

Based on analysis above, some key points in designing electromagnetic generators with high tunability are summarized as follows:

- The coupling factor, K, has to be as large as possible;
- The bigger the generator, the higher K is needed to keep the output power of the generator unchanged;
- The ratio of load resistance to coil resistance should be kept low;
- To achieve large K, the coil coefficient must be large, i.e. the coil must have higher filling factor and larger thickness;
- The layout of magnets must be well designed so that the maximum change in flux linkage can be achieved within the minimum displacement of the magnets;
- Mass, Q-factor and coil resistance do not affect the tunability of the electromagnetic generator;
- With large K and *r*, the mass of the generator must be large to ensure high output power;
- The larger the coil resistance, the smaller the load capacitances are needed to achieve frequency tuning.

7.4 Micro Scale Electromagnetic Generator with Electrical Frequency Tuning

7.4.1 Overview of the Generator, G_et1

Figure 7.11 shows the overall design of the electromagnetic micro-generator for frequency tuning using the electrical method. In Figure 7.11(b), a DIP-16 socket is placed next to the generator as a reference of its dimensions. This generator is called 'G_et1'[1] in the rest of this section.

[1] 'G' stands for 'Generator' and 'et' stands for Electrical Tuning. The name 'G_et1' means 'the generator for electrical tuning, No. 1'.

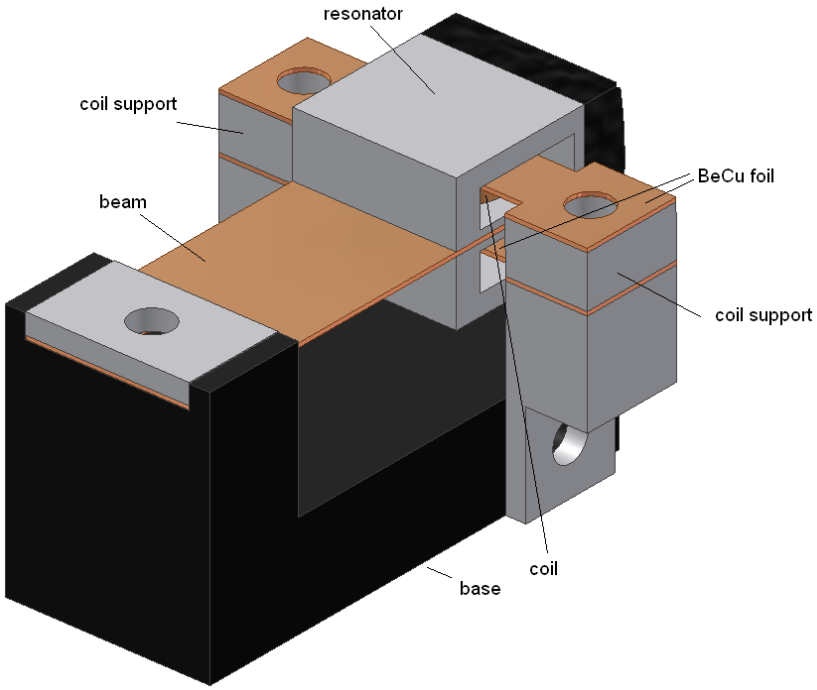

(a) Model

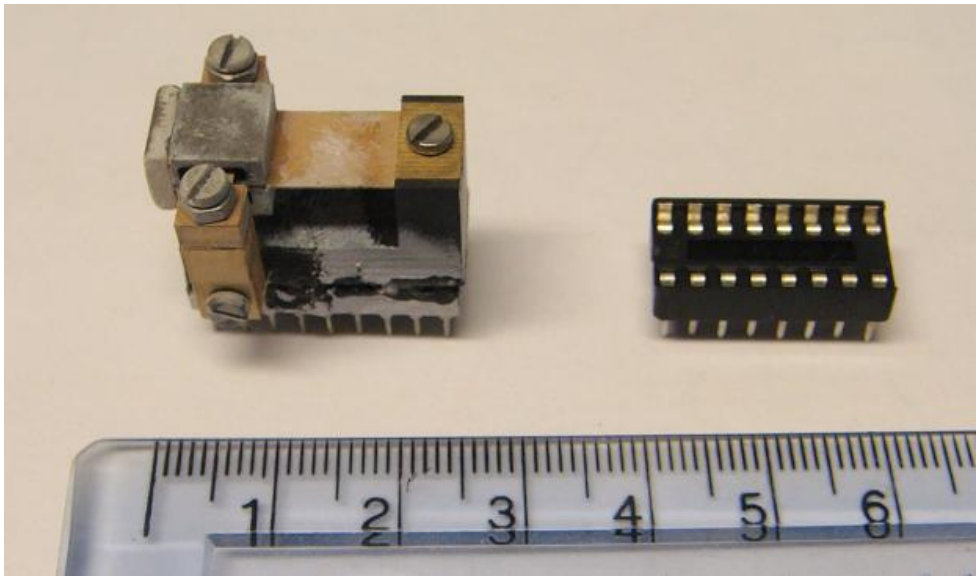

(b) Photo

Figure 7.11. Overview of G_et1.

G_et1 has a fixed coil and a resonator consists of two magnets and a set of magnetic flux guide. Figure 7.12 and 7.13 show the exterior and interior of the resonator, respectively. Figure 7.14 presents the cross-sectional view of the resonator of the A-A' plane in the Figure 7.13.

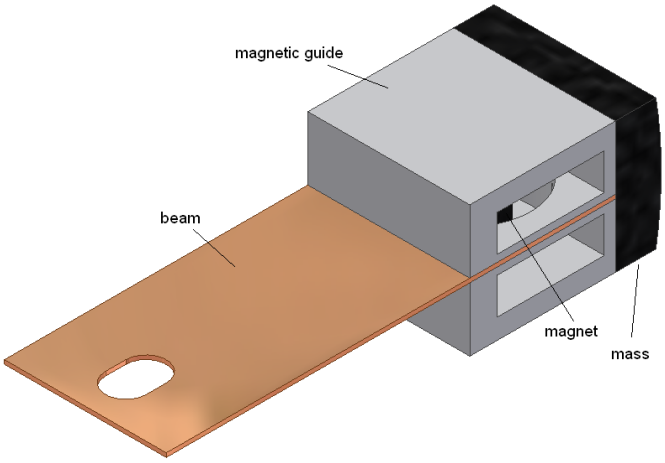

Figure 7.12. Exterior of the resonator of G_et1.

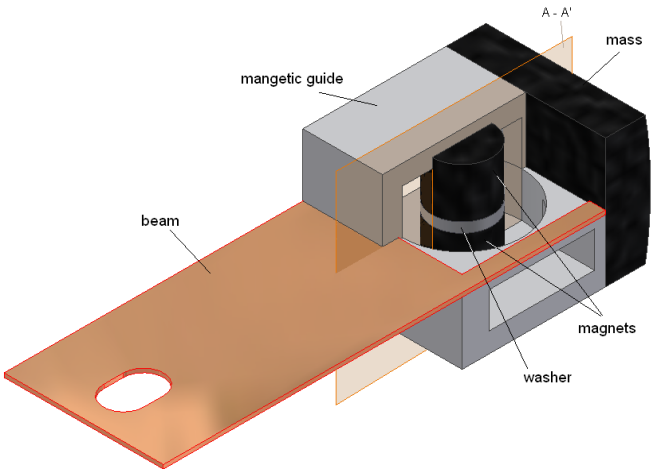

Figure 7.13. Interior of the resonator of G_et1.

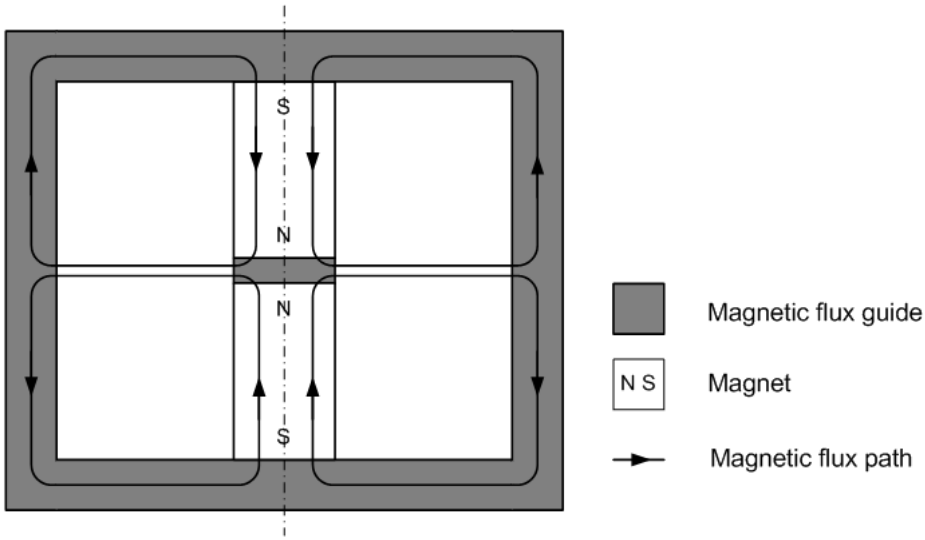

Figure 7.14. Cross-sectional view of the resonator of G_et1.

The identical poles of the two magnets are facing each other so that there forms the four magnetic flux paths. The magnet material is NdFeB, a strong permanent magnet. The magnetic flux guide is made of mild steel that has very high permeability. One piece of 1 mm thick mild steel washer is placed between two magnets to (a) reduce the compelling force between them to make it easy to assemble the generator and (b) divert the magnetic flux to the side magnetic flux guide. The beam is made of BeCu, which has good mechanical properties as mentioned in Section 5.4.1. All components are then glued together using cyanoacrylate. An inertial mass is glued to the free end of the cantilever. Figure 7.15 and Table 7.2 show the dimensions of this generator. The total volume of the generator is 11 cm^3 including the base.

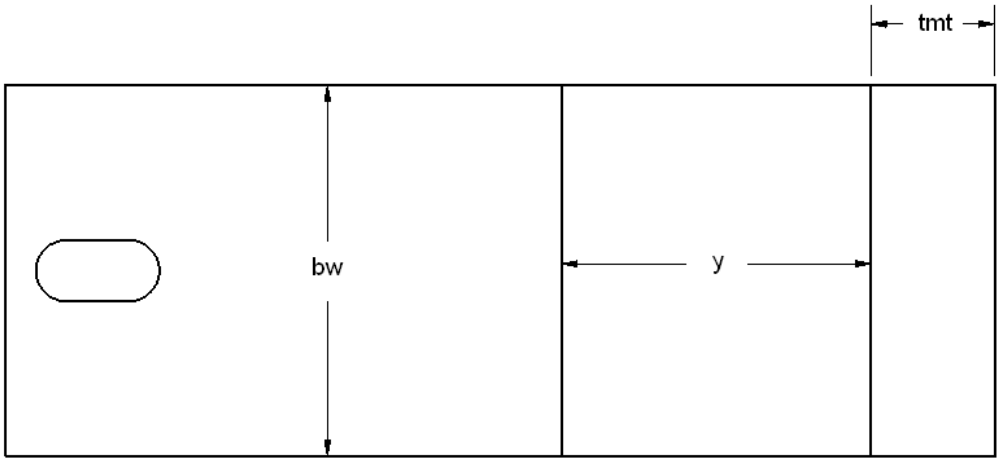

(a) Top view

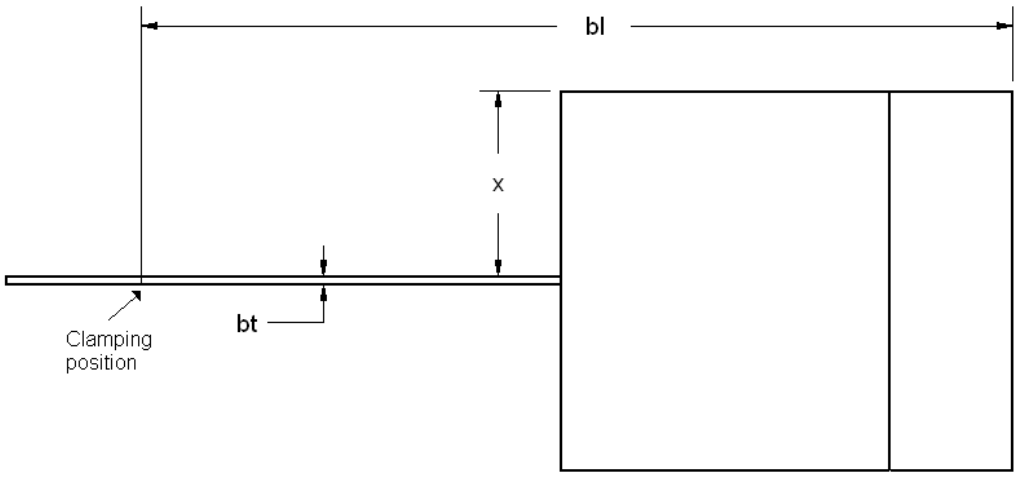

(b) Side view

Figure 7.15. Dimensions of the resonator of G_et1.

Table 7.2. Dimensions of the resonator.

x	y	bw	bl	bt	tmt
6	7	8	19	0.2	2

(Unit: mm)

The cylinder coil is fixed by two coil supports that are attached to both sides of the generator. Two pieces of BeCu foil connect the two coil supports and hold the coil so that the coil sits around the magnets. The outer and inner diameters of the coil are 5mm and 4mm, respectively. The height of the coil is 2.5mm. The coil wire diameter is 25μm. The coil resistance is measured as 697Ω. The number of coil turns is around 1430 and the fill factor is 0.56. In addition, the coil inductance is measured as 0.3mH. The coil supports and foils are screwed together using M2 screw. Figure 7.16 shows the overall structure of the generator, G_et1.

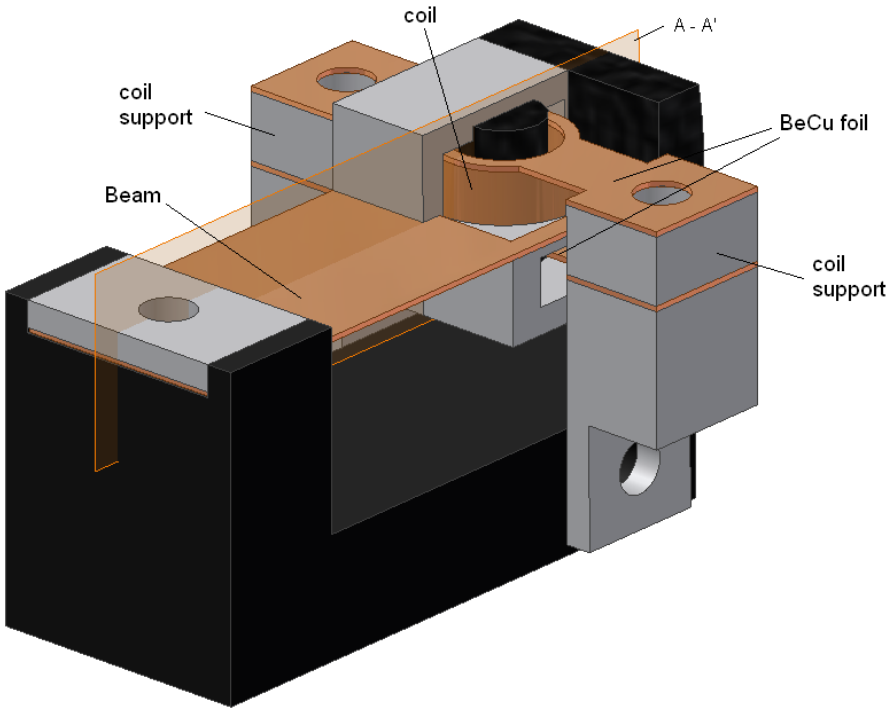

Figure 7.16. Structure of the generator, G_et1.

Figure 7.17 shows the cross sectional view of the A-A' plane in the Figure 7.16. When the resonator vibrates, the magnets together with the magnetic flux guide move up and down relative to the fixed coil. The coil cuts the magnetic flux thus inducing voltage across the coil.

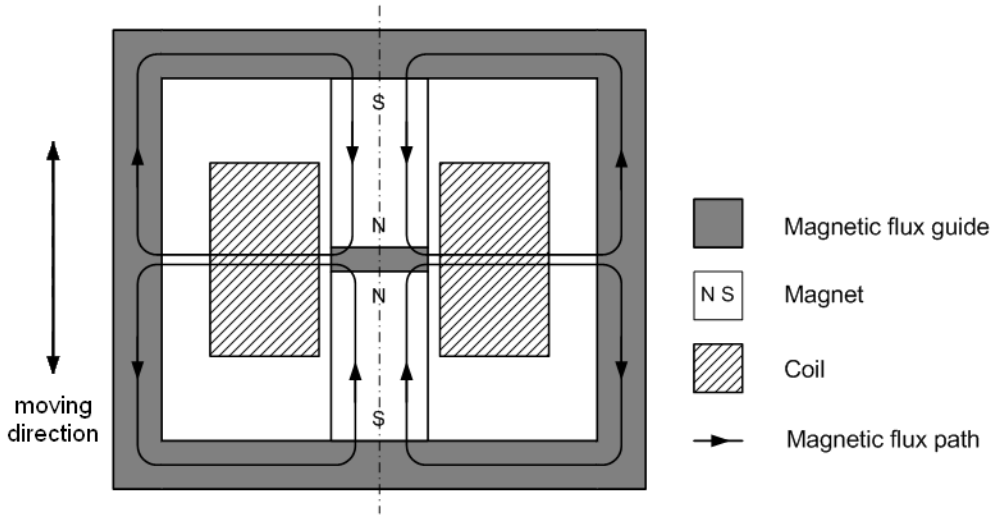

Figure 7.17. Cross-sectional view of the generator, G_et1.

7.4.2 Performance of the Generator, G_et1

The total mass of the generator is 5g and, for the dimensions mentioned in the previous section, the generator has a resonant frequency of 70.05Hz experimentally. The Q-factor of the generator is measured as 120 and the optimum load resistance is 3700Ω. The electromagnetic coupling factor, K, is calculated to be 0.0035 according to Equation (7.41).

Figure 7.18 shows the maximum power at the optimum resistive load and the open circuit voltage of the untuned generator when the generator was excited at various excitation levels, respectively. The maximum RMS output power is 18.4μW when the generator is excited at 30m***g***.

The largest excitation the generator can work at is 30m***g***. When the excitation level is beyond 30m***g***, the resonator would collide with the coil holder and the coil. To avoid the collision and protect the generator, all future tests on this generator were based on an excitation level of 30m***g***.

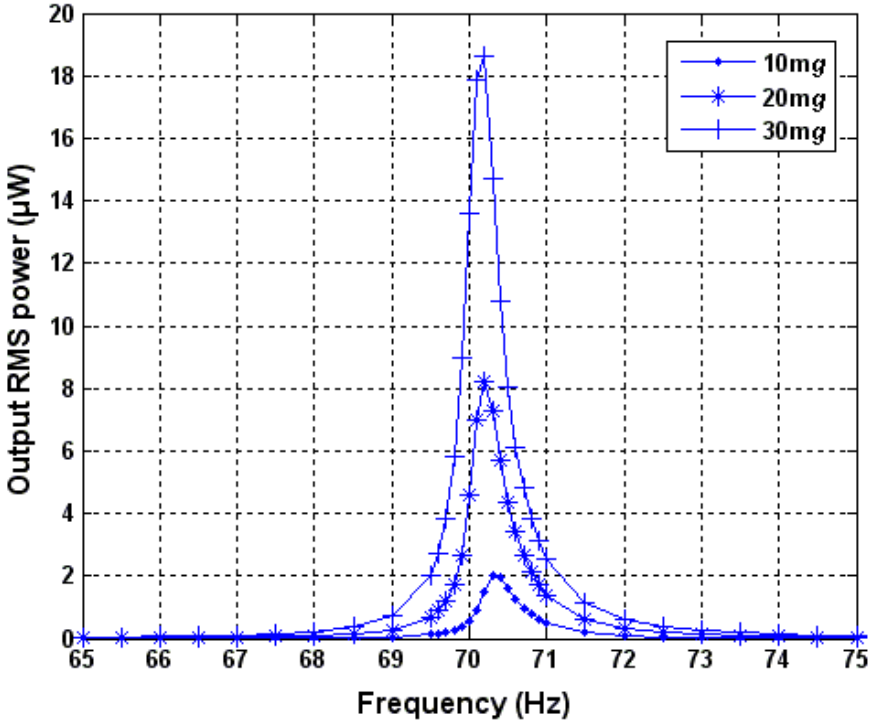

(a) Output RMS power at the optimum load

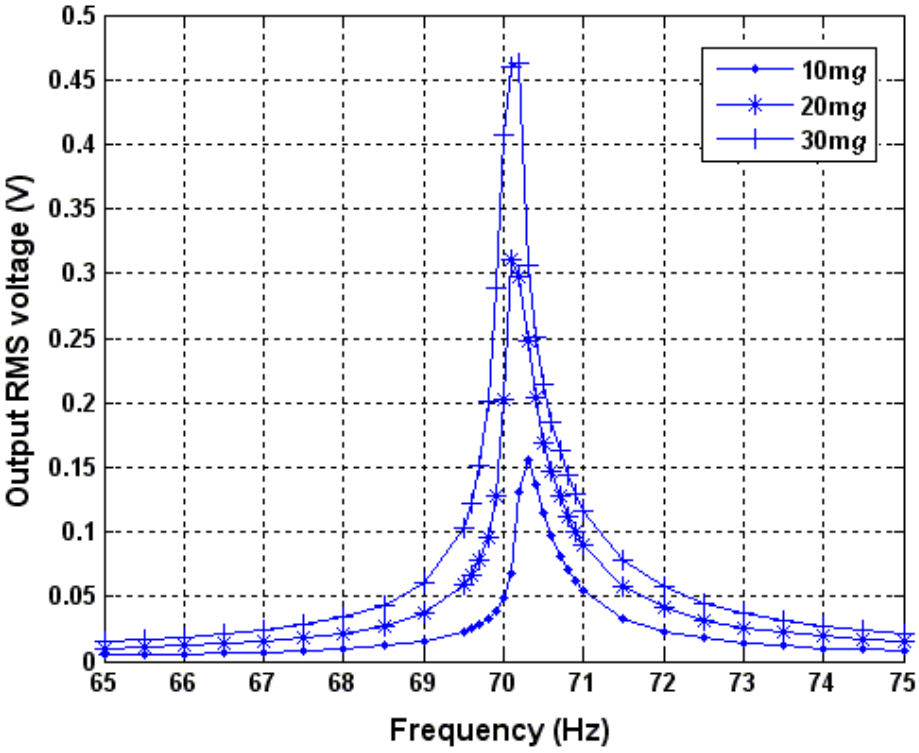

(b) Open circuit output RMS voltage

Figure 7.18. Performance of the untuned generator, G_et1.

Figure 7.19 compares test results and theoretical analysis of the resonant frequency of the generator with variations of load capacitance. The theoretical curve is drawn according to Equation (7.29). Note that, in this test, no capacitor is connected in series with the coil to cancel the coil inductance. The reason is as follows. As the coil inductance is 0.3mH and given the resonant frequency of 70.5Hz, the impedance of the coil inductance is only 0.132Ω which is much smaller than the coil resistance of 697Ω. Therefore, the effect of the coil inductance on the performance of the generator in this case can be ignored. Figure 7.20 compares test results and theoretical analysis of the maximum output power of the generator with variation of load capacitances. The theoretical curve is drawn according to Equation (7.30). Combining Figure 7.19 and 7.20 leads to Figure 7.21 which shows the maximum output power at various resonant frequencies. It is found through Figure 7.19 to 7.21 that the experimental resonant frequencies of the generator agree with the theory while the maximum output power at various resonant frequencies are less than the theory suggests. The overall tuning range is 0.2Hz. The operational frequency range over which the output power is reduced by less than 3dB of the untuned generator is 0.13Hz.

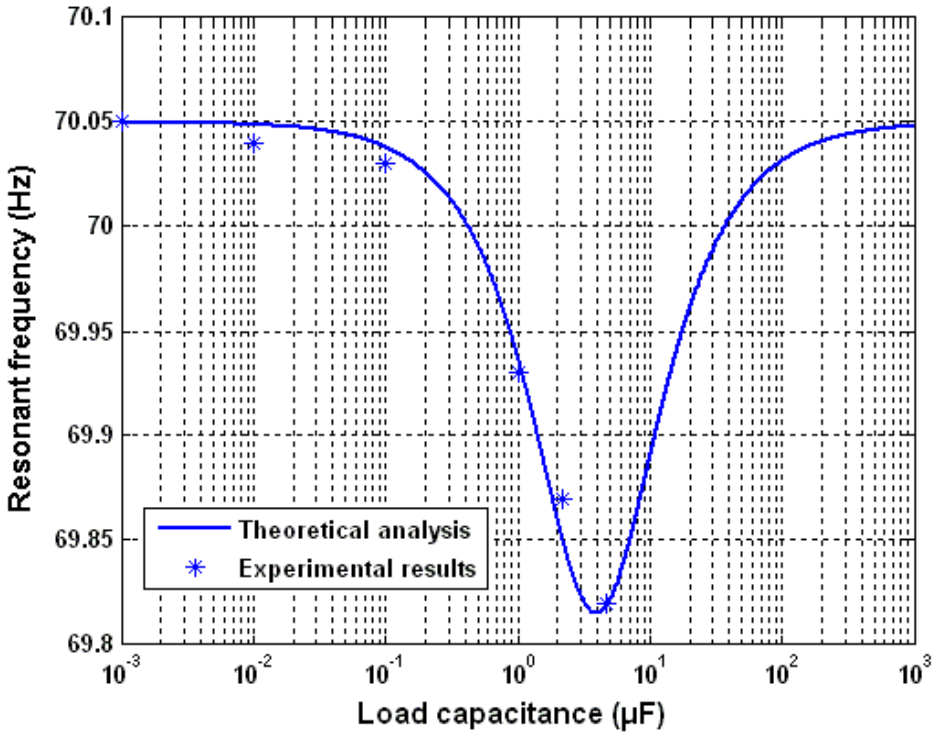

Figure 7.19. Resonant frequency of G_et1 with variations of load capacitances.

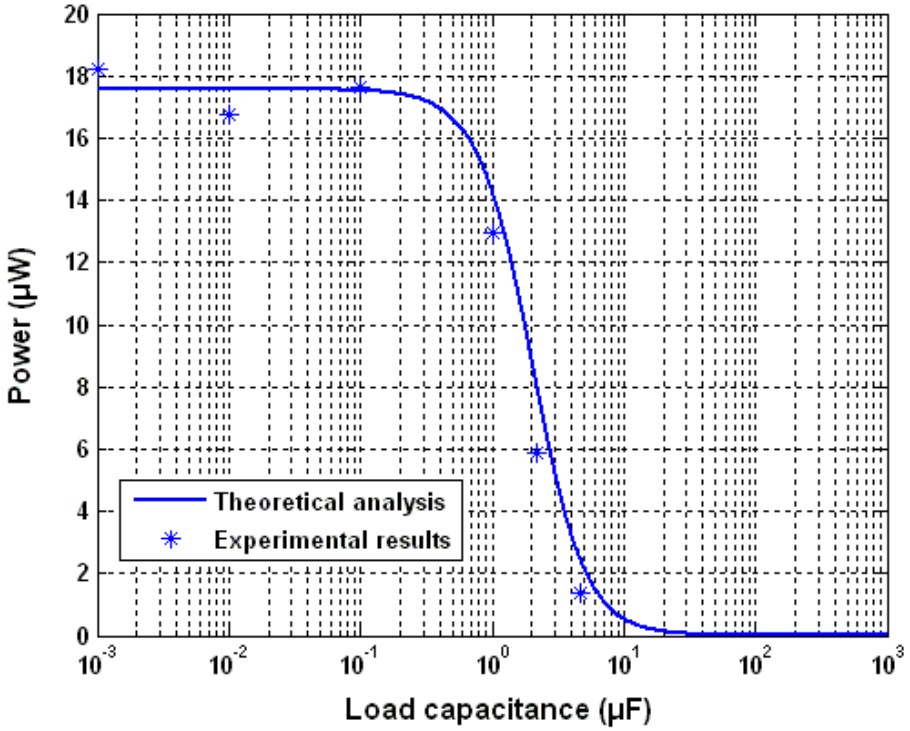

Figure 7.20. Maximum output power of G_et1 with variations of load capacitances.

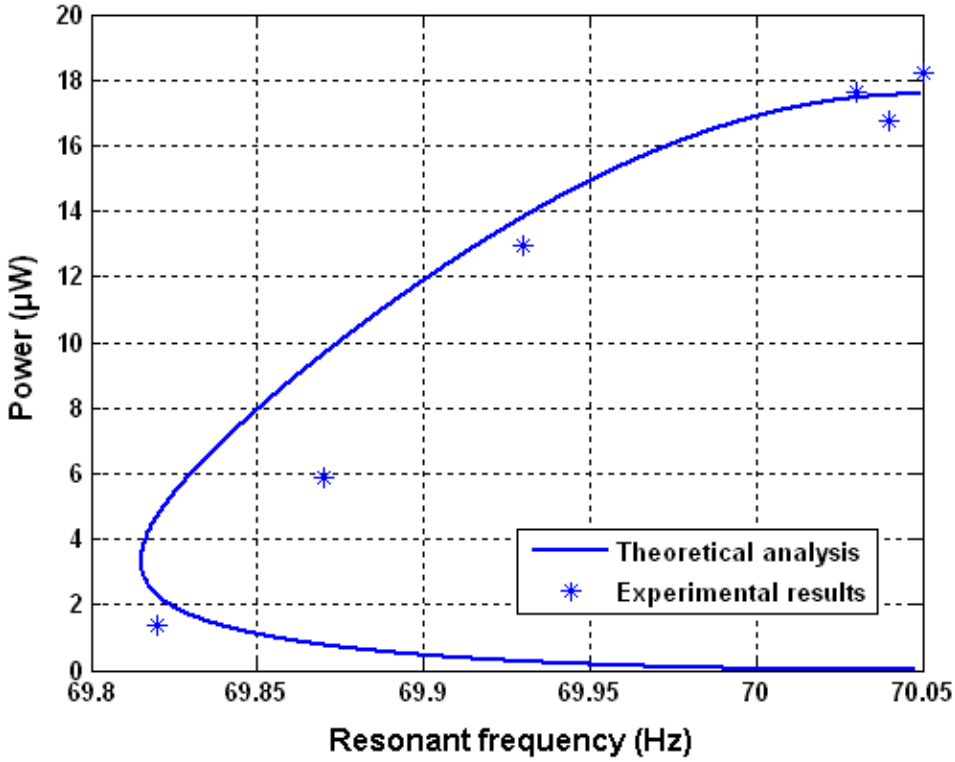

Figure 7.21. Maximum output power at various resonant frequencies of G_et1.

7.5 Macro Scale Electromagnetic Generator with Electrical Frequency Tuning

7.5.1 Overview of the Generator, G_et2

The macro scale electrically tunable electromagnetic generator described in this section was designed and built by Mr Thomas Mouille from Perpetuum Ltd. Tests have been done on this generator to further verify the mathematical model mentioned earlier in this chapter. This generator is called 'G_et2'[1] in the rest of this section.

The generator is a cylinder whose diameter is 7cm and height is 7.5cm as shown in Figure 7.22. The total volume of the generator is 289cm^3. Figure 7.23 shows the schematic cross sectional view of the generator along the centre axis. The generator consists of a stator (as shown in Figure 7.24) and a resonator (as shown in Figure 7.25). Note that in Figure 7.23, the centre rod is not part of the resonator. It is where the two springs are fixed.

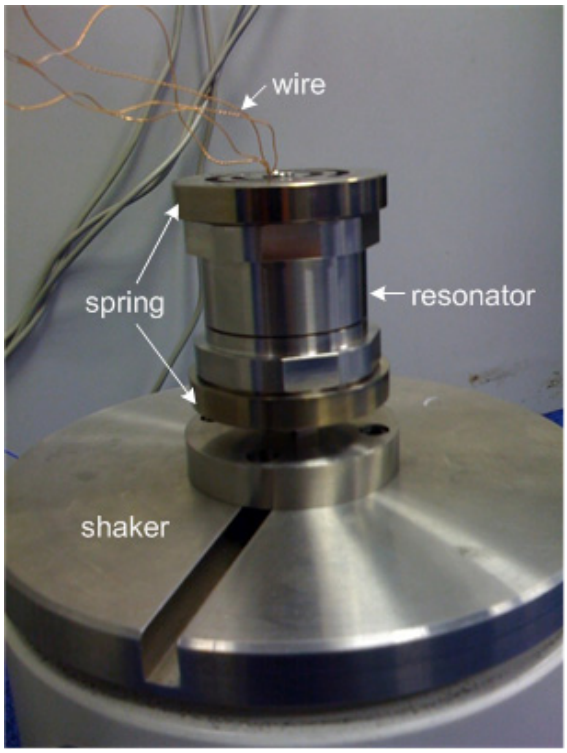

Figure 7.22. Photo of electrically tunable macro generator, G_et2 (Courtesy of Perpetuum Ltd.).

[1] 'G' stands for 'Generator' and 'et' stands for Electrical Tuning. The name 'G_et2' means 'the generator for electrical tuning, No. 2'.

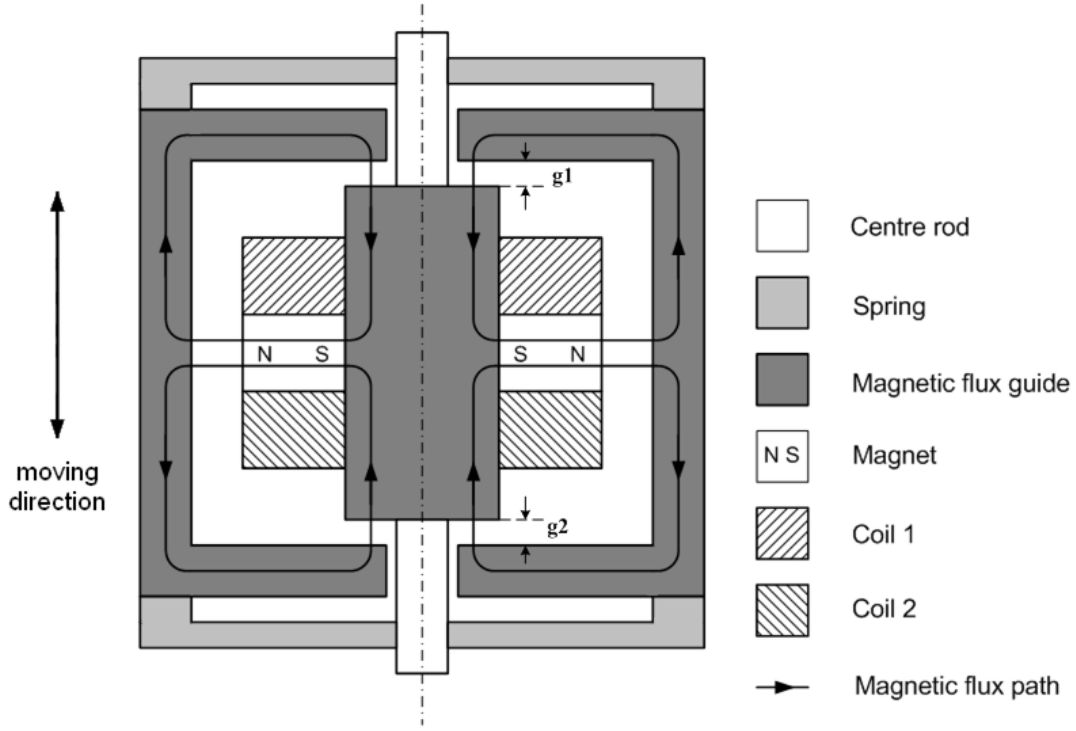

Figure 7.23. Schematic cross sectional view of G_et2.

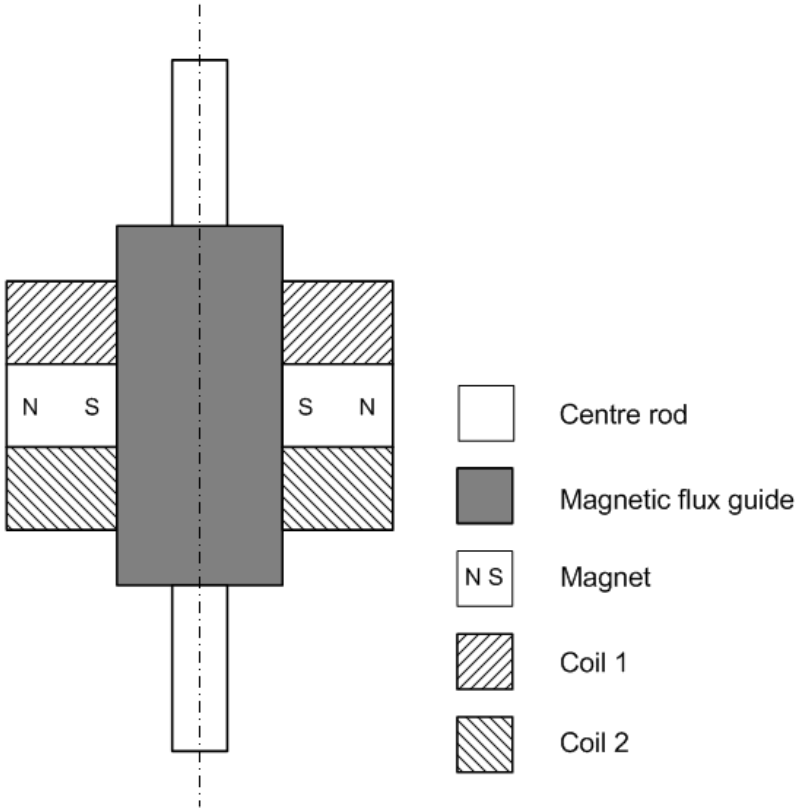

Figure 7.24. The stator of G_et2.

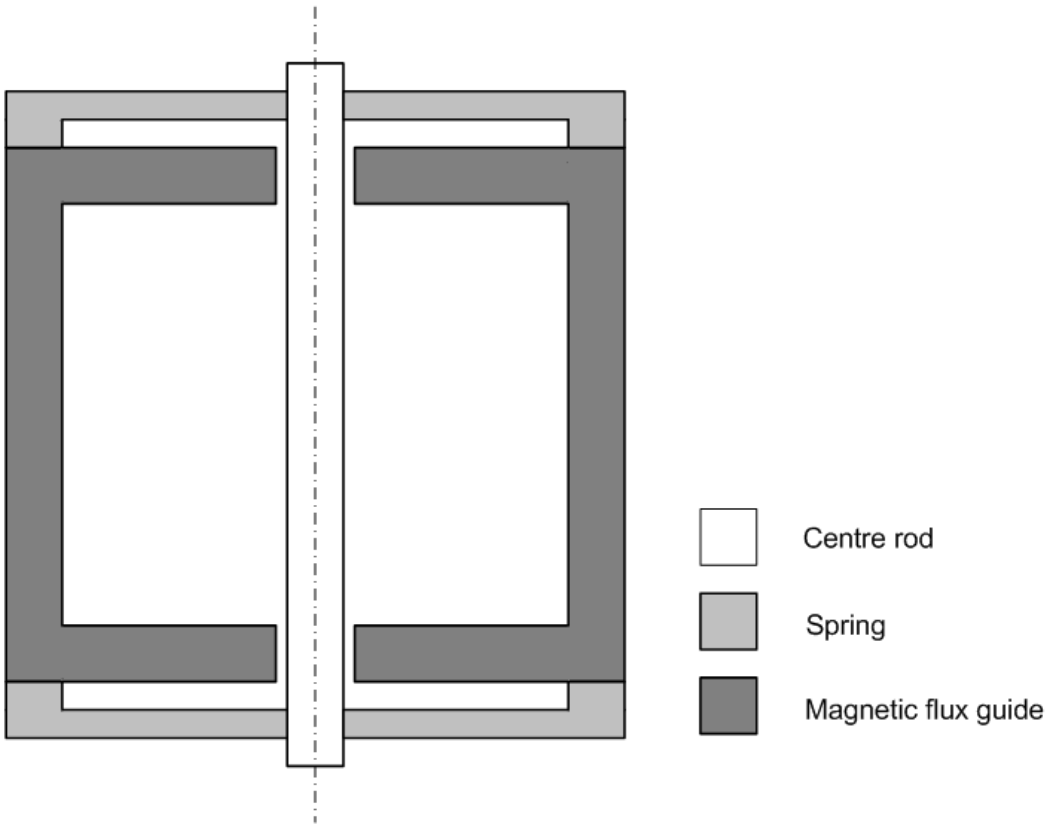

Figure 7.25. The resonator of G_et2.

The stator consists of a centre rod, a centre magnetic flux guide, two coils and a ring magnet magnetized radially. The centre magnetic flux guide is screwed and fixed on the centre rod and coils and the ring magnet are then fixed by plastic holders around the centre magnetic flux guide. The resonator consists of two springs which are screwed and fixed on both sides of the centre rod and the outer magnetic flux guide is fixed between the two springs. The outer magnetic flux guide also acts as the inertial mass.

During operation, the generator is fixed by attaching the centre rod to the vibration source. The little air gap between the centre magnetic flux guide and the outer magnetic flux guide, g1 and g2, vary with the movement of the resonator, which changes magnetic filed flux going through the two coils and thus induces voltage across the coils. The air gaps, g1 and g2, are both 0.2mm long when the generator is static. Therefore, the maximum displacement of the resonator should never exceed 0.2mm or the generator may be damaged.

The magnet and the magnetic flux guide are made of hard and soft ferrite, respectively. The spring is made of stainless steel. Magnet and coil holders are made of plastic and the coil is wound using copper wire.

The total mass of the generator is 830g. The electromagnetic coupling factor, K, is calculated to be 552.25 according to Equation (7.41). The coil resistance and inductance is measured as 99.5Ω and 4H, respectively.

7.5.2 Performance of the Generator, G_et2

The generator has been tested under the excitation level of 10m***g*** and 25m***g*** for comparison. The resonant frequencies of the generator are 95.1Hz and 95.5Hz when excited at 10m***g*** and 25m***g***, respectively. The Q-factor of the generator is measured as 1350 when excited at 10m***g*** and 1250 when excited at 25m***g***.

As the coil inductance is 4H and given the resonant frequency of 95.1Hz and 95.5Hz, the impedance of the coil inductance is 2390Ω and 2400Ω when excited at 10m***g*** and 25m***g***, respectively. They are much bigger than the coil resistance of 99.5Ω. Therefore, a capacitor of 680nF (according to Equation (7.20)) was connected in series with the coil to cancel the effect of the coil inductance on the performance of the generator in the tests described in this section.

Figure 7.26 shows the output RMS power and output RMS voltage at the designated resistive load of the untuned generator when the generator was excited at various excitation levels, respectively. The designated resistances are 10kΩ and 4kΩ when the generator is excited at 10m***g*** and 25m***g***, respectively. The purpose of using designated resistances rather than the optimum load resistance is to verify the generalization of the theory. The output RMS powers are 1.1mW at 10kΩ when excited at 10m***g*** and 2.8mW at 4kΩ when excited at 25m***g***.

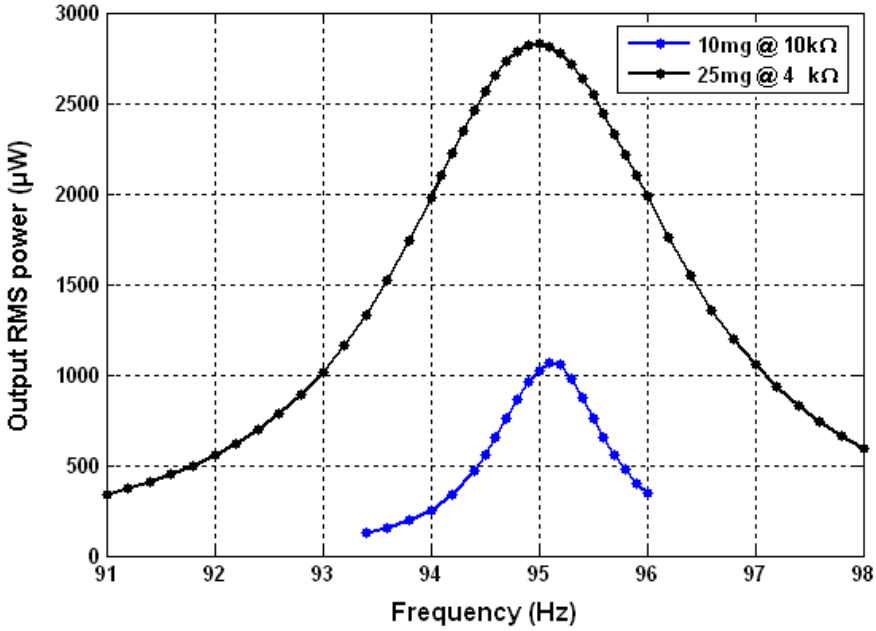

(a) Output RMS power at designated load resistance

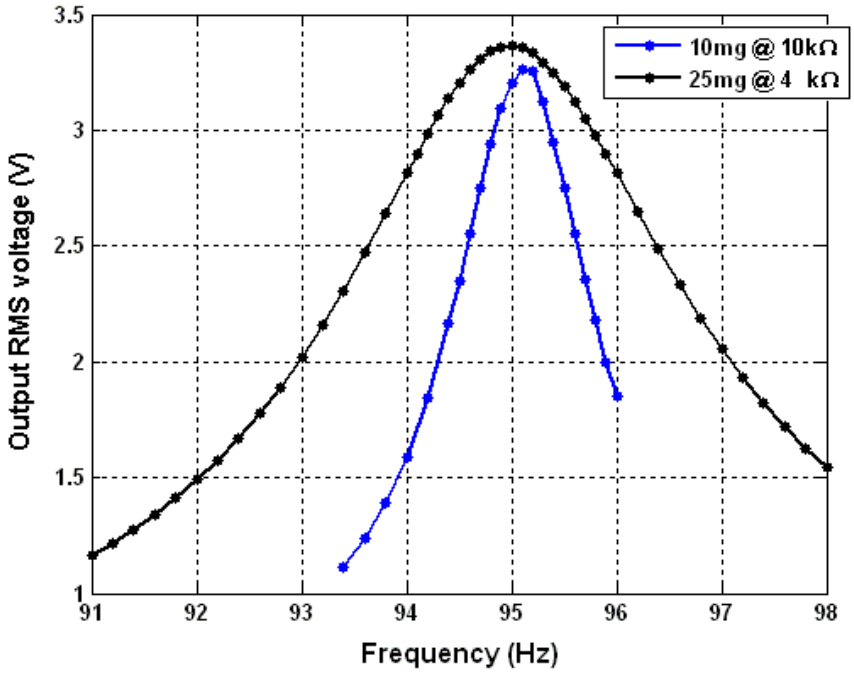

(b) Output RMS voltage at designated load resistance

Figure 7.26. Performance of the untuned generator, G_et2.

Figure 7.27 shows the power spectrum of the generator with a resistive load of 10kΩ and various capacitances ranging from 0 to 1400nF when excited at 10m***g***. Figure 7.28 and 7.29 compare test results and theoretical analysis of the resonant frequency and the maximum output power of the generator with variation of load capacitances,

respectively. The theoretical curves are drawn according to Equation (7.29) for resonant frequency and Equation (7.30) for output power. Combining Figure 7.28 and 7.29 leads to Figure 7.30 which shows the maximum output power at various resonant frequencies. It is found the resonant frequency together with the maximum output power reduces with the increase of the load capacitance as expected. The experimental results agree with the theory. The operational frequency range of the generator over which the output power is reduced by less than 3dB of the untuned generator is 2.2Hz.

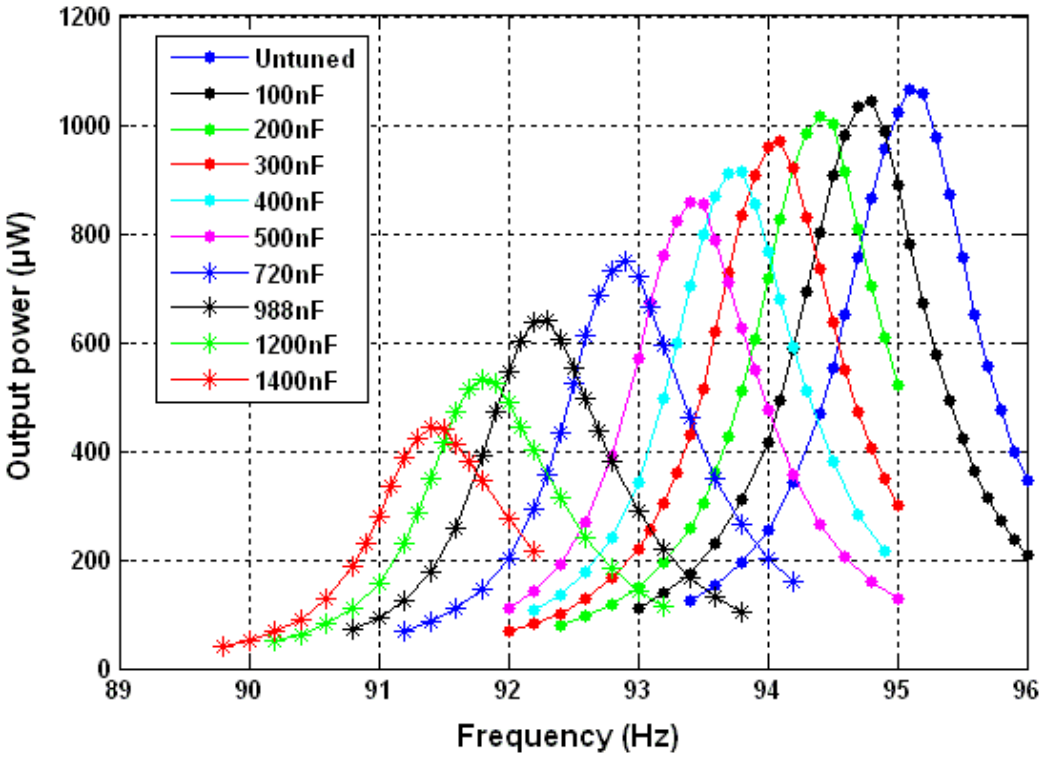

Figure 7.27. Power spectrum of G_et2 with variations of load capacitances when excited at 10m***g*** (load resistance is 10kΩ).

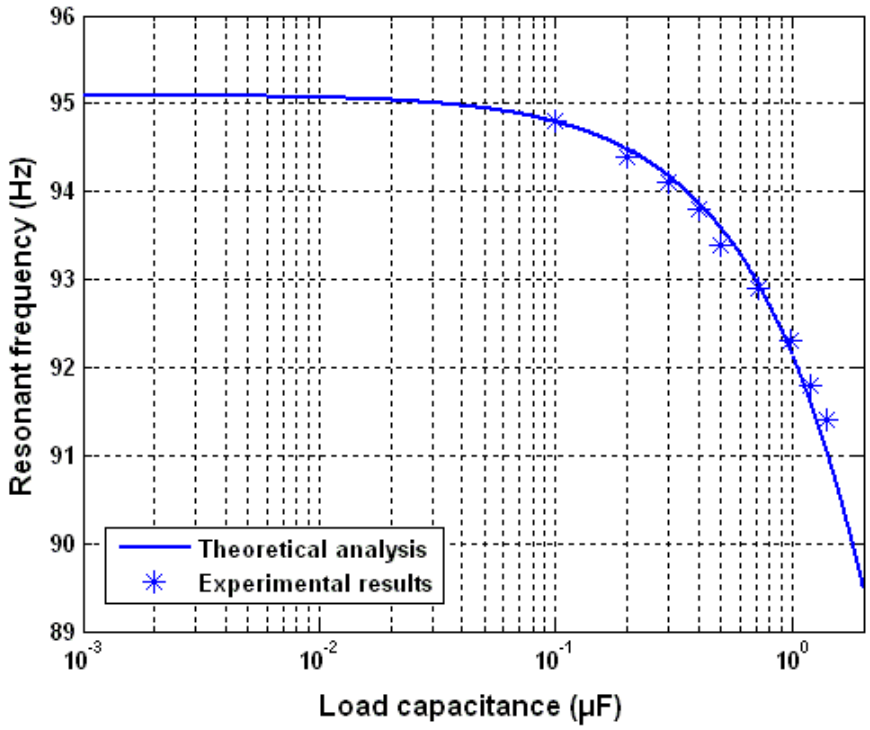

Figure 7.28. Resonant frequency of G_et2 with variations of load capacitances (excited at 10m***g***).

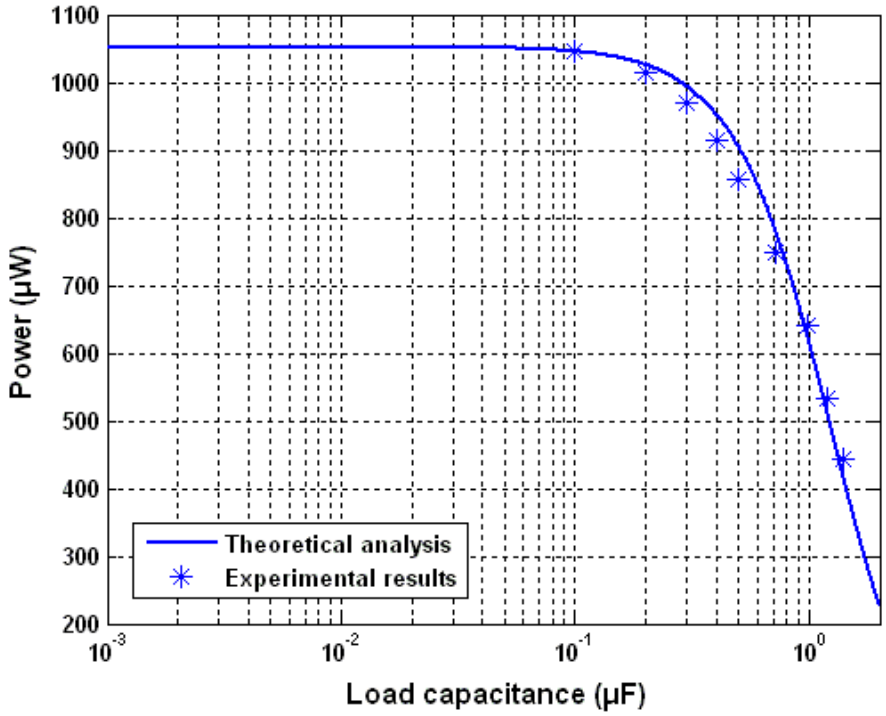

Figure 7.29. Maximum output power of G_et2 with variations of load capacitances (excited at 10m***g***).

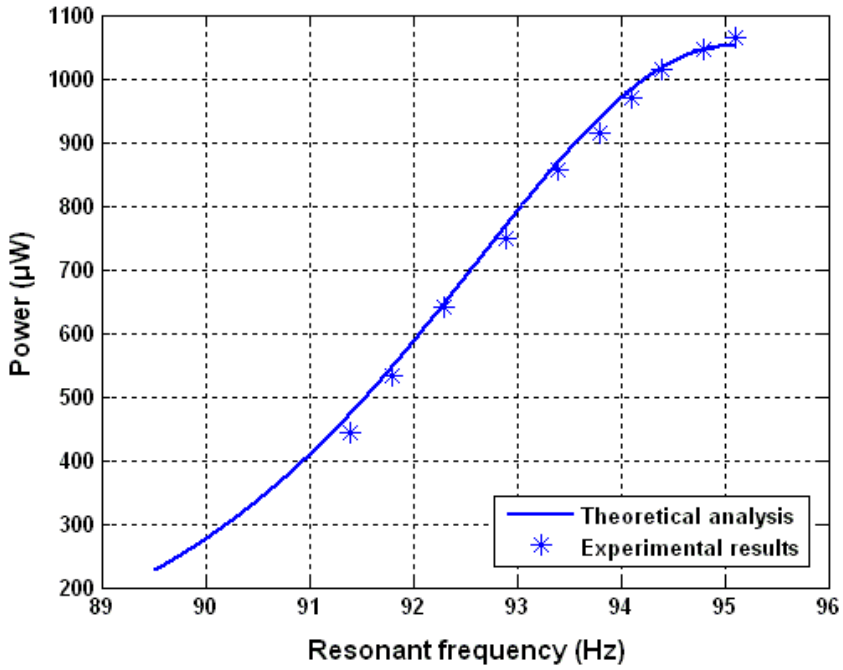

Figure 7.30. Maximum output power at various resonant frequencies of G_et2 (excited at 10m***g***).

Figure 7.31 shows the power spectrum of the generator with a resistive load of 4kΩ and various capacitances ranging from 0 to 1600nF when excited at 25m***g***.

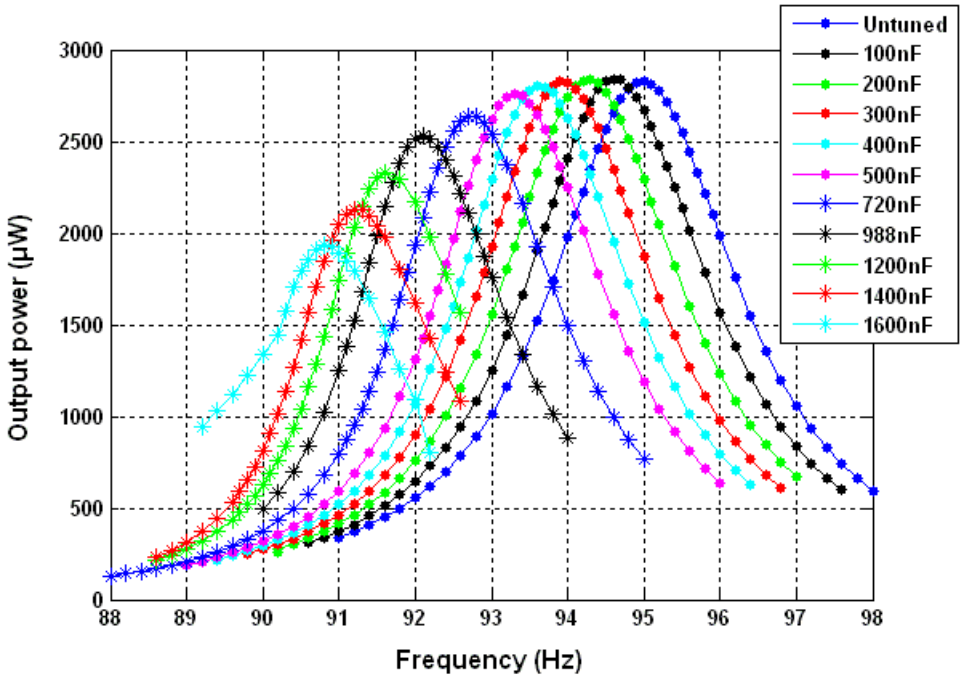

Figure 7.31. Power spectrum of G_et2 with variations of load capacitances when excited at 25m***g*** (load resistance is 4kΩ).

Comparisons of test results and theoretical analysis of the resonant frequency and the maximum output power of the generator with variations of load capacitances are shown in Figure 7.32 and 7.33, respectively. The theoretical curves are drawn according to Equation (7.29) for resonant frequency and Equation (7.30) for output power. Combining Figure 7.32 and 7.33 results in Figure 7.34 which shows the maximum output power at various resonant frequencies.

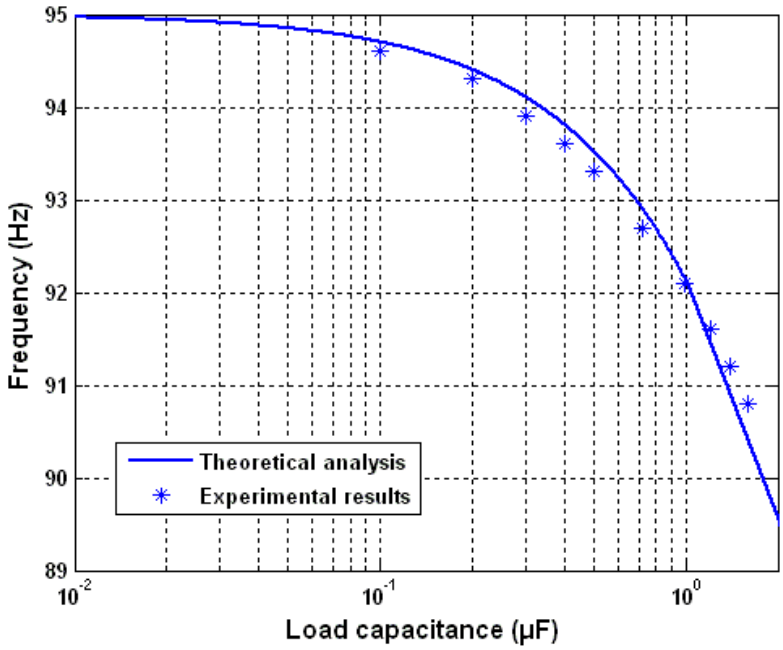

Figure 7.32. Resonant frequency of G_et2 with variations of load capacitances (excited at 25m***g***).

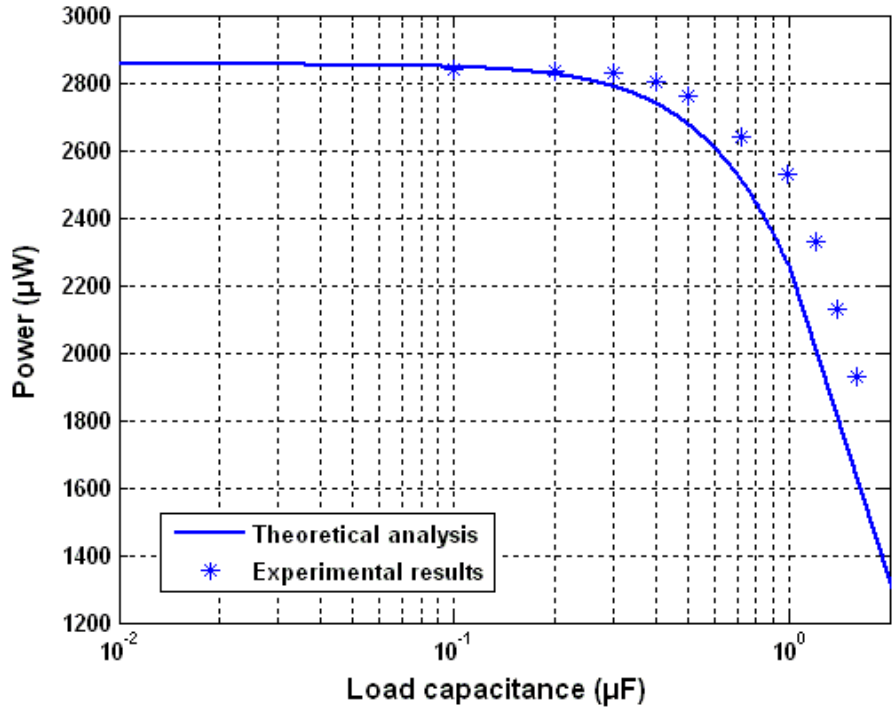

Figure 7.33. Maximum output power of G_et2 with variations of load capacitances (excited at 25m***g***).

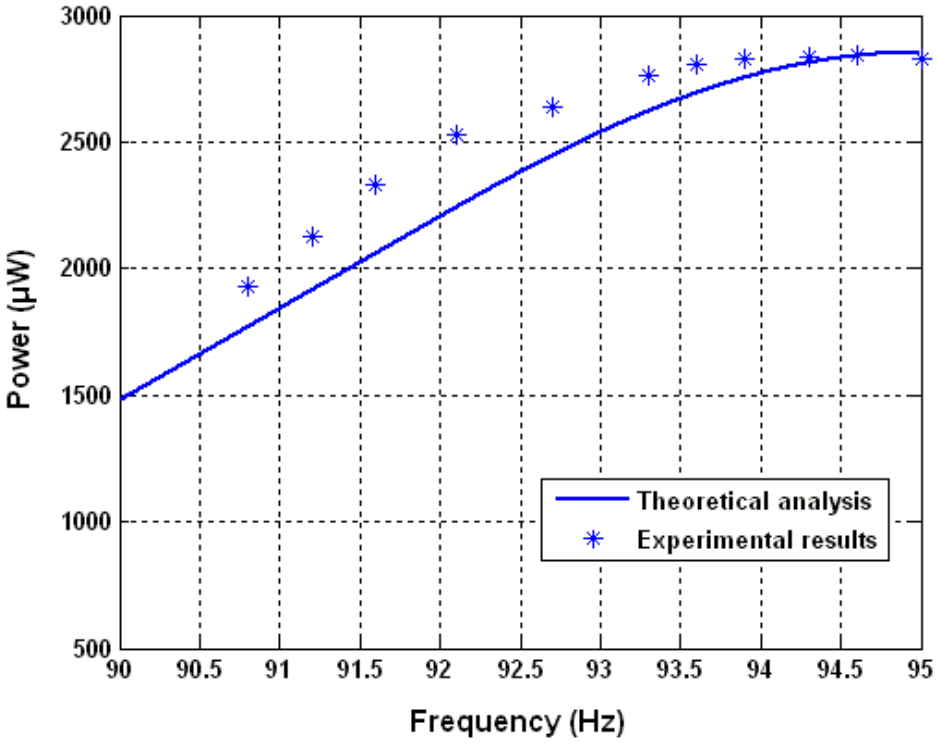

Figure 7.34. Maximum output power at various resonant frequencies of G_et2 (excited at 25m***g***).

It is found the resonant frequency reduced with the increase of the load capacitance as expected. When the load capacitance was small, the maximum power output remained unchanged while the resonant frequency reduced. Then the maximum power output started decreasing as the load capacitance increased. The experimental results of the resonant frequency agree with the theory while the experimental results of the maximum output power are bigger than the theory suggests. The reason is that there are hard cores inside the two coils, the coil inductance varies according to the change in magnetic flux within the hard core and also the movement of the resonator. The coil inductance changes with the vibration level of the generator. The coil inductance of 4H was measured when the generator is static. When the vibration level is small (e.g. 10m***g***), the coil inductance does not change much. Thus the value of the capacitor needed to be connected in series with the coil is close to the calculation based on the static situation. This is why the experimental results and theoretical analysis agree with each other in the case when the excitation level is 10m***g***. As the vibration level increases, the value of the capacitor needed to be connected in series with the coil is different from the calculation based on the static situation. The effect of the coil inductance on the performance of the generator becomes apparent and therefore causes the mismatch between the experimental results and the theoretical analysis. The operational frequency range of the generator over which the output power is reduced by less than 3dB of the untuned generator is 4.2Hz.

7.6 Comparisons of the Two Electrically Tunable Generators

Table 7.3 summarizes the performance of the two generators presented in Section 7.4 and 7.5. It is found that the macro generator, G_et2 has better performance regarding frequency tuning than the micro generator, G_et1. The volume and mass of the generator G_et2 are 166 and 26 times larger than those of the generator G_et1, respectively. However, the electromagnetic coupling factor, K, of G_et2 is over 150,000 times higher than that of G_et1. By comparing the magnetic circuits of these two generators, the reason for the huge difference in tunability of them can be unveiled.

Table 7.3. Comparisons of performance of G_et1 and G_et2.

	Mass (g)	Volume (cm^3)	K (T·m)	Vibration (m***g***)	Untuned resonant frequency (Hz)	Q	3dB frequency range[a] (Hz)	Tuning efficiency[b] (%)	Maximum load capacitance[c] (nF)
G_et1	5	11	0.0035	30	70.05	120	0.13	0.19	1000
G_et2	830	289	552.25	10	95.1	1350	2.2	2.3	700
				25	95.5	1250	4.2	4.4	1400

[a] The frequency range of the generator over which the output power is reduced by less than 3dB

[b] The ratio of the 3dB frequency range to the untuned resonant frequency

[c] The maximum load capacitance that the generator is connected to keep the resonant frequency within the 3dB frequency range

Figure 7.35 shows the magnetic circuit of these two generators. $\mathscr{R}_{ci}$[1] and $\mathscr{R}_{ai}$ represent the reluctances of the magnetic flux guide and the air gap, respectively. The components in the dashed line boxes are magnets. $\mathscr{F}_i$ represents the magnetomotive forces of the magnets and $\mathscr{R}_{mi}$ are the reluctances of the magnets.

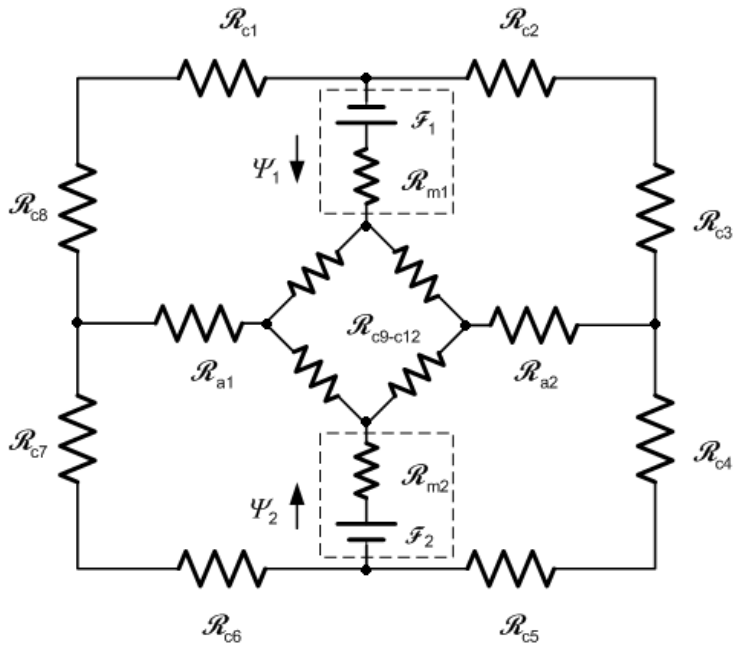

(a) G_et1

[1] i represents the integral.

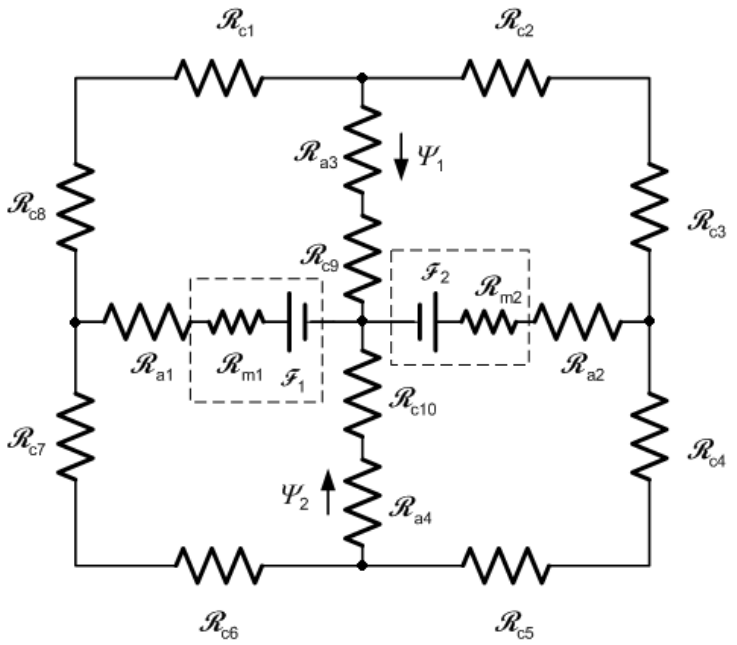

(b) G_et2

Figure 7.35. Magnetic circuits of the two electrical tunable generators.

As the structures of both generators are symmetric with the centre axis, the following equations apply when the generators are in operation.

For the micro generator, G_et1,

$$\mathcal{R}_{c1} = \mathcal{R}_{c2} = \mathcal{R}_{c5} = \mathcal{R}_{c6} \tag{7.56}$$

$$\mathcal{R}_{c3} = \mathcal{R}_{c8} \tag{7.57}$$

$$\mathcal{R}_{c4} = \mathcal{R}_{c7} \tag{7.58}$$

$$\mathcal{R}_{c9} = \mathcal{R}_{c10} = \mathcal{R}_{c11} = \mathcal{R}_{c12} \tag{7.59}$$

$$\mathcal{R}_{a1} = \mathcal{R}_{a2} = \mathcal{R}_{a} \tag{7.60}$$

$$\mathcal{R}_{m1} = \mathcal{R}_{m2} = \mathcal{R}_{m} \tag{7.61}$$

$$\mathcal{F}_1 = \mathcal{F}_2 = \mathcal{F} \tag{7.62}$$

For the macro generator, G_et2,

$$\mathcal{R}_{c1} = \mathcal{R}_{c2} = \mathcal{R}_{c5} = \mathcal{R}_{c6} \tag{7.63}$$

$$\mathcal{R}_{c3} = \mathcal{R}_{c8} \tag{7.64}$$

$$\mathcal{R}_{c4} = \mathcal{R}_{c7} \tag{7.65}$$

$$\mathcal{R}_{a1} = \mathcal{R}_{a2} = \mathcal{R}_{a}' \tag{7.66}$$

$$\mathcal{R}_{m1} = \mathcal{R}_{m2} = \mathcal{R}_{m} \tag{7.67}$$

$$\mathcal{F}_1 = \mathcal{F}_2 = \mathcal{F} \tag{7.68}$$

Based on Equation (7.56) to (7.66), magnetic flux in both magnetic circuits can be estimated. For G_et1, the magnetic flux passing through the coil, Ψ_1 and Ψ_2 are given by:

$$\Psi_{G\_et1a} = \Psi_1 = \frac{\mathcal{F}}{0.5\,\mathcal{R}_{c1} + 0.5\,\mathcal{R}_{c8} + 0.5\,\mathcal{R}_{c9} + \mathcal{R}_{m} + \mathcal{R}_{a}} \tag{7.69}$$

$$\Psi_{G\_et1b} = \Psi_2 = \frac{\mathcal{F}}{0.5\,\mathcal{R}_{c6} + 0.5\,\mathcal{R}_{c7} + 0.5\,\mathcal{R}_{c9} + \mathcal{R}_{m} + \mathcal{R}_{a}} \tag{7.70}$$

For G_et2, the magnetic flux passing through the coil, Ψ_1 and Ψ_2 are given by:

$$\Psi_{G\_et2a} = \Psi_1 = \frac{\mathcal{F}}{0.5\,\mathcal{R}_{c1} + 0.5\,\mathcal{R}_{c8} + \mathcal{R}_{c9} + \mathcal{R}_{m} + \mathcal{R}_{a1} + \mathcal{R}_{a3}} \tag{7.71}$$

$$\Psi_{G\_et2b} = \Psi_2 = \frac{\mathcal{F}}{0.5\,\mathcal{R}_{c6} + 0.5\,\mathcal{R}_{c7} + \mathcal{R}_{c10} + \mathcal{R}_{m} + \mathcal{R}_{a1} + \mathcal{R}_{a4}} \tag{7.72}$$

When G_et1 is working, the reluctances of magnetic flux guide, $\mathcal{R}_{c7}$ and $\mathcal{R}_{c8}$ vary with the movement of the resonator. They are given by:

$$\mathcal{R}_{c7} = \frac{L + \Delta y_1}{\mu_c \cdot \mu_0 \cdot S_c} \tag{7.73}$$

$$\mathcal{R}_{c8} = \frac{L - \Delta y_1}{\mu_c \cdot \mu_0 \cdot S_c} \tag{7.74}$$

where L is the original length of the magnetic flux guide, μ_c is the relative permeability of the magnetic flux guide material, μ_0 is the permeability of free space and S_c is the cross section area of the magnetic flux guide. Δy_1 is the displacement of the resonator relative to the static part.

When G_et2 is working, the reluctances of the air gaps, $\mathcal{R}_{a3}$ and $\mathcal{R}_{a4}$ vary with the movement of the resonator. They are given by:

$$\mathcal{R}_{a3} = \frac{g1 + \Delta y_2}{\mu_0 \cdot S_a} \tag{7.75}$$

$$\mathcal{R}_{a4} = \frac{g2 - \Delta y_2}{\mu_0 \cdot S_a} \tag{7.76}$$

where g1, g2 are the air gap between the resonator and the stator as shown in Figure 7.23. S_c is the cross sectional area of the air gap. Δy_2 is the displacement of the resonator relative to the stator. As the magnetic flux guides are made of ferromagnetic material, their permeability is much higher than that of air. Any small changes in the dimensions of air gaps will results in huge change in their reluctances while any small changes in the dimensions of the magnetic flux guides results in much less change in their reluctances. Furthermore, as reluctances of air gaps are much larger than those of magnetic flux guides, reluctances of air gaps dominate the total reluctance in the magnetic circuit. Small changes in reluctance of magnetic flux guide have little effect on the magnetic flux in the circuit while small changes in reluctance of air gap can change the magnetic flux significantly.

In the micro generator G_et1, the magnetic flux does not change while the mass is vibrating. Only the magnetic flux cutting the coil is changed due to the change in reluctances of the magnetic flux guides. In the macro generator G_et2, the magnetic flux is changed by varying the reluctances of the air gaps. Due to the space limit, the maximum displacements of both generators are similar (around 0.2mm). Apparently, magnetic flux change per unit displacement in G_et2 is much larger than that in G_et1. This is the reason why the electromagnetic coupling factor, K, in G_et2 is much higher than that in G_et1 and the macro generator G_et2 has larger tuning range than the micro generator G_et1.

7.7 Conclusions

In this chapter, frequency tuning by varying the electrical load, particularly, the capacitive load has been presented. The theoretical analysis of piezoelectric generator

suggests that the material of the substrate layer and mass does not affect the tunability. If a piezoelectric material with higher Young's modulus, strain coefficient and smaller permittivity is used, the generator can have a larger tuning range. The ratio of the thickness of the piezoelectric layer to the thickness of the substrate layer should be small to increase the tuning range. The capacitance of the piezoelectric layer should be minimized to increase the tuning range. If both piezoelectric layers are used for tuning, connection of these two layers in parallel gives a larger tuning range than connection in series. The total damping should be kept low to increase the tuning range.

For the electromagnetic generator, it was found, based on theoretical analysis, that a high electromagnetic coupling factor, K, must be achieved to realize the generators with large tuning range. Increasing the coil resistance results in using small load capacitances to achieve a large tuning range. For bigger generators, K must be higher to keep the output power of the generator unchanged. To achieve a large K, the coil must have a higher fill factor and larger thickness. Furthermore, the layout of magnets must be well designed so that the maximum change in magnetic field strength can be achieved within the minimum displacement of the magnets. It was also found that the mass, Q-factor and coil resistance do not affect the tunability of the electromagnetic generator. The mass of the generator must be large to ensure high output power if K is high.

Resonant frequencies of a micro electromagnetic generator as well a macro electromagnetic generator have been tuned by varying their capacitive load. The micro generator named G_et1 has an untuned resonant frequency of 70.05Hz. The electromagnetic coupling factor of G_et1 is 0.0035. It has been tuned by 0.13Hz while changing its capacitive load from 0 to 1000nF when excited at 30m***g***. The macro generator named G_et2 has untuned resonant frequencies of 95.1Hz and 95.5Hz when excited at 10m***g*** and 25m***g***, respectively. The electromagnetic coupling factor of G_et1 is 552.25. It has been tuned by 2.2Hz by changing its capacitive load from 0 to 700nF when excited at 10m***g***. When the generator was excited at 25mg, its resonant frequency has been tuned by 4.2Hz by changing its capacitive load from 0 to 1400nF. Most results were found to agree with the theoretical analysis. It needs to be pointed

out that due to the existence of the coil inductance; a capacitor is needed to be connected to the coil in series to cancel the effect of the coil inductance. The value of this capacitor varies with the vibration frequency. Some disagreement between experimental results and theoretical analysis is caused by inaccurately choosing the value of this capacitor. If this method is to be designed as an automatic process, the value of this capacitor together with the capacitive load should both be adjusted according to the vibration frequency.

The macro generator G_et2 has a larger tuning range than the micro generator G_et1. The reason for that is in the micro generator G_et1, the magnetic flux does not change while the mass is vibrating and only the magnetic flux cutting the coil is changed due to the change in reluctances of the magnetic flux guides while in the macro generator G_et2, the magnetic flux is changed by varying the reluctances of the air gaps. As reluctances of air gaps are much larger than those of magnetic flux guides, reluctances of air gaps dominate the total reluctance in the magnetic circuit. Small changes in reluctance of magnetic flux guide have little effect on the magnetic flux in the circuit while small changes in reluctance of air gap can change the magnetic flux significantly. Since the maximum displacements of both generators are similar, magnetic flux change per unit displacement in G_et2 is much larger than that in G_et1. Therefore, the macro generator G_et2 has much higher electromagnetic coupling factor, K than G_et1 and thus larger tuning range. This also agrees with the key points concluded in Section 7.33 for designing electromagnetic generators capable of frequency tuning using electrical method.

The problem with building a generator like G_et2 is that if the magnet is strong and the magnetic flux guide has very high permeability, there will be strong magnetic force in the small air gap between the resonator an the stator, which will cause non linearity of the generator. If this force is too big, the movement of the resonator can be seriously restricted. This has to be taken into consideration when designing such generators.

Chapter 8

Conclusions and Future Work

8.1 Summary of Work

A vibration based micro-generator is an energy harvesting device that couples a certain transduction mechanism to the ambient vibration and converts mechanical energy to electrical energy. Once installed, it can provide electrical energy persistently with little maintenance need. Therefore, it has been considered one of the most promising energy sources to replace batteries in some applications where maintenance is difficult or complex, such as wireless sensor networks. Theoretical analysis suggests that the maximum output power is generated when the resonant frequency of the generator matches the ambient vibration frequency. Once these two frequencies do not match, the output power drops significantly due to high Q-factor of the generator.

This thesis has addressed some possible methods to overcome this limit of the vibration based micro-generator, in particular, the methods of tuning the resonant frequency of the generator to match the ambient vibration frequency.

Chapter 2 introduced some transduction mechanisms that have been commonly used in vibration energy harvesting, such as electromagnetic, electrostatic, piezoelectric and magnetostrictive. A wide variety of studies regarding these mechanisms were reviewed and summarized. The theory behind the vibration based micro-generator was reviewed. It was found that if the mechanical damping factor approaches zero, i.e. no mechanical damping, the output power is totally dependent on the electrical loads. Therefore, it is highly important to minimize the mechanical damping in designing the micro-generator. The limitation of the vibration-based micro-generators, i.e. their narrow operational bandwidth, was highlighted. Solutions to this problem include widening the bandwidth and tuning the resonant frequency of the micro-generator.

Chapter 3 reviewed a wide range of studies reported so far about tuning resonant frequency of resonators and widening the bandwidth of the resonator and their applications in vibration based micro-generator.

The methods of tuning the resonant frequency include mechanical and electrical. The mechanical tuning method requires a certain mechanism to change the mechanical property of the structure of the generator to tune the resonant frequency. Possible mechanical tuning methods include:

- Changing dimensions;
- Moving the centre of gravity of proof mass;
- Varying spring stiffness;
- Straining the structure.

Mechanical tuning method can be classified as continuous tuning, i.e. the tuning mechanism is always on even when the two frequencies match, and intermittent tuning, i.e. the tuning mechanism is on only when frequency tuning is required. Intermittent tuning has advantages over continuous tuning as it is more efficient because the tuning mechanism is turned off when the generator is at the right

frequency thereby consuming negligible energy, which makes producing a net output power more probable.

The electrical tuning method realizes resonant frequency tuning by adjusting the electrical load, in particular the capacitive load. This method consumes little energy as it does not involve any change in mechanical properties. By comparison, it is much easier to implement than mechanical methods.

The suitability of different tuning approaches will depend upon the application but in general terms, the key factors for evaluating a tuning mechanism for adjusting the resonant frequency of vibration-based micro-generators are:

- Energy consumed by the tuning mechanism should be as small as possible and must not exceed the energy produced by the generator;
- The mechanism should achieve a sufficient operational frequency range;
- The tuning mechanism should achieve a suitable degree of frequency resolution;
- The generator should have as high as possible Q-factor to achieve maximum power output and the strategy applied should not increase the damping, i.e. decrease Q-factor, over the entire operational frequency range.

The method of widening the bandwidth of the generator can be achieved by, for example, employing:

- An array of structures each with a different resonant frequency;
- An amplitude limiter;
- Non-linear (e.g. magnetic) springs;
- Bi-stable structures;
- A large inertial mass (large device size) with a high degree of damping.

It was concluded that, for vibration energy harvesting, possible strategies to increase the operation frequency range include:

- Changing spring stiffness intermittently (preferred) or continuously;
- Straining the structure;
- Adjusting capacitive load;

- Using generator array;
- Employing non-linear and bi-stable structures.

In this thesis, frequency tuning methods by changing spring stiffness intermittently and adjusting capacitive load were studied.

Chapter 4 detailed the realization of resonant frequency tuning of a vibration-based generator by applying axial loads to the cantilever structure. The axial loads are provided by the interacting force between two tuning magnets. An axial tensile load can increase the resonant frequency while an axial compressive load can decrease the resonant frequency. A prototype of generator has been tested to compare to the theoretical analysis. Under the tensile loads, it is found that, when the tuning force became large, the resonant frequency was lower than expected because, when a tensile load much greater than the buckling force is applied to a beam, the resonant frequency approaches that of a straight tensioned cable and does not increase any more because the force associated with the tension in the beam becomes much greater than the beam stiffness. Furthermore, the Q-factor of the generator with tensile loads became higher than that of the generator without any tuning and the output power reduces with the increase of the resonant frequency as predicted. However, the Q-factor decreased when the tensile load became large. Under compressive loads, the resonant frequency decreased significantly for a small tuning force. Furthermore, the Q-factor of the generator dropped a lot as the resonant frequency decreased, i.e. the compressive load increased, which is a fatal drawback for this method as a useful tuning mechanism. Therefore, it was concluded that applying axial tensile loads to a cantilever is the better method to tune the resonant frequency of the vibration-based micro-generator with a cantilever structure compared to applying axial compressive loads.

Chapter 5 presented a tunable vibration-based electromagnetic micro-generator designed for this project. Its resonant frequency can be tuned by applying an axial tensile load using a pair of tuning magnets. The resonant frequency of the micro-generator can be tuned from 67.6 to 98Hz by changing the distance between two tuning magnets from 5 to 1.2mm, respectively. The generator has an efficiency of 44

and delivered a power of 61.6 to 156.6μW to the electrical load over the tuning range when it was excited at a constant low vibration acceleration level of 0.59m·s^{-2}. The tuning performance of this generator was similar to that of the one investigated in Chapter 4. Importantly, it was found that the tuning mechanism does not affect the damping of the micro-generator over most of the tuning range. Only when the tuning force became larger than the inertial force caused by vibration, was total damping increased and the output power less than that in the constant damping situation.

Chapter 6 investigated a closed loop tuning system developed to tune the resonant frequency of the generator introduced in Chapter 5 to match the ambient vibration frequency. A microcontroller was used to detect the output voltage of the micro-generator and control a linear actuator to adjust the distance between the two tuning magnets and hence the tuning force to realize frequency tuning. In the test, all parts in the closed loop tuning system, including microcontroller and linear actuator, were powered by a separate power supply to initially evaluate tuning principles and algorithms. Two tuning algorithms, i.e. voltage-only feedback and voltage-frequency feedback, were tested and compared. The voltage-only feedback algorithm judged whether the resonant frequency matches the vibration frequency based only on the amplitude of the output voltage of the generator while the voltage-frequency feedback algorithm judged whether the resonant frequency matches the vibration frequency based on both the amplitude and frequency of the output voltage of the generator. The experimental results showed that the closed loop frequency tuning system using both algorithms successfully traced the ambient vibration frequency.

The duty cycle, defined as the period of time in which the system accumulates enough energy to perform tuning, of systems using these two algorithms was studied. It is found that the average duty cycle increases linearly with the increase of the tuning range for both algorithms. It was concluded that the duty cycle can be shortened by

- Increasing the output power from the micro-generator;
- Increasing the efficiency of the generator, i.e. using more efficient power conditioning circuitry;
- Selecting actuators that are more efficient in transferring energy from the electrical domain to the mechanical domain;

- Reducing the work done by the actuator, i.e. decrease the tuning range as well as the starting frequency.

It was concluded that the duty cycle of a closed loop tuning system using voltage-frequency feedback algorithm is approximately half (55%) of that of the same tuning system using voltage-only feedback algorithm. Additionally, the tuning system using voltage-only feedback algorithm is only able to detect the change in frequency of ambient vibration while the tuning system using voltage-frequency feedback algorithm can detect not only the change in resonant frequency but also the change in amplitude and phase.

Chapter 7 investigated the method of frequency tuning by varying the electrical load, particularly, the capacitive load. Models of frequency tuning of both piezoelectric and electromagnetic using electrical method were studied. Focus was on the electromagnetic generator. The theoretical analysis of piezoelectric generator suggests that some important considerations relating to the tunability of the piezoelectric generator include:

- The material of the substrate layer and mass does not affect the tenability;
- A piezoelectric material with higher Young's modulus, strain coefficient and smaller permittivity provides a larger tuning range;
- The ratio of the thickness of the piezoelectric layer to the thickness of the substrate layer should be small to increase the tuning range;
- The capacitance of the piezoelectric layer should be minimized to increase the tuning range;
- If both piezoelectric layers are used for tuning, connection of these two layers in parallel gives a larger tuning range than connection in series;
- The total damping should be kept low to increase the tuning range.

From theoretical analysis, some key points in designing electromagnetic generators with high tunability include:

- The coupling factor, K, has to be as large as possible;
- The bigger the generator, the higher K is needed to keep the output power of the generator unchanged;

- The ratio of load resistance to coil resistance should be kept low;
- To achieve large K, the coil coefficient must be large, i.e. the coil must have higher fill factor and larger thickness;
- The layout of magnets must be well designed so that the maximum change in magnetic field strength can be achieved within the minimum displacement of the magnets;
- Mass, Q-factor and coil resistance do not affect the tunability of the electromagnetic generator;
- With large K and *r*, the mass of the generator must to be large to ensure high output power;
- The larger the coil resistance, the smaller the load capacitances are needed to achieve frequency tuning.

Two electrically tunable electromagnetic generators were tested and the experimental results were compared with theoretical analysis. Most results were found to agree with the theoretical analysis. Due to the existence of the coil inductance, a small capacitor is needed to be connected to the coil in series to cancel the effect of the coil inductance. However, the value of this capacitor varies with the vibration frequency. Disagreements between experimental results and theoretical analysis were caused by inaccurately choosing the value of this capacitor. If this method is to be designed as automatic process, the value of this capacitor together with the capacitive load should both be adjusted according to the vibration frequency. If the coil inductance is so small that the impedance of the coil inductance is neglectable compared to the coil resistance, the effect of the coil inductance on the model can be ignored and no capacitor is needed for compensation.

In conclusion, this thesis has highlighted mechanical and electrical methods of resonant frequency tuning of a vibration based micro-generator. The mechanical method involves applying an axial tensile force to strain the cantilever structure of the generator. The electrical tuning method is realized by changing the load capacitance of the generator. Although resonant frequency methods discussed in this thesis are based on electromagnetic generators, they can also be applied to generators using other transduction mechanism such as piezoelectric and electrostatic. Additionally, a

closed loop frequency tuning system as well as the frequency searching algorithms has been developed to realize automatic frequency tuning using the mechanical tuning method presented in this thesis. The duty cycle of the system was investigated and it was proved theoretically that there could be a reasonable duty cycle if the generator and tuning system is designed properly. Furthermore, models of piezoelectric and electromagnetic generators using electrical tuning methods have been established. The model of the electromagnetic generator has also been experimentally verified. It is concluded that frequency tuning using mechanical methods presented in the thesis has a larger tuning range than that using electrical methods. However, frequency tuning using electrical tuning methods consumes less power than that using mechanical methods for the same amount of tuning range. This is because that electrical tuning method does not need to change mechanical properties of the generator. All energy consumed in electrical tuning method is by electronic components while in mechanical tuning methods, an actuator that consumes much more energy than electronic components is always necessary.

8.2 Future Work

The research that has been undertaken for this thesis has successfully met the research objectives proposed in Section 1.1. However, there are still many more additional investigations that could be done in the research area of increasing operating frequency range of vibration based micro-generators. Some of these potential research areas are as follows.

8.2.1 Optimization of Closed Loop Frequency Tuning System for Mechanical Tuning Methods

Although the closed loop frequency tuning system described in this thesis has successfully tuned the resonant frequency of the generator according to the ambient vibration, all components in this system, including the microcontroller, actuator and control circuit, were powered by an external power source, not by the generator itself. Furthermore, none of these components were optimized to minimize the power consumption in frequency tuning. The component that consumes most of the power is the actuator. Power consumptions of most currently commercially available actuators are very high compared to the power generated by most micro-generators developed

so far. How to reduce the gap between power consumption in the actuator and power generated by the micro-generator is the key to make self-powered automatically tunable vibration based micro-generator practical. In addition, most currently commercially available linear actuators are still large in size compared to mm scale micro-generator. To keep tunable generators of reasonable size, it is important to minimize the dimensions of the actuators.

The ideal self-powered automatically tunable vibration based micro-generator should be that the generator can not only power its main clients, such as sensors and transceivers, but also accumulate enough power to tune the resonant frequency according to the vibration frequency within a reasonable period of time. Additionally, it should be of a reasonable size compared to the generator without the frequency tuning system.

8.2.2 Electrically Tunable Micro-Generator with Large Tuning Range

The electrically tunable micro-generator, G_et1, built for this project has small 3dB frequency range of 0.13Hz. Its tuning efficiency is only 0.19%. Although the electrically tunable macro-generator, G_et2, built by Perpetuum Ltd has a larger 3dB frequency range of 4.2 Hz and tuning efficiency of 4.4 %, its dimensions are well over the standard of 'micro'. Potential future research could be to minimize the size of the electrically tunable generator while the tunability of the generator, i.e. 3dB frequency range and tuning efficiency, exceeds or at least remains the same level as its macro scale counterpart. The challenge is to design the magnetic circuit properly so that not only the magnetic flux can change significantly with small displacement of the resonator but also that the strong electromagnetic coupling does not affect the dynamics of the resonator. Furthermore, a closed loop control system must be developed so that the load capacitance and thus the resonant frequency of the generator can be adjusted according to the vibration frequency just like the one developed in this project for the mechanical tuning method.

8.2.3 Other Strategies

It has been detailed in Chapter 3 that there are two possible methods to increase the operating frequency range of vibration based micro-generators. Only the method of

tuning the resonant frequency was studied in this thesis. There are many potential investigations about the other methods, i.e. widening the bandwidth of the micro-generator. As analyzed in Chapter 3, possible strategies to increase the operating frequency range by widening the bandwidth of the micro-generator include:

- Using generator array;
- Employing non-linear and bi-stable structures.

When designing generator arrays, the key point is to find a balance between the total size of the generator array and its operating frequency range. If the same amount of output power is produced, the wider the operating frequency range to be achieved, the more individual generators are needed and thus the larger the generator array will be.

For non-linear micro-generators, a crucial problem is the complexity in modeling and design. As discussed in Section 3.5.3, the output power and bandwidth of the non-linear generators depends on the direction of approach of the vibration frequency to the resonant frequency. For a hard non-linearity, this approach will only produce an improvement when approaching the device resonant frequency from a lower frequency. For a soft non-linearity, this approach will only produce an improvement when approaching the device resonant frequency from a higher frequency. So far, there is no reported method to estimate whether a non-linear device has a hard or soft non-linearity before actually building and testing one. More investigations in non-linear devices must be conducted before applying this technique to micro-generators to increase their operating frequency range.

The merit of the micro-generators with bi-stable structures is that the output power of the generator is independent of the vibration frequency. They can basically work at any frequency as long as the vibration can provide enough force to make the mobile part travel between two stable positions. So far, little work has been reported in this area. A comprehensive theory of bi-stable structures must be established to lay the foundation for its practical applications.

Appendix A

Model of Vibration Based Micro-Generator

Figure A.1 shows a generic model of such a generator, which consists of a seismic mass, m and a spring with the spring constant of k. When the generator vibrates, the mass moves out of phase with the generator housing. There is a relative movement between the mass and the housing. This displacement is sinusoidal in amplitude and can drive a suitable transducer to generate electrical energy. b is the damping coefficient that consists of mechanically induced damping (parasitic damping) coefficient b_m and electrically induced damping coefficient b_e, i.e. $b = b_m + b_e$. $y(t)$ is the displacement of the generator housing and $z(t)$ is the relative motion of the mass with respect to the housing. For a sinusoidal excitation, $y(t)$ can be written as $y(t) = Y \cdot \sin\omega t$, where Y is the amplitude of vibration and ω is the angular frequency of vibration.

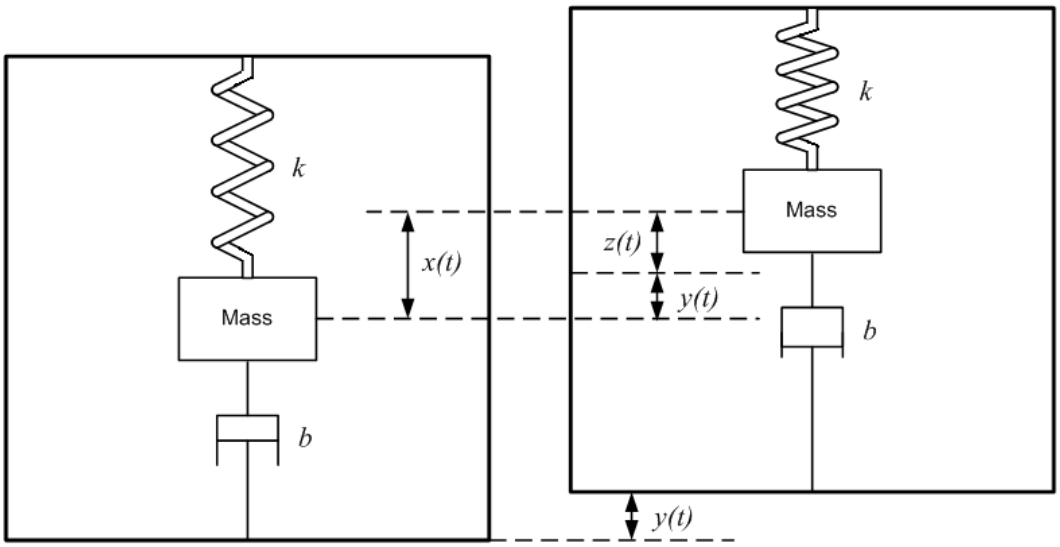

Figure A.1. Generic model of vibration-driven generator.

The transduction mechanism itself can generate electricity by exploiting the mechanical strain or relative displacement occurring within the system. The strain effect utilizes the deformation within the mechanical system and typically employs active materials (e.g. piezoelectric). In the case of relative displacement, either the velocity or position can be coupled to a transduction mechanism. Velocity is typically associated with electromagnetic transduction whist relative position is associated with electrostatic transduction. Each transduction mechanism exhibits different damping characteristics and this should be taken into consideration while modeling the generators. Thermechanical system can be increased in complexity, for example, by including a hydraulic system to magnify amplitudes or forces, or couple linear displacements into rotary generators.

A.1 Transfer Function

For the analysis, it is assumed that the mass of the vibration source is much greater than the mass of seismic mass in the generator and the vibration source is unaffected by the movement of the generator. Then the differential equation of the movement of the mass with respect to the generator housing from the dynamic forces on the mass can be derived as follows:

$$m \cdot \frac{d^2 z(t)}{dt^2} + b \cdot \frac{dz(t)}{dt} + k \cdot z(t) = -m \cdot \frac{d^2 y(t)}{dt^2} \tag{A.1}$$

which can be written in the form after the Laplace Transform as:

$$m \cdot s^2 \cdot z(s) + b \cdot s \cdot z(s) + k \cdot z(s) = -m \cdot a(s) \tag{A.2}$$

where $a(s)$ is the Laplace expression of the acceleration of the vibration, $a(t)$, which is given by:

$$a(t) = \frac{d^2 y(t)}{dt^2} \tag{A.3}$$

Thus, the transfer function of a vibration-based micro-generator is:

$$\frac{z(s)}{a(s)} = \frac{1}{s^2 + \frac{b}{m}s + \frac{k}{m}} = \frac{1}{s^2 + \frac{\omega_r}{Q}s + \omega_r^2} \tag{A.4}$$

where $Q = \frac{\sqrt{km}}{b}$ is the quality factor and $\omega_r = \sqrt{\frac{k}{m}}$ is the resonant frequency.

A.2 Equivalent Circuit

An equivalent electrical circuit for a vibration-based micro-generator can be found from Equation (A.4), which, when rearranged, gives:

$$-m \cdot a(s) = s \cdot Z(s)\left(ms + b + \frac{k}{s}\right) \tag{A.5}$$

Equation (A.3) can be rewritten as:

$$-I(s) = E(s)\left(sC + \frac{1}{R} + \frac{1}{sL}\right) \tag{A.6}$$

where $I(s) = m \cdot a(s)$, $E(s) = s \cdot Z(s)$, $C = m$, $R = \frac{1}{b}$, $L = \frac{1}{k}$. Based on Equation (A.6), an equivalent electrical circuit can be built shown in Figure A.2.

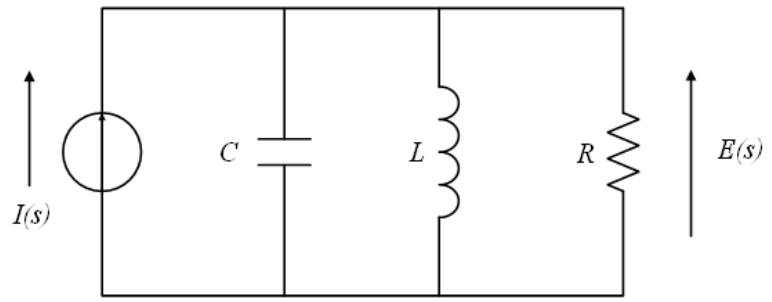

FigureA.2. Equivalent circuit of a vibration-based micro-generator.

A.3 Damping in EM Micro-generators

For electromagnetic generators, the voltage, *u*, and current, *i*, generated can be described by the following equations, respectively:

$$u = \mathrm{K}\frac{dz(t)}{dt} - i(R_c + j\omega L_c) \tag{A.7}$$

$$i = \frac{F_e}{\mathrm{K}} \tag{A.8}$$

where F_e is the damping force generated by the electromechanical coupling, R_c and L_c are the resistance and inductance of the coil, respectively. K is the electromagnetic coupling factor and can be expressed as:

$$\mathrm{K} = N \cdot B \cdot l \tag{A.9}$$

where N is the number of turns, B is the average flux density through the coil and l is the effective length of the coil.

Assume that the micro-generator is connected to a resistive load R_L, the damping force F_e becomes:

$$F_e = \frac{\mathrm{K}^2 \frac{dz(t)}{dt}}{R_L + R_c + j\omega L_c} \tag{A.10}$$

The electrically induced damping coefficient, b_e, is as follows:

$$b_e = \frac{\mathrm{K}^2}{R_L + R_c + j\omega L_c} \tag{A.11}$$

For a micro-generator that works at low resonant frequencies, the inductive impedance of the coil is much lower than its resistive impedance. Hence, the inductive impedance can be ignored in this case. Thus, the electrically induced damping coefficient, b_e, can be simplified to:

$$b_e = \frac{\mathrm{K}^2}{R_L + R_c} \tag{A.12}$$

The electrically induced damping factor, ζ_e, is:

$$\zeta_e = \frac{\mathrm{K}^2}{2m\omega(R_L + R_c)} \tag{A.13}$$

The overall damping factor of the system, ζ_T, is given by:

$$\zeta = \frac{b}{2m\omega_r} = \frac{b_e + b_m}{2m\omega_r} = \zeta_e + \zeta_m \tag{A.14}$$

where $\zeta_m = \frac{b_m}{2m\omega_r}$ is the mechanically induced damping factor.

Quality factor (Q-factor) is a function of damping factor. The total Q-factor is given by:

$$Q_T = \frac{1}{2\zeta_T} \tag{A.15}$$

It is the Q-factor when the generator is connected to the optimum load. The relationship between total quality factor and the electrical and mechanical damping is given by:

$$\frac{1}{Q_T} = \frac{1}{Q_{OC}} + \frac{1}{Q_e} \tag{A.16}$$

where Q_{OC} is the open circuit Q-factor, i.e. $Q_{OC} = \frac{1}{2\zeta_m}$ and $Q_e = \frac{1}{2\zeta_e}$.

A.4 Output Power of EM Micro-generators

Assume that the input is a sinusoid excitation, i.e. $y(t) = \sin\omega t$. The solution to Equation (A.3) is given by:

$$z(t) = \frac{m\omega^2 Y}{k - m\omega^2 + j\omega b}\sin\omega t \tag{A.17}$$

or

$$z(t) = \frac{\omega^2}{\sqrt{\left(\omega_r^2 - \omega^2\right)^2 + \left(\frac{b\cdot\omega}{m}\right)^2}} Y\sin\left(\omega t + \varphi\right) \tag{A.18}$$

where φ is the phase angle given by:

$$\varphi = \tan^{-1}\left(\frac{b\cdot\omega}{k - \omega^2\cdot m}\right) \tag{A.19}$$

The average power dissipated within the damper, i.e. the sum of the power extracted by the transduction mechanism and the power lost in mechanical damping is given by:

$$P = b\left(\frac{dz(t)}{dt}\right)^2 \tag{A.20}$$

Equation (A.18) and (A.20) provide us with the average power dissipated within the damper as follows:

$$P = \frac{m\zeta_T Y^2 \left(\frac{\omega}{\omega_r}\right)^3 \omega^3}{\left[1-\left(\frac{\omega}{\omega_r}\right)^2\right]^2 + \left[2\zeta_T \frac{\omega}{\omega_r}\right]^2} \tag{A.21}$$

When the generator is at resonance, i.e. $\omega = \omega_r$, the power dissipation reaches maximum. The maximum dissipated power is:

$$P = \frac{mY^2\omega_r^3}{4\zeta_T} \tag{A.22}$$

Appendix B

Measurement of Damping

In this appendix, the method of measuring damping as well as the Q-factor of the generator will be introduced.

Figure B.1 shows the attenuation plot of a resonator when the vibration suddenly disappears. It is found that the peak value of the impulse response in one cycle of vibration attenuates gradually.

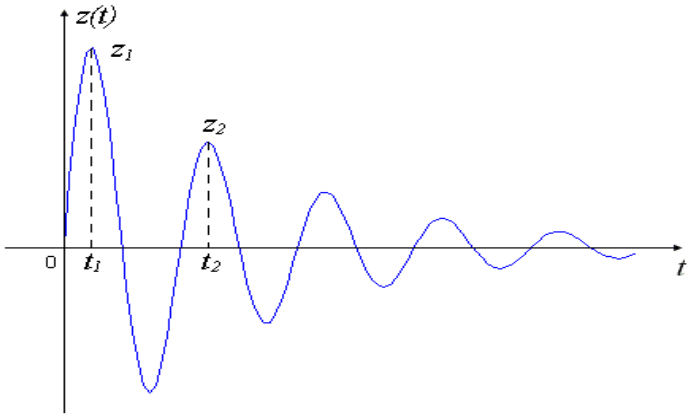

Figure B.1. Example of an underdamped system response

This curve can be expressed as:

$$z(t) = \frac{F}{m\omega_d} e^{-\zeta\omega_r t} \sin \omega_d t \tag{B.1}$$

where m is the mass, F is the magnitude of the excitation. ζ is the damping factor and ω_r and ω_d are the resonant frequency and the frequency of damped oscillation, respectively. ω_d is given by:

$$\omega_d = \omega_r \sqrt{1-\zeta^2} \tag{B.2}$$

The term $e^{-\zeta\omega_r t}$ causes the attenuation in magnitude. More specifically, it is the existence of the damper that results in the drop of the magnitude. Therefore, the damping factor can be measured by observing peak value in each cycle of vibration.

According to Equation (B.1),

$$z_1 = z(t_1) = \frac{F}{m\omega_d} e^{-\zeta\omega_r t_1} \sin \omega_d t_1 \tag{B.3}$$

$$z_2 = z(t_2) = \frac{F}{m\omega_d} e^{-\zeta\omega_r t_2} \sin \omega_d t_2 \tag{B.4}$$

where $t_2 = t_1+T$, $T = \frac{2\pi}{\omega_d}$ is the period of damped oscillation. Their ratio is:

$$\frac{z_1}{z_2} = \frac{\frac{F}{m\omega_d} e^{-\zeta\omega_r t_1} \sin \omega_d t_1}{\frac{F}{m\omega_d} e^{-\zeta\omega_r t_2} \sin \omega_d t_2} \tag{B.5}$$

If t_2 is replaced by t_1,

$$\frac{z_1}{z_2} = \frac{e^{-\zeta\omega_r t_1}\sin\omega_d t_1}{e^{-\zeta\omega_r (t_1+T)}\sin\omega_d (t_1+T)} = e^{\zeta\omega_r T} \tag{B.6}$$

When natural logarithm are taken on both sides in Equation (B.6), the damping factor can be written as:

$$\zeta = \frac{1}{\omega_r T}\ln\frac{z_1}{z_2} = \frac{\omega_d}{2\pi\omega_r}\ln\frac{z_1}{z_2} \tag{B.7}$$

Substitution of Equation (B.2) into Equation (B.7) leads to:

$$\zeta = \frac{\omega_r\sqrt{1-\zeta^2}}{2\pi\omega_r}\ln\frac{z_1}{z_2} \tag{B.8}$$

Thus, the damping factor is given by:

$$\zeta = \frac{\alpha}{\sqrt{4\pi^2+\alpha^2}} \tag{B.9}$$

where α is defined as $\alpha = \ln\frac{z_1}{z_2}$. Therefore, if peak values in the first two cycles of vibration can be measured, the damping factor can be determined.

The damping factor can be more accurately determined by measuring the displacements at two times separated by a given number of periods for the reason that these two peak values cover longer time period, which gives a clearer view of the attenuation. Suppose that the two sampling times are separated by n periods and z_1 and z_{n+1} are the peak displacements corresponding to the times t_1 and $t_{n+1} = t_1 + nT$, so:

$$\frac{z_1}{z_{n+1}} = \frac{x_1}{x_2}\cdot\frac{x_2}{x_3}\cdots\frac{x_n}{x_{n+1}} = \left(e^{\zeta\omega_r T}\right)^n = \left(e^{2\pi\zeta\omega_r/\omega_d}\right)^n \tag{B.10}$$

Substituting Equation (B.2) into (B.10) results in:

$$\frac{z_1}{z_{n+1}} = e^{n2\pi\zeta / \sqrt{1-\zeta^2}} \tag{B.11}$$

From Equation (B.11), the logarithmic decrement is given by:

$$\alpha = \frac{2\pi\zeta}{\sqrt{1-\zeta^2}} = \frac{1}{n}\ln\frac{z_1}{z_{n+1}} \tag{B.12}$$

which can be inserted in Equation (B.9) to obtain the more accurate damping factor.

Although determination of damping factor based on two peak values separated by several period is more accurate than that based on two consecutive peak values, it can still cause some errors, especially when measuring small damping. Basically, there are two methods to improve the accuracy. The first step of these two methods is both to measure peak values in every cycle and then calculate α set of a as well as a set of ζ. Method one takes the mean value of the set of ζ, $\bar{\zeta}$ and $\bar{\zeta}$ is regarded as the accurate value of damping factor. Method two uses error-minimizing approach to find the accurate ζ. The basic idea is to find a value $\tilde{\zeta}$ that makes the accumulative error $e = \sum_i \left(\zeta_i - \tilde{\zeta}\right)^2$ minimum. $\tilde{\zeta}$ is the damping factor. The calculation of $\tilde{\zeta}$ can be done using following equations.

Suppose X=[x_1, x_2, …, x_n] is a set of peak amplitudes of the attenuation. A straight line to fit the set of points that represents the natural logarithm of the measurements X has to be found. The equation of the straight line in the discrete form is given by:

$$z_i = ay_i + b \tag{B.13}$$

Note that z_i corresponds to lnx_i, a to $-\alpha$, y_i to i-1 and b to lnx_1. The error is:

$$\varepsilon = \sum_{i=1}^{n} (\ln x_i - z_i)^2 = \sum_{i=1}^{n} (\ln x_i - a y_i - b)^2 \tag{B.14}$$

To minimize the error, the following equations must be satisfied.

$$\begin{aligned} \frac{\partial \varepsilon}{\partial a} &= 0 \\ \frac{\partial \varepsilon}{\partial b} &= 0 \end{aligned} \tag{B.15}$$

Thus,

$$\begin{aligned} \left(\sum_{i=1}^{n} y_i^2 \right) a + \left(\sum_{i=1}^{n} y_i \right) b &= \sum_{i=1}^{n} (\ln x_i) y_i \\ \left(\sum_{i=1}^{n} y_i \right) a + nb &= \sum_{i=1}^{n} \ln x_i \end{aligned} \tag{B.16}$$

Solving Equation (B.16), α and the damping factor can be obtained by Equation (B.9).

By comparison, values obtained using these two methods are of little difference. Therefore, either method can be adopted.

The Quality (Q) factor of the system is given by:

$$Q = \frac{1}{2\zeta} \tag{B.17}$$

where ζ is the damping factor of the system. Therefore, measurement of quality factor is in fact measurement of damping factor.

Bibliography

[1] Beeby S P, Tudor M J and White N M 2006 Energy harvesting vibration sources for microsystems applications *Measurement Science and Technology* **17** 175-95.

[2] Perpetuum Ltd, http://www.perpetuum.co.uk

[3] Mide Technology Corporation, http://www.mide.com

[4] EnOcean GmbH, http://www.enocean.com

[5] K. Römer and F. Mattern 2004 The Design Space of Wireless Sensor Networks *IEEE Wireless Communications* **11(6)** 54-61.

[6] Elvin N G, Lajnef N and Elvin A A 2006 Feasibility of structural monitoring with vibration powered sensors Smart Materials and Structures **15** 977–86

[7] Nezhad-Ahmadi M R, Weale G, El-Agha A, Griesdorf D; Tumbush G, Hollinger A, Matthey M, Meiners H and Asgaran S 2008 A 2mW 400MHz RF transceiver SoC in 0.18μm CMOS technology for wireless medical applications *Radio Frequency Integrated Circuits Symposium, 2008. RFIC 2008. IEEE* 285-88

[8] Wong A C W, Kathiresan G, Chan C K T, Eljamaly O, Omeni O, McDonagh D, Burdett A J and Toumazou C 2008 A 1 V Wireless Transceiver for an Ultra-Low-Power SoC for Biotelemetry Applications *IEEE Journal of Solid-State Circuits* **43(7)** 1511-21

[9] Paradiso J A and Starner T 2005 Energy Scavenging for Mobile and Wireless Electronics *IEEE Pervasive Computing* **4(1)** 18-27

[10] Mitcheson P D, Yeatman E M, Rao G K, Holmes A S and Green T C 2008 Energy Harvesting From Human and Machine Motion for Wireless Electronic Devices *Proceedings of the IEEE* **96(9)** 1457-86

[11] Norman B C 2007 Power options for wireless sensor networks *IEEE Aerospace and Electronic Systems Magazine* **22(4)** 14-7

[12] Huesgen T, Woias P and Kockmann N 2008 Design and fabrication of MEMS thermoelectric generators with high temperature efficiency *Sensors and Actuators A: Physical* **145-146** 423-29

[13] Roundy S, Wright P K and Rabaey J 2003 A study of low level vibrations as a power source for wireless sensor nodes *Computer Communications* **26** 1131-44

[14] Arnold D P 2007 Review of microscale magnetic power generation *IEEE Transactions on Magnetics* **43(11)** 3940-51

[15] Roundy S, Wright P and Pister K 2002 Micro-electrostatic vibration-to-electricity converters *Proceddings of IMECE* 2002 1-10

[16] Sodano H A, Inman D J and Park G 2004 A review of power harvesting from vibration using piezoelectric materials *Shock Vibration Digest* **36(3)** 197-205

[17] Beeby S P, Tudor M J, Torah R N Roberts S O'Donnell T and Roy S 2007 Experimental comparison of macro and micro scale electromagnetic vibration powered generators *Microsystem Technology* **13** 1647-53

[18] Williams C B, Shearwood C, Harradine M A, Mellor P H, Birch T S and Yates R B 2001 Development of an electromagnetic micro-generator *IEE Proceedings of Circuits Devices Systems* **148** 337-42

[19] Ching N N H, Wong H Y, Li W J, Leong P H W and Wen Z 2002 A laser-micromachined vibrational to electrical power transducer for wireless sensing systems *Sensers and Acuators A* **97-98** 685-90

[20] Glynne-Jones P, Tudor M J, Beeby S P and White N M 2004 An electromagnetic, vibration-powered generator for intelligent sensor systems *Sensors and Actuators A* **110** 344-9

[21] Koukarenko E, Beeby S P, Tudor M J, White N M, O'Donnell T, Saha T, Kulkani S and Roy S 2006 Microelectromechanical systems vibration powered electromagnetic generator for wireless sensor applications *Microsystem Technologies* **12 (11)** 1071-7

[22] Saha C R, O'Donnell T, Loder H, Beeby S P and Tudor M J 2006 Optimization of an electromagnetic energy harvesting device *IEEE Transactions on Magnetics*

42(10) 3509-11

[23] Beeby S P, Torah R N, Tudor M J, Glynne-Jones P, O'Donnell T, Saha C R and Roy S 2007 A micro electromagnetic generator for vibration energy harvesting *Journal of Micromechanics and Microengineering* **17** 1257-65

[24] Wang P H, Dai X H, Fang D M and Zhao X L 2007 Design, fabrication and performance of a new vibration-based electromagnetic micro power generator *Microelectronics Journal* **38** 1175-80

[25] Külahand H and Najafi K 2008 Energy scavenging from low-frequency vibrations by using frequency up-conversion for wireless sensor applications *IEEE Sensors Journal* **8(3)** 261-8

[26] Meninger S, Mur-Miranda J, Lang J, Chandrakasan A, Slocum A, Schmidt M and Amirtharajah R 2001 Vibration to electric energy conversion *IEEE Transactions on Very Large Scale Integration (VLSI) Systems* **9** 64–76.

[27] Tashiro R, Kabei N, Katayama K, Tsuboi F and Tsuchiya K 2002 Development of a electrostatic generator for a cardiac pacemaker that harnesses the ventricular wall motion *Journal of Artificial Organs* **5(4)** 239–45

[28] Mitcheson P, Stark B, Miao P, Yeatman E, Holmes A and Green T 2003 Analysis and optimisation of MEMS on-chip power supply for self powering of slow moving sensors *Eurosensors 03, 17th European conference on sensors and actuators, University of Minho, Guimaraes, Portugal* 48-51

[29] Arakawa Y, Suzuki Y and Kasagi N 2004 Micro seismic power generator using electret polymer film *PowerMEMS Conference, Kyoto, Japan* 187-90

[30] Despesse G, Jager T, Chaillout J, Leger J, Vassilev A, Basrour S and Chalot B 2005 Fabrication and characterisation of high damping electrostatic micro devices for vibration energy scavenging *Proceedings of Design, Test, Integration and Packaging of MEMS and MOEMS* 386–90

[31] Kuehne I, Frey A, Eckstein G, Schmid U and Seidel H 2006 Design and analysis of a capacitive vibration-to-electrical energy converter with built-in voltage *Proceeding of the 36th European Solid-State Device Research Conference* 138-41

[32] Yen B C and Lang J H 2006 A variable-capacitance vibration-to-electric energy harvester *IEEE Transactions on circuits and systems-I: Regular papers* **53(2)** 288-95

[33] Sterken T, Fiorinil P, Altena G, Van Hoof C and Puers R 2007 Harvesting energy from vibrations by a micromachined electret generator *International Solid-State*

Sensors, Actuators and Microsystems Conference, Lyon, France 129-32

[34] Lo H and Tai Y C 2008 Parylene-based electret power generators *Journal of Micromechining and Microengineering* **18** 104006

[35] Anton S R and Sodano H A 2007 A review of power harvesting using piezoelectric materials (2003–2006) *Smart Materials and Structures* **16** R1–R21

[36] Sodano H A and Inman D J 2005 Comparison of piezoelectric energy harvesting devices for recharging batteries *Journal of Intelligent Material Systems and Structures* **16(10)** 799-807

[37] White N M, Glynne-Jones P and Beeby S P 2001 A novel thick-film piezoelectric micro-generator *Smart Materials and Structures* **10** 850-2

[38] Lu F, Lee H P and Lim S P 2004 Modeling and analysis of micro piezoelectric power generators for micro-electromechanical-systems applications *Smart Materials and Structures* **13** 57-63

[39] Jeon Y B, Sood R, Jeong J-h and Kim S G 2005 MEMS power generator with transverse mode thin film PZT *Sensors Actuators A* **122** 16–22

[40] Fang H B, Liu J-Q, Xu Z Y, Dong L, Wang L, Chen D, Cai B C and Liu Y 2006 Fabrication and performance of MEMS-based piezoelectric power generator for vibration energy harvesting *Microelectronics Journal* **37** 1280-4

[41] Marzencki M, Ammar Y and Basrour S 2007 Integrated power harvesting system including a MEMS generator and a power management circuit *Sensors and Actuators A* **145-146** 363-70

[42] Jeong S-J, Kim M-S, Song J-S and Lee H-K 2008 Two-layered piezoelectric bender device for micro-power generator *Sensors and Actuators A* **148** 158-67

[43] Kok S W, White N W and Harris N H 2008 A novel piezoelectric thick-film free-standing cantilever energy harvester *EUROSENSORS XXII, Dresden, Germany* 395-9

[44] Huang J, O'Handley R C and Bono D 2003 New, high-sensitivity, hybrid magnetostrictive/electroactive magnetic field sensors *Proceedings of the SPIE* **5050** 229–37

[45] Wang L and Yuan F G 2008 Vibration energy harvesting by magnetostrictive material *Smart Materials and Structures* **17** 045009

[46] Roundy S, Wright P H and Rabaey J M 2004 *Energy scavenging for wireless sensor networks with special focus on vibrations* Norwell, Massachusetts 02061 USA (Kluwer Academic Publishers) pp 47-9

[47] Volture PEH20w Piezoelectric Vibration Energy Harvester, Mide Technology Corporation, http://www.mide.com/products/volture/peh20w/peh20w.php

[48] Volture PEH25w Piezoelectric Vibration Energy Harvester, Mide Technology Corporation, http://www.mide.com/products/volture/peh25w/peh25w.php

[49] PMG-17 datasheet, Perpetuum Ltd, http://www.perpetuum.co.uk/home.php?page_id=11

[50] PMG-27 datasheet, Perpetuum Ltd, http://www.perpetuum.co.uk/home.php?page_id=12

[51] Williams C B and Yates R B 1996 Analysis of a micro-electric generator for microsystems *Sensers and Acuators A* **52** 8-11

[52] Roundy S and Zhang Y 2005 Toward self-tuning adaptive vibration based micro-generators *Proceedings of SPIE, Smart Structures, Devices, and Systems II* **5649** 373-84

[53] Thomson W T 2003 *Theory of vibration with application* (Nelson Thornes Ltd) p 66

[54] Blevins R D 2001 *Formulas for natural frequency and mode shape* (Krieger Publishing Company) p 158

[55] Gieras J F, Oh J-H, Huzmezan M and Sane H S 2007 Electromechanical energy harvesting system *Patent publication number: WO2007070022(A2), WO2007070022(A3)*

[56] Roylance L and Angell J B 1979 A batch fabricated silicon accelerometer *IEEE Transactions on Electron Devices* **26(12)** 1911-7

[57] Wu X, Lin J, Kato S, Zhang K, Ren T and Liu L 2008 A frequency adjustable vibration energy harvester *Proceedings of PowerMEMS 2008+ microEMS2008, Sendai, Japan, November 9-12, 2008* 245-8

[58] Scheibner D, Mehner J, Reuter D, Kotarsky U, Gessner T and Dötzel W 2004 Characterization and self-test of electrostatically tunable resonators for frequency selective vibration measurements *Sensors and Actuators A* **111** 93-9

[59] Scheibner D, Mehner J, Reuter D, Gessner T and Dötzel W 2005 A spectral vibration detection system based on tunable micromechanical resonators *Sensors and Actuators A* **123-124** 63-72

[60] Adams S G, Bertscht F M, Shawt K A, Hartwell P G, MacDonald N C and Moon F C 1995 Capacitance based tunable micromechanical resonators *The 8th International Conference on Solid-State Sensors and Actuators, and Eurosensors*

IX. Stockholm, Sweden 438-41

[61] Lee K B, Lin L and Cho Y H 2008 A closed-form approach for frequency tunable comb resonators with curved finger contour *Sensors and Actuators A* **141** 523-9

[62] Piazza G, Abdolvand R, Ho G K and Ayazi F 2004 Voltage-tunable piezoelectrically transduced single-crystal silicon micromechanical resonators, *Sensors and Actuators A* **111** 71-8

[63] Yao J J and MacDonald N C 1996 A micromachined, single-crystal silicon, tunable resonator *Journal of Micromechical Microengineering* **6** 257-64

[64] Thiesen J and G P O'Brian 2006 Energy harvester with adjustable resonant frequency *Patent publication number: WO2006046937(A1), EP1803170(A1), US2008129147(A1), EP1803170(A0), CN101002343(A)*

[65] Peters C, Maurath D, Schock W and Manoli Y 2008 Novel electrically tunable mechanical resonator for energy harvesting *Proceedings of PowerMEMS 2008+ microEMS2008, Sendai, Japan, November 9-12, 2008* 253-6

[66] Challa V R, Prasad M G, Shi Y and Fisher F T 2008 A vibration energy harvesting device with bidirectional resonance frequency tunability *Smart Materials and Structures* **17** 015035

[67] Remtema T and Lin L 2001 Active frequency tuning for micro resonators by localized thermal stressing effects *Sensors and Actuators A* **91** 326-32

[68] Syms R R A 1998 Electrothermal frequency tuning of folded and coupled vibrating micromechanical resonators *Journal of microelectromechanical systems* **7(2)** 164-71

[69] Blevins R D 2001 *Formulas for natural frequency and mode shape* (Krieger Publishing Company) p 144

[70] Blevins R D 2001 *Formulas for natural frequency and mode shape* (Krieger Publishing Company) p 109

[71] Blevins R D 2001 *Formulas for natural frequency and mode shape* (Krieger Publishing Company) p 149

[72] Cabuz C, Fukatsu K, Hashmoto H, Shoji S, Kurabayashi T, Minami K and Esashi M 1994 Fine frequency tuning in resonant sensors 245-50

[73] Leland E S and Wright P K 2006 Resonance tuning of piezoelectric vibration energy scavenging generators using compressive axial preload *Smart Materials and Structures* **15** 1413-20

[74] Mukherjee R 2007 MEMS resonator using frequency tuning *Patent publication number: US20070214890A1*

[75] Hu Y, Xue H and Hu H 2007 A piezoelectric power harvester with adjustable frequency through axial preloads *Smart Materials and Structures* **16** 1961-6

[76] Eichhorn C, Goldschmidtboeing F and Woias P 2008 A frequency piezoelectric energy convert based on a cantilever beam *Proceedings of PowerMEMS 2008+ microEMS2008, Sendai, Japan, November 9-12, 2008* 309-12

[77] Zhu D, Roberts S, Tudor M J and Beeby S P 2008 Closed loop frequency tuning of a vibration-based micro-generator *Proceedings of PowerMEMS 2008+ microEMS2008, Sendai, Japan, November 9-12, 2008* 229-32

[78] Charnegie D 2007 Frequency tuning concepts for piezoelectric cantilever beams and plates for energy harvesting *MSc Dissertation* School of Engineering, University of Pittsburgh, USA

[79] Wu W-J, Chen Y-Y, Lee B-S, He J-J and Peng Y-T 2006 Tunable resonant frequency power harvesting devices *Proceedings of SPIE* **6169** 55-62

[80] Shahruz S M 2006 Design of mechanical band-pass filters for energy scavenging *Journal of Sound and Vibration* **292** 987-98

[81] Xue H, Hu Y and Wang Q-M 2008 Broadband piezoelectric energy harvesting devices using multiple bimorphs with different operating frequencies *IEEE Transactions on Ultrasonics , Feroelectrics and Frequency Control* **55(9)** 2104-8

[82] Feng G-H and Hung J-C 2007 Optimal FOM designed piezoelectric microgenerator with energy harvesting in a wide vibration bandwidth *Proceedings of the 2nd IEEE International Conference on Nano/Micro Engineered and Molecular Systems, January 16-19, 2007, Bangkok, Thailand* 511-4

[83] Ferrari M, Ferrari V, Guizzetti M, Marioli D and Taroni A 2008 Piezoelectric multifrequency energy converter for power harvesting in autonomous microsystems *Sensors and Actuators A* **142** 329-35

[84] Sari I, Balkan T and Kulah H 2007 A wideband electromagnetic micro power generator for wireless microsystems *International Solid-State Sensors, Actuators and Microsystems Conference, Lyon, France* 275-8

[85] Soliman M S M, Abdel-Rahman E M, El-Saadany E E and Mansour R R 2008 A wideband vibration-based energy harvester *Journal of Micromechanics and Microengeering* **18** 115021

[86] Ramlan R, Brennan M J, Mace B R and Kovacic I 2008 An investigation into *the benefits of using a nonlinear stiffness in an energy harvesting device (submitted)*

[87] Spreemann D, Folkmer B, Maurath D and Manoli Y 2006 Tunable transducer for low frequency vibrational energy scavenging *Proceedings of EurosensorsXX, Göteborg, Sweden*

[88] Mann B P and Sims N D 2008 Energy harvesting from the nonlinear oscillations of magnetic levitation *Journal of Sound and Vibration* doi:10.1016/j.jsv.2008.06.011

[89] Burrow S G and Clare L R 2007 A Resonant Generator with Non-Linear Compliance for Energy Harvesting in High Vibrational Environments *IEEE International Electric Machines & Drives Conference, IEMDC '07* **1** 715-20

[90] Burrow S G, Clare L R, Carrella A.and Barton D 2008 Vibration energy harvesters with non-linear compliance *Active and Passive Smart Structures and Integrated Systems 2008, Proceedings of the SPIE* **6928** 692807

[91] Dogheche K, Cavallier B, Delobelle P, Hirsinger, L, Cattan E, Rèmiens D, Marzencki M, Charlot B, Basrour S and Ballandras S 2006 A bi-stable micro-machined piezoelectric transducer for mechanical to electrical energy transformation *Integrated Ferroelectrics* **80:1** 305-15

[92] Akoun G and Yonnet J P 1984 3D analytical calculation of the forces exerted between two cuboidal magnets *IEEE Transactions on Magnetics* **20(5)** 1962-4

[93] High Strength Copper – Beryllium Alloys http://www.key-to-metals.com/Article63.htm

[94] Table of Properties of NdFeB Magnets http://www.magnetsales.com/Neo/Neoprops.htm

[95] ET-126B Specifications, Labworks Inc., http://www.labworks-inc.com/products/shakers/ET_126b.htm

[96] LabVIEW, National Instruments, http://www.ni.com/labview

[97] Haydon hybrid linear actuator Mode 21000, http://kerk-haydon.com/Products/StepperMotorLinearActuators/HybridLinearActuators/21000Series/tabid/74/Default.aspx

[98] Table of Properties of NdFeB Magnets, http://www.magnetsales.com/Neo/Neoprops.htm

[99] Mechanical Simulation with ANSYS Workbench, ANSYS Inc., http://www.ansys.com/solutions/simulation-environment.asp

[100] Hildebrand F B 1974 *Introduction to numerical analysis* (McGraw-Hill, Inc.) p 290

[101] Koukarenko E, Beeby S, Tudor M, White N, O'Donnell T, Saha T, Kulkani S and Roy S 2006 Microelectromechanical systems vibration powered electromagnetic generator for wireless sensor applications *Microsystem Technologies* **12**(11) 1071-7

[102] Torah R, Beeby S, Tudor M, O'Donnell T and Roy S 2006 Kinetic energy harvesting using microscale electromagnetic generators *Micromechanics Europe, 2006, Southampton*

[103] Beeby S, Tudor M, Torah R, Koukarenko E, Roberts S, O'Donnell T and Saha C 2006 Macro and Micro Scale Electromagnetic Kinetic Energy Harvesting Generators *DTIP, Stresa, Italy*

[104] All Magnetics Inc. http://www.800amagnet.com/index.htm

[105] Sadiku M N O 1994 *Elements of electromagnetics* (Saunders College Publishing) p 383

[106] Hoole S R H and Hoole P R P 1996 *A modern short course in engineering electromagnetics* (Oxford University Press) p 284

[107] Ansoft Maxwell 3D, http://www.ansoft.com/maxwell/

[108] NISA EMAG, http://www.nisasoftware.com/Products/MechanicalApplications/EMAG/tabid/63/Default.aspx

[109] ANSYS Emag, http://www.ansys.com/products/emag.asp

[110] INTEGRATED's CAE software http://www.integratedsoft.com/applications/MagneticsApplications.aspx

[111] PIC16F684 Data Sheet, available at http://ww1.microchip.com/downloads/en/DeviceDoc/41202E.pdf

[112] Microchip Application Note: AN879 - Using the Microchip Ultra Low-power Wake-up Module, available at http://ww1.microchip.com/downloads/en/AppNotes/00879C.pdf

[113] Roundy S, Wright P K and Rabaey J M 2004 *Energy scavenging for wireless sensor networks with special focus on vibrations* (Kluwer Academic publishers) pp 181-8

[114] http://www.memsnet.org/material/